DYNAMIC REACTIVE POWER CONTROL OF ISOLATED POWER SYSTEMS

A Dissertation

by

MILAD FALAHI

Submitted to the Office of Graduate Studies of
Texas A&M University
in partial fulfillment of the requirements for the degree of

DOCTOR OF PHILOSOPHY

Approved by:

Co-Chairs of Committee,	Mehrdad Ehsani
	Karen Butler-Purry
Committee Members,	Shankar Bhattacharyya
	John Hurtado
Head of Department,	Chanan Singh

December 2012

Major Subject: Electrical Engineering

ABSTRACT

This dissertation presents dynamic reactive power control of isolated power systems. Isolated systems include MicroGrids in islanded mode, shipboard power systems operating offshore, or any other power system operating in islanded mode intentionally or due to a fault. Isolated power systems experience fast transients due to lack of an infinite bus capable of dictating the voltage and frequency reference. This dissertation only focuses on reactive control of islanded MicroGrids and AC/DC shipboard power systems. The problem is tackled using a Model Predictive Control (MPC) method, which uses a simplified model of the system to predict the voltage behavior of the system in future. The MPC method minimizes the voltage deviation of the predicted bus voltage; therefore, it is inherently robust and stable. In other words, this method can easily predict the behavior of the system and take necessary control actions to avoid instability. Further, this method is capable of reaching a smooth voltage profile and rejecting possible disturbances in the system. The studied MicroGrids in this dissertation integrate intermittent distributed energy resources such as wind and solar generators. These non-dispatchable sources add to the uncertainty of the system and make voltage and reactive control more challenging. The model predictive controller uses the capability of these sources and coordinates them dynamically to achieve the voltage goals of the controller. The MPC controller is implemented online in a closed control loop, which means it is self-correcting with the feedback it receives from the system.

DEDICATION

Dedicated to my parents who sparked my passion to learn, encouraged me to move forward, and gave me the fear of being mediocre.

ACKNOWLEDGEMENTS

I would like to thank my committee co-chairs for their patience and support. Special thanks to Dr. Ehsani since I would not be able to finish this research without his help and support. Thanks to Dr. Butler-Purry for her efforts to improve the quality of this research, and for long pleasant discussions throughout my PhD at Texas A&M University. I would also like to thank my committee members, Dr. Bhattacharyya, and Dr. Hurtado, for their guidance and support throughout the course of this research.

Special thanks go to my friends and colleagues at Power System Automation Lab (PSAL) and Sustainable Energy Vehicle Engineering and Power Electronics Lab for their help and support during the long hard days that we spent together. I would also like to thank the staff of Electrical Engineering Department for making my time at Texas A&M University a great experience. Finally, thanks to my mother and father for their encouragement and support throughout my studies at Texas A&M University. Meanwhile, I hope this achievement is encouraging to my siblings that both selected to do a PhD in Electrical Engineering at NC-State University and UCLA.

NOMENCLATURE

DER	Distributed Energy Resource
DFIG	Doubly Fed Induction Generator
DG	Distributed Generator
MILP	Mixed Integer Linear Programming
MIQP	Mixed Integer Quadratic Programming
MLD	Mixed Logical Dynamics
MPC	Model Predictive Control
PWA	Piecewise Affine System
SPS	Shipboard Power System
STATCOM	STAtic synchronous COMpensator
SVC	Static Var Compensator
VVC	Volt/Var Control

TABLE OF CONTENTS

Page

LIST OF FIGURES

Page

LIST OF TABLES

Page

1 INTRODUCTION

An isolated power system is typically a small system that has no possibility of support from an interconnected neighboring system due to a fault or intentional islanded operation. Isolated systems commonly have limited generation capacity from local distributed generators with small inertia. Due to minimal or non-existent transmission system, isolated systems are more vulnerable to disturbances than stiff distribution systems. These systems can easily move from one state to another due to load or generation changes. Due to these distinguishing features, the power management procedures of conventional terrestrial power systems cannot be effectively used for isolated power systems. With these key traits in mind, it is desirable to develop a dynamic power management scheme that accounts for the following criteria: economics, reliability, security, and survivability. Dynamic is emphasized because system dynamics or transients are very important when it comes to isolated power systems since load demand is comparable to generation capacity.

The main objective of a dynamic power management scheme is to ensure continuous power supply for electric loads with optimal utilization of power sources, thereby enhancing system reliability and survivability. Dynamic power management strategy for an isolated power system should include the following control modules that should work together as needed to supply power to the loads: dynamic source management (economic dispatch and unit commitment), dynamic phase/load balancing and grid management, dynamic voltage and reactive power control, dynamic demand side management.

However, the proposed work in this dissertation only addresses dynamic reactive control.

The objective of this dissertation is to develop a dynamic reactive power control strategy for Volt/Var optimization of isolated systems. Volt/Var Optimization (VVO) or generally Volt/Var Control (VVC) is concerned with coordinating the sources and sinks of reactive power to achieve a smooth and stable voltage profile. Generally speaking, bus voltage is coupled with reactive power in power systems. Therefore, coordinating reactive power generation and consumption is helpful in keeping the bus voltages within limits.

Load behavior as a response to voltage variation in a distribution system is very important in volt/Var studies. Load studies show that typically about 50% of the loads in a distribution system are motor loads. Motor loads in a conventional distribution system are often a combination of industrial, residential and commercial motors [1]. The remaining loads in the distribution system are typically constant power loads which can be electronics, motor drives, etc. (about 20%), discharge lighting CFLs (about 10%) and constant impedance loads which can be incandescent lighting, ranges, irons, etc. (about 20%). The behavior of each of these load types in response to voltage changes is predictable. Discharge lighting usually turns off when voltage drops below 70 to 80%. Adjustable speed drives temporarily shut down when the voltage level drops below 90% and constant-impedance loads draw less active power from the network as the bus voltage drops. Large industrial motors have contactors that turn the motor off when voltage drops to about 75% and small motors such as those used in air-conditioning

which do not have electromagnetic contacts may stall, drawing large levels of current from the power system when voltage sags to 70% or less. In the stall condition, the motor continues to draw a large amount of current until it trips the over current protection, which may take from 10 seconds up to a few minutes.

The amount of motor load has a significant impact on voltage stability of the isolated distribution system. Small motors that do not disconnect are more problematic due to stall at low voltage levels. Especially, low-inertia small motors that stall faster drag down system voltage. Unfortunately, the new high-efficiency AC motors have remarkably low inertia.

In the past, the induction motor's speed slowed down slightly when its terminal voltage dropped which resulted in a reduction in the total motor load. This reduction in speed had a "healing" effect for the system when a voltage drop occurred in the system. However, the new generation of adjustable speed drives, still supply the same voltage and frequency to the motor even when the distribution bus voltage drops and thus eliminate some of the inherent self-healing effect in the distribution system.

It is necessary to understand and classify the power quality problems in a power system to be able to solve the problem [2]. There are different classifications for power quality issues in distribution systems. Each of these classifications uses a specific property to categorize the problem. Some standards classify the events as "steady-state" or "non-steady-state" phenomena. Other standards such as ANSI C84.1 use the duration of the event as the key factor for classification. Other guidelines such as IEEE-519 use

the wave shape of each event to classify power quality problems. Finally, standards such as IEC use the frequency range of the event for the classification.

IEC presents the following list of phenomena causing electromagnetic disturbances:

- Conducted low-frequency phenomena
    1. Harmonics, interharmonics
    2. Signaling voltage
    3. Voltage imbalance
    4. Power frequency variations
    5. Induced low-frequency voltages
    6. DC components in AC networks
    7. Voltage fluctuations
    8. Voltage dips
- Radiated low-frequency phenomena
    1. Electric fields
    2. Magnetic fields
- Conducted high-frequency phenomena
    1. Unidirectional transients
    2. Induced continuous wave (CW) voltages or currents
    3. Oscillatory transients
- Radiated high-frequency phenomena
    1. Magnetic fields
    2. Electric fields

3. Electromagnetic field
4. Steady-state waves
5. Transients

- Electrostatic discharge phenomena (ESD)
- Nuclear electromagnetic pulse (NEMP)

Although all the mentioned phenomena are considered as power quality issues, the power system industry usually classifies power quality events according to their magnitude and duration. A sample classification table of power quality issues based on magnitude and duration of the event is shown in Figure 1-1.

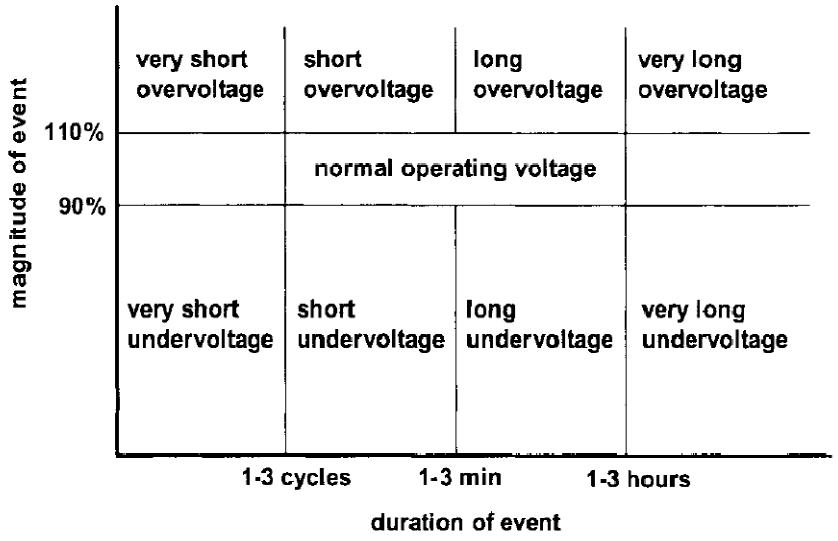

Figure 1-1 Magnitude-duration plot for classification of power quality events [2]

There are nine different regions in the voltage-magnitude plot shown in Figure 1-1 and various standards give different names to events in each of these regions.

Classification based on the voltage magnitude divides power quality events into three regions:

- interruption: voltage magnitude is zero
- Under-voltage: voltage magnitude is below its nominal value by a certain percent
- Over-voltage: voltage magnitude is above its nominal value by a certain percent

Based on the duration of the event, these events are split into four regions, namely, very short, short, long, and very long. The borders in this plot are somewhat arbitrary and the user can set them according to the system requirements or the standard that is used.

1.1 Isolated Power Systems

This dissertation presents a generic study of power management for the integrated isolated power systems. Some examples of isolated power systems include MicroGrids, shipboard power systems, offshore oil platforms, and power systems of the physical islands [3],[4],[5],[6],[7]. This dissertation only focuses on shipboard power systems and MicroGrids. However, the developed method can be easily extended to control voltage and reactive power of other types of isolated power systems.

It is worth mentioning that MicroGrids and all-electric AC/DC shipboard power systems have some similarities in topology and behavior. Thus, offshore shipboard power systems can be considered as a class of MicroGrids operating in the islanded

mode. However, while the structure of these systems is quite similar, different operation and performance criteria differentiates them from one another. In the next part, we will discuss these systems and their specifications in more detail.

1.1.1 Integrated Shipboard Power Systems

A Shipboard Power System (SPS) provides electrical power to propulsion motors and loads in all-electric ships. The SPS uses a power management scheme that enables the use of high energy weapons such as advanced sensors, railguns, and lasers and allows operators to optimize system operation which leads to cost savings and efficiency while maintaining survivability of the system [5],[8].

An SPS may experience several events that can cause transient disturbances, such as, lightning strikes, faults, pulsed loads and damage to the system [9]. To the date of this dissertation, many schemes have been proposed for all-electric shipboard power systems. The latest scheme, which is of more interest, is an AC/DC scheme with high voltage AC generation and DC zonal distribution. In this scheme, the generation is AC typically from synchronous generators and the distribution system is composed of several DC zones [8]. The AC voltage is rectified to DC at the connection point with the DC zones. The zonal scheme has the advantage of mitigating faults within one zone and keeping other zones operational when faults occur, thus it increases system survivability [5]. In this scheme, loads are typically connected to the system inside the distribution zones. However, some loads such as propulsion motors, power installations and high power pulsed weapons are usually directly connected to the AC supplies. Figure 1-2 shows an example of an AC/DC zonal SPS.

The number and size of generators depend on the design but usually the system has some Main Turbine Generators (MTG) and some Auxiliary Turbine Generators (ATG). MTG are typically large synchronous generators and ATGs are smaller and faster synchronous generators. For example, one SPS design of a war cruise ship uses two MTGs of 36MW and two ATGs of 4MW [10]. Propulsion motors, high power weapons, radars, and air conditioners, are the typical loads in the SPS. These loads usually have different priorities defined by the operator based on the mission. The energy management unit disconnects the low priority loads during overload, supply shortage, or damage in the system.

This dissertation only focuses on voltage and reactive power control of the AC/DC zonal SPS; however, other SPS designs can be analyzed and controlled with a similar method. In this work, reactive power control of the SPS is approached through optimizing the setpoints of the reactive compensators and generators in the system while considering the specific limits of the shipboard generators and compensators.

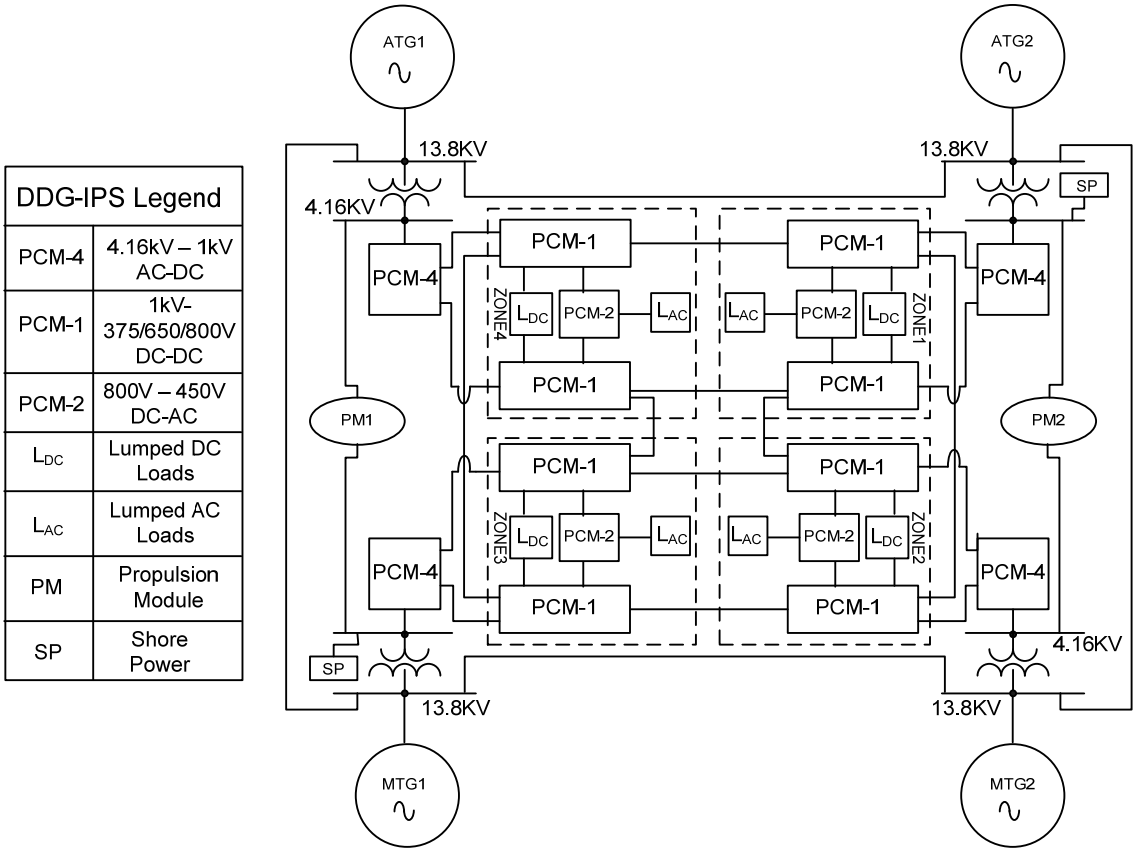

Figure 1-2 A notional zonal AC/DC shipboard power system

1.1.2 MicroGrids

Several issues are increasingly challenging security, reliability, and quality of conventional utility power systems, namely, aging of transmission/distribution infrastructure, changes in customer needs, additional stress due to deregulation, the need to connect non-traditional generation (i.e. renewable sources), and demand for a more reliable/resilient power delivery infrastructure and introduction of Plugged in Hybrid Electric Vehicle (PHEV). Incremental changes to grid infrastructure will not achieve the

demanded reliability; therefore, power system researchers are currently exploring new infrastructures and operational concepts.

High penetration of renewable energy devices to the grid can significantly change the structure of the existing grid. For example, due to the environmental and technical advantages of local power generation, some large power plants will soon be disconnected from the grid and the distributed generators will take their place. However, these sources are intermittent and not dispatchable and have different characteristics than the conventional generators.

A new power system concept that is under extensive study and will possibly replace the current structure in the future is the concept of MicroGrid. A MicroGrid is defined as an aggregation of loads and generation. The generators in MicroGrids are usually consisted of microturbines, wind generators, fuel cells, photovoltaic sources, reciprocating engines, or any other power sources depending on the application. MicroGrids can also be designed to have the ability to use the waste heat from the generators as an energy resource for environment heating to improve overall efficiency.

To the upper system, which is the main grid, a MicroGrid is a controllable electrical load that can be controlled to act as a constant load. Further, It can demand more power when electricity is cheaper, and also can be controlled at zero power demand or isolated mode during the intervals of system stress. This flexibility helps the utilities to operate the system more efficiently, increase the reliability of the system and potentially reduce the total cost of distribution.

MicroGrids require an Energy Management System (EMS) to make decisions regarding the best use of the generators for producing electric power and heat, and the operating mode of the system. These decisions are made based on many factors including the environmental factors, the price of electric power, the cost of generation of each source of energy, and many other considerations [11]. The EMS should be able to control the MicroGrid during all operating modes, namely, connected to the grid, islanded mode (isolated mode), and the ride-through between grid connected and islanded mode.

To summarize, MicroGrids provide thermal and electrical needs at enhanced reliability with reduced emissions. They are also designed to have improved power quality (controlling voltage), and lower costs of energy supply then conventional power systems.

According to the MicroGrid whitepaper from the U.S. Department of Energy, MicroGrids can be grouped into a number of different classes as shown in Table 1[12].

A MicroGrid can operate in three modes:

- Partial Baseload, where DGs provide baseload power to a portion of the site loads and the main grid provides supplemental/back-up power
- Full Baseload (Island), where DGs provide baseload power to all site loads and the main grid provides back-up power when needed
- Back-up/Peaking, where the main grid provides power to all site loads and DGs provide back-up power when needed

Components of a MicroGrid typically consist of:

1) DER: small scale power generation technologies typically (3kW-10MW) and are used to provide an alternative/enhancement to the traditional power system. There are two types: Distributed Generation (DG) - small sources of energy located near the point of use) and Distributed Storage (DS). Micro turbines, wind turbines, PV arrays, reciprocating internal combustion engines with generator, and Combined Heat and Power (CHP) are typical DG units. Typical DS units are batteries, fuel cells, super capacitors, and flywheels.
2) Interconnection Switch: Ties the point of common connection between the MicroGrid and the grid. This switch consolidates various types of power/switching functions into one system with a digital signal processor: metering, power switching, protective relaying, and communications. Grid conditions are measured on both the MicroGrid and the utility sides of the switch to determine operational conditions
3) Energy Management System: EMS is designed to safely operate the MicroGrid in any mode. In islanded mode, the EMS should provide a reference for voltage/frequency since the reference signal form the grid is not available anymore. Voltage control is necessary for local reliability and stability. Frequency during islanded-mode varies freely if none of the DG units dominantly forces a base frequency for the system. Thus, EMS assigns one of the DG units to control to dynamically balance real power and dictate the frequency. This DG unit, which is called the master generator, must provide/absorb

instantaneous real/reactive power difference between generation and loads and protect the internal MicroGrid.

Although, MicroGrids have the potential to solve many of the existing problems in distribution systems, designing them to be able to operate in grid connected mode, the islanded mode and the ride through between these modes has technical challenges in control, protection and power quality. This dissertation is only focusing the power quality and voltage issues of islanded MicroGrids.

Table 1 MicroGrid characteristics for different classes

	Simple (class I)	Master Control (class II)	Peer-to-Peer Control (Class III)
Specific MicroGrid Characteristics for different classes	• Master control system to both meet the loads and provide voltage and frequency support to the MicroGrid. • Generators located in central power plant	• Master control system to both meet the loads and provide voltage and frequency support to the MicroGrid. • Generators distributed among buildings (separate buses)	• No master control exists • Local control at each generator's location maintaining voltage and frequency stability
Common MicroGrid Characteristics	• Multiple generators serve loads in multiple locations. • The generators and facilities are connected by a distribution grid which is interconnected with utility-owned area electrical power system. • Event detection and response control are included		

Figure 1-3 shows an example of a distribution system with divided into several MicroGrids.

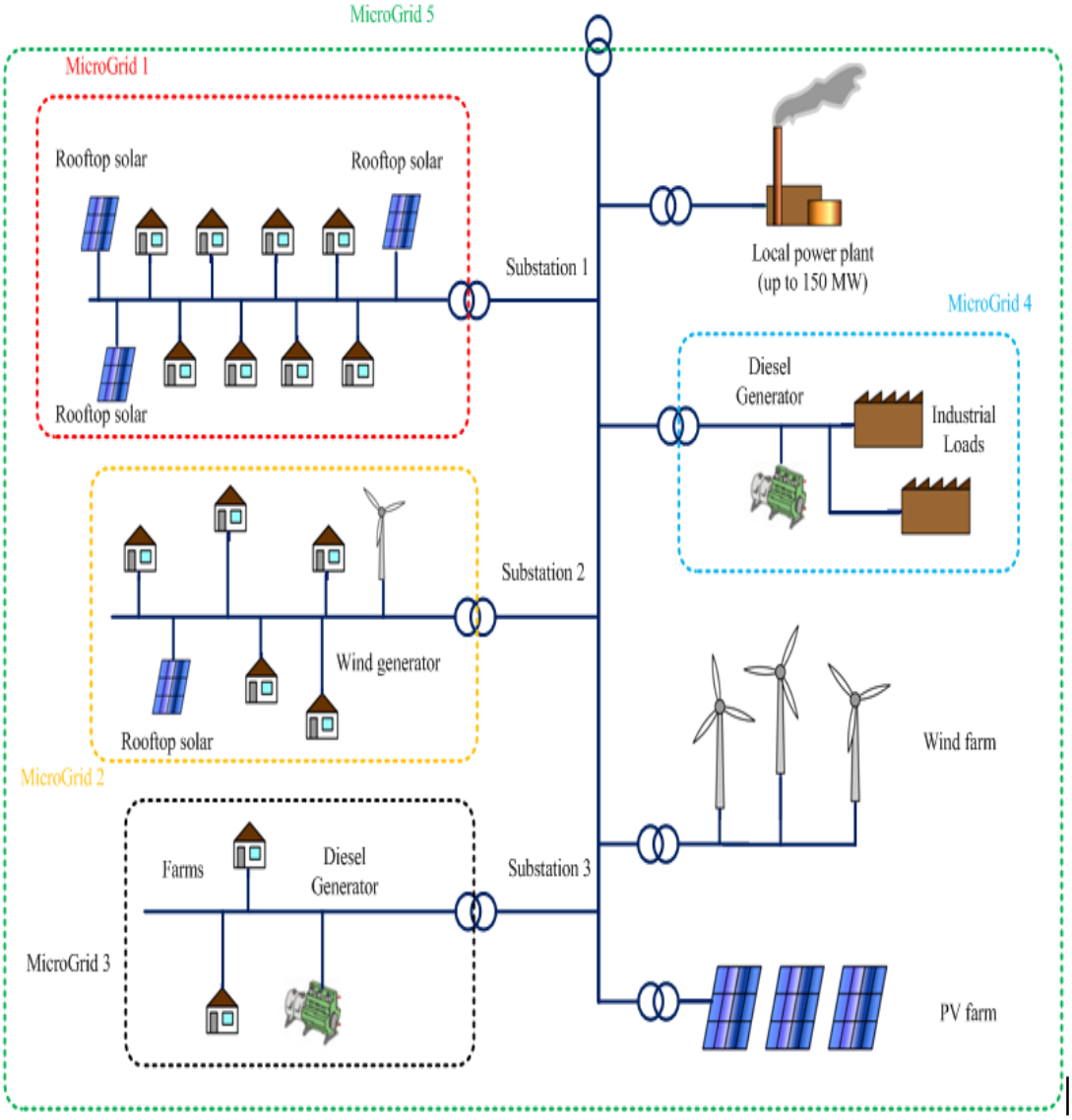

Figure 1-3 An example of possible hierarchical structure of MicroGrids

Figure 1-4 shows a sample of an AC/DC MicroGrid.

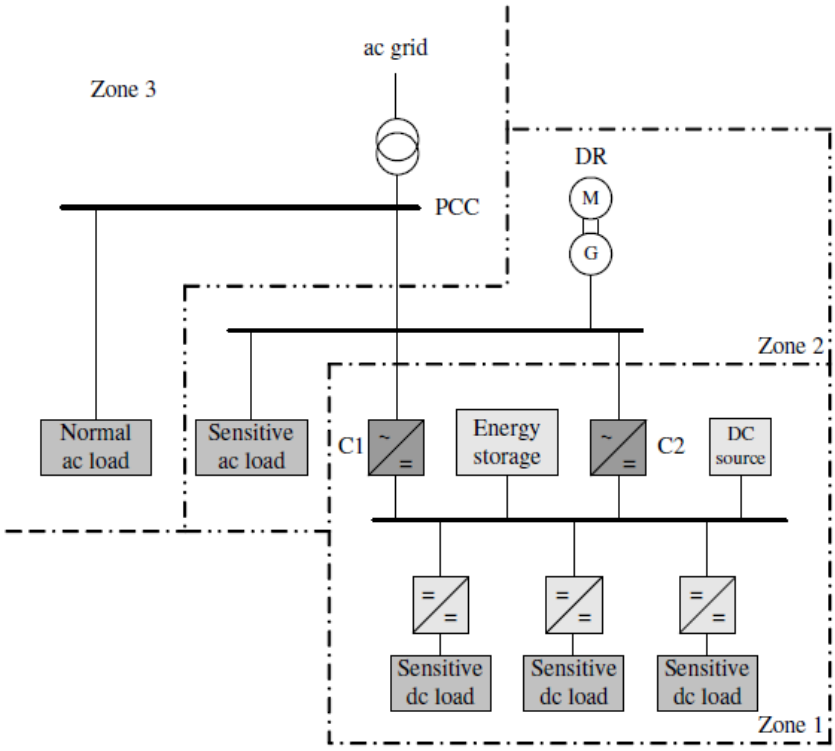

Figure 1-4 An example of a zonal AC/DC MicroGrid [13]

During the short time since the invention of the concept, MicroGrid testbed facilities with different energy sources have been built in different locations such as in the United States, Japan, Canada, and Europe [14]. Those examples vary quite differently from case to case. For example, the CERTS MicroGrid in the United States is a test site based on the class III MicroGrid concept. The renewable energy sources have not been installed into it up to date [15]. The Aichi MicroGrid project in Japan utilized renewable energy sources, battery storage and the capability for heat supply [16, 17]. The EU MicroGrid projects also built up couples of test sites with different topologies [18].

The focus of this work is on control of distribution MicroGrids integrating renewable energy sources. Reactive power control will be approached by optimizing the setpoints of the reactive compensators and possibly the dispatchable generators. A good survey of the current topologies and implementations of distribution MicroGrid could be found in [19],[20].

The conventional control methods usually do not include the dynamics of the system and average values of power, voltage and current are usually used in system studies. However, these methods are not efficient for isolated power systems such as shipboard power system or the autonomous MicroGrid because of the following reasons:

- Since the size of the system is small, changes in the loads and capacitor banks have significant impact on the system
- The system is tightly coupled with relatively large dynamic loads and limited generator inertia. Thus changes in loads can lead to large voltage and frequency deviations
- Changes in the system applied by the reactive controller may result in unacceptable transients which may lead to relay tripping and isolation of the DG's in the system which is not desirable

On the other hand, the demand for high quality power is increasing in the past decades. Thus, voltage regulation methods with real-time voltage control capability and fast transient response are playing a more and more important role in the distribution level [1]. The current efforts for dynamic voltage control and reactive compensation could be divided into two categories, i.e., is adding dynamic power electronics devices

for voltage control in distribution level and designing dynamic control schemes which are capable of controlling the devices dynamically.

The SVC, static synchronous compensator (STATCOM), SC, and DER are some of the devices in the distribution level that are capable of performing as dynamic reactive power compensators. A typical SVC is made of a thyristor-controlled reactor and a capacitor bank or banks in which each capacitor can be switched on or off individually. A STATCOM is a voltage source converter with a capacitor on the DC side and connected in parallel on the AC side to the power system. STATCOM is placed in the system to control power flow and improve the transient stability of the power system. The percentage of penetration of DERs has significantly increased in the past few decades. There are several types of DERs currently operating in the distribution system: micro-turbines, industrial gas turbines, fuel cells, reciprocating engine generators, PVs, wind turbines, etc. Most of these DERs are operated as active power sources, but they have great potential for local voltage regulation by generating or absorbing reactive power for two reasons. First, DERs are usually connected to the power system through a power electronics interface, which is easily capable of injecting reactive power to the system, by simple modifications in the control scheme. Second, the distributed location of DER is ideally suited for voltage regulation.

2 LITERATURE REVIEW OF REACTIVE POWER CONTROL METHODS OF DISTRIBUTION SYSTEMS

2.1 Introduction

Various solution techniques exist in the literature that address the VVC problem of the distribution systems. These techniques range from fully analytical techniques that try to model the distribution system and the problem formulation as rigorously as possible, to fully heuristic techniques that rely upon the engineering judgments of utility engineers. Each methodology has its own advantages and disadvantages that are associated with the structure of the system under study. Also time span of the problem plays an important role on the effectiveness of the solution technique applied. During the planning stage, time is not an issue which justifies using time-consuming techniques with large computational intensities that yield exact solutions. At the operation stage, however, the time period required for convergence of the solutions is of greatest importance, and is a limiting factor for selecting the appropriate solution technique. Also, some of these solution techniques result in finding the local minimum, while others lead to global minima. It should be noted that in distribution systems, a local minimum is not necessarily a disadvantage, since often times it is very satisfactory to find a feasible solution, which can be reached, in the minimum number of network switching operations. Naturally, a higher number of control variables might need to be applied in order to reach the global minimum. This may result in a set of network switching operations too large for practical operational purposes [21].

In general, the solution techniques for solving the VVC problem can be broadly classified as follows.

2.2 Network Model Based Techniques

These techniques require a detailed mathematical model of the distribution system, and can be divided into three categories based on the mathematical approach adopted to solve the optimization problem.

2.2.1 Calculus Based Techniques

In these techniques, the relationship between the control variables and the objective function is explicitly derived using mathematical formulation. In most cases, the solution for minimizing the objective function is derived by solving a linear set of equations or a closed form mathematical equation. Clearly, the efficiency of these techniques is inversely affected by an increase in the size of the problem. Simplifying assumptions are often necessary to make the solution feasible for larger scale systems.

2.2.2 Explicit Enumeration Techniques

From a mere mathematical standpoint, exhaustive search of the problem space for all the possible solutions is the simplest of all the approaches. While this class of techniques is sufficiently efficient for a small-scale problem with a few number of control variables, it drastically loses efficiency as the dimensions of the power system and the optimization problem increase. A modified version of this technique uses an oriented descent search in the negative direction of the gradient of the objective function.

2.2.3 Analytical Optimization Techniques

Various mathematical programming approaches can be adopted to solve the VVC problem. Depending on the nature of the problem formulation, these techniques range from nonlinear programming methods to mixed-integer nonlinear programming, integer programming or dynamic programming methods. Systematic search algorithms such as the branch-and-bound and dynamic programming are considerably more effective than enumerative techniques since they only look at the feasible solutions and not possible solutions. This way, they drastically reduce the search space. However, these techniques still suffer from the curse of dimensionality as the dimensions of the optimization problem increase. This specifically poses a major problem for online applications where a solution is required during the operation of the system within a window of a few minutes to a few hours. Simplified formulation of the optimization problem, for instance linearizing the objective function and/or the constraints, or decomposing the problem into multiple smaller sub-problems, can prove helpful, although at the price of obtaining a sub-optimal solution.

2.2.4 Meta-heuristics Optimization Techniques

During the past few years, meta-heuristic optimization techniques such as simulated annealing (SA) [22], Tabu Search (TS) [23], Genetic Algorithms (GA) [24], Particle Swarm Optimization (PSO) [25], and Ant Colony Optimization (ACO) [22] have been successfully employed for solving optimization problems where the combinatorial solution is difficult or impractical to solve. These are techniques that are based on

evolutionary algorithms, social concepts or other physical and biological phenomena that can iteratively solve complicated multi-variable multi-objective optimization problems, such as the VVC problem. These techniques do not need any rigorous mathematical formulation of the problem, which is a big advantage. Moreover, there are various methods to prevent these techniques from being trapped in the local minima, so that they converge to the global minimum and the near-optimal solution. However, each of these techniques has several parameters associated with it that have crucial impacts on its performance. Unfortunately, there are no definitive rules for selecting these parameters and they are often derived based on trial and error, or from experience.

2.3 Rule Base Techniques

These techniques are based on a set of heuristic rules for switching capacitors and regulating transformers in order to minimize the objective functions while meeting the inequality constraints. As opposed to the previous category of techniques, these methods are independent of a detailed system model, and are often characterized by simplifying assumptions and rules of thumb; however, they achieve this by making approximations and therefore they do not always lead to an optimal solution. Such techniques can be very effective for radial distribution systems with few lateral branches, but as the dimensions of the system increase or the structure of the system becomes a meshed network, their efficiency is reduced. In these cases, there is often a need for combining the rule base technique with other analytical approaches to develop a hybrid approach.

2.4 Intelligent Techniques

Intelligent neural network based techniques are another alternative for solving the VVC problem. They rely on the data available on the system in terms of measurements, and as opposed to the previous techniques they do not require expert knowledge or the system model, as their parameters can be initialized randomly before being trained using the system data. However, the major challenge in using these techniques is associated with training the neural network and selecting its design parameters, which are often chosen based on trial and error or based on experience.

2.5 Model Predictive Control (MPC)

To the knowledge of the author, Beccuti et al. [26], [18] were the first group that used Model Predictive Control (MPC) method for voltage control. They used MPC for voltage stability of transmission systems during emergency voltage condition. They used a small-scale test system with three On-Load Tap Changers (OLTC) and three capacitor banks as control inputs to demonstrate the efficiency of their method in avoiding voltage collapse. They demonstrated that MPC was able to keep the voltages stable and stabilize the transmission system during emergency voltage conditions while other methods result in instability. Zima et al. [27], further explored this method by simplifying the algorithm and allowing relatively fast optimization computations, while keeping an accurate tracking of the nonlinear behavior of the system. The major difference between this method and previous methods was that the authors simplified the problem formulation to be able to solve it in real time for larger scale systems. In addition, Gong et. al. [28], [29] proposed a two-stage model predictive control (MPC) strategy for alleviating voltage

collapse. In their method, the second stage used an MPC using trajectory sensitivities proposed by Hiskens et. al. in [30]. The MPC resulted in a linear Programming (LP) since binary or integer inputs were not considered in the system design.

As MPC showed promising results, researcher started using the MPC method to solve various control, management, and protection problems in power system. For example, Jin et al. [31] used MPC for protection coordination of power systems. They presented an approach to determine a real-time system protection scheme to prevent voltage instability and maintain a desired amount of post-transient voltage stability margin after a contingency using reactive power control. In addition, Kienast [32] studied the reliability and analyzed the efficiency of MPC for control of power systems. Table 2 summarizes some of the key advantages and disadvantages of the solution techniques for the VVC problem.

2.6 Traditional Problem: Capacitor Placement and Sizing

This section briefly reviews the historic origin of reactive power control in power systems. Reactive power control of distribution systems was first addressed by considering shunt capacitors only [33],[34],[35],[36]. The early research focused on radial distribution systems and the objective was to find the number, locations, sizes, and types (i.e., fixed or switched) of capacitors to be installed along the feeders and laterals, in order to minimize power and energy losses, the number of capacitor installations, the number of capacitor switching actions, and/or the capital investment required for capacitors. The acceptable upper and lower limits for node voltages were the main constraints for the optimization problem.

Table 2 Comparison of the available techniques for solving the VVC problem

Methodology	Advantages	Disadvantages
Calculus Based	• Is simple and straightforward • Normally does not require iterations, so no convergence issues	• Often uses major approximations in order to simplify the equations • Is largely dependent on the accuracy of the mathematical model used for the power system • Is not easy to implement for large systems with many control variables
Explicit Enumeration	• Does not require a mathematical model of the power system • Is problem independent • Always guaranteed to reach the local optimal solution	• Is not easy to implement for large systems with many control variables • Might take a very long time to find the solution; therefore, might not be suitable for online applications
Analytical Optimization	• Is mathematically proven • If converges, the solution will be the truly optimal solution • Considers the feasible solutions which reduce the problem space	• Can easily suffer from the curse of dimensionality • In majority of cases, is not easy to solve • Often times needs to make simplifying assumptions in order to ensure convergence
Meta-heuristic Optimization	• Often deals efficiently with large scale problems • Does not necessarily make simplifying assumptions • Sometimes can be tuned and modified to converge to global minimum	• Is not proven mathematically • Convergence might take too long for online applications • Many problem-dependent design parameters must be set by the user, which are crucial to the convergence of the solution
Heuristic Rule-Based	• Is easy to understand and interpret by utility engineers and technicians • Does not require an explicit mathematical model for the power system	• Is difficult to implement for large scale systems with many control variables • Is largely problem-dependent and once designed for one system, cannot be readily applied to other systems
Neural Network Based	• Does not require an explicit mathematical model for the power system • Can be trained offline without any expert knowledge • With enough data in the form of system measurements, can be trained to truly reflect the dynamics of every system	• Is difficult to implement for large scale power systems with many control variables • Requires considerable learning time for the neural network to converge and accurately model the problem • Depends on design parameters that are problem-dependent and are often derived based on trial and error
Model Predictive Method	• Predicts the behavior of system in future and chooses the best solution • Can easily avoid instability • Can find optimal solution in presence of discrete control actions such as capacitor banks	• Requires a model of the system • May result in too much control action • Weight factors have to be defined by user

Initial solutions were based on closed form mathematical formula [37]. Later, mathematical optimization based approaches were introduced such as mixed-integer [38] and dynamic programming [39], [40], [41]. The main challenge for solving the optimization algorithm was the size of the problem and the consequent curse of dimensionality. In order to resolve this, many authors attempted to break the original problem into multiple smaller size sub-problems. For instance, Lee and Grainger [42] proposed a set of three sequential sub-problems for determining the optimum capacitor bank sizes, the optimum switching time of the capacitors and their optimum locations independently. The problem started from a set of proper initial conditions and the three sub-problems were solved one by one by solving linear mathematical equations assuming at each stage that the other two unknowns are specified. Baran and Wu [38] decomposed the problem into two sub-problems: a master problem which was used to determine the locations of the capacitors through integer programming, and a slave problem which was called by the master problem to determine the size and type of the capacitors using heuristics.

Others, such as Hsu and Yang [43] solved the dynamic programming problem offline for finding the truly optimal capacitor switching scenarios for various load patterns in the system. They then used an artificial neural network to cluster the load patterns into different classes. In the online stage of the application, the forecasted load pattern was read and its nearest clusters were retrieved. Then by averaging the associated switching scenario in the cluster, a capacitor-switching schedule for the load pattern under study was retrieved from the database.

Simplifying assumptions have been made in the literature; for instance, using only fixed capacitors [39] or fixed capacitors that could only be switched on or off [41], to make the problem solvable. However, with the assumption that the number of capacitors in the system is small enough, Kaplan [44] used an explicit enumeration approach where all the feeder branches were scanned in an attempt to place the smallest standard size capacitor bank at consecutive nodes moving along the branch towards the substation. At the time this paper was published in 1984, the proposed scheme was in use at the Central Illinois Public Service Company.

In a different attempt to further simplify the previously proposed methods, Salama and Chikhani [45] proposed a simplified network model where the capacitor sizes were represented by dependent current sources located at the branch connected buses. The solution of this equivalent circuit using the Gauss-Seidel iteration method would yield the values of the voltages at any bus. The compensation levels and the capacitor locations were then directly solved for knowing the obtained voltages and using the equations derived in [46].

Meta-heuristic optimization techniques have also been used for solving the capacitor allocation problem. Chiang *et al*. [47], [48] applied simulated annealing to find the near-optimal capacitor sizing and locations based on a set of allowed search space derived through heuristics and engineering judgment.

Sundhararajan and Pahwa [49] used genetic algorithms for solving the problem. Similar to [48], they considered various discrete load levels for the distribution system. However, sensitivity analysis was done in order to select locations which had maximum

impact on the system real power losses with respect to the nodal reactive power. The relationship between the incremental losses and the Jacobian matrix of the system was expressed [50] as shown in (2-1).

$$\left[\frac{\partial P_{loss}}{\partial \underline{Q}}\right] = \begin{bmatrix} J_1 & J_2 \end{bmatrix} \times \left[\frac{\partial P_{loss}}{\partial \underline{\Theta}} \quad \frac{\partial P_{loss}}{\partial \underline{V}}\right]^T \tag{2-1}$$

where J_1 and J_2 are the related sub-matrices of the inverse Jacobian matrix, and the derivatives of the system losses with respect to the voltage angles and magnitudes of the system nodes can be directly calculated at any operating point. Once the sensitivity analysis is applied and the buses with highest factors are selected as the candidate locations, a GA based approach was used to determine the sizes, locations, types and number of the shunt capacitors. For this purpose, each genome in the GA program is selected as a string of $N_c \times N_L$ variables, where N_c and N_L denote the possible capacitor locations and possible load levels respectively. Later, Kim and You [51] adopted a similar approach but used integer strings instead of binary strings in order to save processing time. In their study they used length mutation operator to randomly change the length of the genes in order to account for the unknown number of the capacitors installed [51].

The concept of sensitivity analysis in [49] was also adopted by Huang *et al*. [23] who used Tabu search (TS) to find the number/location/sizing/control of fixed and switched capacitors, and showed faster convergence than simulated annealing. However, it should be noted that the sensitivity analysis based initialization adopted in [49], [23] was performed for the base case conditions, i.e. with no capacitors added to the system. This

could at times lead to solutions with poor quality. Gallego *et al*. [52] proposed a new initialization method to find more efficient initial configurations. Similar to [23], they proposed a method based on Tabu search; however, as opposed to the previous methods with single sensitivity analysis, they proposed an iterative sensitivity based algorithm that would include all the capacitors installed at the previous steps of the algorithm. This way, a larger set of buses would appear in the initial configuration, which would lead to more diversity in the search space and superior results in terms of quality and cost of the solutions [52].

In addition, Ramakrishna and Rao [53] proposed a fuzzy logic based system for controlling discrete switched capacitors. Two parallel Fuzzy Inference System (FIS) rule bases were designed to control the bus voltages and reduce the losses. Typical fuzzy rules for the corresponding rule bases were developed as:

Rule *n*: If $\Delta V_i/\Delta Q_j$ is A_n and If Load is B_n, Then Switched Capacitor Size ΔQ_j is C_n,

Rule *m*: If $\Delta P_i/\Delta Q_j$ is A_m and If Load is B_m, Then Switched Capacitor Size ΔQ_j is C_m, (2-2)

where the voltage sensitivity factors $\Delta V_i/\Delta Q_j$ and power loss sensitivity factors $\Delta P_i/\Delta Q_j$ are obtained from the load flow solution. The parameters A, B and C in (2-2) denote the fuzzy sets associated with the input and output variables. The two fuzzy rule bases are iterated back and forth until it could be ensured that all the voltage constraints are met and the power losses are minimized.

2.7 Present Status of Reactive Power Control Methods of Isolated Power Systems

Reactive power control is a fundamental issue in isolated power system since there is usually no “infinite bus” capable of keeping voltage and frequency constant and satisfying the reactive power needs of the loads. In addition, due to the small size of the system changes in the loads usually significantly impact the system and can cause voltage and frequency deviations. Further, frequent generator termination and restarts due to energy saving and generator output power change due to the non-dispatchable characteristics of the renewable energy sources cause the system to operate far from optimal operating point. In addition, presence of pulsed loads with significant magnitude in the system causes increased disturbance levels in the system compared to the terrestrial power system, which increases the need for VVC consequently.

Some examples of isolated power systems are the MicroGrids and shipboard power systems. Both of these systems should be able to operate in both isolated mode and connected to the grid mode. In next part, we will discuss these systems in more detail.

2.7.1 Present Status of Reactive Control of Electric Shipboard Power system

Continuity of power in all operating conditions is vital to the operation of shipboard power system. One of the functionalities in power management of the shipboard power system is reactive power control. Reactive power control is a fundamental issue in shipboard power systems because of many reasons. Reactive power control is a fundamental issue in all electric shipboard power systems due to the existence of large magnetic pulsed loads such as magnetic weapons that need power supply for a short

period of time, startup and shutdown of the generators and the absence of an infinite bus in the system. Due to these issues and complexity of shipboard power systems, power quality problems from abnormal distortions in voltage and frequency to black-outs are not unusual even in the most recent shipboard plants [54]. Jonasson and Soder [54] report the answers of the ship owners to a questionnaire regarding power quality issues and blackouts in the shipboard power system. The issues studied include, black outs, abnormal changes in voltage and frequency, voltage dips, electromagnetic fields, electrostatic discharges, voltage flickers, transients, harmonics and three phase unbalance. The following reasons cause the need for a new VVC scheme for shipboard power systems.

2.7.1.1 Lack of infinite bus and small generator inertia

When operating in offshore, the SPS is an isolated power system meaning that it does not have power support from any other system. Thus, the generators and the energy storage devices in the system are the only sources of power in the SPS. The generators in an SPS are small compared to those in terrestrial systems and therefore have smaller inertia. Hence, the shaft of the generator may not be able to follow when abrupt changes occur in the system, which in turn results in frequency and voltage fluctuations.

It should also be noted that the shipboard power system is tightly coupled with generators placed close to the loads. Hence, some papers suggest that modeling of the system for reactive power control requires integrating higher order models of generators and loads and constant voltage and frequency models are not sufficient for such studies [55]. However, integration of dynamics should be done carefully since too detailed

models may increase the convergence time of the algorithm while they might not necessarily make the simulation more accurate.

2.7.1.2 Generator start-up and shut down

Due to limited amount of fuel in the SPS, usually the power management scheme tries to keep as many generators as possible off. Typically, an extra generator starts up only if more than 80% of current generation is consumed by the loads for a duration of more than 30 seconds. Hence, when the load decreases in the system, the power management scheme starts shutting down the generators. Typically, the power management system starts shutting down the generators from the largest possible generator since larger generators consume more fuel than the smaller ones.

Although these startups and shutdowns help with energy saving in the system, they cause significant disturbance in the system, which is specific to the SPS. This disturbance can start from voltage or frequency fluctuations and lead into tripping of the relays. Relay trips may isolate part of the system or in severe cases may cause cascaded tripping and result in a total blackout [56]. Quaia [57] studied some sample case studies of such voltage and frequency deviations due to startup and shutdown of generators. This paper shows a case study where the shutdown of a generator causes underfrequncy and since there is not enough time for load shedding, the protective relays of the generators trip which results in a general blackout in the system.

2.7.1.3 Pulsed loads

Some high-energy weapons in SPS need a large amount of power for a short period. These pulsed loads are usually vital and with high priority since their operation help with survival of the system. Thus, in some operating conditions, the generators should be started up or loads should be shed from the system to supply these load. These changes in the system cause transient dynamics in the system. The power management system should decide which load to shed and which generator to start. If unsuitable control actions are taken such as shedding a load where it is not needed, the system may experience huge voltage deviations and fluctuations in the frequency which may result in not only the load not being supplied but also relay trips and isolation of part of the system or total blackout.

Arcidiacono *et al.* [55] studied some sample case studies of voltage and frequency deviation in the system as a result of a pulsed load getting energized. This paper shows that when a pulsed load gets energized, a frequency drop occurs on one of the main generators and voltage distortion occurs at the connection point of the pulsed load.

With all that being said, in most of the existing shipboard power systems, Coordination between power station control and propulsion management, to match demand and generation of reactive power is poor [58]. Currently, studies are being performed on voltage and reactive control of the next generation shipboard power systems to overcome this issue.

The possible control inputs for reactive power control in a shipboard power system are reactive compensators, load shedding and generators. Static filters are also

sometimes placed in the system to help with voltage control. This work mainly focuses on controlling the reactive compensators and the gas generators to achieve voltage and reactive power control.

Since the length of the lines is short in a ship and hence the total loss in the lines is negligible, although possible, but it is not practical to consider loss minimization as the objective function. Better candidates for the objective function are minimizing deviations of voltage, power factor or Vars. In this work we will use voltage deviations in the objective function which means that the optimization tries to minimize the deviations of the voltage from its nominal value.

2.7.2 Present Status of Reactive Control of MicroGrids

Considering that reactive power control of renewable energy sources individually is a challenging problem, reactive power control of the MicroGrid integrating wind and photovoltaic sources has many challenges. Generally speaking, significant integration of DERs in the MicroGrid can affect the frequency, angle and voltage stability of the system [59], [60]. Wind and PV energy sources are sometimes referred to as negative loads since they are intermittent and not dispatchable. These energy sources are usually operated at the maximum power point tracking to reach the highest efficiency [61].

Abrupt changes in the wind energy resource can lead to sudden loss of production causing frequency excursions which may result in dynamically unstable situations if these frequency fluctuations cause the frequency relay to trip [59]. Similar issues occur for the PV source when it starts operating in the morning time or during the cloudy weather conditions. Thus, the capacity of these sources for active and reactive

production changes depending on the weather. Therefore, the controller should be able to adjust the limits dynamically to use this capacity to the best.

Chowdhury et al. [62] studied the challenge of operating a wind power plant within a MicroGrid. They presented some case studies on a system with one doubly fed induction wind generator. The results showed that if there is no rotor speed control or pitch angle control of the wind generator or a STATCOM is not present in the system, the voltage of the point of common coupling (PCC) bus and frequency of the system drops significantly. They also compared the results of no control case with the cases where pitch angle control, inertia control, and STATCOM are present and showed stability improvement in the latter cases. It can be concluded from their study that MicroGrids integrating renewable sources need an advanced voltage control scheme.

Laaksonen et al. [63] studied a MicroGrid integrating battery storage and a Photovoltaic energy source. The battery inverter with fast response was considered to act as the master generator to control voltage and frequency when operating the MicroGrid in islanded mode. The operation of the MicroGrid after islanding was studied in the case studies and the significant voltage and frequency changes were demonstrated when the MicroGrid intentionally or unintentionally starts operating in isolated mode. These changes are due to either lack of external frequency reference or power shortage in the isolated system after the MicroGrid gets disconnected from the main grid.

Another challenge occurs when the MicroGrid has to operate in the islanded mode intentionally or due to a fault. In this case, the infinite bus and the references of voltage and frequency from the grid are not present anymore. Therefore, a suitably sized DG

unit with fast dynamic response has to perform as the master generator and the other DGs perform as PQ source in the islanded case. The voltage setpoint of the master generator and the reactive power setpoints of the PQ control mode sources are possible control inputs for reactive power control. So, the DG has the ability to enhance the power quality as well as the reliability of the system [61].

In some MicroGrid designs, the buses have the same voltage level with no transformers between the buses. Hence, in these designs tap changers may not be added for voltage control. Thus, capacitor banks or power electronics compensators are usually added close to the load buses in the design stage for voltage support. These capacitor banks along with the D-STATCOM, if present, are possible control inputs for reactive power control in a MicroGrid. In addition, as mentioned before, the DG units can be used to inject reactive power at their connection point to the system. The energy storage units with power electronics interface to the MicroGrid can also be used as a possible candidate for reactive control. In this work, we only use compensators and DGs for voltage control and assume that no storage is present in the system.

The classic methods for voltage profiling and studying the impact of the DG on the system usually incorporate the use of load flow analysis. However, classic methods do not give a realistic impression of where and when overvoltage and undervoltage occurs in the system, because these methods are based on some selected combinations of consumer loads and DG power productions [59]. Therefore, dynamic modeling of MicroGrids with relative amount of detail, gives better information of the dynamic

behavior of the system, which is more accurate and more efficient for reactive power control than static models.

Dynamics behavior and transients of MicroGrids consisting of multiple DGs and the effect of power electronics interfaces on MicroGrids are studied in [64],[4],[65]. Katiraei et al. [4] presented a good study on the dynamic behavior of MicroGrids after preplanned and unintentional islanding. The Studied MicroGrid included two DG units and the time constant of the DG units were far apart. Hence, the DG units studied in this paper did not exhibit any dynamic interaction during transients. The results demonstrated that if the DG unit is interfaced to the grid through fast power electronics circuits instead of governor and exciter control, the MicroGrid can maintain angle stability due to fast active power control and can enhance voltage quality due to fast reactive power control. The transient under and overvoltage were not studied in this paper, and the focus was on active and reactive power interactions of the DG units in different working conditions. In a later work, Katiraei and Iravani [65] studied some local power management strategies for MicroGrids with electronically interfaced DG units. They used a systematic method to develop a small signal model of the MicroGrid and the system was analyzed using an eigenvalue approach. They proposed a power management scheme for controlling the MicroGrid and showed that utilizing a power management scheme to control the electronically interfaced DGs has a significant impact on the dynamics of the system especially in islanded mode. Majumder et al. [65] further explored the effect of power electronics interfaces and DG units on the MicroGrid. They used two voltage source converters connected to ideal DC sources as DG units in their

study. They proposed using a local control method consisting of two modes to control the DGs in a MicroGrid. When the DGs are working below their available power limits, the system is working in mode 1 and once the DGs reach their available power limits, the system is marked as working in mode 2. Considering two operating modes makes power sharing between the DGs easier for the energy management system. They authors performed case studies on islanding and resynchronization of MicroGrid, variable power supply from the grid, fluctuations in the frequency and voltage of the utility, and fluctuations in the DC MicroGrid voltage, and reported frequency deviations in some of the case studies.

Capacitor placement and Volt/Var optimization of MicroGrids has been studied in [66],[67],[68],[69]. Al-Askari et al. [66] used genetic algorithm to solve a capacitor allocation problem for the MicroGrid operating in the islanded mode. They formulated the problem to minimize the total power loss in the MicroGrid and to minimize the total cost of capacitor banks. The genetic chromosome assigned a four digit binary value to each power system bus corresponding to the size of shunt capacitor at that specific bus. Then, the genetic algorithm tried to find the optimal location and optimal number of capacitor banks in each bus. It is questionable whether isolated systems need a different capacitor placement strategy than conventional distribution systems. However, using the same strategy for the same system may lead to different placement results in islanded and grid-connected mode.

Ghadimi and Rastegar [67] formulated the reactive power control of MicroGrids subject to power flow equations and constraints of the system. They used a small signal

model of small islanded MicroGrids integrating inverter interfaced distributed generation (DG) units. They used an active management strategy of the distribution system with three control levels. These three layers include Distribution Management System (DMS), MicroGrid Management System (MMS), and Local Controllers (LC) with communication ability with each other. They formulated reactive power control problem to minimize the total loss of the system subject to load flow information and inequality constraints of the system and used MATLAB's optimization toolbox to solve the problem. They performed some case studies on a MicroGrid integrating two DG units and used reactive generation capacity of these units as control input. In a case study, a fault occurred in the system which results in the islanding of the MicroGrid with two DG units and the proposed scheme optimizes the reactive power flow of the isolated system using the DGs.

Madureira and Lopes [68] studied reactive power control of a system including multiple MicroGrids, a diesel generator, a wind generator, a hydro unit and a combined heat and power unit. They selected the objective function to minimize the power losses in the system subject to the limits of the MicroGrids. They used capacitor banks, position of tap changers, and reactive power injection capacity of the DG units as control input for reactive control and solved the problem with particle swarm intelligence based algorithm. Same authors further proceeded the work by adding the concept of "Micro-Generation shedding" in [69]. In this paper, the amount of Micro-Generation shedding is added to the objective function of [68]. The solution methodology in this paper is similar to [68]. In an interesting case study, they showed that in a sunny day where the PV

sources generate more power than the total load, Micro-Generation shedding results in lower power loss in the system.

2.7.3 Shortcomings of the Current Reactive Control Methods and Motivation for New Methods

To summarize, the following issues and limits in the current MicroGrid triggers the need for a need reactive power control scheme:

- Changes in non-dispatchable sources (Abrupt changes in wind, solar in the morning)
- No infinite bus in the isolated operation
- Ride through between the grid connected and isolated mode
- DG limits

Current formulations of reactive power control do not consider the dynamics of the system. The problem is usually formulated locally or as an optimization problem with load flow equations as constraints. However, average system studies are not efficient for the islanded power system because:

- The islanded power system is more vulnerable to changes in voltage and the changes can be sharp
- The capacity of renewable sources change in time depending on many factors such as weather change
- Assigning the control inputs and setpoints dynamically can help reduce the overall loss in the power system while keeping the voltages within limits

- Adding a control horizon to the optimization can help the controller to determine and eliminate possible voltage breakdowns in the system
- Some control actions may result in unacceptable transient response in the islanded power system and the average methods do not reflect the transient

For the shipboard power systems, the following issues are not addressed by current reactive power control methods.

- Lack of infinite bus and small generator inertia
- Generator start-up and shut down
- Pulsed loads

2.8 Summary

This section presented a literature review of voltage and reactive power control methods. Further, it summarized the advantages and disadvantages of each of these methods. In addition, it presented the current status of reactive power control of shipboard power systems and MicroGrids and listed the shortcomings of current approaches.

3 DYNAMIC REACTIVE POWER CONTROL OF ISOLATED POWER SYSTEMS

3.1 Introduction

Reactive power control is a large-scale optimization problem with real, discrete, and binary variables [70]. The objective reactive power control is to achieve an adequate voltage profile while satisfying the operational constraints. Minimizing the active loss is an alternative goal for reactive power control as well which is sometimes included directly in the objective function or achieved indirectly by smoothing the voltage profile. Volt, Var, Power factor, losses or a combination of them are possible candidates for the objective function of the VVC and tap changer position, setpoint of switchable shunt capacitor banks and reactive power setpoint of compensators and DGs are possible candidates for control input.

One of the main difficulties remaining in the industry is solving the mixed integer VVC problem which includes binary, integer, and discrete variables [70]. In addition, the mathematical model of a power system is nonlinear with unknown convexity. Therefore, a major challenge of volt/Var control is to formulate VVC in a form that could be solved with existing optimization methods. Thus, system equations are usually linearized if model based control methods are used or heuristic and intelligent methods may be applied if linearization is not possible.

Several approaches have been used to solve the reactive power control problem using classical or intelligent optimization methods as discussed in section 2. Some of these approaches have been successfully implemented on the industrial distribution system. These methods are targeting the conventional distribution system. Nevertheless,

they provide the necessary background for volt/Var control of the isolated power systems. The current solution methods for VVC problem were discussed in section 2.

3.2 Problem Formulation of Dynamic Reactive Power Control of Isolated Power Systems

The focus of this work is on reactive power control of distribution MicroGrid and shipboard power system. In this section, the specifications of these two systems and the assumptions used to solve the reactive control problem are discussed in more detail.

3.2.1 Assumptions, Issues, and Problems

In the studied distribution MicroGrid, the DER units are a combination of wind generator, photovoltaic generator and diesel synchronous generator. The renewable DERs are interfaced to the system through power electronics inverters. It is assumed that the local controller of the units is designed such that each of the AC/DC interface inverters of DERs is able to inject active and reactive power to the system with some limitations.

As mentioned in the last section, solar and wind energy sources are affected by climate, environment, time and many other factors with strong randomness. Therefore, the operation of the system integrating distributed wind and solar energy sources has great uncertainties. This can result in a challenge to the safety, reliability and economical efficiency of the power system. So it is necessary to assess power quality challenges of the distributed wind-solar power generating system before starting to formulate the problem [71].

Some characteristics of wind and solar energy are listed below:

a) Wind:

- Wind is variable and uncertain and has limited dispatchability
- Wind peak output power is not usually coincident with the peak load
- Wind is an energy resource and not a capacity resource

b) Solar:

Solar DER has almost the same limits as the wind DER and if a storage unit is not available in the system, it is not dispatchable [72]. In addition, solar DER may introduce sharp changes to the system that can result in voltage ringing effect.

The problem that is solved in this dissertation is the global voltage control and optimization problem of the isolated power system. However, the control method has two layers of control, i.e., local and global control layers. The local control layer is consisted of the local control of each DER unit that controls the reactive power output of that specific unit, and the local controllers of the power electronics compensators that regulates their reactive output to the give setpoint. It is assumed that the local control is already designed and operating efficiently throughout this dissertation. The global control layer, which is the focus of this dissertation, is a centralized voltage and reactive power controller, which sends the control setpoints to each unit in a timely manner.

As mentioned, the focus of this work is on the centralized control layer. However, local and droop controllers are present in the system to adjust the final resulting setpoint of the general controller and assure the stability of the system.

One assumption in this research is that the studied systems do not have energy storage or has limited energy storage. Storage devices are added in systems with high penetration of renewable sources for active and reactive support. The price of energy storage is high and therefore it is desirable to have limited or no energy storage if possible [73], [74]. Even if they are present in the system, it is not desirable to turn battery storage devices on and off frequently for reactive control due to battery aging. In addition, a new reactive control scheme can reduce the need for energy storage devices for reactive support.

Another assumption in this research is that there is always a backup synchronous generator available in the MicroGrid which is capable of acting as the master generator and regulating the voltage and frequency in the system while the system is operating in the islanded mode. Although it is possible to use other DERs or even storage devices as the master generator in the MicroGrid [75], those cases are not studied in this dissertation.

Accurate modeling of the dynamics of the loads is critical in this study, since changes in the loads are the main cause of voltage drop in the nearby buses. The dynamic loads are modeled with relative restoring time constants. The non-dynamic loads in the system are considered to be constant power or constant impedance loads. Plugged in Hybrid Electric Vehicle (PEHV) loads, which are short-term loads, could also be modeled as dynamic or static loads depending on the dynamics of the charger.

Reactive power compensators are also present in the system and need to be included in the model. Reactive compensators include capacitor banks or power electronics

compensators such as SVC or STATCOM. Modeling the dynamics of power electronics compensators is not necessary since they have short response time comparing to dynamics of the power system.

The control inputs in this problem are capacitor bank switches, dynamic compensator setpoints and the voltage and reactive power setpoint of DERs. The goal of the controller is to keep the voltage of the load buses close to their nominal voltage. Further, an AC/DC zonal shipboard power system is another plant that will be studied in this work. The system includes generators, a high voltage AC system and DC distribution zones that supply power to AC and DC loads.

The sources in the system are synchronous generators connected to gas turbines. Synchronous generators are classified as Main Turbine Generators (MTG) and Auxiliary Turbine Generators (ATG) and the MTGs are typically significantly larger than the ATGs. It is assumed that one of the generators, typically one of the MTGs, is operating as the master generator and is responsible for regulating the voltage and frequency and all the other generators are operating in PQ control mode.

The generalized reactive power controller is responsible for setting the generator voltage and reactive power setpoints. Thus, the voltage setpoint of the master generator and reactive power setpoint of PQ control mode generators are the main control inputs for reactive control, which are assigned by the generalized reactive power controller.

Shipboard power system may also include dynamic reactive compensators in some of the buses close to loads depending on the initial system design. Setpoints of dynamic

compensators if they are present in the system are additional control inputs of the problem.

The loads are classified as vital or non-vital loads based on the importance of their functionality to the survival of the ship. The propulsion motor in this system is an induction motor, which can either be modeled as a dynamic load or as a constant power load depending on the operating mode of the motor. The system also includes pulsed loads, which are electromagnetic weapons that need supply for a short period of time. The loads in the SPS could be static or dynamic. The dynamic loads need to be modeled with their relative time constant. The static loads can be modeled as constant power or constant impedance loads.

The reactive power control problem can be decoupled by cutting the system into smaller pieces at DC capacitors since no reactive power is transmitted through a DC capacitor. Therefore, the high voltage AC system sees the DC distribution zones as AC loads. However, inside the zones the voltage control problem can be formulated as a local control problem. Power electronics devices are used to control the voltage in the DC distribution zones. Cascaded power electronics devices can help with voltage control in this level since if the output voltage of the rectifier drops, the next level converter may still be able to compensate and achieve the necessary output voltage by adjusting its duty cycle. The local voltage control problem inside the zones is not the focus of this dissertation and will be discussed briefly.

Similar to the MicroGrid case, since power loss in the system is not significant, the main goal of the controller is to keep the voltage of the load buses close to their nominal

voltage. Thus, the objective function should be chosen to minimize the voltage deviation of the critical buses from their nominal voltage.

Since the system is operating offshore, the VVC formulation should include dynamics of the sources and loads. However, including the full dynamics of the components may result in the problem to be cumbersome for the optimization software to solve which typically results in several numerical errors or unfeasible conditions. Thus, mathematical model of the shipboard power system may need to be simplified and linearized in order to be able to solve the optimization problem using the classic optimization methods.

Although shipboard power systems are distribution systems, unlike terrestrial power systems the general structure of the system includes generators and loads at a short distance from each other. Hence, the reactive power control scheme of shipboard power system includes some constraints of the generators as well. Similar to the conventional distribution systems, the reactive control power includes compensator and line limits in the formulation.

Due to limited amount of fuel in the SPS, usually the power management scheme tries to keep as many generators as possible off and an extra generator starts up only if more than 80% of current generation is consumed. Hence, when the load decreases in the system, the power management scheme starts shutting down the generators. Startup and Shut down of generators cause disturbance in the system and naturally moves the system out of optimality. Therefore reactive power optimization should be performed after each disturbance is mitigated.

Throughout this dissertation, it is assumed that the active power dispatch problem is already solved. In other words, the governors and active power loops of the DERs are controlling the device locally and a dispatch is determining the active power setpoint of the devices in the system. Hence, this dissertation is only addressing the reactive power control problem, which determines the reactive setpoints and voltage reference setpoint of the components in the system.

Further, it is assumed that the DERs are capable of meeting the active power needs of the loads during all operating conditions. This means that the system is capable of maintaining the frequency stability during all operating conditions. It is also assumed that the frequency of the system is very close to 60 Hz during all operating conditions of the controller. This assumption is reasonable since power systems are designed to operate within a rather strict frequency range. If the frequency deviates beyond that limit, the frequency relay gets triggered and isolates the system. In addition, reactive power control is usually performed as a response to regular system changes or after a fault has been cleared or after a reconfiguration has been performed in the power system. Thus, its main objective does not involve dealing with severe frequency stability issues in the power system.

Throughout this dissertation, it is assumed that the voltages V, the currents I and the apparent power S can be represented by phasors. The voltage V for example may be written as follows.

$$V = V_m e^{\delta} = V_d + jV_q \tag{3-1}$$

where the absolute value (or magnitude) of the voltage is $V_m = |V|$, the angle is $\delta = \arg(V)$, and the direct and quadrature components are $V_d = \Re\{V\}$ and $V_q = \Im\{V\}$, respectively. Also, variables and parameters are normalized using the per-unit system in all the equations in this dissertation unless mentioned otherwise.

The assumption in using the phasor of voltage and current is that the frequency of the power system remains very close to the nominal frequency even during voltage disturbances.

3.2.2 Background on Discrete-Time Hybrid Modeling

Hybrid systems are heterogeneous systems that include continuous and discrete variables such as finite state machines, if-then-else rules, on/off switches. In general, hybrid systems switch between different operating modes and each mode is governed by a set of dynamic equations. Mode transitions may be triggered by certain variables of the system crossing predefined thresholds, at certain time periods, or by external inputs to the system [18].

Power systems are good examples of hybrid systems. In power systems, many control variables such as load shedding and capacitor switching are discrete inputs. In addition, secondary controllers such as under load tap changers incorporate thresholds, logic and finite state machines. Further, saturation of some components such as active voltage regulators of the synchronous generators, which protect the generator from overheating, could be considered as a hybrid behavior. However, power systems are typically nonlinear systems while the general hybrid system framework is typically

developed for piecewise linear systems. Thus, mathematical manipulations are necessary to derive linear models for the power system. Piecewise linear models are a stage between linear and nonlinear models where the system is typically modeled by several linear models in different operating regions.

$$\begin{cases} \frac{d}{dt}x = Ax + Bu \\ y = Cx + Du \end{cases} \quad \Longleftrightarrow \quad \begin{cases} \frac{d}{dt}x = f(x,u,t) \\ y = g(x,u,t) \end{cases} \tag{3-2}$$

Linear systems Hybrid systems Nonlinear systems

In the next part, three typical discrete-time linear frameworks for hybrid systems will be presented: Discrete Hybrid Automata (DHA), Mixed Logical Dynamical (MLD) systems and PieceWise Affine (PWA) systems.

3.2.2.1 Piecewise affine systems

Polyhedral piecewise affine systems [76], [77] partition the state-space into polyhedral and assign an set of affine state space equations to each polyhedron.

$$\begin{gathered} x(k+1) = A_{j(k)}x(k) + B_{j(k)}u(k) + f_{j(k)} \\ y(k) = C_{j(k)}x(k) + D_{j(k)}(k)u(k) + g_{j(k)} \\ \text{With } j(k) \text{ such that } \begin{bmatrix} x(k) \\ u(k) \end{bmatrix} \in \mathcal{P}_{j(k)} \end{gathered} \tag{3-3}$$

where $k \epsilon \mathbb{N}$ is the discrete time instant, $x \in \chi$ is the continuous states of the system, $u \in U$are the inputs and $y \in Y$are the outputs and $j(k)$ is the mode of the system and $\mathcal{P}_{j(k)}$ is a polyhedral of the form $\mathcal{P}_{j(k)}: H_{j(k)}x(k) + J_{j(k)}(k)u(k) \leq K_{j(k)}$. The following lemma defines well-posedness for PWA functions.

Lemma: Let ΣPWA be a PWA model. If $\{\mathcal{P}_j\}_{j\in J}$ is a polyhedral partition of $\chi \times \mathcal{U}$, then ΣPWA is well-posed.

PWA model can approximate nonlinear and discontinuous dynamics arbitrarily well as shown in Figure 3-1.

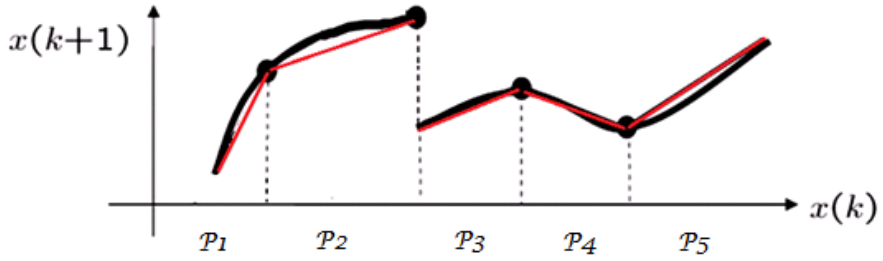

Figure 3-1 PWA model

3.2.2.2 Discrete hybrid automata

One design procedure for hybrid systems is to divide the system into two hierarchical layers, considering the continuous controllers in the lower level controlling the subsystems and the discrete controllers supervising in the higher level. Discrete Hybrid Automata (DHA) [18] is an interconnection of a Finite State Machine (FSM) which provides the discrete part providing the discrete part and a Switched Affine System (SAS) which providing the continuous part of the system. Two connecting elements are required for the interaction between these two parts, namely, The Event Generator (EG) and the Mode Selector (MS). The Event Generator extracts binary signals from the continuous dynamics of the system. These binary signals and other exogenous binary inputs trigger switches of the Finite State Machine states. The Mode Selector combines

all binary variables of the system to determine the operating mode of the system and based on the mode it selects the corresponding continuous dynamic from the Switched Affine System (SAS) [18].

3.2.2.2.1 Switched affine system

A Switched Affine System is a set of affine systems operating together. The switched affine system can be presented as follows.

$$\begin{aligned} x(k+1) &= A_i(k)x_r(k) + B_i(k)u_r(k) + f_i(k) \\ y_r(k) &= C_i(k)x_r(k) + D_i(k)u_r(k) + g_i(k) \end{aligned} \tag{3-4}$$

where $k \in \mathbb{N}_0$ is the discrete time-instant, $x_r \in \chi_r \subseteq \mathbb{R}^{n_r}$ is the real state, $u_r \in \mathcal{U}_r \subseteq \mathbb{R}^{m_r}$ is the exogenous real input, $y_r \in Y_r \subseteq \mathbb{R}^{p_r}$ is the real output, $\{A_i, B_i, f_i, C_i, D_i, g_i\}_{i\in I}$ is a set of matrixes with appropriate dimensions that describe the system in each mode, and $i \in I \subset \mathbb{N}$ is the mode of the system which is an input and selects the appropriate matrixes and chooses the output.

The state-update equation can be rewritten as a difference equation + if-then-else conditions as follows.

$$\begin{aligned} z_1(k) &= \begin{cases} A_1(k)x_r(k) + B_1(k)u_r(k) + f_1(k) & i(k) = 1 \\ 0 & \text{otherwise} \end{cases} \\ &\vdots \\ z_s(k) &= \begin{cases} A_s(k)x_r(k) + B_s(k)u_r(k) + f_s(k) & i(k) = s \\ 0 & \text{otherwise} \end{cases} \\ x_r(k+1) &= \sum_{i=1}^{s} z_i(k) \end{aligned} \tag{3-5}$$

where, $z_i \in \mathbb{R}^{n_r}$, i=1,…,s. Figure 3-2 shows the general structure of a switched affine system.

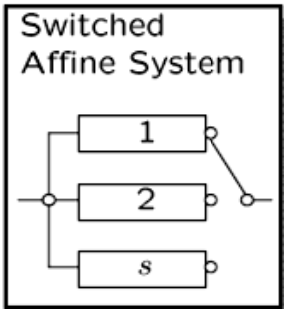

Figure 3-2 Switched affine system

3.2.2.2.2 Event generator

An event generator generates a binary signal, δ_e, based on the affine constraints of the system as follows.

$$\delta_e(k) = f_H(x_r(k), u_r(k)) \tag{3-6}$$

where $f_H: \mathbb{R}^{n_r} \times \mathbb{R}^{m_r} \longrightarrow \mathcal{D} \subseteq \{0,1\}^{n_c}$ is a vector of descriptive functions of a set of affine constraints. The threshold events are modeled as $[\delta_e(k) = 1] \rightarrow \left[f_H^i\left(x_r(k), u_r(k)\right) \leq 0\right]$, and time events are modeled by adding a clock variable t which is defined as $t(k+1) = t(k) + T_s$ and setting $[\delta_e(k) = 1] \rightarrow [t(k) \geq t_0]$.

3.2.2.2.3 Finite state machine

A finite state machine or automaton is a discrete dynamic process, which evolves according to a binary state update function. A finite state machine is generally described as follows.

$$x_b(k+1) = f_b(x_b(k), u_b(k), \delta_e(k))$$
$$y_b(k) = g_b(x_b(k), u_b(k), \delta_e(k)) \tag{3-7}$$

where $x_b \in \chi_b \subseteq \{0,1\}^{n_b}$ is the binary state, $u_b \in U_b \subseteq \{0,1\}^{m_b}$ the exogenous binary input, $y_b \in Y_b \subseteq \{0,1\}^{P_b}$ the binary output, δ_e is the binary event, and $f_B: \chi_b \times \mathcal{U}_b \times \mathcal{D} \longrightarrow \chi_b$, $g_B: \chi_b \times \mathcal{U}_b \times \mathcal{D} \longrightarrow Y_b$ are the deterministic binary functions.

Mode Selector (MS): The binary state, x_b, the binary input, u_b, and the event δ_e selects the mode of the system through the binary function $f_M: \chi_b \times \mathcal{U}_b \times \mathcal{D} \longrightarrow I$ which is therefore called Mode Selector. The output of the mode selector which is called the active mode is as follows.

$$i(k) = f_b(x_b(k), u_b(k), \delta_e(k))$$

Naturally, the mode of the system changes when $i(k)$ changes from the pervious time instant.

Definition: Assuming $x = \begin{bmatrix} x_r \\ x_b \end{bmatrix}, u = \begin{bmatrix} u_r \\ u_b \end{bmatrix}, y = \begin{bmatrix} y_r \\ y_b \end{bmatrix}$, a *DHA* is well-posed on χ, U, Y, if for any initial condition $x(0) \in \chi$ and for all inputs $u(0) \in U$, the state trajectory, $x(k) \in \chi$ and the output trajectory, $y(k) \in Y$ are uniquely defined for all $k \in \mathbb{N}_0$. Figure 3-3 shows the general structure of discrete hybrid automata.

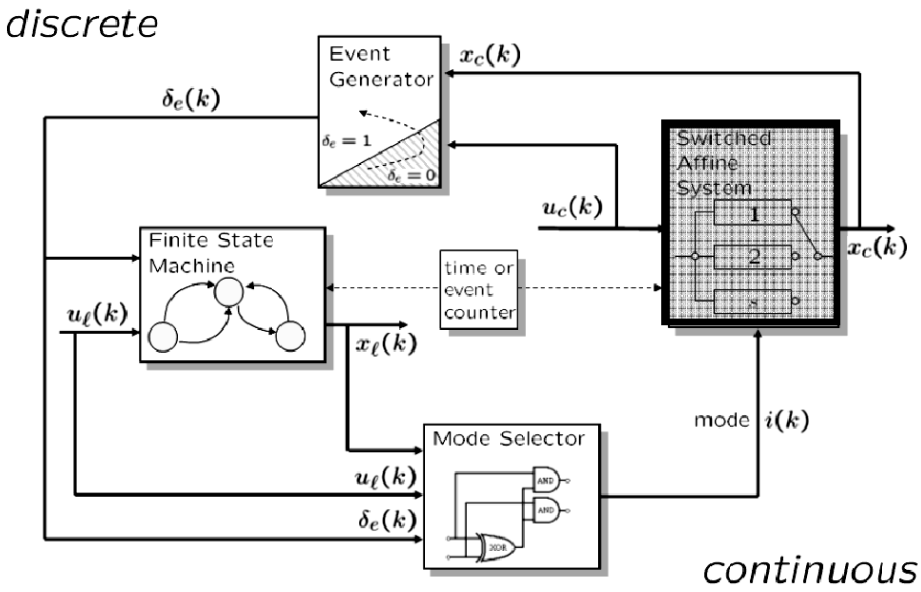

Figure 3-3 Discrete hybrid automata [78]

3.2.2.3 Mixed logical dynamical systems

Mixed Logical Dynamics (MLD) is another design procedure for hybrid systems, which transform the logics into linear inequalities. These inequalities include integer and continuous variables. Thus, MLD describes the system by linear dynamic equations subject to linear mixed-integer inequalities. A wide range of systems including power systems can be described in the MLD form. The MLD form is more suitable than the hierarchical form for power systems studies since there is no need for decoupling the system into two layers.

The MLD of a hybrid system can be described in the following general form [79].

$$
\begin{aligned}
x(k+1) &= A(k)x(k) + B_1u(k) + B_2\delta(k) + B_3z(k) \\
y(k) &= C(k)x(k) + D_1u(k) + D_2\delta(k) + D_3z(k) \\
E_2\delta(k) + E_3z(k) &\leq E_4x(k) + E_1u(k) + E_5
\end{aligned}
\tag{3-8}
$$

where $k\epsilon\mathbb{N}$ is the discrete time instant, $x \in \chi$ is the continuous states of the system, $u \in U$are the inputs and $y \in Y$are the outputs, $\delta \in \{0,1\}^{n_\delta}$ are the binary variable and $z \in \mathbb{R}^{n_z}$ are auxiliary continuous variables which are introduced while translating PWA functions into linear inequalities. The general MLD form presented in (3-8) contains all constraints on states, inputs, outputs and auxiliary variables and all the state space equations of the system. It should be noted that the equality equations, which include the dynamics of the system in discrete form, are linear equations. However, the nonlinearity is hidden in the integrality constraints on the binary variables. A combination of a binary state x_b, binary input u_b, and binary variable δ is called a mode. If for a given (x_b, u_b, δ), there exists a $x_r \in \chi_r, u_r \in U_r$ and $z \in \mathbb{R}^{n_z}$ such that the inequality in (3-8) holds, the mode is called feasible; else it is infeasible [79], [18]. An MLD representation of a system is Well-posedness if the following Lemma holds.

Lemma: If for every given pair $x(k) \in \chi$ and $u(k) \in U$, the values of $\delta(k)$ and $z(k)$ are uniquely defined by the inequality in (3-8), the MLD model is well-posed.

All the MLDs in this dissertation are considered to be well-posed. It should be noted that this assumption is not restrictive and is always satisfied when real physical plants are described in the MLD form [79]. It should also be noted that automata, propositional logic, if . . . then . . . else statements, and PWA functions can all be described in MLD form. However, nonlinear functions such as network equations in power systems cannot

be directly described in MLD form and should be approximated by PWA functions. Hereafter, we will mainly consider the hybrid systems in the form of MLDs. This assumption is not limiting since a hybrid system defined in any other form could be converted to MLDs. Table 3 shows how each of the elements of hybrid systems are converted to the MLD form.

Table 3 MLD transform [78]

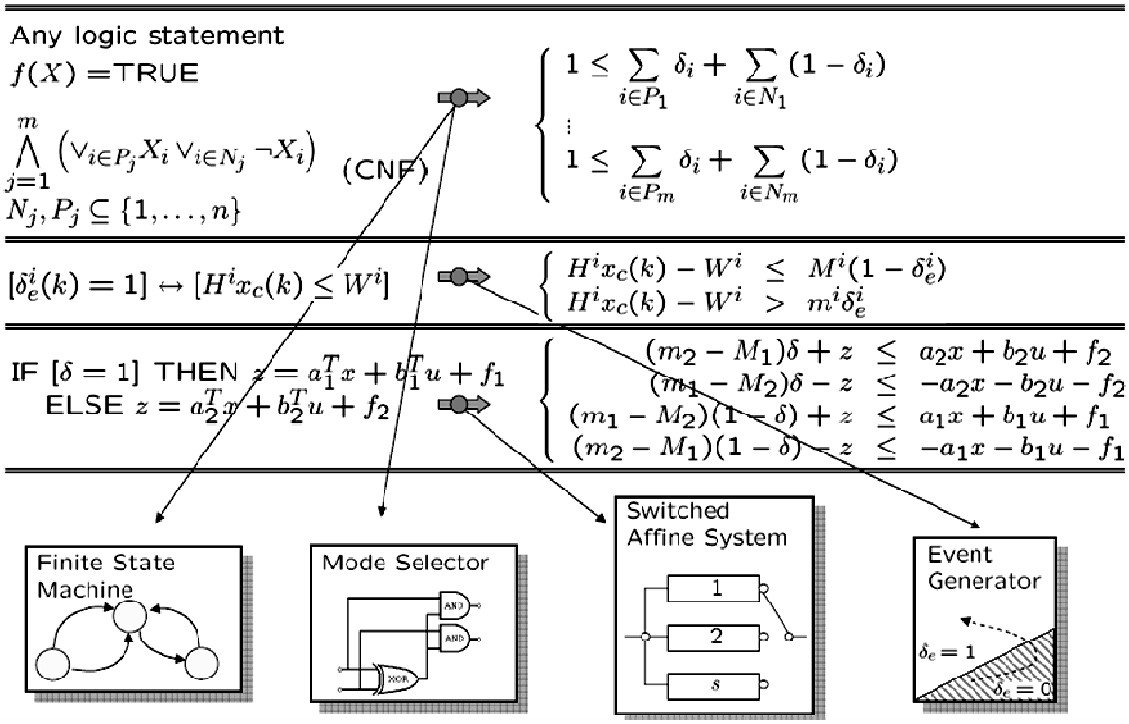

A generalized stabilizing controller can also be derived for the systems described in the MLD form. For example, a stabilizing model predictive control scheme that can force the system to follow a desired reference trajectories is discussed in [79].

Although all the above-mentioned models are avoid nonlinear equations, all of them can approximate nonlinear systems arbitrarily accurate. Further, all of these hybrid

models may include thresholds on states, inputs and internal variables. Also, they may include binary states that are part of a finite state machine or an automaton. Thus, all of the aforementioned hybrid system models are equivalent and several programs exist for systematical transforming to each other [80], [18].

Despite of being equivalent, each of these modeling frameworks has their specific benefits. DHAs models have separate blocks and are easily understandable by the user, which makes it more convenient for user interface. MLD models are suitable for online optimal control and PWA models are suitable offline optimal control [81], to design observers for hybrid systems [82], and to perform analysis tasks.

As mentioned earlier, direct modeling of hybrid systems in MLD or PWA form is usually excruciating. Researchers at ETHZ University developed a program called HYbrid Systems DEscription Language (Hysdel) [83] which allows the designer to describe a hybrid system on a textual basis. This is very similar to DHA models and describes the hybrid system in blocks. They also developed a compiler that converts the input text to PWA and MLD forms, which is basically transforming DHA hybrid system to PWA and MLD. The Hysdel language has been used to develop most of the models in this dissertation.

- **Example1:**

$$x(k+1) = \begin{cases} x(k) + u(k) \;\; if \;\; x(t) \geq 0 \\ -x(k) + u(k) \;\; if \;\; x(t) < 0 \end{cases} \tag{3-9}$$

In this case the constraint $x(k) \geq 0$ could be assigned to an auxiliary binary variable, $\delta(k)$. Therefore, when this switch is on the system is in one state and when it is off the system is in another state.

$$[\delta(k) = 1] \leftrightarrow [x(k) \geq 0] \tag{3-10}$$

According to [79] we have the following general equation.

$$[f(x) \geq 0] \leftrightarrow [\delta = 1] \text{ is true if and only if } \begin{cases} f(x) \leq M(1-\delta) \\ f(x) \geq \varepsilon + (m-\varepsilon)\delta \end{cases} \tag{3-11}$$

where, *M* and *m* are the maximum (or supremum) and minimum (or infimum) or $f(x)$ Thus, assuming that the Maximum and minimum of the $x(k)$ are +10 and -10 (*M*=+10 and *m*=-10), (3-10) is equivalent to the following two inequalities.

$$\begin{aligned} -\mathrm{m}\delta(k) &\leq \mathrm{x}(k) - \mathrm{m} \\ -(M+\varepsilon)\delta(k) &\leq -x(k) - \varepsilon \end{aligned} \tag{3-12}$$

Then the system's differential equation (3-9) could be rewritten in the following unique form.

$$x(k+1) = 2\delta(k)x(k) - x(k) + u(k) \tag{3-13}$$

Defining the auxiliary variable $z(k) = \delta(k)x(k)$, we have the following equations.

$$
\begin{aligned}
z\ \ (k) &\le M\delta\ \ (k)\\
z\ \ (k) &\ge m\delta\ \ (k)\\
z\ \ (k) &\le x(k) - m(1-\delta\ \ (k))\\
z\ \ (k) &\ge x(k) - M(1-\delta\ \ (k))
\end{aligned}
\tag{3-14}
$$

- **Example 2:**

Consider the following piecewise linear system from [79].

$$
\begin{aligned}
\boldsymbol{x}(k+1) &= 0.8\begin{bmatrix}\cos\ \alpha(k) & -\sin\alpha(k)\\ \sin\alpha(k) & \cos\ \alpha(k)\end{bmatrix}\boldsymbol{x}(k) + \begin{bmatrix}0\\1\end{bmatrix}u(k)\\
y(k) &= [1 \quad 0]\,\boldsymbol{x}(k)
\end{aligned}
\tag{3-15}
$$

where,

$$
\begin{aligned}
\alpha(t) &= \begin{cases}\dfrac{\pi}{3} & if\ \ [1\ \ 0]x(k) \ge 0\\ -\dfrac{\pi}{3} & if\ \ [1\ \ 0]x(k) < 0\end{cases}\\
\boldsymbol{x}(k)\ &\in [-10\ \ 10]\times[-10\ \ 10]\\
u(k) &\in [-1\ \ 1]
\end{aligned}
\tag{3-16}
$$

Using auxiliary variables $\boldsymbol{z}(k) \in \mathbb{R}^4$ and $\delta \in \{0,1\}$ such that $[\delta(k) = 1] \leftrightarrow [[1\ 0]x(k) \ge 0$ equation (3-15) can be rewritten as follows.

$$x(k+1) = [I \quad I]z(k)$$

Thus in this case we have the following equations for the system in the two cases.

$$\boldsymbol{x}(k+1) = \begin{bmatrix} 0.4 & -0.69 \\ 0.69 & 0.4 \end{bmatrix} \boldsymbol{x}(k) + \begin{bmatrix} 0 \\ 1 \end{bmatrix} u(k) \qquad \leftrightarrow [[1\ 0]\mathrm{x(k)} \geq 0]$$

$$\boldsymbol{x}(k+1) = \begin{bmatrix} 0.4 & 0.69 \\ -0.69 & 0.4 \end{bmatrix} \boldsymbol{x}(k) + \begin{bmatrix} 0 \\ 1 \end{bmatrix} u(k) \qquad \leftrightarrow [[1\ 0]\mathrm{x(k)} < 0] \tag{3-17}$$

where,

$$\boldsymbol{A_1} = \begin{bmatrix} 0.4 & -0.69 \\ 0.69 & 0.4 \end{bmatrix}$$

$$\boldsymbol{A_2} = \begin{bmatrix} 0.4 & 0.69 \\ -0.69 & 0.4 \end{bmatrix} \tag{3-18}$$

Using the MLD approach discussed earlier,

$$z_1(k) \leq M\delta_1(k)$$

$$z_1(k) \geq m\delta_1(k)$$

$$z_1(k) \leq \boldsymbol{A_1}\boldsymbol{x}(k) + \boldsymbol{B_1}u(k) - m(1-\delta_1(k)) \tag{3-19}$$

$$z_1(k) \geq \boldsymbol{A_1}\boldsymbol{x}(k) + \boldsymbol{B_1}u(k) - M(1-\delta_1(k))$$

Expanding in the matrix form, results in the following.

$$\begin{bmatrix} 10 \\ -10-\epsilon \\ -M \\ -M \\ M \\ M \\ M \\ M \\ -M \\ -M \\ 0 \\ 0 \\ 0 \\ 0 \end{bmatrix} \boldsymbol{\delta}(k) + \begin{bmatrix} 0 & 0 \\ 0 & 0 \\ I & 0 \\ -I & 0 \\ 0 & I \\ 0 & -I \\ I & 0 \\ M & 0 \\ -I & I \\ 0 & -I \\ 0 & 0 \\ 0 & 0 \\ 0 & 0 \\ 0 & 0 \end{bmatrix} \boldsymbol{z}(k) \leq \begin{bmatrix} 0 \\ 0 \\ 0 \\ 0 \\ 0 \\ B \\ -B \\ B \\ -B \\ 0 \\ 0 \\ 1 \\ -1 \end{bmatrix} \boldsymbol{u}(k) + \begin{bmatrix} 10 \\ -10 \\ 0 \\ 0 \\ 0 \\ A_1 \\ -A_1 \\ A_2 \\ -A_2 \\ I \\ -I \\ 0 \\ 0 \end{bmatrix} \boldsymbol{x}(k) + \begin{bmatrix} 10 \\ -\epsilon \\ 0 \\ M \\ M \\ M \\ M \\ M \\ 0 \\ 0 \\ N \\ N \\ 1 \\ 1 \end{bmatrix}$$

where ϵ is a small positive scalar, $B = [0\ 1]^T$, $M = \left(1+\sqrt{3}\right)[1\ 1]^T + B$, $N = 10[1\ 1]^T$, and A_1, A_2 are obtained from (3-15) by setting $\alpha = \frac{\pi}{3}, -\frac{\pi}{3}$ respectively.

3.2.3 Background on the optimization of hybrid systems

An optimization problem could be expressed in the following general form.

$$\min_{\xi} f_0(\xi)$$
$$\text{Subj. to } f_i(\xi) \leq 0\,, i = 1, \dots, n_f \tag{3-20}$$

where ξ is the optimization variable which can be defined in the general form of $\xi \triangleq \begin{bmatrix}\xi_r \\ \xi_b\end{bmatrix}$. The general form contains the real-valued part ξ_r and the integer-valued part ξ_b. The optimization problem tries to find a vector ξ^* that minimizes the objective function $f_0(\xi)$ such that the inequality constraints $f_i(\xi) \leq 0$ hold.

A point ξ is called feasible if it satisfies all the constraints $f_i(\xi)$ and the optimization problem (3-20) is called feasible if there exists at least one feasible point in the input domain. The set of all feasible inputs is referred to as the feasible set. The optimal value J^* of the problem (3-20) is defined as follows.

$$J^* = \inf\{ f_0(\xi) \mid f_0(\xi) \leq 0;\ i = 1, \dots, n_f \} \tag{3-21}$$

The solution to the optimization problem from the feasible set of inputs,ξ^*, is referred to as the optimizer. The optimizer is called a local optimizer if it minimizes the cost function in a subset of the feasible set and a global optimizer if it minimizes the cost for the whole feasible set.

If the objective function and the inequality constraints in optimization problem (3-20) are convex and no binary variables are present in the optimization variable the problem is referred to as a convex optimization problem. In a convex optimization problem the feasible set is convex, and any locally optimal point is also globally optimal.

If the objective function and constraints of the optimization problem (3-20) are linear, the problem is referred to as a Mixed Integer Linear Programming (MILP) problem, which can be expressed as follows.

$$\begin{aligned} &\min_{\xi} C\xi^T \\ &\text{Subj. to } G\xi \leq g \end{aligned} \tag{3-22}$$

where G is a matrix and c and g are row vectors. Although the objective function and constraints are linear, the optimization problem is not convex due to the existence of integer variables. Thus locally optimal points are not necessarily globally optimal. Further, MILPs are NP-hard which means the solution time grows exponentially with the number of binary variables [84].

Several algorithms have been proposed to solve MILP problems including branch and bound, cutting plane, decomposition and logic-based methods. Details of these algorithms could be found in [85]. Obviously, if the optimization vector ξ contains only real and no integer components, problem (3-22) reduces to a Linear Program (LP), which is convex which means a local minimize to the problem is in fact the global minimize and the problem can be solved in polynomial time. Similarly, the Mixed Integer Quadratic Programming (MIQP) problem can be formulated as follows.

$$\min_{\xi} \frac{1}{2}\xi^T Q\xi + C\xi^T$$
$$\text{Subj. to } G\xi \leq g \tag{3-23}$$

$$\xi \triangleq \begin{bmatrix}\xi_r \\ \xi_b\end{bmatrix}, \xi_r \in \mathbb{R}^{n_c}, \xi_b \in \{0,1\}^{n_d} \tag{3-24}$$

where Q is a weight matrix.

Mixed integer programming problems are classified in general as NP-hard, which means that with the available algorithms in the worst case, the solution time grows exponentially with the number of integer variables [84].

In this dissertation, the objective function is defined to penalize the predicted evolution of the state, control input and output over the finite horizon N using a norm. Also the weight matrices and Q are always defined to be full column rank matrices. The prediction is performed using the MLD model of the system at every time-step within the prediction horizon which means the MLD model is augmented for N steps to predict the behavior of the system ahead of time.

If the MIQP problem is solved subject to the MLD model of the system the optimization vector can be written as follows.

$$\xi = [\boldsymbol{u}(0), \ \ldots, \boldsymbol{u}(N-1), \boldsymbol{\delta}(0), \ldots, \boldsymbol{\delta}(N-1), \boldsymbol{z}(0), \ldots, \boldsymbol{z}(N-1)]^T \tag{3-25}$$

where $\boldsymbol{u}, \boldsymbol{\delta}, \boldsymbol{z}$ are the vectors of continuous, discrete and auxiliary variables, respectively. As can be seen in (3-25), the optimization vector includes discrete and continuous variables.

The control input at time-instant k is obtained by minimizing the objective function subject to the evolution of the MLD model and its mixed-integer linear inequality constraints. This yields to Constrained Finite Time Optimal Control (CFTOC) problem which can be expressed as follows.

$$U^*(k) = \arg\min J\big(x(k), u(k)\big)$$
$$\text{Subject to MLD model} \tag{3-26}$$

Furthermore, additional integrality constraints are present on the binary variables and on binary inputs. Solving this problem yields a sequence of optimal control inputs $U^*(k) = [u(k), \dots, u(k+N-1)]^T$. If a linear norm is used in the cost function of (3-31), the CFTOC problem leads to solving an MILP and if a quadratic norm is used, it leads to solving MIQP, respectively.

Several algorithms have been proposed and applied successfully to medium and large size application MIQP problems [86], the four major ones being:

- Cutting plane methods, where new constraints (cuts) are generated and added to reduce the feasible domain until the optimal solution is found
- Decomposition methods, where the mathematical structure of the models is exploited via variable partitioning, duality, and relaxation methods
- Logic-based methods, where disjunctive constraints or symbolic inference techniques are utilized, which can be expressed in terms of binary variables
- Branch and bound (B&B) methods, where the 0-1 combinations are explored through a binary tree, the feasible region is partitioned into sub-domains

systematically, and valid upper and lower bounds are generated at different levels of the binary tree.

More details and analysis of the multi of multi-parametric programming for MILPs and MIQPs could be found in [87],[88],[89]. In this dissertation, branch and bound method is used for solving the MILP/MIQP problem and will be discussed in more detail in section 3.3.1.

3.2.4 Dynamic Reactive Power Control of Power Systems

The objective of reactive power control is to minimize losses and to keep the bus voltages within limits while satisfying all system constraints. As mentioned earlier, cables are usually short in isolated power systems; therefore, minimizing loss is not be the best option as the objective function in these systems. In this case, a better candidate is the sum of voltage deviations of critical buses in the system. It should be noted that when the total voltage deviation is minimized, the total loss of the system is minimized indirectly. Reactive power control of an isolated power system can be formulated in the following general form.

$$\min_{u(0,..N-1),\boldsymbol{\sigma}(0,...,N-1)} J(\boldsymbol{x}(k), \boldsymbol{u}(k), k) \tag{3-27}$$

$$\dot{x}(k) = f(\boldsymbol{x}(k), \boldsymbol{u}(k), k) \tag{3-28}$$

$$g(\boldsymbol{x}(k), \boldsymbol{u}(k), \boldsymbol{\sigma}(k), k) = 0 \tag{3-29}$$

$$h(\boldsymbol{x}(k), \boldsymbol{u}(k), k) \leq 0 \tag{3-30}$$

The cost function given by (3-27) can be chosen to minimize the voltage deviation of the buses that are more likely to have voltage drop, i.e., load buses. In this problem, the cost function is chosen to minimize the voltage deviation over a prediction horizon on *N*.

The prediction horizon and step size is chosen by the operator to cover the slowest dynamic of the system and not to exceed the maximum possible computation time for online control. Hence, assuming the current time instant as t_0, the voltages of the critical buses of the system should be predicted over the horizon of N to calculate the cost function. The control action should also be included in the cost function to reduce the possibility of having too much control action which may result in actuator aging and damage in the system. Thus, the objective function (3-27) could be written as follows.

$$J(\boldsymbol{x},\boldsymbol{u},k)=\sum_{k=0}^{N-1}\left\{\begin{array}{l}\left\{\sum_{i\in N_t}\left\|V_i(k+t_0|t_0)-V_i^{Nom}\right\|_{\{1,\infty\}}\right\}+\cdots\\ \ldots+\|\boldsymbol{W_1}\Delta\boldsymbol{v}(k)\|_{\{1,\infty\}}+\|\boldsymbol{W_2}\Delta\boldsymbol{\sigma}(k)\|_{\{1,\infty\}}\end{array}\right\} \tag{3-31}$$

In (3-31), N_t is the set of the buses which are more important for voltage control, i.e., the buses that are close to the loads, N is the horizon of the optimization, $\boldsymbol{W_1}$ and $\boldsymbol{W_2}$ are user definable input weight matrices and $V_i(k+t_0|t_0)$ is the phasor of estimated voltage of bus i at the time t_0+k based on the bus voltage measurement at time t_0.

As shown in (3-28) and (3-29), the optimization problem is subject to the following simplified and discretized differential algebraic equations.

$$\begin{aligned}x_1(k+1)&=x_1(k)+\Delta t\left(\frac{-1}{T_V}x_1(k)+V_{Ref,DG1}(k)\right)\\ V_1(k)&=V_{DG1}(k)=\frac{1}{T_V}x_1(k)\end{aligned} \tag{3-32}$$

$$x_i(k+1) = x_i(k) + \Delta t\left(\frac{-1}{T_{Q,i}}x_i(k) + Q_{Ref,DGi}(k)\right)$$
$$Q_{DG\ i}(k) = \frac{1}{T_{Q,i}}\ x_i(k)\ \ ,\quad i = 2, \dots, N_{DG} \tag{3-33}$$

$$x_j(k+1) = x_j(k) - \Delta t\left(\frac{x_j(k)}{T_{q\,j}} + Q_{L0\,j}(V^{b_s}(k) - V^{b_t}(k))\right)$$
$$Q_{L\,j}(k) = \left(\frac{x_j(k)}{T_{q\,j}} + Q_{L0\,j}\left(V^{b_t}(k)\right)\right)\ ,\ j = N_{DG}+1, \dots, N_{DG}+N_{DL} \tag{3-34}$$

$$\sum P_n(k) = \sum_{j=1}^{N}|V_n(k)||V_j(k)|\left(G_{nj}\cos(\theta_n(k)-\theta_j(k)) + B_{nj}\sin(\theta_n(k)-\theta_j(k))\right)$$
$$\sum Q_n(k) = \sum_{j=1}^{N}|V_n(k)||V_j(k)|\left(G_{nj}\sin(\theta_n(k)-\theta_j(k)) - B_{nj}\cos(\theta_n(k)-\theta_j(k))\right) \tag{3-35}$$

where $N_{DG}$is the number of DGs and N_{DL} is the number of dynamic loads. The DAE equations (3-32) through (3-35) are simplified DAE equations of the sources and loads and the network equations of the system. Equation (3-32) represents the dynamics of the master generator; (3-33) the dynamics of *PQ* controlled DERs and (3-34) the dynamics of the loads and (3-34) are the network equations. In (3-36), $\sum Q_n(k)$ is the sum of the reactive power injected and withdrawn from bus *n* as follows.

$$\sum Q_n(k) = \left(\sum_{i=1}^{N_{DG\,n}} Q_{DG\,i}(k)\right) + \left(\sum_{c=1}^{N_{c\,n}} Q_{Cc}(k)\right) - \left(\sum_{j=1}^{N_{DL\,n}} Q_{L\,j}(k)\right) - \left(\sum_{p=1}^{N_{L\,n}} Q_{L\,p}(k)\right) \tag{3-36}$$

where, $N_{DG\,k}, N_{c\,n}, N_{DL\,n}, N_{L\,n}$ are the number of DGs, compensators, dynamic loads and static loads connected to bus *n* respectively. Figure 3-4 shows the injection and withdrawal of reactive power to and from bus *n*.

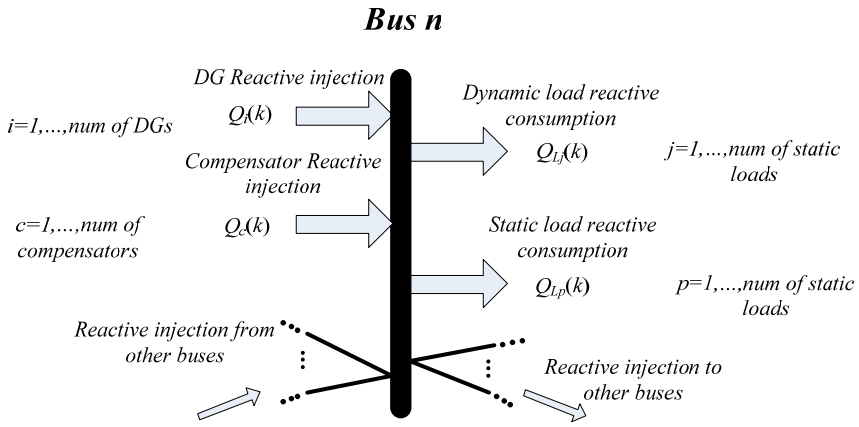

Figure 3-4 Injection and withdrawal of reactive power from bus *n*

The simplified nonlinear system equations should be converted to the MLD form following the procedure depicted in Figure 3-5.

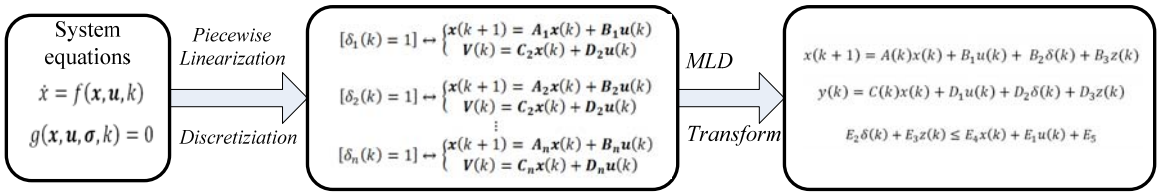

Figure 3-5 Converting the system to MLD form

Equations (3-29) and (3-30) include the bus voltage limits, compensator limits, cable thermal limits and power equality of the system given by following equations:

$$\begin{aligned} V_{b\,min} \leq |V_b(k)| \leq V_{b\,Max} \qquad & b = 1, \dots, N_{Bus} \\ Q_{c\,min}(k) \leq Q_c(k) \leq Q_{c\,Max}(k) \quad & c = 1, \dots, N_{comp} \\ |I_{cl}(k)| \leq I_{cl\,Max} \qquad & cl = 1, \dots, N_{cl} \end{aligned} \tag{3-37}$$

where N_{Bus} is the number of buses, N_{Comp} is the number of compensators and N_{cl} is the number of the cables, $|V_b(k)|$ is the voltage magnitude of bus b at time k, $Q_c(k)$ reactive power setpoint of compensator c at time k and $|I_{cl}(k)|$ is the current of cable cl at time k. The thermal rating of an overhead line is the maximum current that the line can handle without overheating and it is highly dependent on the conductor and insulator materials and the working condition.

Figure 3-6 shows the prediction of the voltages in the system using the model (3-32) through (3-35). This figure shows the predicted voltage profile of two buses in the system over a horizon of N with step time of k. The objective of model predictive control is to select a control sequence force the voltage to follow the reference voltage profile. In the voltage and reactive control of the isolated power system, the main goal is to make

the bus voltages achieve the nominal voltage value which is usually constant and equal to 1 per unit.

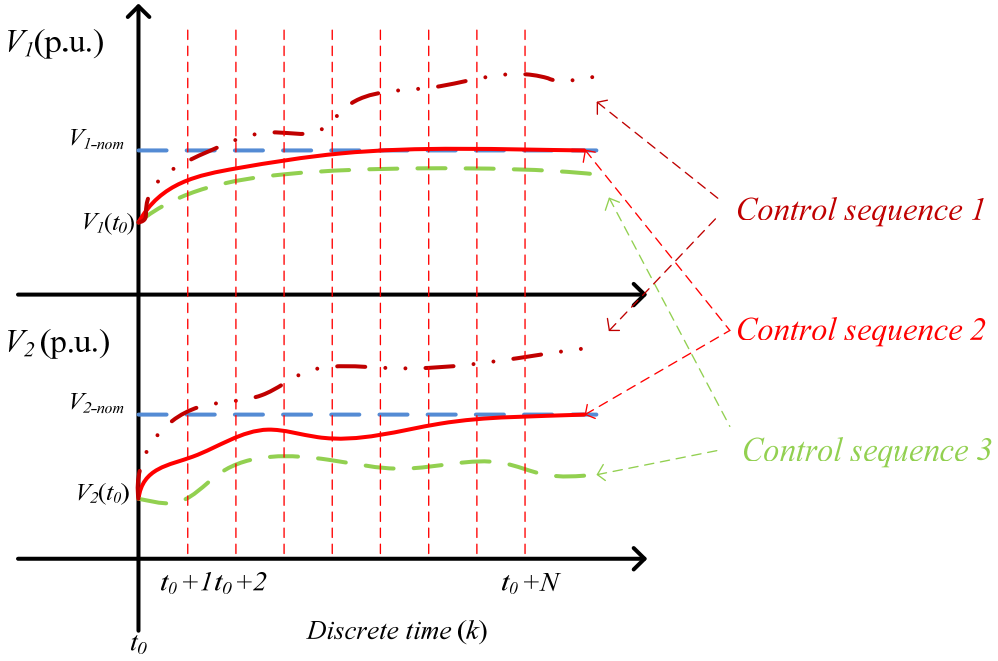

Figure 3-6 Prediction of the voltage profile of buses in the system for MPC

Hypothetically, if the system has only one control input, the control sequences discussed in Figure 3-6 may look like Figure 3-7.

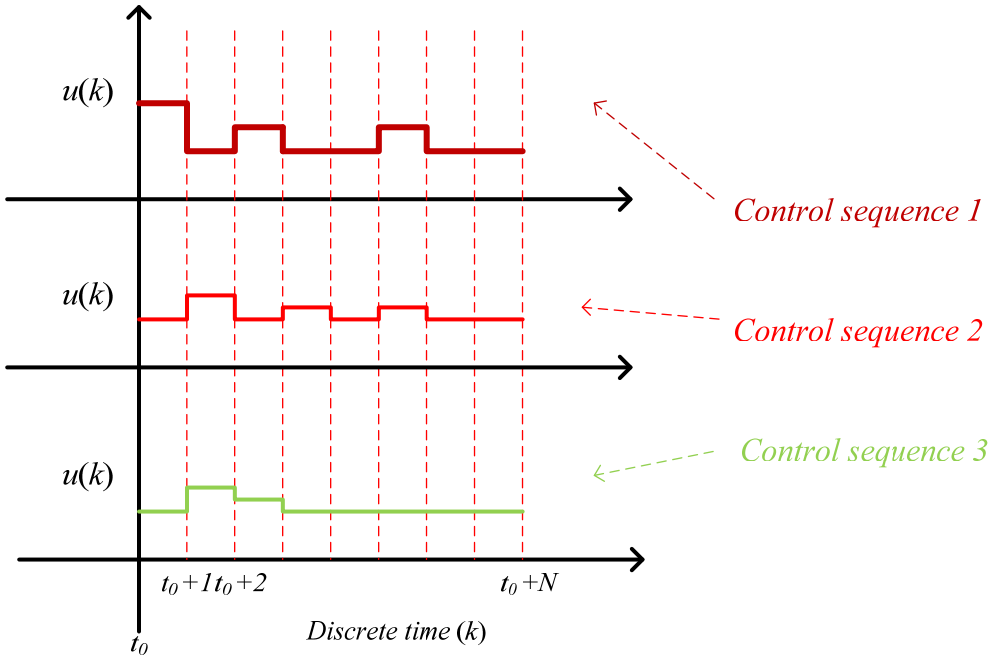

Figure 3-7 Sequence of control inputs

By combining Figure 3-6 and Figure 3-7 Sequence of control inputsFigure 3-7, Figure 3-8 show the concept of model predictive control with a discrete prediction of voltage over the horizon *N*.

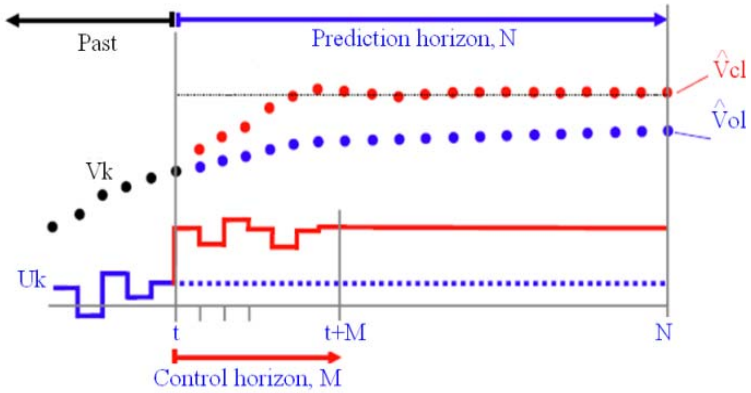

Figure 3-8 General concept of model predictive control

Each step of the time horizon is subject to one set of MLD equations. For example the step 19 of the time horizon of an example system is subject to the following MLD equations.

#1	Numeric value	Element-wise inequality 6x1	umin < u_19 < umax
#2	Numeric value	Equality constraint (derived) 1x1	u_19(3) in [0 1 2]
#3	Numeric value	Element-wise inequality 4x1	xmin < x_19 < xmax
#4	Numeric value	Element-wise inequality 4x1	xmin < x_20 < xmax
#5	Numeric value	Element-wise inequality 2x1	ymin < y_19 < ymax
#6	Numeric value	Equality constraint 2x1	x_20 == A*x_19 + B1*u_19 + B2*d_19 + B3*z_19 + B5
#7	Numeric value	Equality constraint 1x1	y_19 == C*x_19 + D1*u_19 + D2*d_19 + D3*z_19 + D5
#8	Numeric value	Element-wise inequality 6x1	E2*d_19 + E3*z_19 <= E1*u_19 + E4*z_19 + E_5
#9	Numeric value	Element-wise inequality 6x1	MLD.zl < z_19 < MLD.zu
#10	Numeric value	Element-wise inequality 6x1	umin < u_18 < umax
#11	Numeric value	Equality constraint (derived) 1x1	u_18(3) in [0 1 2]
#12	Numeric value	Element-wise inequality 4x1	xmin < x_18 < xmax
#13	Numeric value	Element-wise inequality 2x1	ymin < y_18 < ymax

Thus, the MLD equations are repeated *N* times in the constraints of the optimizations with *N* being the time horizon of the optimization. Thus, the MLD constraints are augments to the number of step times in the time horizon. This process replaces the difference equations with chained algebraic equations with each step depending on the pervious step, which makes it understandable for the optimization software. The concept of augmenting MLD constraints at each step time is shown in Figure 3-9.

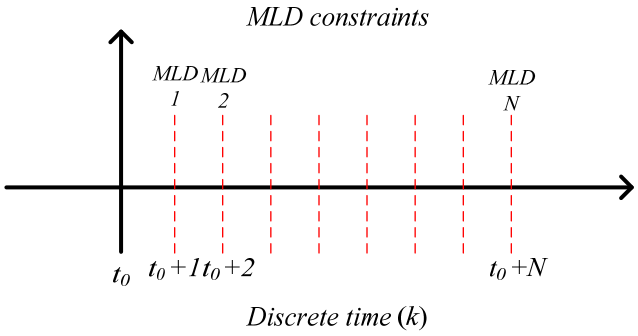

Figure 3-9 MLD constraints of the optimization problem at each step time

In (3-28), $\boldsymbol{x}(k)$ is the vector of the state space variables as follows.

$$\boldsymbol{x}(k) = \left[x_1(k) \dots\ x_{DG\,i}(k) \dots\ \ x_{L_q j}(k) \dots\right]^T \quad i = 2, \dots, N_{DG}\ ,\ j = 1, \dots, N_{Load} \tag{3-38}$$

where N_{DG} is the number of DGs and N_{Load} is the number of loads, $x_1(k)$ is the state variable of the master generator which is numbered as the first DG, $x_{DG\,i}(k)$ is the state variable of the *i*'th DG, $x_{L_q j}$ is the reactive power state variable of *j*'th load.

In (3-28), the control variables in the $\boldsymbol{v}(k)$ vector can include voltage and reactive power of generators, Generated reactive power of compensators. Some or all of these inputs may be used in the reactive power control based on the studied power system and based on the needs. Thus, $\boldsymbol{v}(k)$ which is the vector of continuous control inputs is defined as follows.

$$\boldsymbol{v}(k) = \left[\, V_{Ref,DG1}\,(k)\ \ Q_{Ref,DG\,i}(k) \dots\ \ Q_c\,(k) \dots\right]^T \quad i = 2, \dots, N_{DG}\ ,\ c = 1, \dots, N_{Comp} \tag{3-39}$$

where $V_{Ref,DG1}\,(k)$ is the reference voltage of the master generator and $Q_{Ref,DG\,i}(k)$ is the reference reactive power injection of *i*'th DG, $Q_c\,(k)$ is the reactive power reference of *c*'th dynamic compensator if dynamic compensators are present in the system. $\boldsymbol{\sigma}(k)$ is the vector of the discrete control inputs to the system, i.e., $\boldsymbol{\sigma}(k) = \left[\sigma_1 \dots \sigma_{N_{sw}}\right]$ where N_{SW} is the number of controllable discrete inputs in the power system. The augmented control vector $\boldsymbol{u}(k)$ is defined as the augmented vector of discrete control and continuous control inputs, i.e. $\boldsymbol{u}(k) = [\,\boldsymbol{v}(k)\ \boldsymbol{\sigma}(k)]$**.** Figure 3-10 shows the process of calculation of the objective function in (3-31).

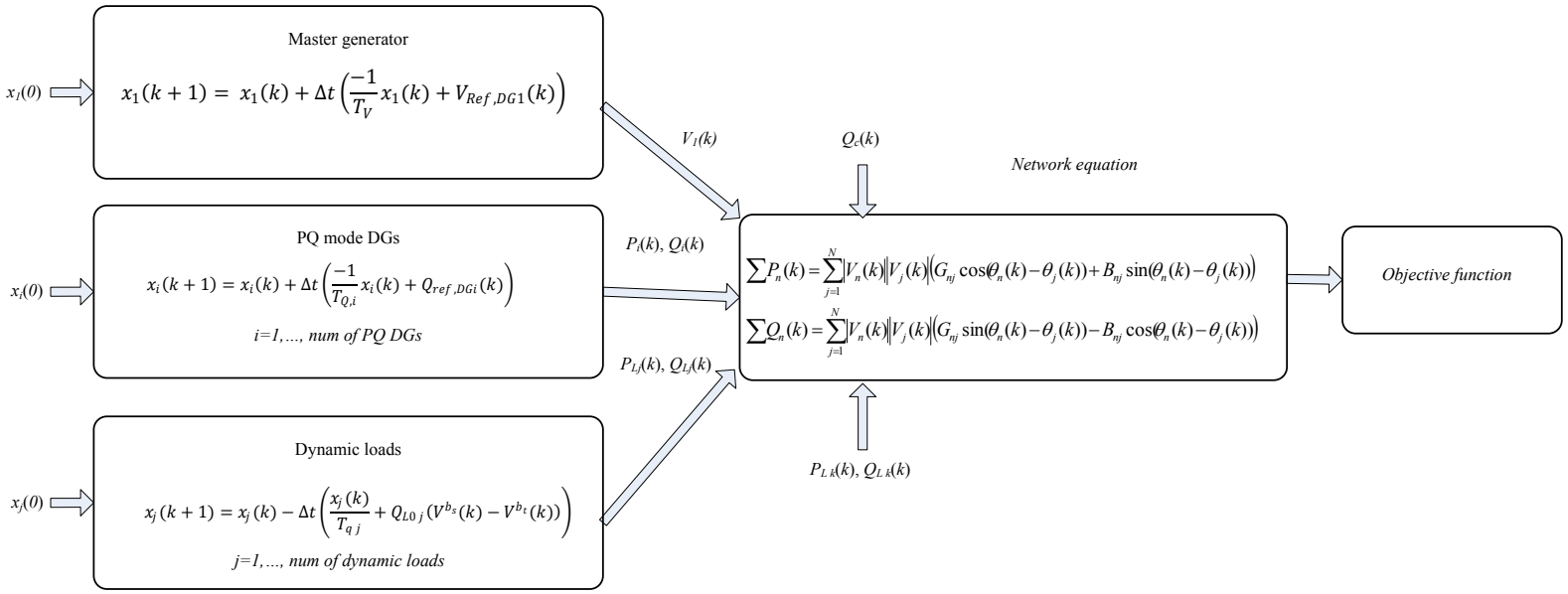

Figure 3-10 Process of calculation of the objective function

In the next part we will discuss how we derived the simplified differential equations defined by (3-28), the algebraic equations defined by (3-29). The differential constraints of the system expressed in (3-28) include the dynamics of the generators and the loads in the power system. These equations are usually expressed in continuous time domain and then discretized and linearized. First of all, we discuss the dynamics of the sources in time domain. Then we will discuss how we simplified and discretized the equations for reactive power control.

3.2.4.1 Sources

Generators should be modeled with appropriate amount of detail for the study. For synchronous generators, the model should include automatic voltage regulator, exciter, turbine and governor [90], [91]. Model of the synchronous generator can be significantly simplified by neglecting stator dynamics and the decrease in accuracy of the model is negligible with such simplification. Hence, neglecting generators stator dynamic is very common in the literature [91]. Following equations model the synchronous generator rotor dynamics and exciter dynamics in continuous time domain.

$$T'_{doi}\frac{dE_{qi}(t)}{dt} = -E'_{qi}(t) - (X_{di} - X'_{di})I_{di}(t) + E_{fdi}(t)$$

$$T'_{qoi}\frac{dE_{di}(t)}{dt} = -E'_{di}(t) - \left(X_{qi} - X'_{qi}\right)I_{qi}(t)$$

$$\frac{d\delta_i(t)}{dt} = \omega_i(t) - \omega_s$$

$$\frac{2H}{\omega_s}\frac{d\omega_i(t)}{dt} = T_{Mi}(t) - E_{di}(t)I_{di}(t) - E_{qi}(t)I_{qi}(t) - \left(X'_{qi} - X'_{di}\right)I_{di}(t)I_{qi}(t) - D_i(\omega_i(t) - \omega_s) \quad (3\text{-}40)$$

$$T_{Ei}\frac{dE_{fdi}(t)}{dt} = -\left(K_{Ei} + S_{Ei}\left(E_{fdi}\right)\right)E_{fdi}(t) + V_{Ri}(t)$$

$$T_{Fi}\frac{dR_{fi}(t)}{dt} = -R_{fi}(t) + \frac{K_{Fi}}{T_{Fi}}E_{fdi}(t)$$

$$T_{Ai}\frac{dV_{Ri}(t)}{dt} = -V_{Ri}(t) + K_{Ai}R_{fi}(t) - \frac{K_{Ai}K_{Fi}}{T_{Fi}}E_{fdi}(t) + K_{Ai}(V_{refi} - V_i(t))$$

δ : rotor angle (radian)

ω : rotor speed (radian per second)

E_{fdi}: exciter voltage on stator base (p.u.)

$\acute{E}_q$ ($\acute{E}_d$): quadrature (direct) axis transient voltage (p.u.).

$I_{qi}(I_{di})$: stator q-axis(d-axis) component of currents (p.u.)

V_i, θ_i: bus voltage magnitude and angle respectively.

$X_{di}, X_{di}{}'$: direct axis synchronous, transient and sub-transient reactance (p.u.) respectively.

$X_{qi}, X_{qi}{}'$: quadrature axis synchronous, transient and sub-transient reactance (p.u.) respectively.

$T_{do}{}'$: direct axis open circuit transient and sub-transient time constants (seconds) respectively.

$T_{qo}{}'$: quadrature axis open circuit transient and sub-transient time constants (seconds) respectively

Also S_E, T_F, K_E are the exciter gains.

Stator algebraic equations are written as follows.

$$\begin{aligned} E'_d(t) - V(t)\sin(\delta(t) - \theta(t)) - R_s I_d(t) + X'_q I_q(t) = 0 \\ E'_q(t) - V(t)\cos(\delta(t) - \theta(t)) - R_s I_q(t) + X'_d I_d(t) = 0 \end{aligned} \tag{3-41}$$

where $R_s$is the stator resistance. In order to derive the network equations, we have to compute the generated active and reactive power of the generator. The generated active power equations are as follows.

$$P_{gen,i}(V_i) = I_{di}(t)V_i(t)\sin(\delta_i(t) - \theta_i(t)) + I_{qi}(t)V_i(t)\cos(\delta_i(t) - \theta_i(t)), \quad i = 1, \dots, m \tag{3-42}$$

where θ_i is the phase of bus *i*. The generated reactive power by this generator is calculated as follows.

$$Q_{gen,i}(V_i) = I_{di}(t)V_i(t)\cos(\delta_i(t) - \theta_i(t)) - I_{qi}(t)V_i(t)\sin(\delta_i(t) - \theta_i(t)), \quad i = 1, \dots, m \tag{3-43}$$

Generators have some physical constraints on the amount of reactive power that they can produce or consume. The reactive capability limits of the generator should be considered in dynamic reactive control studies. The continuous reactive power output

capability is limited by three constraints [90]: the armature current limit, the field current limit, and the end-region heating limit.

Although the model presented in (3-40) to (3-43) may be used as the plant model in reactive studies, using this model as the prediction model makes the computational time of the optimization too long. Thus, the full model may not be used for prediction and simplifications should be applied. We used system identification methods to achieve a simple model of the component that can be used in the prediction model in this research. Since mainly the output voltage of the master generator is important in volt/Var studies, the model should describe the change in output voltage as a result of a change in the input voltage reference. Hence, an input-output model with the reference voltage as the input and estimates the output voltage is enough as the prediction model. In this research, a first order model which is derived based on the step response of the voltage is used as the prediction model for the master generator.

$$\frac{V_{DG\,1}(s)}{V_{Ref,DG1}(s)} = \frac{1}{T_V s + 1} \tag{3-44}$$

where T_V is the time constant which is identified with system identification. For the master DG, the simplified state space equations can be derived by transferring (3-44) into the state space form as follows.

$$\begin{aligned} \dot{x}_1(t) &= \frac{-1}{T_V} x_1(t) + V_{Ref,DG1}(k) \\ V_{DG1}(t) &= \frac{1}{T_V} x_1(t) \end{aligned} \tag{3-45}$$

If more accuracy is needed, especially for small systems with limited number of DGs, a 2nd order model could be used to estimate the voltage. The general form of the 2nd order model is as follows.

$$\frac{V_{DG\,1}(s)}{V_{Ref,DG1}(s)} = \frac{\omega^2}{s^2 + 2\xi\omega s + \omega^2} \tag{3-46}$$

The discretization can be performed using the following formula.

$$\frac{d}{dt}\boldsymbol{x}(t) = \frac{\boldsymbol{x}(k+1) - \boldsymbol{x}(k)}{\Delta t} \tag{3-47}$$

- **Example:**

The master generator state space equation (3-48) can be discretized using (3-47) as follows.

$$x_1(k+1) = x_1(k) + \Delta t\left(\frac{-1}{T_V}x_1(k) + V_{Ref,DG1}(k)\right) \tag{3-48}$$

Figure 3-11 shows the actual generator voltage response and the estimated voltage using 1st and 2nd order models for a step of 0.05 p.u. in the reference voltage of the synchronous generator.

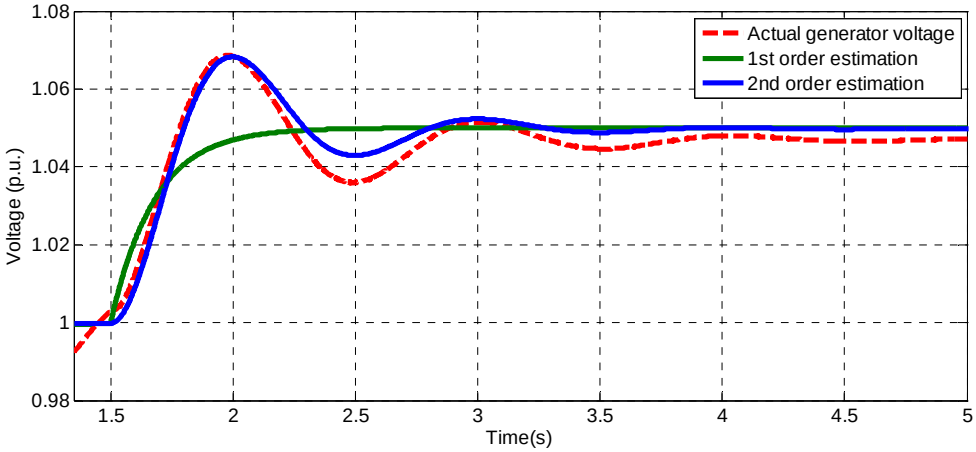

Figure 3-11 Actual synchronous generator voltage and estimated voltage using 1st and 2nd order models

As can be seen in Figure 3-11, the actual response of the generator is smaller than the reference due to saturation and system dynamics; however, the identified model can be adjusted by adding an extra gain on the identified model. Figure 3-12 shows the schematic diagram of a typical controller for DFIG wind generator.

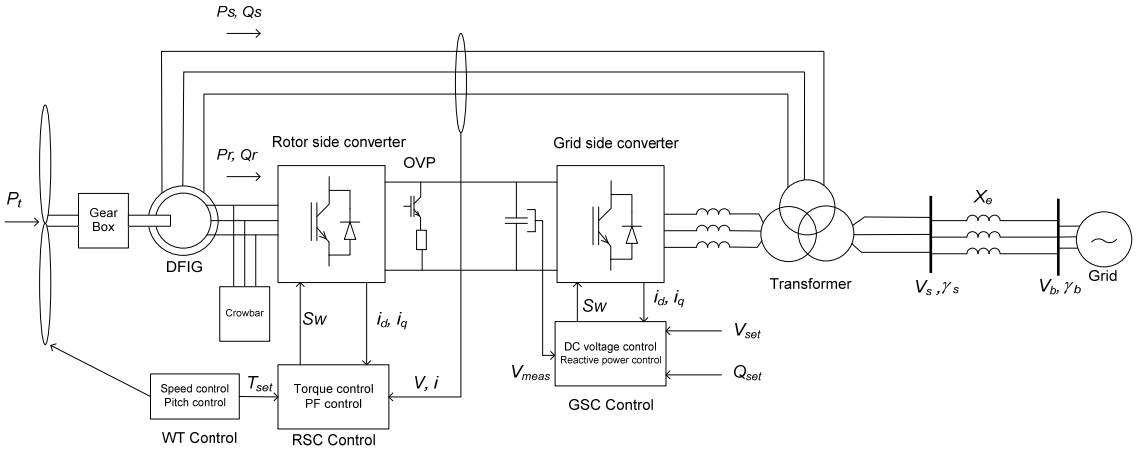

Figure 3-12 Schematic diagram of conventional control of DFIG wind generator

The dynamic equations are obtained from Newton's equations of motion for each mass (rotational speed) and shaft (torsion or twist angle) [92].

$$2H_t \frac{d\omega_t(t)}{dt} = \frac{P_t}{\omega_t} - T_{sh}(t) \tag{3-49}$$

$$\frac{1}{\omega_{elB}} \frac{d\theta_{tw}(t)}{dt} = \omega_t(t) - \omega_r(t) \tag{3-50}$$

$$2H_g \frac{d\omega_r(t)}{dt} = T_{sh}(t) - T_e(t) \tag{3-51}$$

where ω_t and ω_r (p.u.) are the turbine and generator speeds, respectively; θ_{tw} (rad) is the shaft twist angle; H_t and H_g (sec) are the turbine and generator inertias, ω_{elB} (rad/s) is the electrical base speed, P_t (p.u.) is the turbine input power, and T_{sh} and T_e (p.u.) are the shaft and generator torques which are defined as follows.

$$\begin{aligned} T_{sh}(t) &= k\theta_{tw}(t) + c\left(\frac{d\theta_{tw}(t)}{dt}\right) \\ T_e(t) &= \left(\frac{\acute{e}_{qs}(t)}{\omega_s}\right) i_{qs}(t) + \left(\frac{\acute{e}_{0ds}(t)}{\omega_s}\right) i_{ds}(t) \end{aligned} \tag{3-52}$$

where k (p.u./el.rad) and c (p.u.s/el.rad) are the shaft stiffness and damping coefficients.

In this dissertation, the dynamic equations of the DFIG are described in the *dq* frame with the *d*-axis leading. First, following variables are defined.

$$\acute{e}_{qs}(t) = K_{mrr}\omega_s\psi_{dr}$$

$$\acute{e}_{ds}(t) = -K_{mrr}\omega_s\psi_{qr}$$

$$\acute{L_s} = L_{ss} - \frac{{L_m}^2}{L_{rr}} \tag{3-53}$$

$$T_e = \frac{L_{rr}}{R_r}$$

where ψ_{qr} and ψ_{dr} (p.u.) are the rotor q- and d fluxes, R_r (p.u.) is the rotor resistance, $K_{mrr} = L_m/L_{rr}$ and L_{ss}, L_{rr}, and L_m (p.u.) are the stator, rotor, and mutual inductances, respectively.

For balanced and unsaturated conditions, the corresponding p.u. DFIG model is as follows.

$$\frac{\omega_s\acute{L_s}}{\omega_{el}}\frac{di_{qs}(t)}{dt} = -R_1 i_{qs}(t) + \omega_s\acute{L_s} i_{ds}(t) + \frac{\omega_r}{\omega_s}\acute{e}_{qs}(t) - \frac{1}{T_r\omega_s}\acute{e}_{ds}(t) - v_{qs}(t) + K_{mr}v_{qr}(t) \tag{3-54}$$

$$\frac{\omega_s\acute{L_s}}{\omega_{el}}\frac{di_{ds}(t)}{dt} = -R_1 i_{ds}(t) - \omega_s\acute{L_s} i_{qs}(t) + \frac{\omega_r}{\omega_s}\acute{e}_{ds}(t) + \frac{1}{T_r\omega_s}\acute{e}_{qs}(t) - v_{ds}(t) + K_{mr}v_{dr}(t) \tag{3-55}$$

$$\frac{1}{\omega_{el}}\frac{d\acute{e}_{qs}(t)}{dt} = R_2 i_{ds}(t) - \frac{1}{T_r\omega_s}\acute{e}_{qs}(t) + \left(1 - \frac{\omega_r}{\omega_s}\right)\acute{e}_{ds}(t) - K_{mrr}v_{dr}(t) \tag{3-56}$$

$$\frac{1}{\omega_{el}}\frac{d\acute{e}_{ds}(t)}{dt} = -R_2 i_{qs}(t) + \left(1 - \frac{\omega_r}{\omega_s}\right)\acute{e}_{qs}(t) - \frac{1}{T_r\omega_s}\acute{e}_{ds}(t) - K_{mrr}v_{qr}(t) \tag{3-57}$$

where i_{qs} and i_{ds} (p.u.) are the stator q- and d-axis currents, ω_s (p.u.) is the synchronous speed, $\omega_{el} = \omega_{elB}\,\omega_s$, Rs (p.u.) is the stator resistance, and $R_1 = R_s + R_2$ and $R_2 = K_{mrr}^2 R_r$.

The generator dynamic equations could be divided into three parts: stator electrical (3-54), (3-55); rotor electrical (3-56), (3-57) and rotor mechanical (3-51). Similar to synchronous generator, stator transients are neglected without losing accuracy [90]. The ac voltage of the rotor-side converter is dependent on the control objectives of the wind generator. The grid side converter is responsible for controlling the capacitor voltage which is equivalent to sending the maximum active power to the grid and also reactive power control. The controller is usually designed in the converter dq-axis with decoupled control on real and reactive power. The rotor side control is not of interest in this dissertation and more details could be found in [93].

The active and reactive power sharing between the wind generator and the network could be written as follows.

$$P_{grid}(t) = \frac{V_s(t)V_b(t)\sin(\gamma_e(t) - \gamma_b(t))}{X_e}$$

$$Q_{grid}(t) = \frac{{V_s}^2(t) - V_s(t)V_b(t)\cos(\gamma_e(t) - \gamma_b(t))}{X_e} \tag{3-58}$$

Figure 3-13 shows schematic diagram of a typical controller of photovoltaic source [94], [95].

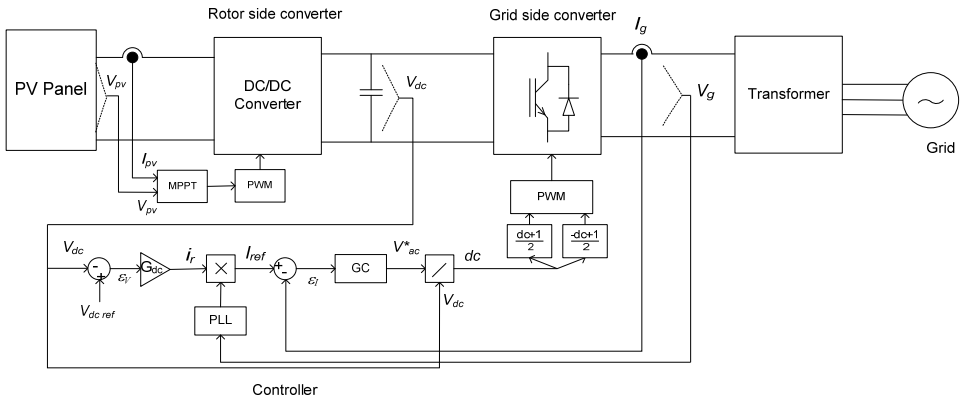

Figure 3-13 Schematic diagram of conventional control of photovoltaic source

The photovoltaic source may be modeled as a current source. In the ideal condition the following equation holds for the output current [96].

$$I(t) = I_{pv,cell} - \underbrace{I_{0,cell}\left[\exp\left(\frac{qV}{akT}\right) - 1\right]}_{I_d} \tag{3-59}$$

where $I_{\mathrm{pv,cell}}$ is the current generated by the incident light which is directly proportional to the Sun irradiation, I_{d} is the Shockley diode equation, $I_{0,\mathrm{cell}}$ is the reverse saturation or leakage current of the diode, q is the electron charge which is equal to $1.60217646 \times 10^{-19}$ C), k is the Boltzmann constant which is equal to $1.3806503 \times 10^{-23}$ J/K, T is the temperature of the *p–n* junction in Kelvin, and a is the diode ideality constant.

The same system identification approach as in (3-44) shall be used to limit the number of dynamic equations for the prediction model. However, since the PV and wind sources are controlled in PQ mode, the dynamic response of reactive power output of the source to changes in reactive power setpoint is required for the prediction model.

$$\frac{Q_{DG\,i}(s)}{Q_{Ref,DG\,i}(s)} = \frac{1}{T_{Q,i}\,s+1} \tag{3-60}$$

where $T_{Q,i}$ is the time constant which is identified with system identification and $Q_{Ref,DG\,i}(s)$ is the reactive power reference and $Q_{DG\,i}(s)$ is the reactive output of *i*'th DG in frequency domain.

For the other DGs in the system, the simplified state space equations are as follows.

$$\begin{aligned} \frac{d}{dt}\,x_i(t) &= \frac{-1}{T_{Q,i}}x_i(t) + Q_{Ref,DGi}(t) \\ Q_{DG,i}(t) &= \frac{1}{T_{Q,i}}\,x_i(t) \end{aligned} \tag{3-61}$$

By simplifying the differential equations, the state space vector of the system presented in (3-38) will change to the following. Figure 3-14 shows the reactive response of a wind DG and the estimated reactive power using system identification when a step in reactive power setpoint is applied to the DG at *t*=0.6s. The time constant, T_Q, for this case is 0.06 seconds.

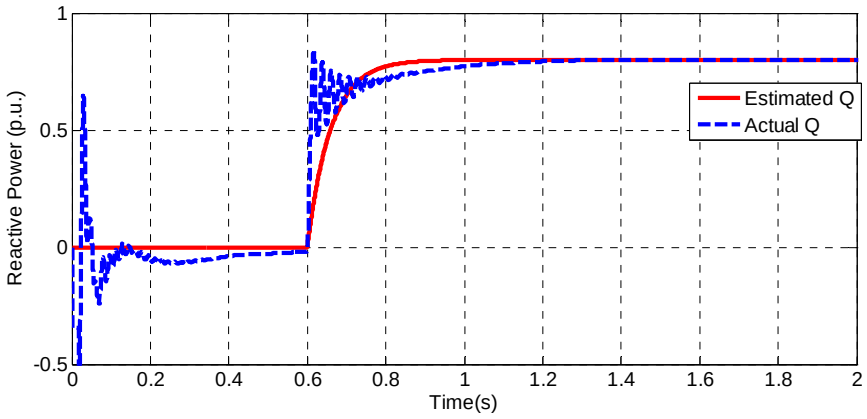

Figure 3-14 Reactive response of a wind DG and the estimated reactive power

$$\boldsymbol{x}(t) = [x_1(t) \dots x_i(t) \dots x_{L_q j}(t) \dots]$$
$$i = 2, \dots, N_{DGs}\ , j = 1, \dots, N_{Load} \tag{3-62}$$

where x_1 is the state of the master generator, x_i's are states of the other sources and $x_{L_q j}$ are the states of the loads.

3.2.4.2 Loads

The power consumed by most of the loads in a power system is voltage dependent. Hence, the load admittance varies dynamically with the voltage which means that when the voltage decreases the consumed power of most of the loads decrease. However, after the disturbance, internal controllers of the most of the loads like thermostats of electrical heating and power electronics converters which regulate the rotational speed of machines restore the power demand of the load. The new power demand usually settles usually below or equal to the pre-disturbance level. This self restoring behavior of the load can be described using second order differential equations as described in [73], [97], [98]. One set of equations model the active power and another set model the reactive power of the load [99].

$$\frac{dx_{L_P\, j}(t)}{dt} = -\frac{x_{L_P\, j}(t)}{T_{P\, j}} + P_{L0\, j}(V^{a_s}(t) - V^{a_t}(t))$$
$$P_{L\, j}(t) = \left(\frac{x_{L_P\, j}(t)}{T_{P\, j}} + P_{L0\, j}(V^{a_t}(t))\right) \tag{3-63}$$

In (3-63), $x_{L_P\, j}(t)$ is an internal state variable which models the load recovery dynamic of the *j*'th load with the time constant T_{pj}. The instantaneous voltage

dependency is expressed by V^{at} and the steady-state voltage dependency is given by V^{as}. In this model, the actual active power P_L can be considered as an output, the absolute value of the load voltage V is the input and $P_{L0\,j}$ is the rated active power of the load. Similarly, the load model for the reactive power is defined as follows.

$$\frac{dx_{L_q\,j}(t)}{dt} = -\frac{x_{L_q\,j}(t)}{T_{q\,j}} + Q_{L0\,j}(V^{b_s}(t) - V^{b_t}(t))$$

$$Q_{L\,j}(t) = \left(\frac{x_{L_q}(t)}{T_{q\,j}} + Q_{L0\,j}(V^{b_t}(t))\right) \tag{3-64}$$

where $Q_{L0\,j}$ is the rated reactive power of the of the j'th load and $Q_{L\,j}(t)$ is the actual reactive power of the j'th load at time t and $T_{q\,j}$ is the load reactive recovery time constant of the j'th load. Figure 3-15 shows the currents and the voltages of the load.

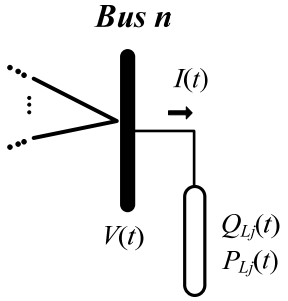

Figure 3-15 Load current and voltage

Linearizing (3-64) around the operating point of the system yields to the following.

$$\frac{dx_{L_q\,j}(t)}{dt} = -\frac{x_{L_q\,j}(t)}{T_{q\,j}} + Q_{L0\,j}[b_s(V^*(t))^{b_s-1} - b_t(V^*(t))^{b_t-1}]\,V(t) \tag{3-65}$$

where, V^* is the operating voltage of the bus connected to the j'th load. Mathematical manipulation of (3-65) yields the following linear transfer function.

$$\Delta Q_{L\,j} = Q_{L0}\left(\frac{C + T_{q\,j}Ds}{T_{q\,j}s + 1}\right)\Delta V \tag{3-66}$$

where the matrices C and D are defined as follows.

$$C = b_s\left(\frac{V^*}{V_0}\right)^{b_s-1} \quad , D = b_t\left(\frac{V^*}{V_0}\right)^{b_t-1} \tag{3-67}$$

where V_0 is the nominal bus voltage and V^* is the operation point of the bus voltage.

It is important to take into account the high reactive power consumed by the motor in the startup [100]. In such a case, the rating of the upstream equipment may need to be rated higher than the steady-state condition and some adaptation should be performed on the controller to alleviate the voltage drop as much as possible [101]. The amount of the voltage dip caused by motor startup is directly related to reactive power need of the motor load during startup. The typical value of the power factor for motors under 1000 HP is about 0.20 [102]. The locked rotor kVA per HP is defined for each NEMA code letter (Appendix A) which can be used to determine the expected startup reactive power need of the motor [103].

In addition, large squirrel-cage induction motors and industrial synchronous motors draw several times their full load current from the supply causing a power factor in the range of 0.15–0.30 lagging during their startup. The actual shape and magnitude of the staring current curve depends on the voltage at the motor terminals, the motor design, and the characteristic of the load which is connected to the motor [104].

3.2.4.3 Network equations for balanced microgrid

The algebraic equations include the network equations of the power system. Network equations can be expressed in either power balance or current balance form. The current balance from is more common in software packages. Figure 3-16 shows the connection of synchronous generator to the rest of the network.

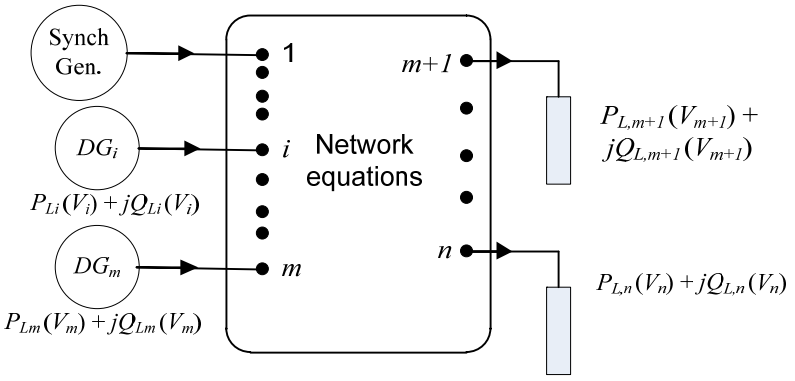

Figure 3-16 Connection of synchronous generators and the rest of the network

In this section, we derive the network equations for balanced and unbalanced networks. If the net apparent power injection into the bus n is defined as $S_n=S_{gn}-S_{dn}$, we can express S_n as follows.

$$S_n(t) = V_n(t)I_n^*(t) \tag{3-68}$$

where V_n is the phasor of the voltage of the bus $V_n(t)=|V_n(t)|\angle\theta_n$ assuming that the voltages are balanced. I_k is net of the injected current into the bus n which can be expressed as follows.

$$I_n(t) = \sum_{j=1}^{N} Y_{nj} V_j(t) \tag{3-69}$$

where, Y_{nj} are the admittance matrix elements and V_j 's are voltages of the buses. Substitution of (3-69) into (3-68) yields to the following equation.

$$S_n(t) = V_n(t)\left(\sum_{j=1}^{N} Y_{nj} V_j(t)\right)^* = V_n(t)\sum_{j=1}^{N} Y_{nj}{}^* V_j{}^*(t) \tag{3-70}$$

If the system is balanced, Y_{nj} which is a complex number can be expressed as $Y_{nj}=G_{nj}+jB_{nj}$ where G_{nj} is the real part and B_{nj} is the imaginary part of the admittance matrix element Y_{nj}. Given that $S_n(t) = P_n(t)+jQ_n(t)$, we can express (3-70) as two equations, one for the real power, P_n, and one for the reactive power, $Q_n(t)$, as follows:

$$\begin{aligned}
\sum P_n(t) &= \sum_{j=1}^{N} |V_n(t)||V_j(t)|\left(G_{nj}\cos(\theta_n(t)-\theta_j(t)) + B_{nj}\sin(\theta_n(t)-\theta_j(t))\right) \\
\sum Q_n(t) &= \sum_{j=1}^{N} |V_n(t)||V_j(t)|\left(G_{nj}\sin(\theta_n(t)-\theta_j(t)) - B_{nj}\cos(\theta_n(t)-\theta_j(t))\right)
\end{aligned} \tag{3-71}$$

The two equations of (3-71) are referred to as power flow equations. Obviously, power flow equations are nonlinear, thus, they need to be linearized in order to be used in the hybrid control scheme. The power flow equations are very complex and are functions of many variables. Thus piecewise linear approximations of any one variable will depend on the value of the other variables. Thus, we seek to simplify the equations based on some observation of the power system.

The resistance of the cables in power system is usually significantly less than the reactance and the x/r ratio is often between 2 and 10. Further, in most of shipboard

power system and MicroGrid applications, the cables are fairly short. Also, angle difference between buses in power systems is directly coupled with the active power flow of the system. Usually, the difference between the voltage angle of the adjacent buses which are connected by a cable is less than 10-15 degrees [105]. It is extremely rare to ever see such angular separation exceed 30 degrees. Figure 3-17 confirms this observation for a MicroGrid which encounters heavy loading and loads changes. As can be seen in Figure 3-17, most of the angles are small and do not experience significant changes during different load conditions of the MicroGrid.

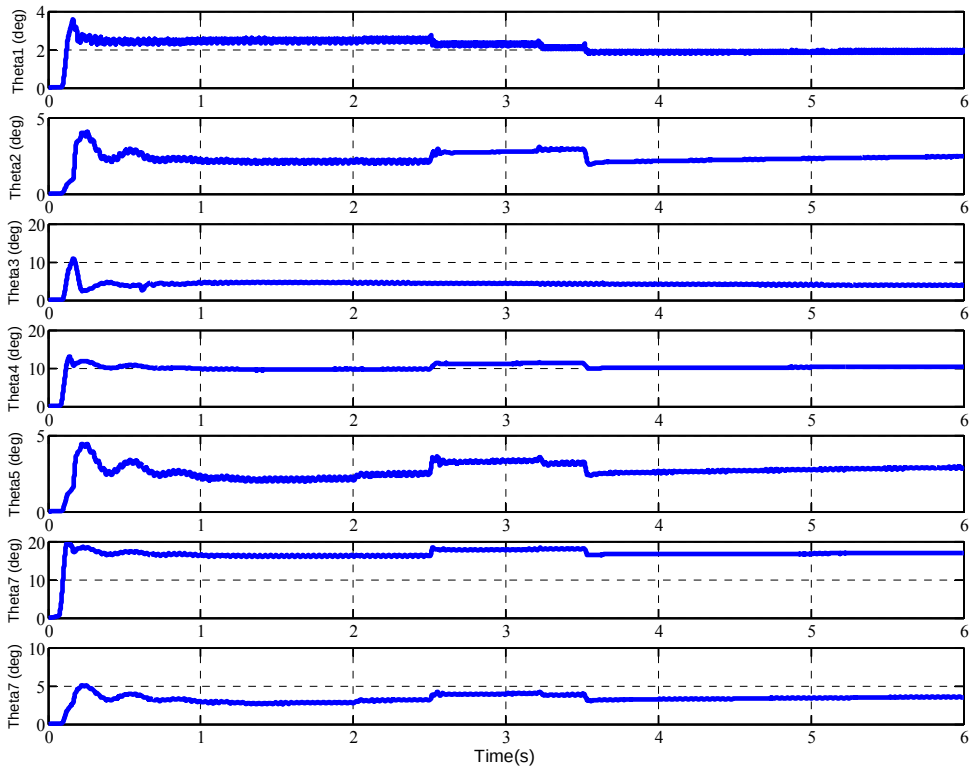

Figure 3-17 Bus angles for a MicroGrid for a case-study with changing loads

This observation can help us to eliminate the trigonometric functions in (3-71) considering the fact that the angular difference across the cables only appears as the argument of the trigonometric functions sine and cosine.

3.2.4.4 Network equations for unbalanced microgrid

Single phase load connected to the buses of the power system or distributed along the lines are the main reason of imbalance in the distribution system. Further, single-phase loads may vary significantly during different times of the day or week, or season [106]. Also, operation of fuses may cause a significant amount of load to be disconnected from the system and substantially increase system imbalance. Large voltage imbalance (>3%) results in high ripple currents on the dc bus of the three-phase inverter-based DERs. These ripples in the current may have a degrading effect on the inverter and the energy sources [106]. It should also be noted that most rotating equipments, specifically generators, are designed to operate with no more than as specified current imbalance (ANSI/NEMA MG 1- 2006). Further, imbalances in the distribution system or load imbalance can cause negative sequence currents. Three-phase DERs and motors have limited negative sequence capability and may be damaged by imbalanced load conditions but the damage can be minimized by the use of a negative sequence current relay. The maximum allowed continuous voltage unbalance in the distribution system is 5% according to NEMA MG1.

It should also be mentioned that in power systems, most voltage unbalance conditions are due to magnitude inequalities while the phase-angles are equal (120° or $2\pi/3$) or nearly equal [1]. If the voltage unbalance is in this category and the inequalities

in the magnitudes is less than 1%, the DER with an inverter interface can compensate for the voltage unbalance by providing different amounts of reactive power on each phase. This local control scheme is beyond the scope of this dissertation and the interested and the interested reader is referred to [1] for more information.

The objective function and power flow equations of the formulation in previous section should be changed for the unbalanced power system.

$$\begin{aligned} J(\boldsymbol{x},\boldsymbol{u},k) = \sum_{k=0}^{N-1}\Bigg\{\sum_{i\in N_t}\Big\{&\left\|{V_i}^{A}(k+t_0|t_0)-V_i^{Nom}\right\|_{\{1,2,\infty\}} \\ &+\left\|{V_i}^{B}(k+t_0|t_0)-V_i^{Nom}\right\|_{\{1,2,\infty\}} \\ &+\left\|{V_i}^{C}(k+t_0|t_0)-V_i^{Nom}\right\|_{\{1,2,\infty\}}\Big\}+\|\boldsymbol{W_1}\Delta\boldsymbol{v}(k)\|_{\{1,2,\infty\}} \\ &+\|\boldsymbol{W_2}\Delta\boldsymbol{\sigma}(k)\|_{\{1,2,\infty\}}\Bigg\} \end{aligned} \tag{3-72}$$

where ${V_i}^{A}(k+t_0|t_0)$, ${V_i}^{B}(k+t_0|t_0)$, ${V_i}^{C}(k+t_0|t_0)$ are the predicted voltage of phase *A*, *B* and *C* of bus *i*, respectively.

The problem is solved subject to differential equations of the sources and loads (3-32), (3-33), (3-34), and the constraints of the system (3-37) and the network equations. The network equations for the unbalanced system are solved in an iteration fashion and each iteration is as follows. A ladder iterative technique can be used to solve the unbalanced power flow [107] , [108]. The power flow equations are as follows for two adjacent nodes.

$$\begin{aligned} \boldsymbol{V_{ABC}}^{\boldsymbol{n}}(k) &= \boldsymbol{a_t}\,\boldsymbol{V_{abc}}^{\boldsymbol{m}}(k)+\boldsymbol{b_t}\,\boldsymbol{I_{abc}}^{\boldsymbol{m}}(k) \\ \boldsymbol{I_{abc}}^{\boldsymbol{n}}(k) &= \boldsymbol{c_t}\,\boldsymbol{V_{abc}}^{\boldsymbol{m}}(k)+\boldsymbol{d_t}\,\boldsymbol{I_{abc}}^{\boldsymbol{m}}(k) \end{aligned} \tag{3-73}$$

Figure 3-18 shows the structure of two adjacent nodes *n*, *m* in the power system.

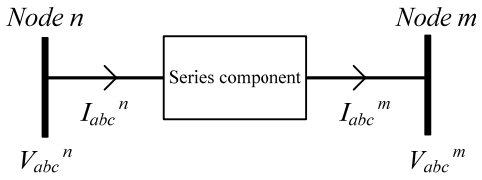

Figure 3-18 A series feeder component

In this formulation the loads and PQ generators should be converted to current as follows.

$$\boldsymbol{I_i}(k) \quad = \left(\frac{\boldsymbol{S_i}(k)}{\boldsymbol{V_i}(k)}\right)^{*} \tag{3-74}$$

The interested reader is referred to [107] for more information about the iterative distribution power flow. Figure 3-19 shows the process of calculation of the objective function in this case.

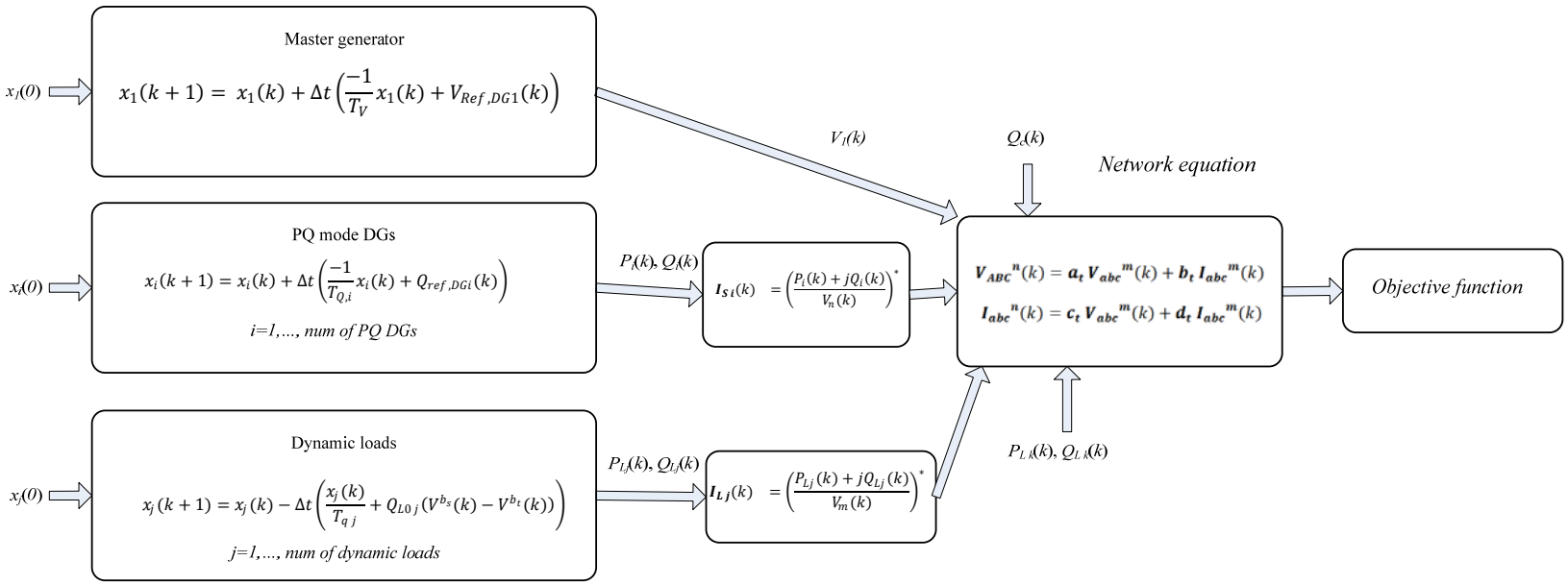

Figure 3-19 Process of calculation of the objective function

In the next part, we will discuss modeling of all the elements in the unbalanced power systems, which are used in the unbalanced power flow.

3.2.4.4.1 Lines

The series impedance of a line section *l* is represented by a 3×3 matrix [109], [107]:

$$\boldsymbol{Z_l} = \begin{bmatrix} z_{aa,l} & z_{ab,l} & z_{ac,l} \\ z_{ab,l} & z_{bb,l} & z_{bc,l} \\ z_{ac,l} & z_{bc,l} & z_{cc,l} \end{bmatrix} \tag{3-75}$$

3.2.4.4.2 Loads

Loads in power system can be modeled as constant current, constant power and constant impedance and either one can be *Y*-connected or Δ-connected. Assuming that load *Li* is connected to bus *i*, V_i is the three-phase voltage in bus *i*, I_{Li} is three phase load current, then following load models can be used in the distribution power flow [108]:

1) Grounded-*Y,* constant power load

$$\boldsymbol{I_{Li}}(k) = \left(\frac{\boldsymbol{S_{Li}}(k)}{\boldsymbol{V_i}(k)}\right)^* \tag{3-76}$$

where,

$$\boldsymbol{S_{Li}}(k) = \begin{bmatrix} S_{a,Li}(k) & 0 & 0 \\ 0 & S_{b,Li}(k) & 0 \\ 0 & 0 & S_{c,Li}(k) \end{bmatrix} \tag{3-77}$$

2) Grounded-*Y,* constant current load

$$\boldsymbol{I_{Li}}(k) = [I_{a,Li} \quad I_{b,Li} \quad I_{c,Li}]^T \tag{3-78}$$

3) Grounded-*Y,* constant impedance load

$$\boldsymbol{I_{Li}}(k) = \boldsymbol{Y_{Li}}\boldsymbol{V_i}(k) \tag{3-79}$$

where,

$$\boldsymbol{Y_{Li}} = \begin{bmatrix} y_{a,Li} & 0 & 0 \\ 0 & y_{b,Li} & 0 \\ 0 & 0 & y_{c,Li} \end{bmatrix} \tag{3-80}$$

4) Ungrounded-Δ, constant power

$$\boldsymbol{I_{Li}}(k) = \boldsymbol{T}^T\left[\boldsymbol{S_{Lppi}}(\boldsymbol{TV_i(k)})^{-1}\right]^* \tag{3-81}$$

where,

$$\boldsymbol{T} = \begin{bmatrix} 1 & -1 & 0 \\ 0 & 1 & -1 \\ -1 & 0 & 1 \end{bmatrix}, \qquad \boldsymbol{S_{Lppi}}(k) = \begin{bmatrix} S_{a,Li}(k) & 0 & 0 \\ 0 & S_{b,Li}(k) & 0 \\ 0 & 0 & S_{c,Li}(k) \end{bmatrix} \tag{3-82}$$

5) Ungrounded-Δ, constant current

$$\boldsymbol{I_{Li}}(k) = T^T\boldsymbol{I_{Lppi}}(k) \tag{3-83}$$

where $\boldsymbol{I_{Lppi}}(k) = [I_{ab,Li}(k) \quad I_{bc,Li}(k) \quad I_{ca,Li}(k)]^T$.

6) Ungrounded-Δ, constant impedance

$$\boldsymbol{I_{Lppi}}(k) = [I_{ab,Li}(k) \quad I_{bc,Li}(k) \quad I_{ca,Li}(k)]^T \tag{3-84}$$

where,

$$\boldsymbol{Y_{Lppi}} = \begin{bmatrix} y_{ab,Li} & 0 & 0 \\ 0 & y_{bc,Li} & 0 \\ 0 & 0 & y_{ca,Li} \end{bmatrix}, \quad \boldsymbol{V_{ppi}}(k) = \begin{bmatrix} V_{ab,i}(k) \\ V_{bc,i}(k) \\ V_{ca,i}(k) \end{bmatrix} \tag{3-85}$$

3.2.4.4.3 Shunt capacitors

Similar to loads, shunt capacitors can be *Y* connected or Δ connected and can be modeled exactly the same as *Y* or Δ connected constant impedance load, respectively.

3.2.4.4.4 Transformers

A general three-phase transformer model is shown in Figure 3-20, where V_p represents primary voltage, V_s represents secondary voltage, Y_m represents core losses, and Z_t represents leakage impedance.

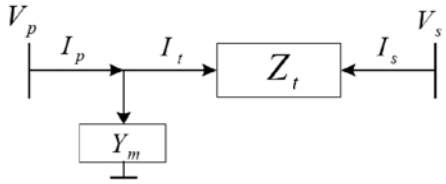

Figure 3-20 Transformer model

All types of three-phase transformers, such as Δ - Y_0 transformer, *Y* - Δ transformer or Y_0-Y_0 transformer can be modeled in this framework [110].

3.2.4.4.5 Distributed energy sources

Distributed energy sources are classified as *PQ* or *PV* depending on their operation mode. If the unit is operating in *PQ* mode, the unit model is identical with constant

power load, except that the current is being injected into the bus instead of being drawn from the bus. However, if the unit is in *PV* mode, the connected bus is modeled as a *PV* bus. In this case, if the computed reactive power generation is out of the reactive generation limits of the unit, then the node can no longer be modeled as a *PV* bus. Thus, the unit acts as a *PQ* unit and the reactive power generation of the unit is set to the maximum limit.

The unbalanced power flow (3-73) needs to be solved iteratively until the voltages and currents converge to the solution. The iterative power flow takes a large amount of computation time even for the static system analysis. Further, the power flow should be solved by the optimization and control algorithm. Thus, we seek to find a linear relation between the variables of the power system and the bus voltages. The linear relation can be introduced by sweeping each of the power system variables in their complete possible range. The sweeping of the parameters can be performed individually which means for example $V_{DG1}(k)$ can be swept from 0.95 to 1.05 and the sensitivity of the bus voltages of the system are calculated to a change in $V_{DG1}(k)$. If for example the linearization yields to two sections for $V_{DG1}(k)$ for a bus voltage of bus *m*, then we have the following two equations.

$$\begin{aligned} &[0.95 \quad 0.95 \quad 0.95]^T < \boldsymbol{V_{DG1}}(k) < [1.02 \quad 1.02 \quad 1.02\ ]^T \rightarrow \boldsymbol{V_m}(k) \\ &\qquad = \boldsymbol{p}_{1,m}^{1}\, \boldsymbol{V_{DG1}}(k) + k \\ &[1.02 \quad 1.02 \quad 1.02]^T < \boldsymbol{V_{DG1}}(k) < [1.05 \quad 1.05 \quad 1.05\ ]^T \rightarrow \boldsymbol{V_m}(k) \\ &\qquad = \boldsymbol{p}_{1,m}^{2}\, \boldsymbol{V_{DG1}}(k) + k \end{aligned} \tag{3-86}$$

Next, $\boldsymbol{V_{DG1}}(k)$ is fixed to a value inside one section and another parameter is swept within its range. This method has an inherent error since the parameters are not changing together. Also, the number of sections can increase fast since each section can get divided multiple times for the next parameter sweeps. The user can decide the accuracy of estimation of the voltages by limiting the total number of sections in each step.

Another method is to sweep the parameters all together and try to find the sections based on the bus voltages. Then a hybrid identification method like the one presented [111] can be used to determine the clusters and the linear regressors. This method usually yields to results that are more accurate especially if the number of clusters is chosen reasonable based on experience with the system. We will discuss the hybrid linear identification method for piecewise linearization with more detail in the next section.

Both of these linearization methods can take several hours depending on the size of the system and number of the variables but the whole process is performed offline. Once the linear relation is driven, it can be used in the reactive power optimization to calculate the cost function.

$$|\boldsymbol{V_m}(k)| = \boldsymbol{p}_{1,m}^{I_i}\,|\boldsymbol{V_{DG1}}(k)| + \sum_{i=2}^{N_{DG}}\left(\boldsymbol{p}_{i,m}^{I_i}\boldsymbol{Q_{DG\ i}}(k)\right) + \sum_{j=1}^{N_{DL}}\left(\boldsymbol{p}_{j+N_{DG},m}^{I_i}\boldsymbol{Q_{L\,j}}(k)\right) + \sum_{c=1}^{N_C}\left(\boldsymbol{p}_{vc+N_{DG}+N_{DL},m}^{I_i}\,\boldsymbol{Q_c}(k)\right) + \boldsymbol{p}_{N_{DG}+N_{DL}+N_C+1,m}^{I_i} \tag{3-87}$$

where $\boldsymbol{p}_{i,m}^{I_i}$ is a regressor matrix.

$$\boldsymbol{p}_{i,m}^{I_i} = \begin{bmatrix} p_{i,m}^{I_i,A} & 0 & 0 \\ 0 & p_{i,m}^{I_i,B} & 0 \\ 0 & 0 & p_{i,m}^{I_i,C} \end{bmatrix}$$

$$|\boldsymbol{V_m}(k)| = \begin{bmatrix} {V_m}^A(k) \\ {V_m}^B(k) \\ {V_m}^C(k) \end{bmatrix}, |\boldsymbol{V_{DG1}}(k)| = \begin{bmatrix} {V_{DG1}}^A(k) \\ {V_{DG1}}^B(k) \\ {V_{DG1}}^C(k) \end{bmatrix}, \tag{3-88}$$

$$\boldsymbol{Q_{DG\,i}}(k) = \begin{bmatrix} {Q_{DG\,i}}^A(k) \\ {Q_{DG\,i}}^B(k) \\ {Q_{DG\,i}}^C(k) \end{bmatrix}, \boldsymbol{Q_{L\,j}}(k) = \begin{bmatrix} {Q_{L\,j}}^A(k) \\ {Q_{L\,j}}^B(k) \\ {Q_{L\,j}}^C(k) \end{bmatrix}$$

It is not necessary to estimate the bus angle to calculate the objective function of the optimization problem. However, the bus voltage angle is required in order to calculate the line current to make sure the current does not pass the maximum current limit. Distribution systems are usually initially designed with a large enough line current margins. Thus, the line currents usually do not pass the maximum line ampacity during normal operation of the system with no faults. However, as the demand for power increases in time, more loads get connected to the distribution system and this increase in loading puts more stress on some of the lines. Therefore, it is necessary for the volt/Var controller to make sure that the current of those specific lines do not pass the ampacity of the line and preferably VVC should try to reduce the stress on the line. Thus, to reduce the computation time of the VVC controller, it is not necessary to estimate all the bus voltage angles of the power system. The bus voltage angle of the buses that are connected to the stressed lines can be estimated with the same linear approximation presented for the bus voltage magnitude. The only difference is that the

bus angle is usually coupled with the active power of the loads and generators and has small coupling with bus voltage magnitude.

3.2.5 Piecewise Linearization

The voltages of the buses in the system can be derived following the piecewise linearization technique discussed in [111]. Figure 3-21 depicts the piecewise linearization algorithm which starts with classification of data points into *s* modes [112]. Then a min squared error algorithm is used to estimate linear hyperplanes that fits the data points. The number of modes, *s*, is provided as an estimate by the user based on the data points to achieve maximum accuracy. The algorithm presented in [111] estimates the regions, χ_i's with linear borders.

The state space equations of the power system could be presented in the piecewise linear form as follows.

$$\boldsymbol{x}(k+1) = \begin{cases} \boldsymbol{A_1 x}\ \ (k) + \boldsymbol{B}_1\, \boldsymbol{u}(k) & \text{if} \quad \boldsymbol{x}(k), \boldsymbol{u}(k) \in \chi_1 \\ \vdots & \\ \boldsymbol{A_1 x}\ \ (k) + \boldsymbol{B}_s\, \boldsymbol{u}(k) & \text{if} \quad \boldsymbol{x}(k), \boldsymbol{u}(k) \in \chi_s \end{cases} \tag{3-89}$$

Equation (3-89) is referred to as piecewise linear dynamic equations of the system. The general piece-wise linear time-invariant dynamic system can be described as follows [79].

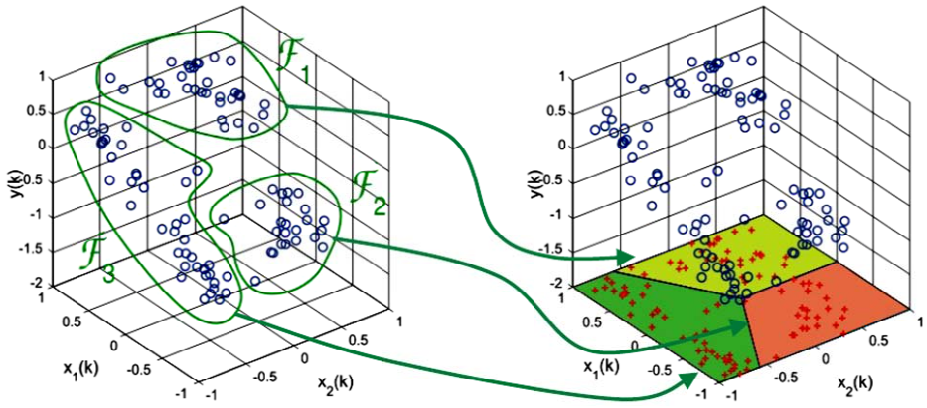

a)

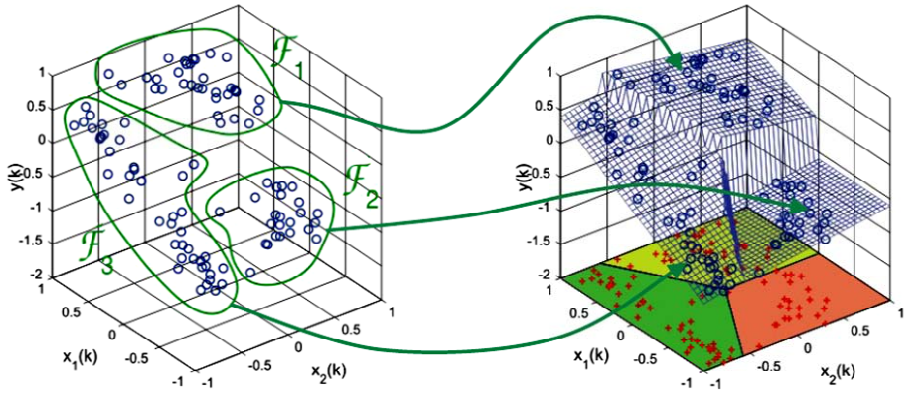

b)

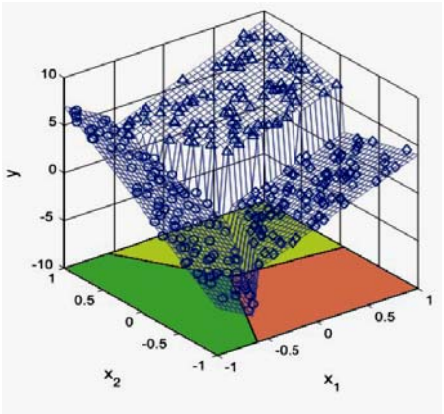

c)

Figure 3-21 Sample result of classification algorithm on 2 dimension data [112]

$$\boldsymbol{x}(k+1) = \begin{cases} \boldsymbol{A_1 x}(k) + \boldsymbol{B_1 u}(k) & if\ \delta_1(k) = 1 \\ \vdots & \\ \boldsymbol{A_s x}(k) + \boldsymbol{B_s u}(k) & if\ \delta_s(k) = 1 \end{cases} \tag{3-90}$$

where $\delta_i(k) \in \{0,1\}$, are 0-1 variables which satisfy the following exclusive-or condition.

$$\oplus_{i=1}^{s}[\delta_i(k) = 1] \tag{3-91}$$

Assuming $\mathcal{C}$ is a bonded polytope, system (3-90) is completely well-posed if and only if $\mathcal{C}$ can be partitioned into *s* non-overlapping parts such that the union of the partitions is equal to $\mathcal{C}$ as follows.

$$\begin{gathered} \mathcal{C}_i \cap \mathcal{C}_j = \emptyset, \ \ \forall i \neq j \\ \cup_{i=1}^{s} \mathcal{C}_i = \mathcal{C} \end{gathered} \tag{3-92}$$

Note that assuming that $\mathcal{C}$ is bounded polytope is not restrictive for power systems because continuous inputs and states are usually bounded by physical reasons in a power system, and logical input/state components are intrinsically bounded. The δ_i's are defined as follows.

$$[\delta_i(k) = 1] \leftrightarrow \left[\begin{bmatrix} x \\ u \end{bmatrix} \epsilon\, \mathcal{C}_i\right] \tag{3-93}$$

Several nonlinear models can be approximated by a model of the form (3-90), although this approximation capability is limited for computational reasons by the number *s* of logical variables.

Knowing that the sets $\mathcal{C}_i$ are polytopes of the form $\mathcal{C}_i = \left\{\begin{bmatrix} x \\ u \end{bmatrix} : S_i^j x + R_i^j u > T_i^j\right\}$, (3-93) could be rewritten as follows.

$$[\delta_i(k) = 0] \leftrightarrow \bigvee_{j=1}^{n_i} [S_i x + R_i^j u > T_i^j] \tag{3-94}$$

where S_i^j denotes the *j*th row of S_i. Equation (3-94) is not easy to solve; however, solving this equation is equivalent to solving (3-91) and (3-92).

$$\begin{aligned} S_i x(k) + R_i \ u(k) - T_i \ &\leq M_i^*[1 - \delta_i(k)] \\ \sum_{i=1}^{s} \delta_i(k) &= 1 \end{aligned} \tag{3-95}$$

where, $M_i^* \triangleq \text{Max}_{x \in \mathcal{C}} \ S_i x(k) + R_i \ u(k) - T_i$. Equation (3-90) can be rewritten as follows.

$$\boldsymbol{x}(k+1) = \sum_{i=1}^{s} [\boldsymbol{A_i x}(k) + \boldsymbol{B_i u}(k)] \, \delta_i(k) \tag{3-96}$$

Equation (3-96) is nonlinear and involves multiplication between logical variables, states, inputs. However, we can translate (3-96) into equivalent mixed-integer linear inequalities. We can start by the following change of variables.

$$\boldsymbol{x}(k+1) = \textstyle\sum_{i=1}^{s} \boldsymbol{z_i}(k) \quad , \quad \boldsymbol{z_i}(k) = [\boldsymbol{A_i x}(k) + \boldsymbol{B_i u}(k)]\delta_i(k) \tag{3-97}$$

And let's define the following min and Max $m = [m_1 \ldots m_n]^T$, $M = [M_1 \ldots M_n]^T$ vectors as follows.

$$M_j \triangleq \text{Max}_{i=1,..,s} \left\{ \text{Max}_{\begin{bmatrix} x \\ u \end{bmatrix} \epsilon C} \quad A_i^j x + B_i^j u \right\}$$
$$m_j \triangleq \min_{i=1,..,s} \left\{ \text{Max}_{\begin{bmatrix} x \\ u \end{bmatrix} \epsilon C} \quad A_i^j x + B_i^j u \right\} \tag{3-98}$$

M and m are finite numbers which can be calculated or estimated. Thus, (3-96) is equivalent to the following set of equations.

$$z_i(k) \leq M\delta_i(k)$$
$$z_i(k) \geq m\delta_i(k)$$
$$z_i(k) \leq A_i x(k) + B_i u(k) - m(1 - \delta_i(k)) \tag{3-99}$$
$$z_i(k) \geq A_i x(k) + B_i u(k) - M(1 - \delta_i(k))$$

3.2.5.1 Example 1 – 2 bus system

This example is formulating the MPC problem for a simple system with one source and one load depicted in Figure 3-22.

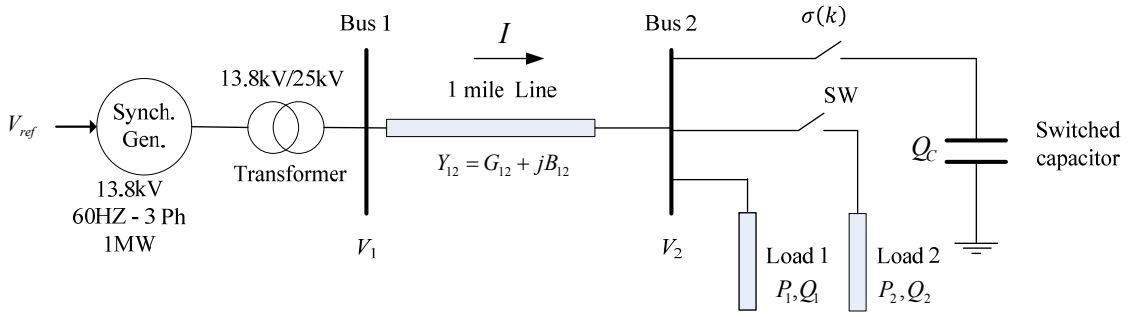

Figure 3-22 Studies on a simple system

The objective function of voltage control for this system is as follows.

$$J(\boldsymbol{x},\boldsymbol{u},k)=\sum_{k=0}^{N-1}\left\{\|V_2(k+t|t)-V_2^{Nom}\|_{\{1,\infty\}}+\left\|W_1\Delta v_{ref}(k)\right\|_{\{1,\infty\}}\right\} \tag{3-100}$$

In addition, the optimization problem is subject to the following simplified differential algebraic equations. In this example we discretized the system assuming that the step time of the system is 1. Assuming that the system has two working conditions only, the DAE equations of the system can be written as follows. In the first operating condition, load 2 is not connected to the system. The system equations in this case are as follows.

$$\begin{aligned} x_1(k+1)&=\frac{-1}{T_V}x_1(k)+v_{ref}(k)\\ V_1(k)&=\frac{1}{T_V}x_1(k)\end{aligned} \tag{3-101}$$

$$\begin{aligned} &P_1(k)=\left|V_2(k)\right|\left|V_1(k)\right|\left(G_{12}\cos(\theta_1(k)-\theta_2(k))+B_{12}\sin(\theta_1(k)-\theta_2(k))\right)\\ &\sigma(k)Q_C(k)+Q_1(k)=\\ &\left|V_2(k)\right|\left|V_1(k)\right|\left(G_{12}\sin(\theta_1(k)-\theta_2(k))-B_{12}\cos(\theta_1(k)-\theta_2(k))\right)\end{aligned} \tag{3-102}$$

In the second operating condition, the equations could be written as follows.

$$\begin{aligned} x_1(k+1)&=\frac{-1}{T_V}x_1(k)+v_{ref}(k)\\ V_1(k)&=\frac{1}{T_V}x_1(k)\end{aligned} \tag{3-103}$$

$$\begin{aligned} &P_1(k)+P_2(k)=\left|V_2(k)\right|\left|V_1(k)\right|\left(G_{12}\cos(\theta_1(k)-\theta_2(k))+B_{12}\sin(\theta_1(k)-\theta_2(k))\right)\\ &\sigma(k)Q_C(k)+Q_1(k)+Q_2(k)=\\ &\left|V_2(k)\right|\left|V_1(k)\right|\left(G_{12}\sin(\theta_1(k)-\theta_2(k))-B_{12}\cos(\theta_1(k)-\theta_2(k))\right)\end{aligned} \tag{3-104}$$

Using the auxiliary variable $\delta(k)$, we have the following equations for the two modes of the system.

$$[\delta(k)=0] \leftrightarrow \begin{cases} x_1(k+1) = a_1 x_1(k) + b_1 v_{ref}(k) \\ V_1(k) = c_{11} x_1(k) + c_{12}\sigma(k) \\ V_2(k) = d_{11} x_1(k) + d_{12}\sigma(k) \end{cases} \tag{3-105}$$

$$[\delta(k)=1] \leftrightarrow \begin{cases} x_1(k+1) = a_2 x_1(k) + b_2 v_{ref}(k) \\ V_1(k) = c_{21} x_1(k) + c_{22}\sigma(k) \\ V_2(k) = d_{21} x_1(k) + d_{22}\sigma(k) \end{cases} \tag{3-106}$$

In this case the differential equation of the system does not change which means, $a_1 = a_2$ and $b_1 = b_2$. This means that the system could be written in the following form.

$$\begin{gathered} x_1(k+1) = a_1 x_1(k) + b_1 v_{ref}(k) \\ V_1(k) = (c_{11} x_1(k) + c_{12}\sigma(k))(1-\delta(k)) + (c_{21} x_1(k) + c_{22}\sigma(k))\delta(k) \\ V_2(k) = \big(d_{11} x_1(k) + d_{12}\sigma(k)\big)(1-\delta(k)) + \big(d_{21} x_1(k) + d_{22}\sigma(k)\big)\delta(k) \end{gathered} \tag{3-107}$$

It should be noted that $\delta(k)$ is an auxiliary variable that models the two working conditions of the system and not a switch controlled by the user. However, $\sigma(k)$ is a switch controlled by the user and is a discrete input to the system. The only continuous control input in this case is the $v_{ref}(k)$ of the master generator.

In this case, the problem is subject to the following inequality constraints.

$$\begin{gathered} 0.95 \le |V_b(k)| \le 1.05 \qquad b = 1,2 \\ \frac{|V_1(k) - V_2(k)|}{|Z_{cl}|} = |I(k)| \le 1 \end{gathered} \tag{3-108}$$

The load parameters of this system are presented in Table 4.

Table 4 Load and capacitor parameters of the 2 bus system

Parameter	Value
P_1	500 kW
Q_1	300 kVar
P_2	400 kW
Q_2	100 kVar
Q_c	150kVar

The system parameters are given in Table 5.

Table 5 Parameters of the 2 bus system

Parameter	Value	Parameter	Value
a_1	-0.33	c_{22}	0
b_1	2	d_{11}	2.95
c_{11}	3	d_{12}	0.0241
c_{12}	0	d_{21}	2.95
c_{21}	3	d_{22}	0.0225

Figure 3-23 depicts the voltage of the buses in the system. Figure 3-24 shows the control inputs to the system.

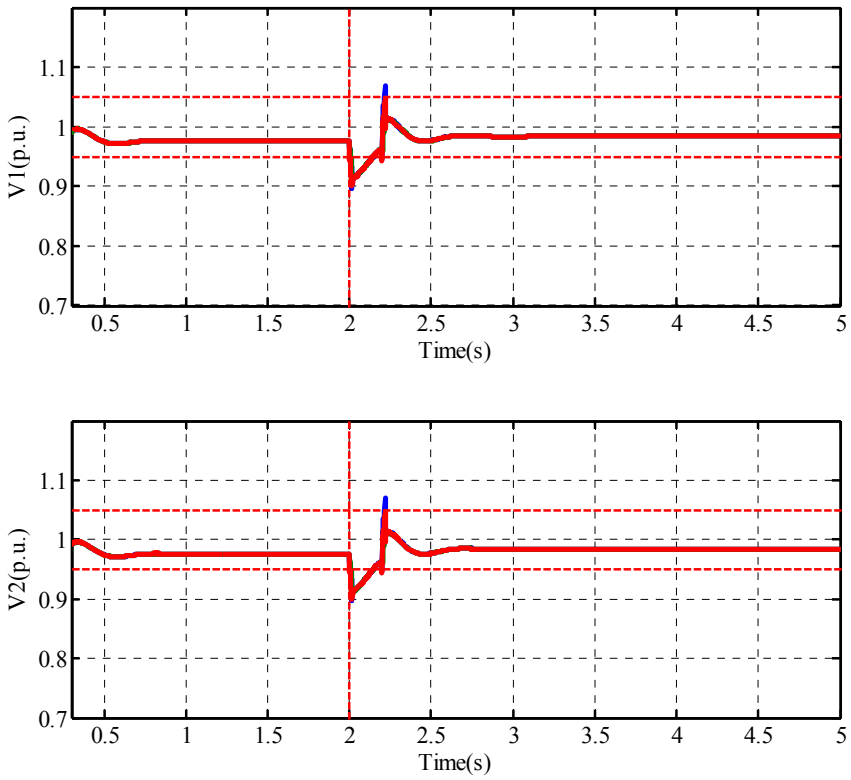

Figure 3-23 Bus voltages of the simple 2 bus system

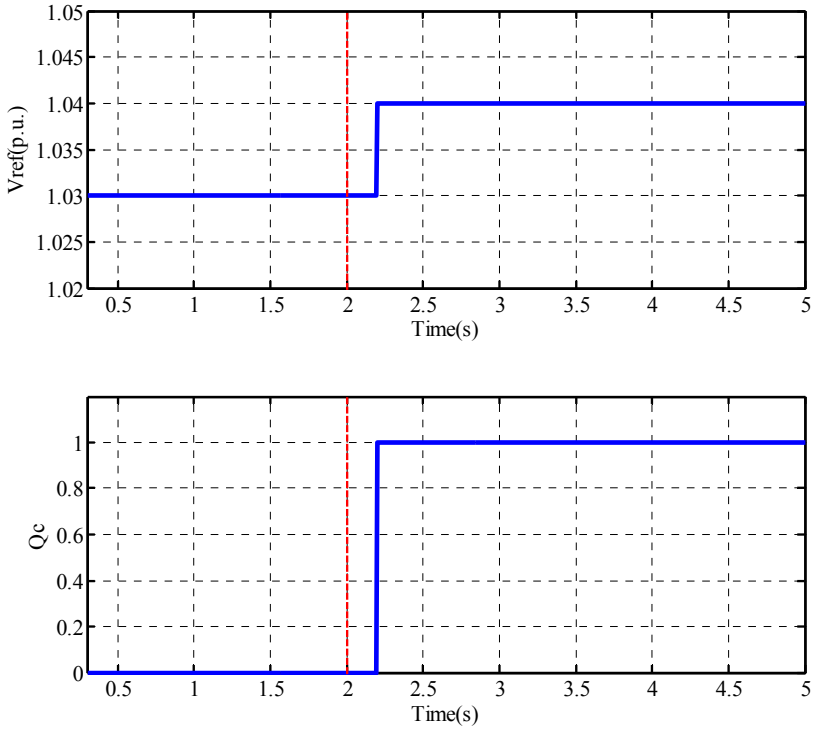

Figure 3-24 Control inputs to the simple 2 bus system

3.2.5.2 Example 2 - IEEE 4 bus system with no capacitor banks

The IEEE 4 bus system shown in Figure 3-25 was studied in this example as a simple test system for the dynamic reactive power control. This system was consisted of a synchronous DG connected to bus 1 which was considered as the master generator. In addition, a wind DG was connected to bus 4 which was controlled as a PQ generator. Two capacitor banks were connected to bus 4 for reactive voltage support. It is assumed that the capacitor banks are disconnected in example 2.

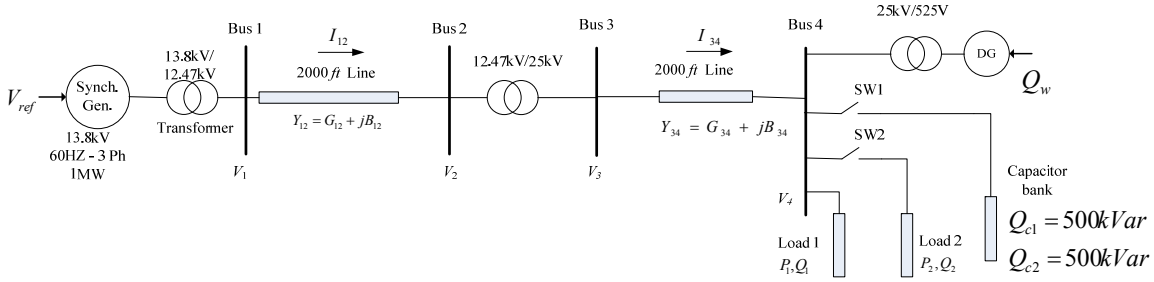

Figure 3-25 Control inputs to the simple 4 bus system

The differential equations in the predictive model include differential equations of the DGs and the dynamic load. Thus, the simplified state space equations include three state variables for this system. The state space model of the components is presented as follows.

DG equations:

$$x_1(k+1) = x_1(k) + \Delta t\left(\frac{-1}{T_V}x_1(k) + V_{Ref}(k)\right) \tag{3-109}$$

$$|V_1(k)| = \frac{1}{T_V}x_1(k)$$

$$x_2(k+1) = x_2(k) + \Delta t\left(\frac{-1}{T_{Q,2}}x_2(k) + Q_{Ref,DG2}(k)\right) \tag{3-110}$$

$$Q_{DG2}(k) = \frac{1}{T_{Q,2}}\,x_2(k)$$

Dynamic load:

$$x_3(k+1) = x_3(k) - \Delta t\left(\frac{x_3(k)}{T_{q,3}} + Q_{L0}\left(V_4{}^{b_s}(k) - V_4{}^{b_t}(k)\right)\right) \tag{3-111}$$

$$Q_L(k) = \left(\frac{x_3(k)}{T_{q,3}} + Q_{L0}\left({V_4}^{b_t}(k) \right) \right)$$

The network equations could be written in the following general form.

$$\sum P_n(k) = \sum_{j=1}^{4} |V_n(k)||V_j(k)| \left(G_{kj}\cos(\theta_n - \theta_j) + B_{nj}\sin(\theta_n - \theta_j) \right) \tag{3-112}$$

$$\sum Q_n(k) = \sum_{j=1}^{4} |V_n(k)||V_j(k)| \left(G_{kj}\sin(\theta_n - \theta_j) - B_{nj}\cos(\theta_n - \theta_j) \right)$$

The network equations (3-112) can be expanded for this system as follows.

For bus 2:

$$\begin{aligned} 0 = {} & |V_1(k)||V_2(k)|(G_{12}\cos(\theta_2 - \theta_1) + B_{12}\sin(\theta_2 - \theta_1)) \\ & + |V_2(k)||V_3(k)|(G_{23}\cos(\theta_2 - \theta_3) + B_{23}\sin(\theta_2 - \theta_3)) \\ 0 = {} & |V_1(k)||V_2(k)|(G_{12}\sin(\theta_2 - \theta_1) - B_{12}\cos(\theta_2 - \theta_1)) \\ & + |V_2(k)||V_3(k)|(G_{23}\sin(\theta_2 - \theta_3) - B_{23}\cos(\theta_2 - \theta_3)) \end{aligned} \tag{3-113}$$

For bus 3:

$$\begin{aligned} 0 = {} & |V_3(k)||V_2(k)|(G_{23}\cos(\theta_3 - \theta_2) + B_{23}\sin(\theta_3 - \theta_2)) \\ & + |V_3(k)||V_4(k)|(G_{34}\cos(\theta_3 - \theta_4) + B_{23}\sin(\theta_2 - \theta_3)) \\ 0 = {} & |V_3(k)||V_2(k)|(G_{23}\sin(\theta_3 - \theta_2) - B_{23}\cos(\theta_3 - \theta_2)) \\ & + |V_3(k)||V_4(k)|(G_{34}\sin(\theta_3 - \theta_4) - B_{34}\cos(\theta_3 - \theta_4)) \end{aligned} \tag{3-114}$$

For bus 4:

$$P_l(k) = |V_4(k)||V_3(k)|(G_{34}\cos(\theta_4 - \theta_3) + B_{34}\sin(\theta_4 - \theta_3))$$
$$Q_l(k) + Q_{DG2}(k) = |V_4(k)||V_3(k)|(G_{34}\sin(\theta_4 - \theta_3) - B_{34}\cos(\theta_4 - \theta_3)) \quad (3\text{-}115)$$

The network equations could be simplified with basic mathematical manipulations as follows.

$$|V_2(k)| = \frac{-|V_4(k)|(G_{34}\sin(\theta_3 - \theta_4) - B_{34}\cos(\theta_3 - \theta_4))}{(G_{23}\sin(\theta_3 - \theta_2) - B_{23}\cos(\theta_3 - \theta_2))} \quad (3\text{-}116)$$

$$|V_3(k)| = \frac{-|V_1(k)|(G_{12}\sin(\theta_2 - \theta_1) - B_{12}\cos(\theta_2 - \theta_1))}{(G_{23}\sin(\theta_2 - \theta_3) - B_{23}\cos(\theta_2 - \theta_3))}$$

$$|V_4(k)| = \frac{Q_L(k) + Q_{DG2}(k)}{|V_3(k)|(G_{34}\sin(\theta_4 - \theta_3) - B_{34}\cos(\theta_4 - \theta_3))}$$

Linearizing the network equations results in the following set of equations.

$$|V_2(k)| = |V_4(k)|\ \frac{-(G_{34}\sin(\theta_3 - \theta_4) - B_{34}\cos(\theta_3 - \theta_4))}{(G_{23}\sin(\theta_3 - \theta_2) - B_{23}\cos(\theta_3 - \theta_2))} \quad (3\text{-}117)$$

$$|V_3(k)| = |V_1(k)|\ \frac{-(G_{12}\sin(\theta_2 - \theta_1) - B_{12}\cos(\theta_2 - \theta_1))}{(G_{23}\sin(\theta_2 - \theta_3) - B_{23}\cos(\theta_2 - \theta_3))}$$

$$|V_4(k)| = \frac{1}{|V_3(k)|}\ \frac{Q_L(k) + Q_{DG2}(k)}{(G_{34}\sin(\theta_4 - \theta_3) - B_{34}\cos(\theta_4 - \theta_3))}$$

Plugging in (3-111) in (3-117) results in the following.

$$|V_2(k)| = |V_4(k)| \frac{-(G_{34}\sin(\theta_3-\theta_4) - B_{34}\cos(\theta_3-\theta_4))}{(G_{23}\sin(\theta_3-\theta_2) - B_{23}\cos(\theta_3-\theta_2))} \tag{3-118}$$

$$|V_3(k)| = \frac{1}{T_V}x_1(k)\frac{-(G_{12}\sin(\theta_2-\theta_1) - B_{12}\cos(\theta_2-\theta_1))}{(G_{23}\sin(\theta_2-\theta_3) - B_{23}\cos(\theta_2-\theta_3))}$$

$$|V_4(k)| = \frac{1}{|V_3(k)|}\frac{\left(\frac{x_3(k)}{T_{q,3}} + Q_{L0}\left(|V_4|^{b_t}(k)\right)\right) + \frac{1}{T_{Q,2}}\,x_2(k)}{(G_{34}\sin(\theta_4-\theta_3) - B_{34}\cos(\theta_4-\theta_3))}$$

The regions χ_i are defined with polytopes in the general form of $\boldsymbol{H}[x_1\ x_2\ x_3]^T \leq \boldsymbol{K}$. Assuming four regions for the system, the following linear equations describe the voltages in the system.

$$x_1(k+1) = x_1(k) + \Delta t\left(\frac{-1}{T_V}x_1(k) + V_{Ref}(k)\right) \tag{3-119}$$

$$x_2(k+1) = x_2(k) + \Delta t\left(\frac{-1}{T_{Q,2}}x_2(k) + Q_{Ref,DG2}(k)\right)$$

$$x_3(k+1) = x_3(k) - \Delta t\left(\frac{x_3(k)}{T_{q,3}} + Q_{L0}(|V_4|^{b_s}(k) - |V_4|^{b_t}(k))\right)$$

$$|V_1(k)| = \frac{1}{T_V}x_1(k)$$

$$|V_2(k)| = |V_4(k)| \frac{-(G_{34}\sin(\theta_3-\theta_4) - B_{34}\cos(\theta_3-\theta_4))}{(G_{23}\sin(\theta_3-\theta_2) - B_{23}\cos(\theta_3-\theta_2))}$$

$$|V_3(k)| = \frac{1}{T_V}x_1(k)\frac{-(G_{12}\sin(\theta_2-\theta_1) - B_{12}\cos(\theta_2-\theta_1))}{(G_{23}\sin(\theta_2-\theta_3) - B_{23}\cos(\theta_2-\theta_3))}$$

$$|V_4(k)| = \frac{1}{|V_3(k)|}\frac{\left(\frac{x_3(k)}{T_{q,3}} + Q_{L0}\left(|V_4|^{b_t}(k)\right)\right) + \frac{1}{T_{Q,2}}\,x_2(k)}{(G_{34}\sin(\theta_4-\theta_3) - B_{34}\cos(\theta_4-\theta_3))}$$

This set of equations could be written in the following general form for each mode of the system.

$$\chi_i: \boldsymbol{H}_i[x_1\ x_2\ x_3]^T \leq \boldsymbol{K}_i \rightarrow \begin{cases} x_1(k+1) = a_{1i}x_1(k) + b_{1i}V_{Ref}(k) \\ x_2(k+1) = a_{2i}x_2(k) + b_{2i}Q_{Ref,DG2}(k) \\ x_3(k+1) = a_{3i}x_3(k) + d_{1i} \\ |V_1(k)| = c_{1i}x_1(k) \\ |V_2(k)| = c_{2i}x_3(k) + c_{3i}x_2(k) + e_{1i} \\ |V_3(k)| = c_{4i}x_1(k) \\ |V_4(k)| = c_{5i}x_3(k) + c_{6i}x_2(k) + e_{2i} \end{cases} \tag{3-120}$$

Four modes are considered for the linearized system.

1st mode:

$$\chi_1: \sigma_1 \& \left\{ \begin{bmatrix} 3.19 & 0 & 0 \\ -3.316 & 0 & 0 \\ 0 & 83 & 0 \end{bmatrix} [x_1\ x_2\ x_3]^T \leq \begin{bmatrix} 1 \\ 1 \end{bmatrix} \right\} \tag{3-121}$$

$$\rightarrow \begin{cases} x_1(k+1) = 0.33\ x_1(k) + 0.2\ V_{Ref}(k) \\ x_2(k+1) = -0.66\ x_2(k) + 0.2Q_{Ref,DG2}(k) \\ x_3(k+1) = 0.9328x_3(k) + 0.0280 \\ |V_1(k)| = 3.33\ x_1(k) \\ |V_2(k)| = 0.122\ V_4(k) \\ |V_3(k)| = 0.168\ x_1(k) \\ |V_4(k)| = -0.0070x_3(k) \end{cases}$$

2nd mode:

$$\chi_2: \sim\sigma_1 \& \left\{ \begin{bmatrix} 3.19 & 0 & 0 \\ -3.316 & 0 & 0 \\ 0 & 83 & 0 \end{bmatrix} [x_1\ x_2\ x_3]^T \leq \begin{bmatrix} -1 \\ -1 \\ -1 \end{bmatrix} \right\}$$

$$\rightarrow \begin{cases} x_1(k+1) = 0.33\, x_1(k) + 0.2\, V_{Ref}(k) \\ x_2(k+1) = -0.66\, x_2(k) + 0.2 Q_{Ref,DG2}(k) \\ x_3(k+1) = 0.9328 x_3(k) + 0.0224 \\ |V_1(k)| = 3.33\, x_1(k) \\ |V_2(k)| = 0.122\, V_4(k) \\ |V_3(k)| = 0.168\, x_1(k) \\ |V_4(k)| = -0.0078 x_3(k) \end{cases} \quad (3\text{-}122)$$

3rd mode:

$$\chi_3: \sigma_1 \& \left\{ \begin{bmatrix} 3.19 & 0 & 0 \\ -3.316 & 0 & 0 \\ 0 & 83 & 0 \end{bmatrix} [x_1\ x_2\ x_3]^T \leq \begin{bmatrix} 1 \\ 1 \\ 1 \end{bmatrix} \right\}$$

$$\rightarrow \begin{cases} x_1(k+1) = 0.33\, x_1(k) + 0.2\, V_{Ref}(k) \\ x_2(k+1) = -0.66\, x_2(k) + 0.2 Q_{Ref,DG2}(k) \\ x_3(k+1) = 0.9328 x_3(k) + 0.0280 \\ |V_1(k)| = 3.33\, x_1(k) \\ |V_2(k)| = 0.093\, V_4(k) \\ |V_3(k)| = 0.294\, x_1(k) \\ |V_4(k)| = -0.007 x_3(k) \end{cases} \quad (3\text{-}123)$$

4th mode:

$$\chi_4: \sim\sigma_1 \& \left\{ \begin{bmatrix} 3.19 & 0 & 0 \\ -3.316 & 0 & 0 \\ 0 & 83 & 0 \end{bmatrix} [x_1\ x_2\ x_3]^{\mathrm{T}} \leq \begin{bmatrix} -1 \\ -1 \\ -1 \end{bmatrix} \right\}$$

$$\rightarrow \begin{cases} x_1(k+1) = 0.33\, x_1(k) + 0.2\, V_{Ref}(k) \\ x_2(k+1) = -0.66\, x_2(k) + 0.2 Q_{Ref,DG2}(k) \\ x_3(k+1) = 0.9328 x_3(k) + 0.0224 \\ |V_1(k)| = 3.33\, x_1(k) \\ |V_2(k)| = 0.093\, V_4(k) \\ |V_3(k)| = 0.294\, x_1(k) \\ |V_4(k)| = -0.0079 x_3(k) \end{cases} \quad (3\text{-}124)$$

where σ_1 is an auxillary state switch which represents the system operating with load profile 1 where only load one is connected to the system and $\sim\sigma_1$ represents the system operating in load profile 2 where load 1 and load 2 are both connected to the system.

Further, Auxiliary binary switches δ_1 through δ_4 are assigned to hyperplanes χ_1 through χ_4 respectively. This assignment of the auxiliary variables can be shown as follows.

$$\begin{aligned} [\delta_1 = 1] &\rightarrow \chi_1 \\ [\delta_2 = 1] &\rightarrow \chi_2 \\ [\delta_3 = 1] &\rightarrow \chi_3 \\ [\delta_4 = 1] &\rightarrow \chi_4 \end{aligned} \quad (3\text{-}125)$$

We can start by the following change of variables.

$$\boldsymbol{x}(k+1) = \sum_{i=1}^{4} \boldsymbol{z_i}(k) \quad , \quad \boldsymbol{z_i}(k) = [\boldsymbol{A_i x}(k) + \boldsymbol{B_i u}(k)]\delta_i(k) \quad (3\text{-}126)$$

where the state vector is presented as follows.

$$\boldsymbol{x}(k) = [x_1(k)\ x_2(k)\ x_3(k)\ \ |\mathrm{V}_1(\mathrm{k})|\ \ |\mathrm{V}_2(\mathrm{k})|\ \ |\mathrm{V}_3(\mathrm{k})|\ |\mathrm{V}_4(\mathrm{k})|]^T \tag{3-127}$$

Further, the control input vector is presented as follows.

$$\boldsymbol{u}(k) = \left[\ V_{Ref}(k)\ \ Q_{Ref,DG2}(k)\right]^T \tag{3-128}$$

And let's define the following min and Max $\boldsymbol{m} = [m_1 \dots m_n]^T$, $\boldsymbol{M} = [M_1 \dots M_n]^T$ vectors as follows.

$$\begin{aligned} M_j &\triangleq \mathrm{Max}_{\,i=1,..,4} \left\{ \mathrm{Max}_{\,\left[\begin{smallmatrix} x \\ u \end{smallmatrix}\right] \epsilon\, \mathcal{C}} \ \ \boldsymbol{A_i^j x} + \boldsymbol{B_i^j u} \right\} \\ m_j &\triangleq \mathrm{min}_{\,i=1,..,4} \left\{ \mathrm{Max}_{\,\left[\begin{smallmatrix} x \\ u \end{smallmatrix}\right] \epsilon\, \mathcal{C}} \ \ \boldsymbol{A_i^j x} + \boldsymbol{B_i^j u} \right\} \end{aligned} \tag{3-129}$$

M and m are finite numbers which can be calculated or estimated. Thus, (3-96) is equivalent to the following set of equations. In this case the supremum of the state variables is 1 and the infimum is -1 as follows.

$$\begin{aligned} M_j &\triangleq [\ 1\ 1\ 1\ 1]^T \ \ j{=}1,..,4 \\ m_j &\triangleq [-1\ \ -1\ \ -1\ \ -1]^{\mathrm{T}} \ \ j{=}1,..,4 \end{aligned} \tag{3-130}$$

The vector of auxiliary variables $\boldsymbol{z}(k)$ can be defined as follows.

$$\boldsymbol{z}(k) = [\boldsymbol{z_1}(k)\ \boldsymbol{z_2}(k)\ \boldsymbol{z_3}(k)\ \boldsymbol{z_4}(k)] \tag{3-131}$$

The vector of auxiliary mode selectors, $\boldsymbol{\delta}(k)$, can be written as follows.

$$\boldsymbol{\delta}(k) = [\delta_1(k)\ \delta_2(k)\ \delta_3(k)\ \delta_4(k)] \tag{3-132}$$

Further, the MLD form can be presented as follows.

$$\boldsymbol{z_i}(k) \le \boldsymbol{M}\delta_i(k)$$

$$\boldsymbol{z_i}(k) \ge \boldsymbol{m}\delta_i(k)$$

$$\boldsymbol{z_i}(k) \le \boldsymbol{A_i x}(k) + \boldsymbol{B_i u}(k) + \boldsymbol{m}(1 - \delta_i(k)) \tag{3-133}$$

$$\boldsymbol{z_i}(k) \ge \boldsymbol{A_i x}(k) + \boldsymbol{B_i u}(k) - \boldsymbol{M}(1 - \delta_i(k))$$

Thus, by enumerating i=1,…,4, the MLD model of the system is presented in the matrix form as follows.

$$\begin{bmatrix} -\boldsymbol{M} & 0 & 0 & 0 \\ 0 & -\boldsymbol{M} & 0 & 0 \\ 0 & 0 & -\boldsymbol{M} & 0 \\ 0 & 0 & 0 & -\boldsymbol{M} \\ \boldsymbol{m} & 0 & 0 & 0 \\ 0 & \boldsymbol{m} & 0 & 0 \\ 0 & 0 & \boldsymbol{m} & 0 \\ 0 & 0 & 0 & \boldsymbol{m} \\ \boldsymbol{m} & 0 & 0 & 0 \\ 0 & \boldsymbol{m} & 0 & 0 \\ 0 & 0 & \boldsymbol{m} & 0 \\ 0 & 0 & 0 & \boldsymbol{m} \\ \boldsymbol{M} & 0 & 0 & 0 \\ 0 & \boldsymbol{M} & 0 & 0 \\ 0 & 0 & \boldsymbol{M} & 0 \\ 0 & 0 & 0 & \boldsymbol{M} \end{bmatrix} \boldsymbol{\delta}(k) + \begin{bmatrix} \boldsymbol{I} & 0 & 0 & 0 \\ 0 & \boldsymbol{I} & 0 & 0 \\ 0 & 0 & \boldsymbol{I} & 0 \\ 0 & 0 & 0 & \boldsymbol{I} \\ -\boldsymbol{I} & 0 & 0 & 0 \\ 0 & -\boldsymbol{I} & 0 & 0 \\ 0 & 0 & -\boldsymbol{I} & 0 \\ 0 & 0 & 0 & -\boldsymbol{I} \\ \boldsymbol{I} & 0 & 0 & 0 \\ 0 & \boldsymbol{I} & 0 & 0 \\ 0 & 0 & \boldsymbol{I} & 0 \\ 0 & 0 & 0 & \boldsymbol{I} \\ -\boldsymbol{I} & 0 & 0 & 0 \\ 0 & -\boldsymbol{I} & 0 & 0 \\ 0 & 0 & -\boldsymbol{I} & 0 \\ 0 & 0 & 0 & -\boldsymbol{I} \end{bmatrix} \boldsymbol{z}(k) \le \begin{bmatrix} 0 \\ 0 \\ 0 \\ 0 \\ 0 \\ 0 \\ 0 \\ 0 \\ \boldsymbol{B_1} \\ \boldsymbol{B_2} \\ \boldsymbol{B_3} \\ \boldsymbol{B_4} \\ -\boldsymbol{B_1} \\ -\boldsymbol{B_1} \\ -\boldsymbol{B_1} \\ -\boldsymbol{B_1} \end{bmatrix} \boldsymbol{u}(k) + \begin{bmatrix} 0 \\ 0 \\ 0 \\ 0 \\ 0 \\ 0 \\ 0 \\ 0 \\ \boldsymbol{A_1} \\ \boldsymbol{A_2} \\ \boldsymbol{A_3} \\ \boldsymbol{A_4} \\ -\boldsymbol{A_1} \\ -\boldsymbol{A_1} \\ -\boldsymbol{A_1} \\ -\boldsymbol{A_1} \end{bmatrix} \boldsymbol{x}(k) + \begin{bmatrix} 0 \\ 0 \\ 0 \\ 0 \\ 0 \\ 0 \\ 0 \\ 0 \\ \boldsymbol{m} \\ \boldsymbol{m} \\ \boldsymbol{m} \\ \boldsymbol{m} \\ \boldsymbol{M} \\ \boldsymbol{M} \\ \boldsymbol{M} \\ \boldsymbol{M} \end{bmatrix} \tag{3-134}$$

The following conditions also hold for the auxiliary mode selectors.

$$\begin{aligned} &[\delta_1 = 1] \rightarrow [\delta_2 = 0], [\delta_1 = 1] \rightarrow [\delta_3 = 0], [\delta_1 = 1] \rightarrow [\delta_4 = 0] \\ &[\delta_2 = 1] \rightarrow [\delta_1 = 0], [\delta_2 = 1] \rightarrow [\delta_3 = 0], [\delta_2 = 1] \rightarrow [\delta_4 = 0] \\ &[\delta_3 = 1] \rightarrow [\delta_1 = 0], [\delta_3 = 1] \rightarrow [\delta_2 = 0], [\delta_3 = 1] \rightarrow [\delta_4 = 0] \\ &[\delta_4 = 1] \rightarrow [\delta_1 = 0], [\delta_4 = 1] \rightarrow [\delta_2 = 0], [\delta_4 = 1] \rightarrow [\delta_3 = 0] \end{aligned} \tag{3-135}$$

Equations (3-135) can be transformed to the following inequality form.

$$\begin{aligned}
&\delta_1 - (1-\delta_2) \le 0, \quad \delta_1 - (1-\delta_3) \le 0, \quad \delta_1 - (1-\delta_4) \le 0 \\
&\delta_2 - (1-\delta_1) \le 0\,, \quad \delta_2 - (1-\delta_3) \le 0, \quad \delta_2 - (1-\delta_4) \le 0 \\
&\delta_3 - (1-\delta_1) \le 0\,, \quad \delta_3 - (1-\delta_2) \le 0, \quad \delta_3 - (1-\delta_4) \le 0 \\
&\delta_4 - (1-\delta_1) \le 0\,, \quad \delta_4 - (1-\delta_2) \le 0, \quad \delta_4 - (1-\delta_3) \le 0
\end{aligned} \tag{3-136}$$

Table 6 presents the load parameters for the 4 bus system.

Table 6 Load parameters of the 4 bus system

Parameter	Value
P_1	2.70 MW
Q_1	1.300 MVar
P_2	2.7 MW
Q_2	1.3 MVar
Q_{c1} and Q_{c2}	500kVar

3.2.5.3 Example 3 - IEEE 4 bus system with capacitor banks

This example uses the same system as example 2, however, the system has a descrete input in the form of a capacitor bank in this case. The linear system equations are as follows.

$$\chi_i: \boldsymbol{H}_i[x_1\ x_2\ x_3]^T \leq \boldsymbol{K}_i \tag{3-137}$$

$$\rightarrow \begin{cases} x_1(k+1) = a_{1i}x_1(k) + b_{1i}V_{Ref}(k) \\ x_2(k+1) = a_{2i}x_2(k) + b_{2i}Q_{Ref,DG2}(k) \\ x_3(k+1) = a_{3i}x_3(k) + d_{1i} \\ |V_1(k)| = c_{1i}x_1(k) \\ |V_2(k)| = c_{2i}x_3(k) + c_{3i}x_2(k) + e_{1i} \\ |V_3(k)| = c_{4i}x_1(k) + b_{3i}\sigma_c\ (k) \\ |V_4(k)| = c_{5i}x_3(k) + c_{6i}x_2(k) + b_{4i}\sigma_c\ (k) + e_{2i} \end{cases}$$

Four modes are considered for the linearized system.

1st mode:

$$\chi_1: \sigma_1 \& \left\{ \begin{bmatrix} 3.19 & 0 & 0 \\ -3.316 & 0 & 0 \\ 0 & 83 & 0 \end{bmatrix} [x_1\ x_2\ x_3]^T \leq \begin{bmatrix} 1 \\ 1 \end{bmatrix} \right\} \tag{3-138}$$

$$\rightarrow \begin{cases} x_1(k+1) = 0.33\ x_1(k) + 0.2\ V_{Ref}(k) \\ x_2(k+1) = -0.66\ x_2(k) + 0.2Q_{Ref,DG2}(k) \\ x_3(k+1) = 0.9328x_3(k) + 0.0280 \\ |V_1(k)| = 3.33\ x_1(k) \\ |V_2(k)| = 0.122\ V_4(k) \\ |V_3(k)| = 0.168\ x_1(k) + \sigma_c\ (k) \\ |V_4(k)| = -0.0070x_3(k) + \sigma_c\ (k) \end{cases}$$

2nd mode:

$$\chi_2: \sim\sigma_1 \& \left\{ \begin{bmatrix} 3.19 & 0 & 0 \\ -3.316 & 0 & 0 \\ 0 & 83 & 0 \end{bmatrix} [x_1\ x_2\ x_3]^T \leq \begin{bmatrix} -1 \\ -1 \\ -1 \end{bmatrix} \right\} \tag{3-139}$$

$$\rightarrow \begin{cases} x_1(k+1) = 0.33\, x_1(k) + 0.2\, V_{Ref}(k) \\ x_2(k+1) = -0.66\, x_2(k) + 0.2 Q_{Ref,DG2}(k) \\ x_3(k+1) = 0.9328 x_3(k) + 0.0224 \\ |V_1(k)| = 3.33\, x_1(k) \\ |V_2(k)| = 0.122\, V_4(k) \\ |V_3(k)| = 0.168\, x_1(k) + \sigma_c\,(k) \\ |V_4(k)| = -0.0078 x_3(k) + \sigma_c\,(k) \end{cases}$$

3rd mode:

$$\chi_3: \sigma_1 \& \left\{ \begin{bmatrix} 3.19 & 0 & 0 \\ -3.316 & 0 & 0 \\ 0 & 83 & 0 \end{bmatrix} [x_1\ x_2\ x_3]^T \leq \begin{bmatrix} 1 \\ 1 \\ 1 \end{bmatrix} \right\} \tag{3-140}$$

$$\rightarrow \begin{cases} x_1(k+1) = 0.33\, x_1(k) + 0.2\, V_{Ref}(k) \\ x_2(k+1) = -0.66\, x_2(k) + 0.2 Q_{Ref,DG2}(k) \\ x_3(k+1) = 0.9328 x_3(k) + 0.0280 \\ |V_1(k)| = 3.33\, x_1(k) \\ |V_2(k)| = 0.093\, V_4(k) \\ |V_3(k)| = 0.294\, x_1(k) + \sigma_c\,(k) \\ |V_4(k)| = -0.007 x_3(k) + \sigma_c\,(k) \end{cases}$$

4th mode:

$$\chi_4: \sim\sigma_1 \& \left\{ \begin{bmatrix} 3.19 & 0 & 0 \\ -3.316 & 0 & 0 \\ 0 & 83 & 0 \end{bmatrix} [x_1\ x_2\ x_3]^{\mathrm{T}} \leq \begin{bmatrix} -1 \\ -1 \\ -1 \end{bmatrix} \right\}$$

$$\rightarrow \begin{cases} x_1(k+1) = 0.33\, x_1(k) + 0.2\, V_{Ref}(k) \\ x_2(k+1) = -0.66\, x_2(k) + 0.2 Q_{Ref,DG2}(k) \\ x_3(k+1) = 0.9328 x_3(k) + 0.0224 \\ |V_1(k)| = 3.33\, x_1(k) \\ |V_2(k)| = 0.093\, V_4(k) \\ |V_3(k)| = 0.294\, x_1(k) + \sigma_c\,(k) \\ |V_4(k)| = -0.0079 x_3(k) + \sigma_c\,(k) \end{cases} \tag{3-141}$$

where σ_1 is an auxillary state switch which represents the system operating with load profile 1 where only load one is connected to the system and $\sim\sigma_1$ represents the system operating in load profile 2 where load 1 and load 2 are both connected to the system.

Further, Auxiliary binary switches δ_1 through δ_4 are assigned to hyperplanes χ_1 through χ_4 respectively. This assignment of the auxiliary variables can be shown as follows.

$$\begin{aligned} [\delta_1 = 1] &\rightarrow \chi_1 \\ [\delta_2 = 1] &\rightarrow \chi_2 \\ [\delta_3 = 1] &\rightarrow \chi_3 \\ [\delta_4 = 1] &\rightarrow \chi_4 \end{aligned} \tag{3-142}$$

We can start by the following change of variables.

$$\boldsymbol{x}(k+1) = \sum_{i=1}^{4} \boldsymbol{z_i}(k) \quad , \quad \boldsymbol{z_i}(k) = [\boldsymbol{A_i x}(k) + \boldsymbol{B_i u}(k)]\delta_i(k) \tag{3-143}$$

where the state vector is presented as follows.

$$\boldsymbol{x}(k) = [x_1(k)\ x_2(k)\ x_3(k)\ \ |\mathrm{V}_1(\mathrm{k})|\ \ |\mathrm{V}_2(\mathrm{k})|\ \ |\mathrm{V}_3(\mathrm{k})|\ |\mathrm{V}_4(\mathrm{k})|]^T \tag{3-144}$$

Further, the control input vector which is consisted of the continuous vector and the discrete vector is presented as follows.

$$\boldsymbol{u}(k) = \left[\ V_{Ref}(k)\ \ Q_{Ref,DG2}(k)\ \ \ \sigma_c(k)\right]^T \tag{3-145}$$

The continuous control vector is as follows.

$$\boldsymbol{v}(k) = \left[\ V_{Ref}(k)\ \ Q_{Ref,DG2}(k)\ \right]^T \tag{3-146}$$

The discrete control vector is as follows.

$$\boldsymbol{\sigma}(k) = [\ \sigma_c\ (k)]^T \tag{3-147}$$

And let's define the following min and Max $\boldsymbol{m} = [m_1 \dots m_n]^T$, $\boldsymbol{M} = [M_1 \dots M_n]^T$ vectors as follows.

$$\begin{aligned} M_j &\triangleq \mathrm{Max}_{\,i=1,..,4}\ \left\{\mathrm{Max}_{\,\left[\begin{smallmatrix}x\\u\end{smallmatrix}\right]\epsilon\ \mathcal{C}}\ \ \boldsymbol{A_i^j x} + \boldsymbol{B_i^j u}\right\} \\ m_j &\triangleq \mathrm{min}_{\,i=1,..,4}\ \left\{\mathrm{Max}_{\,\left[\begin{smallmatrix}x\\u\end{smallmatrix}\right]\epsilon\ \mathcal{C}}\ \ \boldsymbol{A_i^j x} + \boldsymbol{B_i^j u}\right\} \end{aligned} \tag{3-148}$$

M and m are finite numbers which can be calculated or estimated. Thus, (3-96) is equivalent to the following set of equations. In this case, the supremum of the state variables is 1 and the infimum is -1 as follows.

$$\begin{aligned} M_j &\triangleq [\ 1\ 1\ 1\ 1]^T\ \ j{=}1,..,4 \\ m_j &\triangleq [-1\ \ -1\ \ -1\ \ -1]^{\mathrm{T}}\ \ j{=}1,..,4 \end{aligned} \tag{3-149}$$

The vector of auxiliary variables $\boldsymbol{z}(k)$ can be defined as follows.

$$\boldsymbol{z}(k) = [\boldsymbol{z_1}(k)\ \boldsymbol{z_2}(k)\ \boldsymbol{z_3}(k)\ \boldsymbol{z_4}(k)] \tag{3-150}$$

The vector of auxiliary mode selectors, $\boldsymbol{\delta}(k)$, can be written as follows.

$$\boldsymbol{\delta}(k) = [\delta_1(k)\ \delta_2(k)\ \delta_3(k)\ \delta_4(k)] \tag{3-151}$$

Further, the MLD form could be presented as follows.

$$\begin{gathered} \boldsymbol{z_i}(k) \leq \boldsymbol{M}\delta_i(k) \\ \boldsymbol{z_i}(k) \geq \boldsymbol{m}\delta_i(k) \\ \boldsymbol{z_i}(k) \leq \boldsymbol{A_i x}(k) + \boldsymbol{B_i u}(k) + \boldsymbol{m}(1 - \delta_i(k)) \\ \boldsymbol{z_i}(k) \geq \boldsymbol{A_i x}(k) + \boldsymbol{B_i u}(k) - \boldsymbol{M}(1 - \delta_i(k)) \end{gathered} \tag{3-152}$$

Thus, by enumerating *i*=1,…,4, the MLD model of the system is presented in the matrix form as follows.

$$\begin{bmatrix} -M & 0 & 0 & 0 \\ 0 & -M & 0 & 0 \\ 0 & 0 & -M & 0 \\ 0 & 0 & 0 & -M \\ m & 0 & 0 & 0 \\ 0 & m & 0 & 0 \\ 0 & 0 & m & 0 \\ 0 & 0 & 0 & m \\ m & 0 & 0 & 0 \\ 0 & m & 0 & 0 \\ 0 & 0 & m & 0 \\ 0 & 0 & 0 & m \\ M & 0 & 0 & 0 \\ 0 & M & 0 & 0 \\ 0 & 0 & M & 0 \\ 0 & 0 & 0 & M \end{bmatrix} \boldsymbol{\delta}(k) + \begin{bmatrix} I & 0 & 0 & 0 \\ 0 & I & 0 & 0 \\ 0 & 0 & I & 0 \\ 0 & 0 & 0 & I \\ -I & 0 & 0 & 0 \\ 0 & -I & 0 & 0 \\ 0 & 0 & -I & 0 \\ 0 & 0 & 0 & -I \\ I & 0 & 0 & 0 \\ 0 & I & 0 & 0 \\ 0 & 0 & I & 0 \\ 0 & 0 & 0 & I \\ -I & 0 & 0 & 0 \\ 0 & -I & 0 & 0 \\ 0 & 0 & -I & 0 \\ 0 & 0 & 0 & -I \end{bmatrix} \boldsymbol{z}(k) \leq \begin{bmatrix} 0 \\ 0 \\ 0 \\ 0 \\ 0 \\ 0 \\ 0 \\ \acute{B}_1 \\ \acute{B}_2 \\ \acute{B}_3 \\ \acute{B}_4 \\ -\acute{B}_1 \\ -\acute{B}_1 \\ -\acute{B}_1 \\ -\acute{B}_1 \end{bmatrix} \boldsymbol{u}(k) + \begin{bmatrix} 0 \\ 0 \\ 0 \\ 0 \\ 0 \\ 0 \\ 0 \\ 0 \\ A_1 \\ A_2 \\ A_3 \\ A_4 \\ -A_1 \\ -A_1 \\ -A_1 \\ -A_1 \end{bmatrix} \boldsymbol{x}(k) + \begin{bmatrix} 0 \\ 0 \\ 0 \\ 0 \\ 0 \\ 0 \\ 0 \\ 0 \\ m \\ m \\ m \\ m \\ M \\ M \\ M \\ M \end{bmatrix} \quad (3\text{-}153)$$

The following conditions also hold for the auxiliary mode selectors.

$$\begin{aligned} &[\delta_1 = 1] \rightarrow [\delta_2 = 0], [\delta_1 = 1] \rightarrow [\delta_3 = 0], [\delta_1 = 1] \rightarrow [\delta_4 = 0] \\ &[\delta_2 = 1] \rightarrow [\delta_1 = 0], [\delta_2 = 1] \rightarrow [\delta_3 = 0], [\delta_2 = 1] \rightarrow [\delta_4 = 0] \\ &[\delta_3 = 1] \rightarrow [\delta_1 = 0], [\delta_3 = 1] \rightarrow [\delta_2 = 0], [\delta_3 = 1] \rightarrow [\delta_4 = 0] \\ &[\delta_4 = 1] \rightarrow [\delta_1 = 0], [\delta_4 = 1] \rightarrow [\delta_2 = 0], [\delta_4 = 1] \rightarrow [\delta_3 = 0] \end{aligned} \quad (3\text{-}154)$$

Equations (3-135) can be transformed to the following inequality form.

$$\begin{aligned} &\delta_1 - (1 - \delta_2) \leq 0, \quad \delta_1 - (1 - \delta_3) \leq 0, \quad \delta_1 - (1 - \delta_4) \leq 0 \\ &\delta_2 - (1 - \delta_1) \leq 0, \quad \delta_2 - (1 - \delta_3) \leq 0, \quad \delta_2 - (1 - \delta_4) \leq 0 \\ &\delta_3 - (1 - \delta_1) \leq 0, \quad \delta_3 - (1 - \delta_2) \leq 0, \quad \delta_3 - (1 - \delta_4) \leq 0 \\ &\delta_4 - (1 - \delta_1) \leq 0, \quad \delta_4 - (1 - \delta_2) \leq 0, \quad \delta_4 - (1 - \delta_3) \leq 0 \end{aligned} \quad (3\text{-}155)$$

The objective function for this system is chosen as follows.

$$J(\boldsymbol{x},\boldsymbol{u},k)=\sum_{k=0}^{N-1}\begin{Bmatrix}\|V_4(k+t_0|t_0)-V_4^{Nom}\|_{\{1,\infty\}}\cdots\\ \ldots+\|\boldsymbol{W_1}\Delta\boldsymbol{v}(k)\|_{\{1,\infty\}}+\|\boldsymbol{W_2}\Delta\boldsymbol{\sigma}(k)\|_{\{1,\infty\}}\end{Bmatrix} \tag{3-156}$$

As mentioned in the earlier section $\boldsymbol{u}(k)$= [$\boldsymbol{v}(k)$ $\boldsymbol{\sigma}(k)$] and V_4^{Nom} is the nominal voltage of bus 4**.**

In this problem, only voltage of bus 4 was included in the objective function because bus 4 was the main that caused voltage changes in the system, i.e., bus 4 was the only bus that had uncontrollable changes in the load and generation. In other words, bus 4 experienced load changes based on customer demand and reactive power generation of the wind generators changes due to the weather condition.

Six case studies were studied for this system as follows.

3.2.5.3.1 Case-study 1 – one wind generator

In this case study one wind turbine with generation capacity of 1 KVA was connected to bus 4. The synchronous generator in this case study had the capacity of 5.5 KVA. An abrupt load change occurred at t= 6s, where load 2 was connected to the system. This change was a relatively large change comparing to the inertia of the synchronous generator. An active load scheme was designed to control the frequency and supply the active power to the load in timely manner. The active controller is not the focus of this dissertation. In addition, wind speed changed from 15 m/s to 5 m/s at t=10s and changed back to normal speed of 15m/s at t=18s. This change in the wind speed

resulted in a reduction in reactive power capacity of the wind generator, which means that other reactive sources in the system should be used to compensate the voltage drop.

The dynamic reactive controller was designed using the MPC discussed in earlier sections for the objective function (3-156) and the MLD form presented in (3-153). Figure 3-26 shows the voltage profile of the system and Figure 3-27 shows the control inputs.

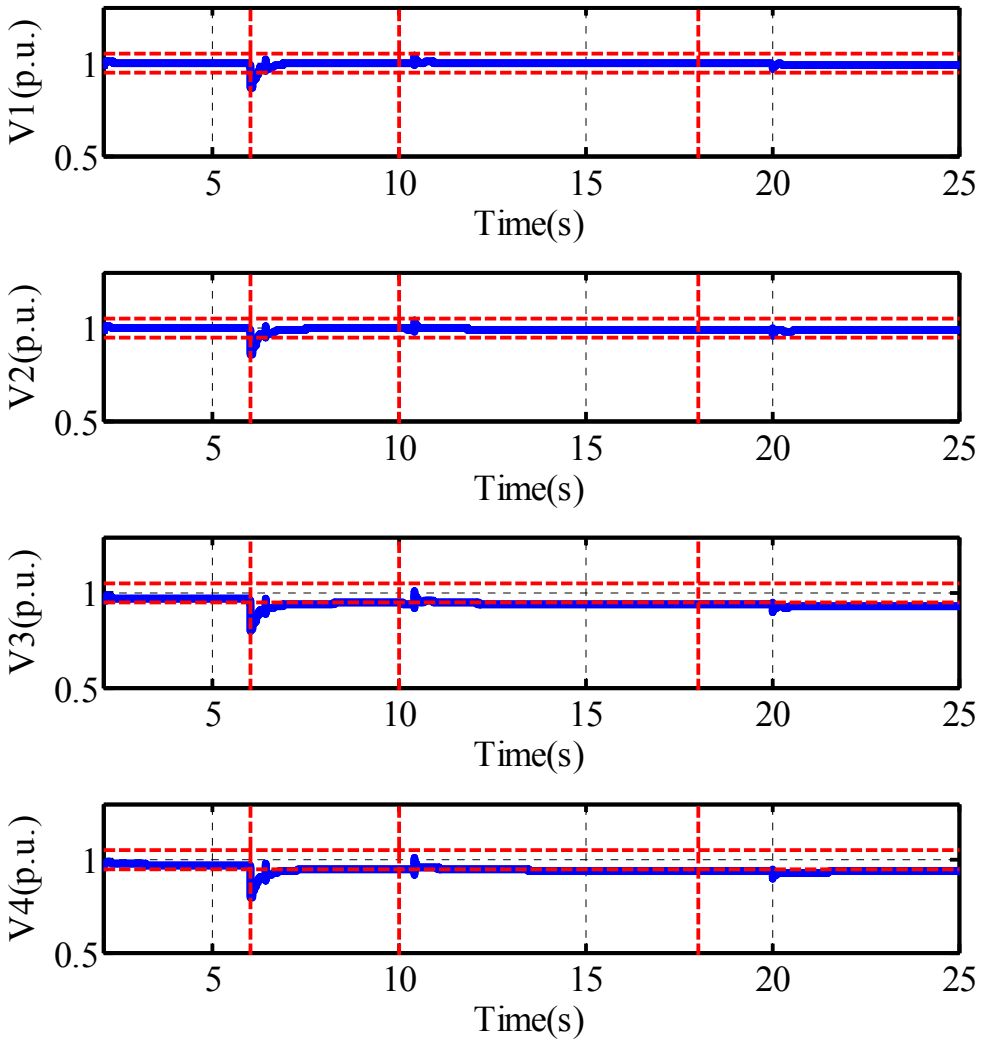

Figure 3-26 Bus voltages of the system for 1 wind generator case

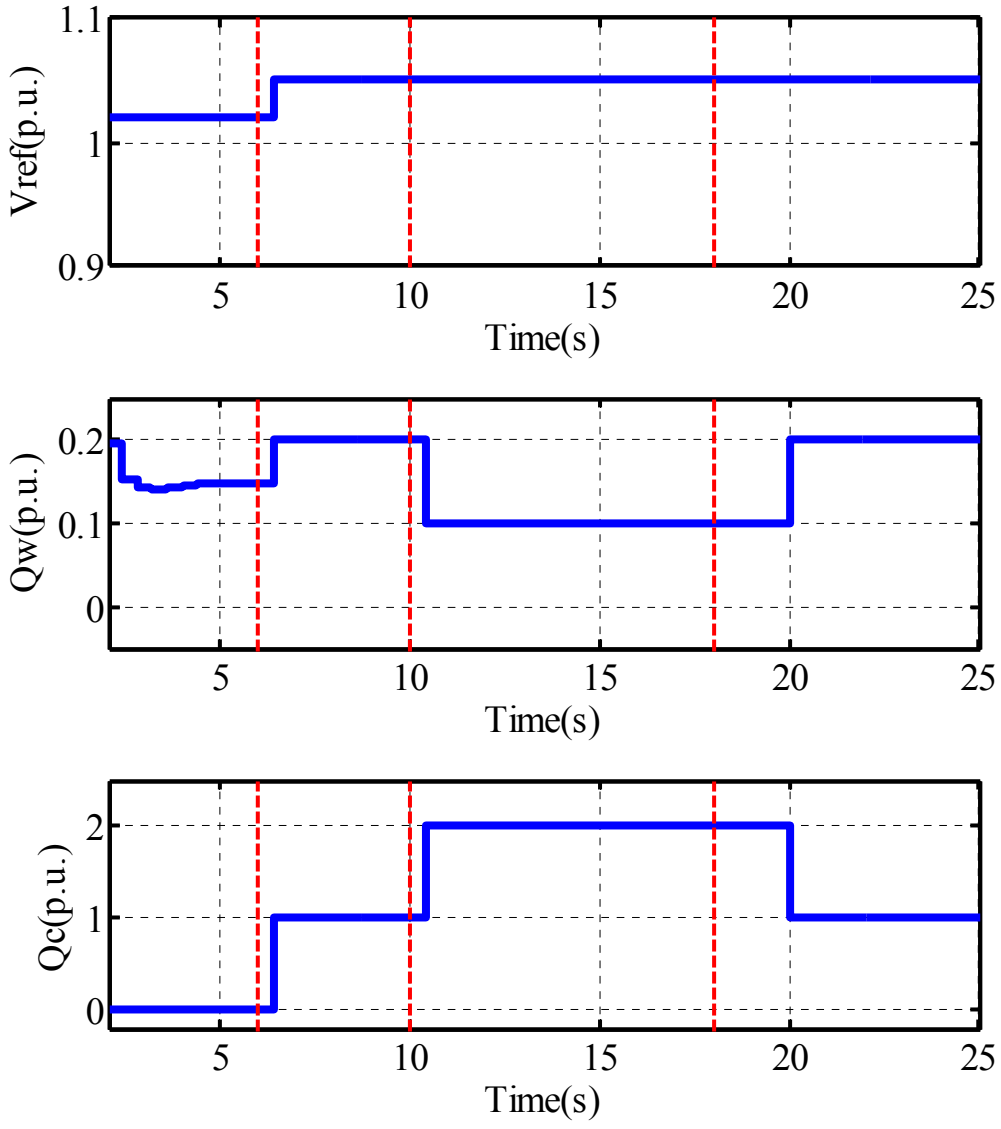

Figure 3-27 Control inputs to the system for 1 wind generator case

As can be seen in Figure 3-27, the MPC sent the control signal to the capacitor bank for a step of 500kVar, 0.4 seconds after the load got connected to the system. This step change in the capacitor bank along with an increase in reactive power production of the wind generator and an increase in the voltage reference of the synchronous generator compensated the voltage drop of the load change in bus 4. Since bus 4 was the main

reactive consumer in the studied system, compensation of the reactive power in bus 4 consequently resulted in a smooth voltage profile in the whole system.

At t=10s, the wind speed changed to 5m/s which resulted in a drop in reactive power capacity of the wind generator, therefore, the MPC controller connected the second capacitor bank to the system to compensate for the reactive power production at bus 4. When the wind speed changed back to the normal speed, the wind generator took a few seconds to get back to normal production capacity. When the wind generator got back to the normal reactive capacity, the MPC controller disconnected one capacitor bank from the system and used the reactive power production capacity of the wind generator to compensate for reactive power need in the system.

3.2.5.3.2 Case-study 2 – two wind generators

In this case study two wind turbines with generation capacity of 1 KVA each, were connected to bus 4. The synchronous generator in this case study had the capacity of 4.5 KVA. The load change and wind change profile was similar to case study 1. Figure 3-28 shows the voltage profile of the system and Figure 3-29 shows the control inputs to the system for this case study.

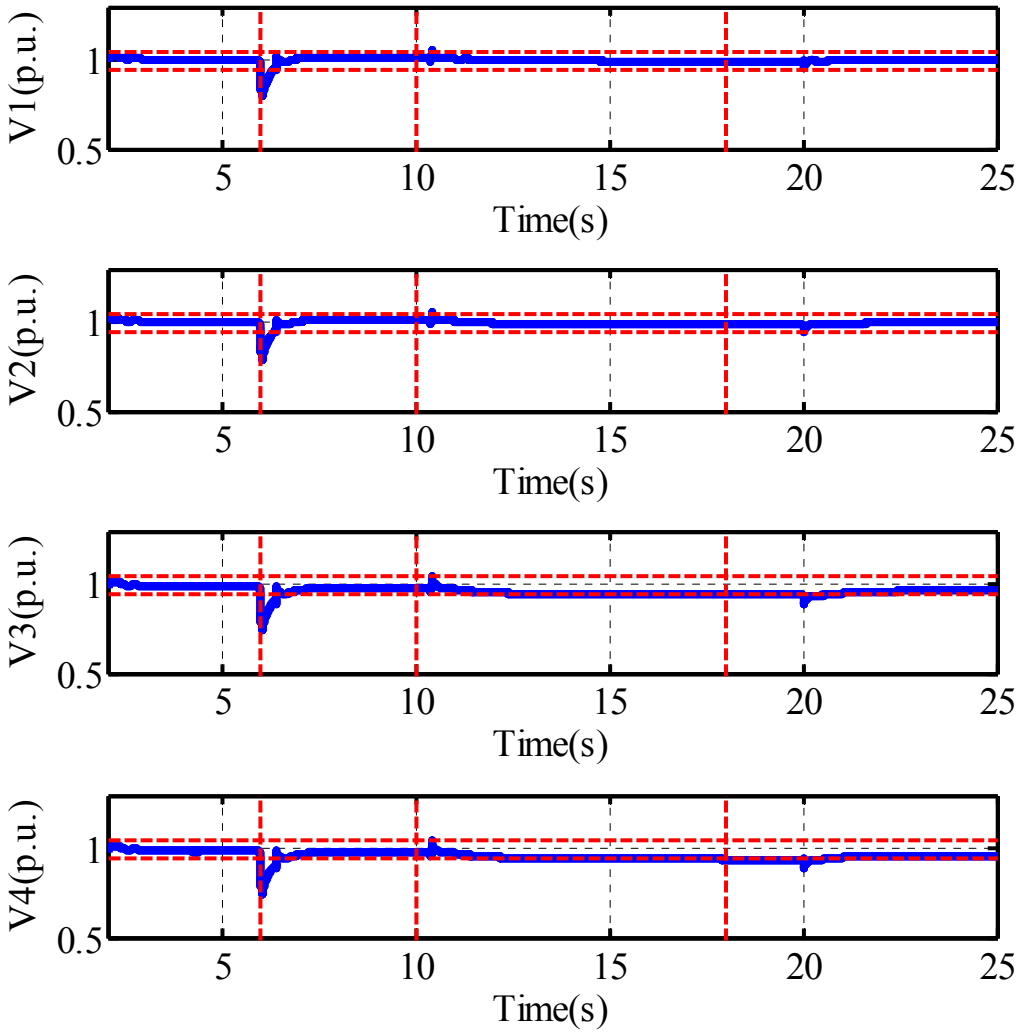

Figure 3-28 Bus voltages of the system for 2 wind generator case

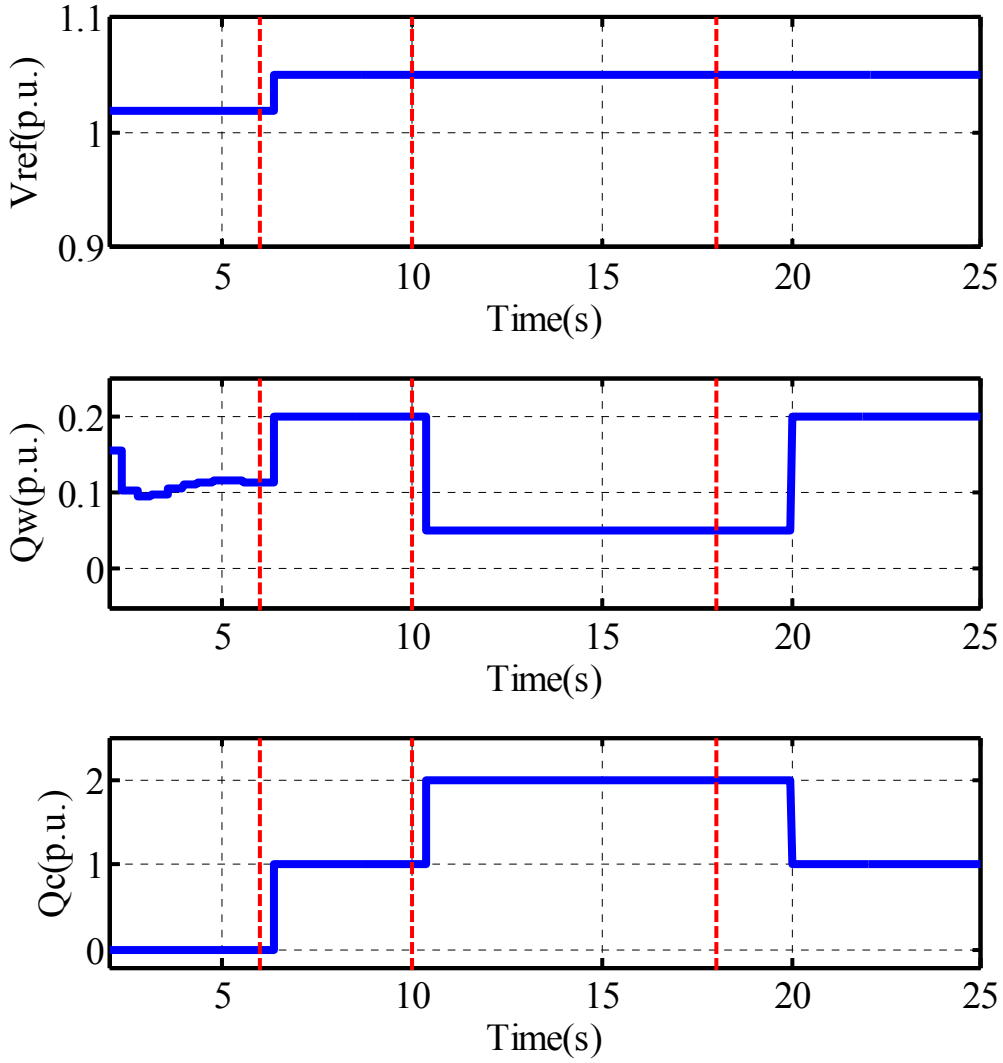

Figure 3-29 Control inputs to the system for 2 wind generator case

Although in this case the reactive production was significantly smaller than case study 1 because the percentage of penetration of wind was higher in the system, the MPC reactive controller was still capable of keeping the bus voltages within limits by adjusting the control inputs.

3.2.5.3.3 Case-study 3 – three wind generators

In this case study three wind turbines with generation capacity of 1 KVA each, were connected to bus 4. The synchronous generator in this case study had the capacity of 3.5 KVA. The load change and wind change profile were similar to case study 1. Figure 3-30 shows the voltage profile of the system and Figure 3-31shows the control inputs to the system for this case-study.

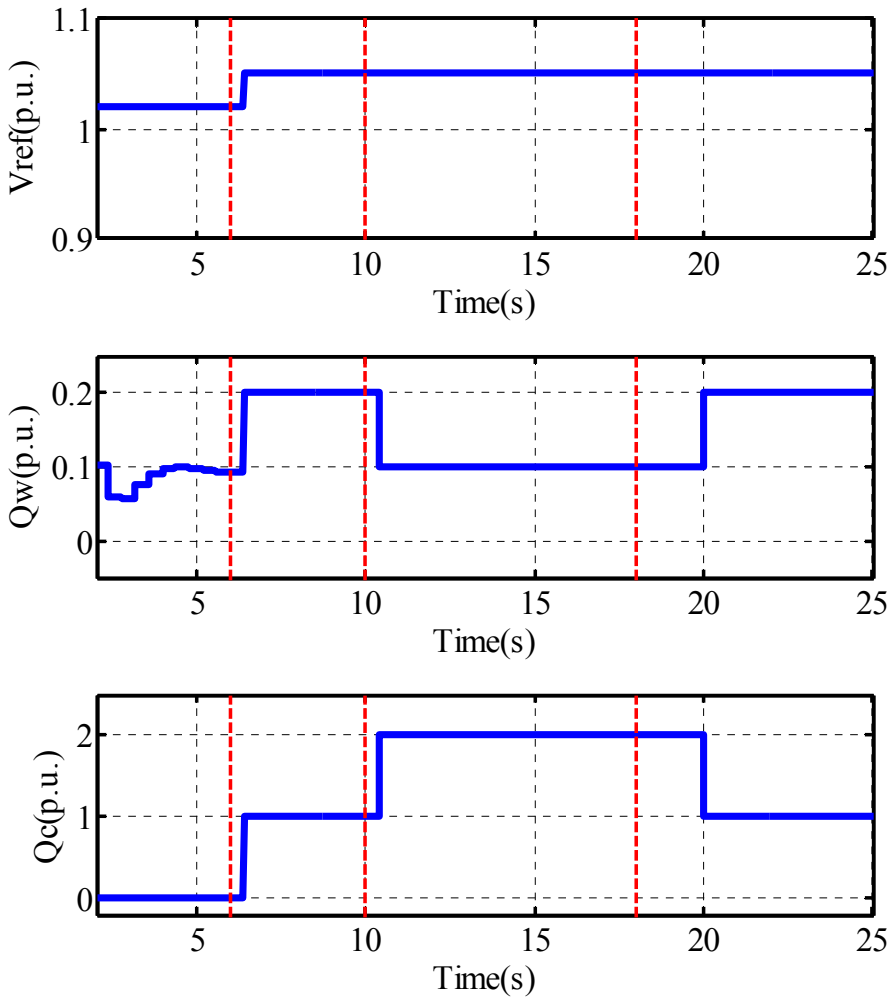

Figure 3-30 Control inputs to the system for 3 wind generator case

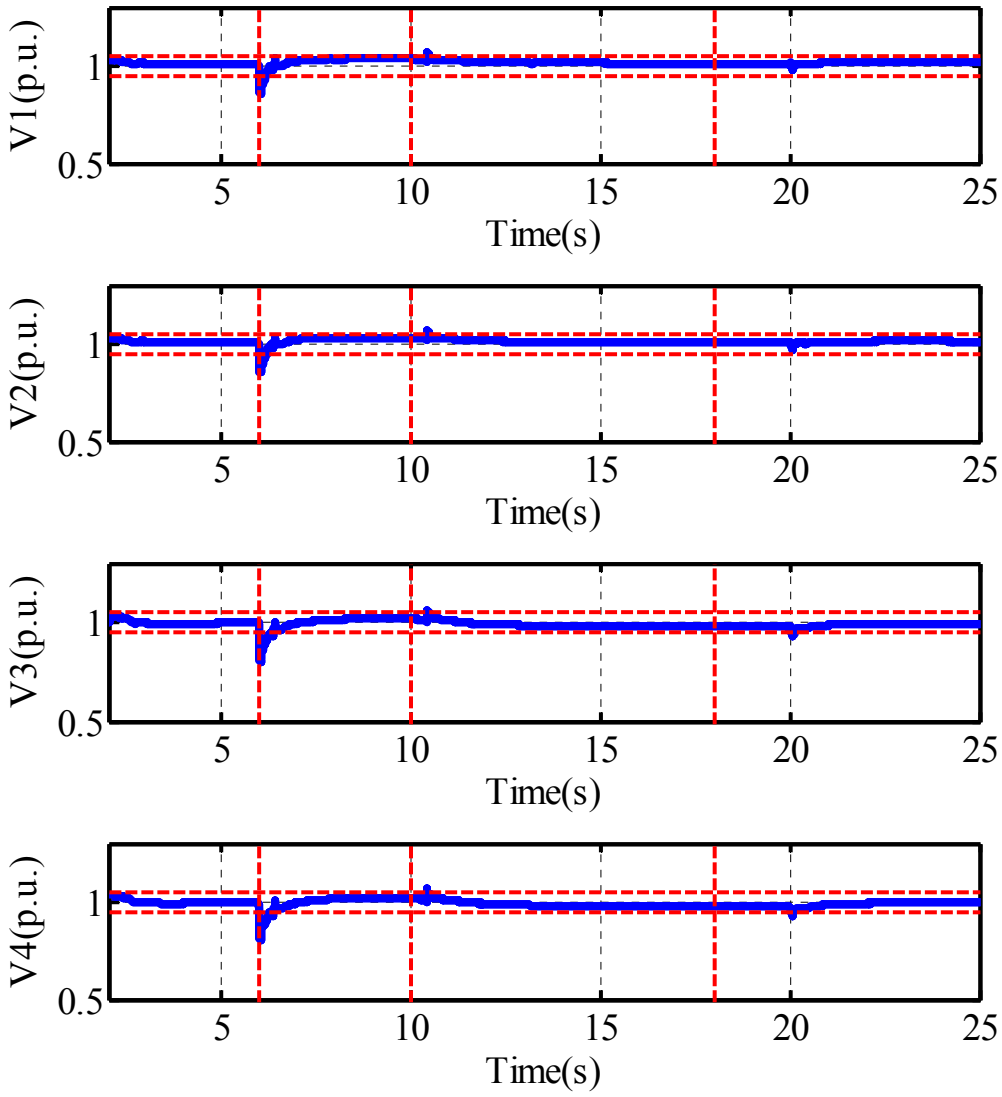

Figure 3-31 Bus voltages of the system for 3 wind generator case

In this case the reactive production was significantly smaller than case-study 1 and case-study 2 because the percentage of penetration of wind was higher. However, the MPC reactive controller was still capable of keeping the bus voltages within limits by adjusting the control inputs.

3.2.5.3.4 Case-study 4 – one wind generator with half load

In this case study one wind turbine with generation capacity of 1 KVA was connected to bus 4 and the synchronous generator connected to bus 1 had the capacity of 5.5 KVA. In this case study only load 1 was connected to the system all through the 25 seconds of operation. The wind speed changed from 15 m/s to 5 m/s at t=6s and returned back to normal speed of 15 m/s at t=18s. The MPC controller tried to eliminate the effect of reduction of the reactive power capacity of the wind generator.

In this case not only the reactive power controller should keep the voltages above the lower voltage limit but also should make sure that the control action does not result in overvoltage in the system. As can be seen in Figure 3-32 and Figure 3-33, the MPC controller was capable of keeping the bus voltages within voltage limits. In addition, as can be seen in the results, after the wind speed got back to normal speed, the controller decided to disconnect the capacitor bank earlier comparing to case-study 1 because the total consumption of reactive power in the system was smaller in this case than case-study 1.

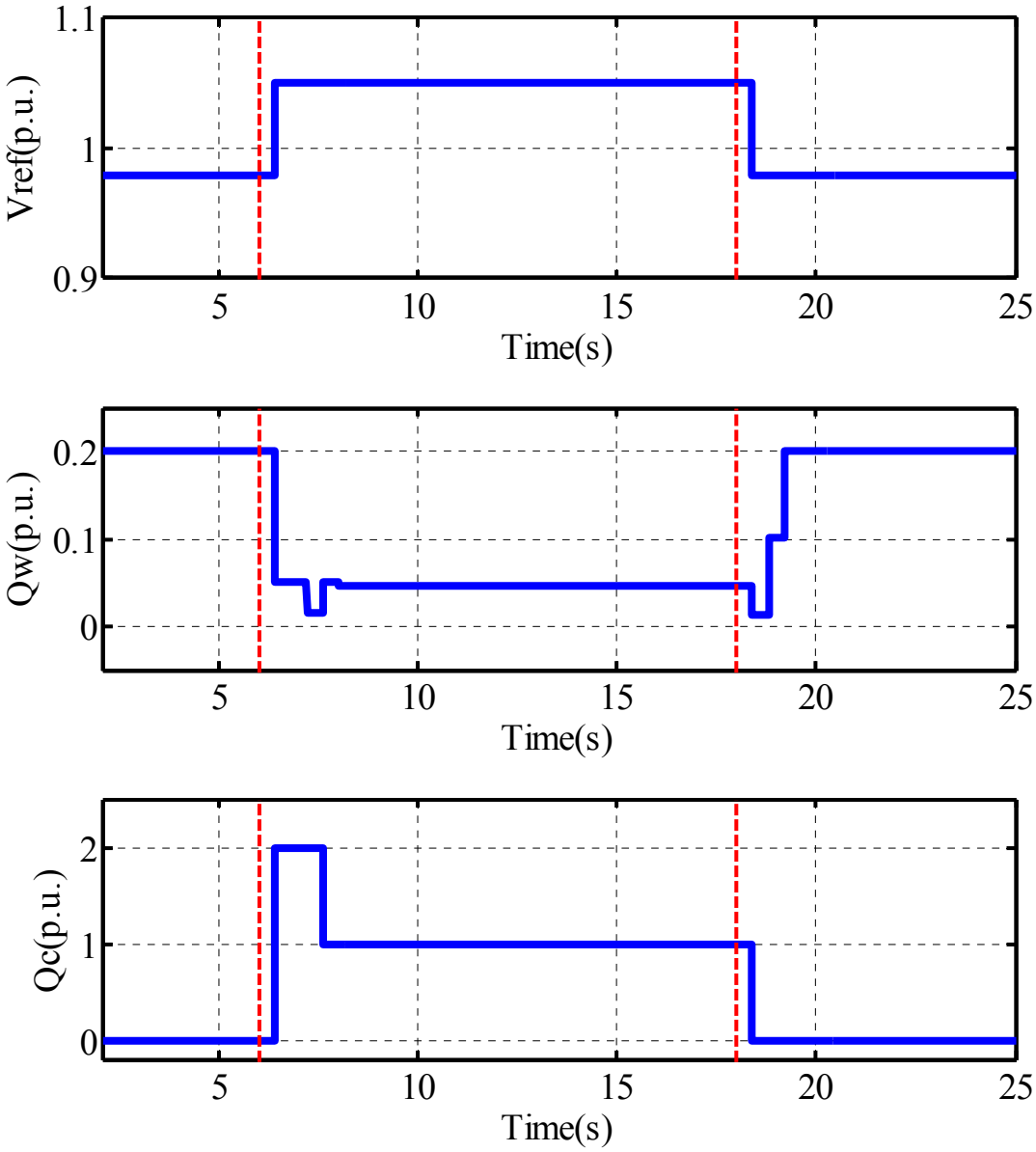

Figure 3-32 Control inputs to the system for 1 wind generator case

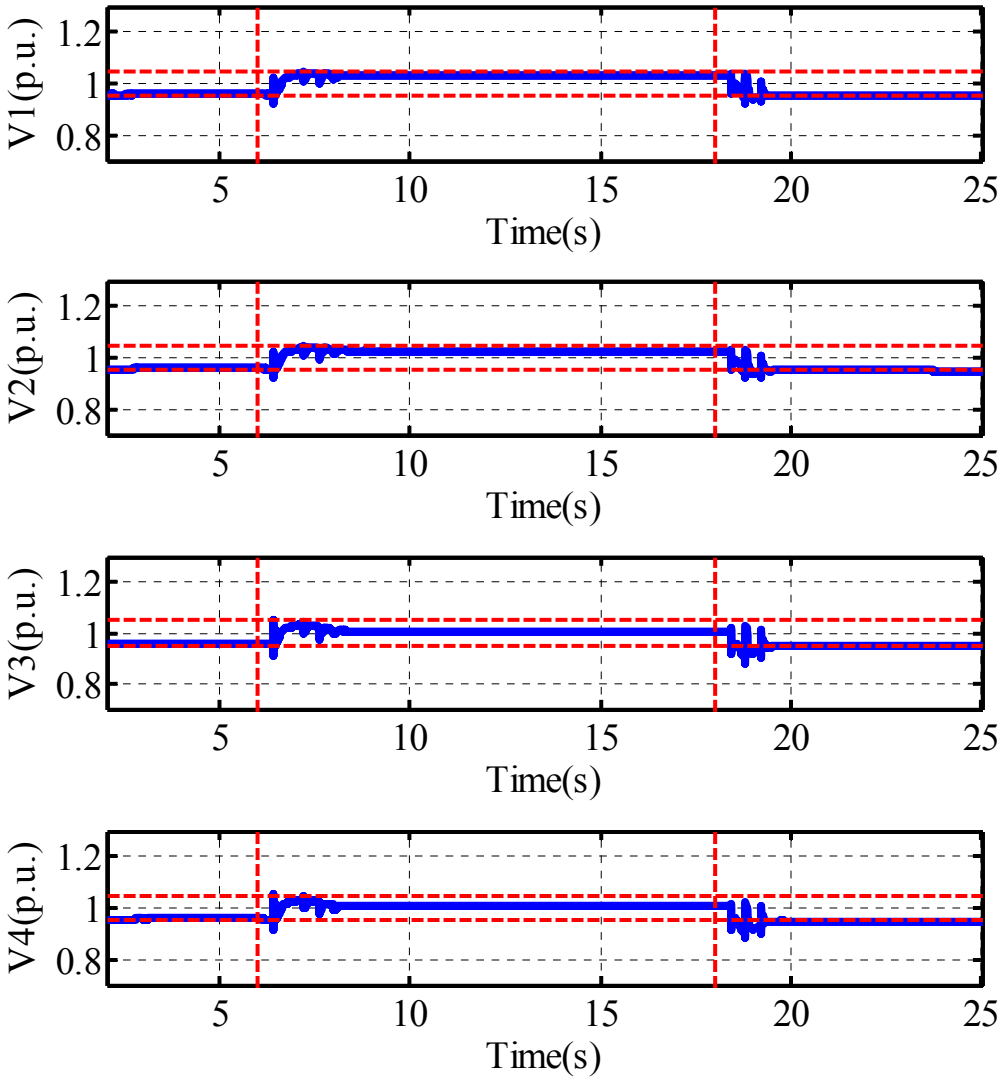

Figure 3-33 Bus voltages of the system for 1 wind generator case

3.2.5.3.5 Case-study 5 – two wind generators with half load

In this case study two wind turbines with generation capacity of 1 KVA each, were connected to bus 4. The synchronous generator in this case study had the capacity of 4.5 KVA. The wind profile in this case-study was similar to case-study 4. Figure 3-34 depicts the control inputs that the MPC controller sent to the system.

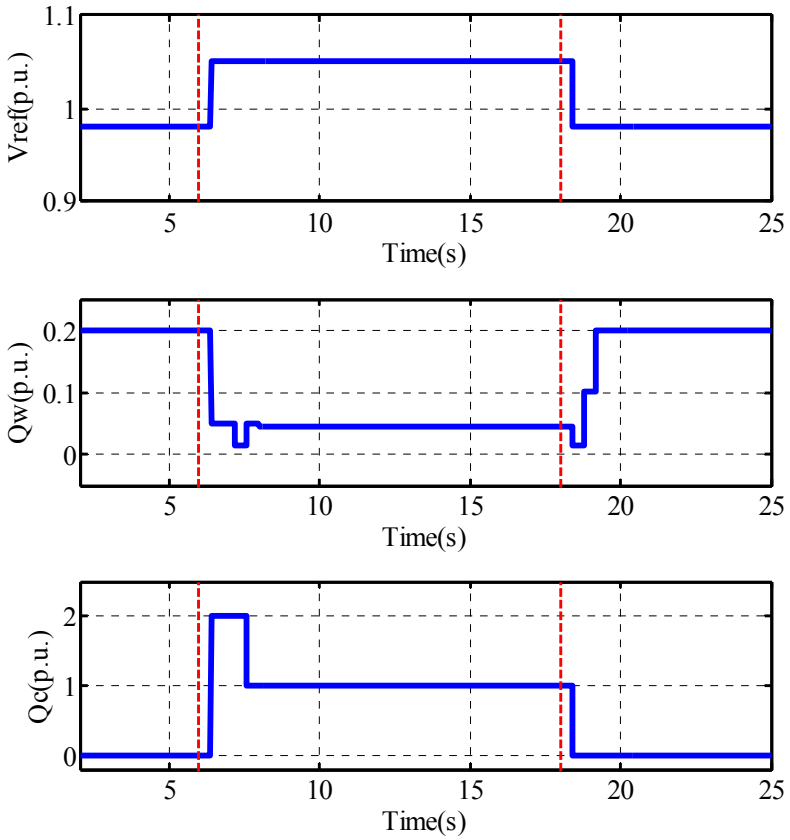

Figure 3-34 Control inputs to the system for 2 wind generator case

In this case-study the wind penetration was higher than case-study 4, but as can be seen in Figure 3-35, the MPC controller was still capable of keeping the bus voltages within limits.

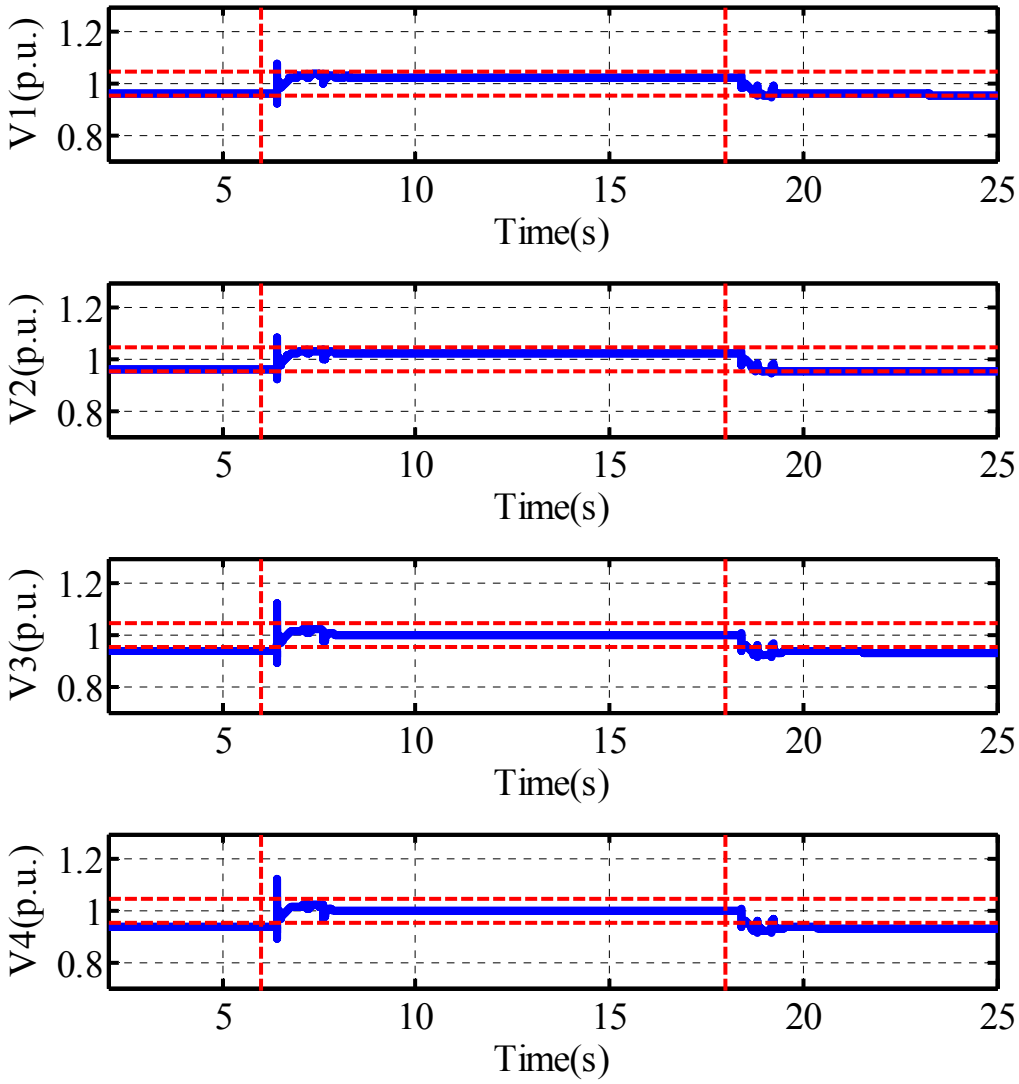

Figure 3-35 Bus voltages of the system for 2 wind generator case

3.2.5.3.6 Case-study 6 – Three wind generators with half load

In this case study three wind turbines with generation capacity of 1 KVA each, were connected to bus 4 and the synchronous generator connected to bus 1 had the capacity of 3.5 KVA.

The wind and load profile in this case-study is similar to case-study 4. However the wind energy penetration is higher in the system. As can be seen in Figure 3-36 and Figure 3-37, the MPC controller was still capable of keeping the voltages within limits in this case.

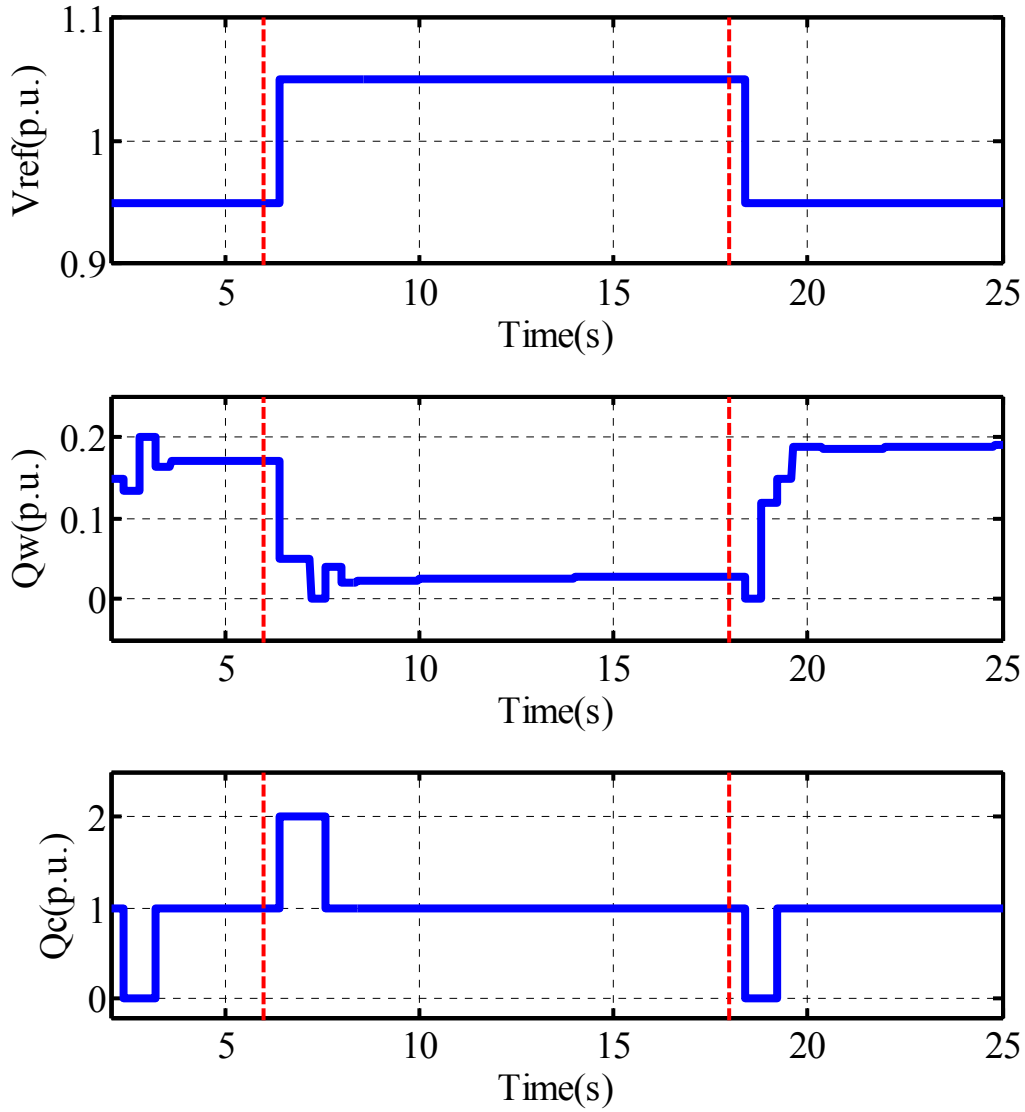

Figure 3-36 Control inputs to the system for 3 wind generator case

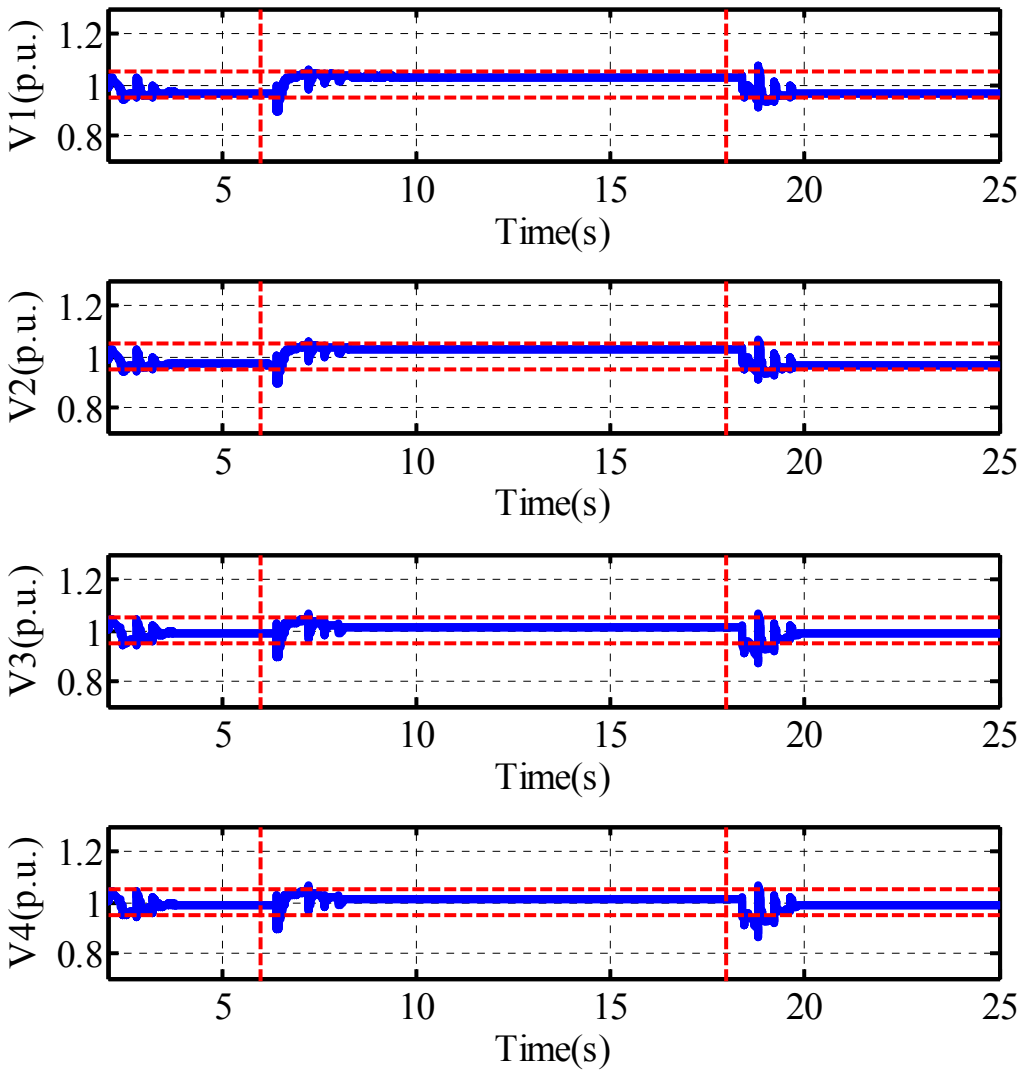

Figure 3-37 Bus voltages of the system for 3 wind generator case

In this case, the controller connected both of the capacitor banks initially after the wind speed drop to keep the system stable and then disconnected one of the banks after the initial disturbance in the system. Similarly, when the wind speed got back to the normal speed, the controller disconnected both of the capacitor banks initially for stability purpose and then reconnected one bank to the system.

3.3 Model Predictive Control Based Reactive Power Control of Isolated Power Systems

In this section, the basic concepts and methodologies needed to solve the hybrid control problem formulated in the section 3.2 will be provided. The section starts with a brief description of Model Predictive Control (MPC) of power system, which leads to a mixed integer linear or quadratic programming. Then Mixed Integer Linear Programming (MILP) and Mixed Integer Quadratic Programming (MIQP) are briefly discussed.

Model is traditionally referred to differential or difference equations derived from the physical or circuit dynamics of the studied system. These equations describe the system as a smooth linear or nonlinear function. Hence, most of the control system theories have been developed for smooth dynamic systems. However, in most of the cases, the real system includes logic such as on-off switches and the model of the system is not smooth. In a power system for example, capacitor banks and tap changers are logic inputs to the system. Therefore, in most applications including power systems, control of the logic inputs is performed using heuristic rules derived based on operator's experience of the physical system. Although these rules achieve the minimum requirements for some of the applications, they are not efficient all the times and can get troublesome especially when the system goes through fast mode changes. Therefore, the relatively new concept of hybrid systems and hybrid control has been introduced in the literature for this class of systems [79]. Obviously, the hybrid model of the system is needed for model

predictive control. In the next section, some typical methods to model a hybrid system will be discussed.

3.3.1 Model Predictive Control of Hybrid Systems Described in the MLD Form

MPC can easily solve problems with multiple inputs and outputs and state, input and output constraint. In addition, most of the hybrid models including MLD and PWA can be used as prediction models for MPC. This is an interesting feature, which makes MPC a good candidate for hybrid control problems. More details about the MPC formulation using MLD models can be found in [79].

MPC works based on a receding horizon policy which means a sequence of future control actions is chosen based on the prediction of the future behavior of the system and these control actions are applied to the system until future measurements are available. When new measurements are available, a new control sequence is calculated over the shifted horizon and replaces the previous one. This means that the receding horizon combines the constrained optimal control, which is an open loop procedure with a receding horizon policy, which provides the feedback to the controller and closes the control loop. More details about MPC could be found in [113],[114],[115]. The flow chart of MPC controller is depicted in Figure 3-38.

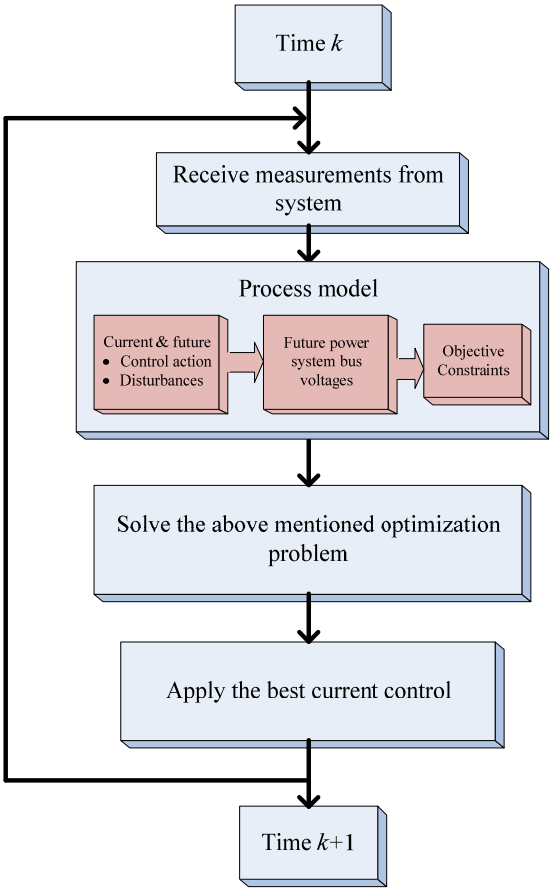

Figure 3-38 Flowchart of the MPC controller

The control sequence is calculated using an optimization which is a Mixed Integer Quadratic Programming (MIQP) or Mixed Integer Linear Programming (MILP) due to presence of integer variables in the system. The problem is solved over a finite or infinite horizon of time using the current state of the plant as initial state. Solving the problem over infinite horizon achieves best overall controller performance, however, in majority of the cases a finite horizon is chosen to limit the calculation time. In this work, a branch and bound algorithm is used to solve the MIQP problem. The branch and bound algorithm is presented to the extent needed for this dissertation. More details and full explanation about branch and bound can be found in [116].

The optimization problems stemming from MLD systems exhibit some predictable structural properties. For example, some blocks of constraints are repeated over the optimization vector due to the evolution of the studied system over the optimization time horizon. Thus, an efficient B&B algorithm can be designed tailored to the problem structure to reduce the amount of computation. The number of relaxed QPs (Quadratic Programs) that have to be solved during B&B gives a measure of complexity of a solution method for an MIQP. Although this number only gives a rough measure of complexity since it does not take complexity of the single QPs into account, it often reflects the time required to find a solution.

The main idea of branch and bound method lies in the fact that QP sub-problems are relatively easy to solve. In other words, the key concepts in branch and bound are:

- Separation of the original MIQP problem into QP sub-problems
- Relaxation of the integrality constraints (3-24), meaning that the integer variables are allowed to span the interval [0, 1].

The optimal solutions to the sub-problems represent lower bounds of the optimal value of the original MIQP problem [85]. A graphical representation of relaxation and separation concepts in B&B algorithms for an MIQP with three integers is shown in Figure 3-39.

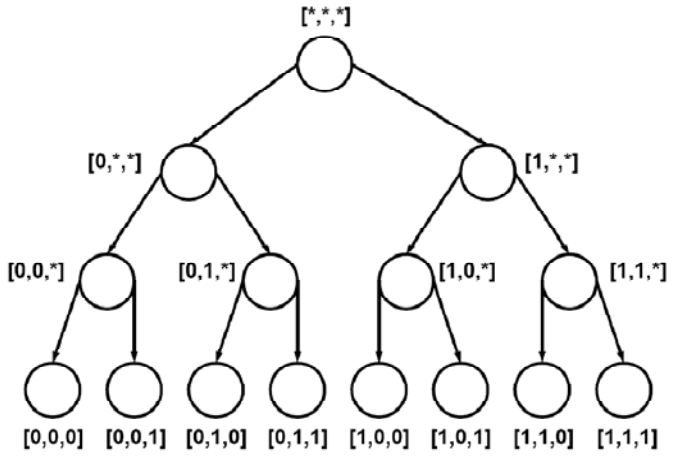

Figure 3-39 The binary tree for a MIQP with 3 integer variables. Each node is marked with the corresponding vector $\boldsymbol{\xi_j}$ [116]

A binary tree consists of nodes and branches and one node of the tree is chosen as the root. Each node except the root has a unique father, which is the predecessor node towards the root. Each node including the root can have subsequent nodes called children and a node without children is called a leave. A tree, where each node except the leaves has exactly *k* children is called a *k*-ary tree. The depth of a node is the number its predecessors towards the root. The *q*-th level of a tree is the set of all nodes with depth *q*. The length of a tree is the maximum depth over all its nodes.

A full *k*-ary tree of length *N* is a *k*-ary tree with k^N leaves, each at depth *N*. The tree obtained from a node ν by deleting the branch to its father and taking ν as root of a new tree is the subtree of node ν.

An MIQP problem can be represented as a tree. Let $\xi \in \{0,1\}^{n_d}$ be a vector having the same dimension as the vector of binary variables x_d, and let the symbol * mean that the corresponding entry of ξ is relaxed and spans the interval [0, 1]. The original MIQP

of (3-23) where all integrality constraints are relaxed is associated to the interval [0, 1] with the following.

$$\xi_{b\,0} = \underbrace{[* * \ldots *]}_{n_d\ times} \tag{3-157}$$

The vector $\xi_{b\,0}$ is assigned to the root of a k-ary tree. The separation of the original MIQP or any sub-problem into relaxed QPs is done by setting selected integer variables to 0 or 1. The resulting new QP problems are assigned to the children of the node. Separating the root [* * … *] to two new sub-problems results in the following.

$$\begin{aligned} \xi_{b\,1} &= [* , 0 , * , \ldots, *] \\ \xi_{b\,2} &= [* , 1 , * , \ldots , *] \end{aligned} \tag{3-158}$$

Figure 3-40 shows the separation of the root on the second variable.

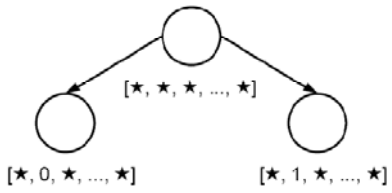

Figure 3-40 Separation of the roots on the second variable [116]

Each child is represented by a vector ξ_j, $\xi_j \in \{* ,0,1\}^{n_d}$ and if the *i*-th component $\xi_j^i = 0$ (or $\xi_j^i = 1$), then the QP corresponding to that node is solved by setting the *i*-th integer variable to 0 (or 1). If $\xi_j^i = *$, then the *i*-th integer variable of ξ_j is regarded as free within [0, 1] in the corresponding QP.

The branch and bound algorithm to solve MIQP can be summarized as follows.

Algorithm 1- Branch and Bound [117]:

1. Initialize a list of sub-problems for the original MIQP problem. Set

$$f_{opt} = +\infty \text{ and } x_{opt} = [\infty, \ldots, \infty]$$

2. If the list of sub-problems is empty, terminate the algorithm and send f_{opt} and x_{opt} to output. If $f_{opt} = +\infty$, send an error message that the MIQP is infeasible.
3. Select one sub-problem in the list of sub-problems to become the current problem and remove it from the list of sub-problems.
4. Relax the current problem, solve it, and denote its solution as f_R and its optimizer as x_R. (Relaxation)
5. If the current problem is infeasible go to step 2.

   Else if $f_R \geq f_{opt}$, go to step 2

   Else if x_R satisfies the integer constraints and $f_R \leq f_{opt}$, then update the current best solution by setting $f_{opt} = f_R$ and $x_{opt} = x_R$ and go to step 2. (fathoming)
6. Generate two new sub-problems from the current problem, add them to the list of sub-problems, and go to step 2. (Separation)

The performance of a B&B algorithm depends largely on steps 6 and 3. Separation in step 6 is performed by setting one binary variable to its two possible values. The chosen binary variable is called branching variable and its selection method defines the branching rule. The strategy of selecting the next current node in step 3 is called tree exploring strategy. A good B&B algorithm quickly fathoms large subtrees and avoids

formation of numerous sub-problems. The most common choices for the branching rule and the tree exploring strategy are presented in [117].

In this work, the outside first tree exploring strategy is used to solve the MIQP problem. The outside first strategy is tailored for optimal control problems using MLD systems where the values of binary variables $\delta(k)$ occasionally change over the time horizon, *N*. The integer optimization vector ξ_d in (3-24) contains samples of $\delta(k)$ taken at different time instants.

$$\xi_d = [\delta(k), \delta(k+1), \ldots, \delta(k+n_d-1)] \tag{3-159}$$

Typically, the binary variables $\delta(k)$ are associated with inequality conditions on continuous states $x(k)$ such as the following.

$$[\delta(k) = 0] \leftrightarrow [x(k) \leq x_0] \tag{3-160}$$

The continuous states, $x(k)$, usually have to satisfy dynamic equations. Therefore, their inertia prevents frequent switches of the binary indicator variable $\delta(k)$. This observation can be incorporated to make the B&B more efficient. In other words, the B&B algorithm should try to solve the QPs where the binary switch does not change prior to the other cases. However, a limited number of switchings should not be imposed over the prediction horizon since, although unlikely, an arbitrary number of switches might indeed occur. Therefore, the concept of guaranteed switches is introduced here to solve the problem.

3.3.1.1 Guaranteed switches definition

Given a subproblem given by ξ, let *I* be the ordered m-tuple collecting the indices *i* for which $\xi^i \neq *$,

$$I \triangleq [i_1\ i_2, \ldots, i_m] \text{ such that } \xi^{i_j} \neq * \quad \forall i_j \text{ and } i_1 < i_2 < \cdots < i_m$$

The number of *guaranteed switches*, *D*, is defined as the number of indices i_q in *I* such that $\xi^{i_q} \neq \xi^{i_{q+1}}$ [116].

Example:

Assume $\xi = [0,0,*,1,*,*,1,0,0,*]$. With the introduced notation, *I* = [1, 2, 4, 7, 8, 9], and *D* = 2. The outside first tree exploring strategy solves a QP in each column of Table 7 before moving on to the next column.

Table 7 Classification of sub-problems according to guaranteed switches in the binary variables for $n_d = 3$ [116]

Column -1, Original problem	Column 0, no guaranteed switches	Column 1, 1 guaranteed switch	Column 2, 2 guaranteed switches
[* * *]	[0 0 0] [0 0 *] [0 * *] [1 1 1] [1 1 *] [1 * *]	[0 0 1] [0 1 1] [1 1 0] [1 0 0] [0 1 *] [1 0 *]	[0 1 0] [1 0 1]

The order of the QPs in each column is arbitrary. Figure 3-41 shows the order that outside first strategy uses for exploration of the 3 binary tree. As can be seen in Figure 3-41 and Table 7, the MIQP tree is explored from the outside to the inside.

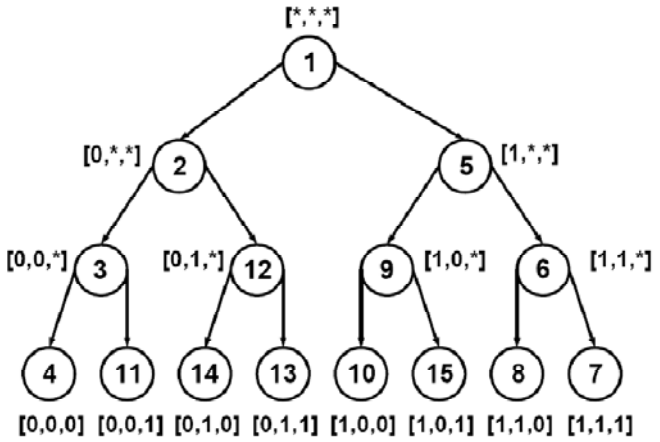

Figure 3-41 Order of solving problems in the outside first strategy, assuming the "first free variable" branching rule [116]

Algorithm 2- Branch and Bound with outside first tree exploring strategy [116]

1. Initialize a list of sub-problems from the original MIQP problem. Set

$$f_{opt} = +\infty \text{ and } x_{opt} = [\infty, \dots, \infty]$$

2. If the list of sub-problems is empty, terminate the algorithm and send f_{opt} and x_{opt} to output. If $f_{opt} = +\infty$, the MIQP problem is infeasible.

3. Determine k^o as the minimum number of guaranteed switches among the problems in the list of sub-problems. Select one problem with k^o guaranteed switches to become the current problem and remove it from the list of sub-problems.

4. Relax the current problem, solve it, and denote its solution as f_R and its optimizer as x_R.

5. If the current problem is infeasible go to step 2.

   Else if $f_R \geq f_{opt}$ go to step 2.

Else if x_R satisfies the integer constraints and $f_R \leq f_{opt}$ update the current best solution by setting $f_R = f_{opt}$ and $x_{opt} = x_R$.

6. Generate two new sub-problems from the current problem, determine their guaranteed switches, add them to the list of sub-problems, and go to step 2.

The hard restrictions on computation time due to time-step severely limit the chances to find a global minimizer to (3-23),(3-24), especially for large power system analysis problems with many binary variables. Therefore, the MIQP optimization method should aim at providing sufficient suboptimal solutions. Thus, the method changes the problem to choosing and solving the problems in the MIQP tree that are most likely to yield to a sub-optimal point close to the global minimum. Adding a maximum number of guaranteed switches, k_{max}, to the outside first tree exploration strategy allows for selecting and solving the QPs that are most promising in giving good suboptimal solutions. Bemporad and Morari [79] proved that for MPC problems using MLD stability is not altered by local minima, even though MPC controller's rate of convergence deteriorates.

The block diagram of the proposed model predictive controller based on MLD model of the MicroGrid is presented in Figure 3-42.

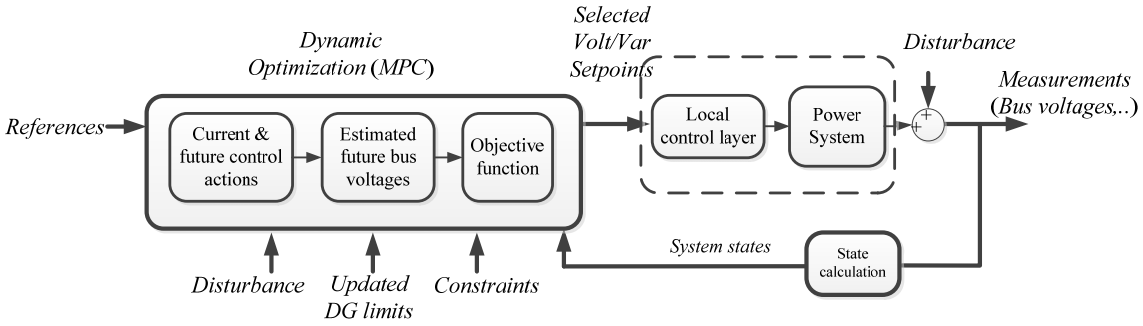

Figure 3-42 Block diagram of MPC for the MicroGrid

Summarizing the formulation of this section, the volt/Var optimization problem for the unbalanced system using the MLD model can be described as follows.

$$J(\boldsymbol{x},\boldsymbol{u},k)=\sum_{k=0}^{N-1}\Bigg\{\sum_{i\in N_t}\Big\{\left\|V_i{}^{A}(k+t_0|t_0)-V_i^{Nom}\right\|_{\{1,\infty\}}+\left\|V_i{}^{B}(k+t_0|t_0)-V_i^{Nom}\right\|_{\{1,\infty\}}+\left\|V_i{}^{C}(k+t_0|t_0)-V_i^{Nom}\right\|_{\{1,\infty\}}\Big\}+\|\boldsymbol{W_1}\Delta\boldsymbol{u}(k)\|_{\{1,\infty\}}+\|\boldsymbol{W_2}\Delta\boldsymbol{\sigma}(k)\|_{\{1,\infty\}}\Bigg\} \tag{3-161}$$

$$\text{Subj. to}\begin{cases}x(k+1|t_0)=Ax(k|t_0)+B_1u(k)+B_2\delta(k|t_0)+B_3z(k|t_0)\\ y(k|t_0)=Cx(k)+D_1u(k)+D_2\delta(k)+D_3z(k|t_0)\\ E_2\delta(k|t_0)+E_3z(k)\le E_4x(k|t_0)+E_1u(k|t_0)+E_5\\ V_{b_{min}}\le|V_b(k)|\le V_{b\,Max} & b=1,\dots.,N_{Bus}\\ Q_{c\,min}\le Q_c(k)\le Q_{c\,Max} & c=1,\dots,N_{comp}\\ |I_{cl}(k)|\le I_{cl\,Max} & cl=1,\dots,N_{cl}\end{cases}$$

3.4 Performance Analysis of the MPC Controller

As mentioned earlier the system presented in the MLD form is equivalent of PWA systems and the proof of this can be found in the appendix of [118]. Thus the

performance of MPC controlling a system presented in PWA platform which is easier to present for the general case is presented here. The PWA system is described in the following general form.

$$x(k+1) = A_i x(k) + B_i u(k) + f_i$$
$$y(k) = C_i x(k) + D_i u(k) + g_i \tag{3-162}$$

where $u(k) \in \mathbb{R}^{\mathrm{m}}$ is the control input to the system and $x(k) \in \mathbb{R}^{\mathrm{n}}$ is the state of the system. A Lyapanov function with the following general structure is used to prove the stability of the MPC controller.

$$V(x_c) = {x_c}^T P_i(x_c)\, x_c \tag{3-163}$$

where x_c is the equilibrium point of the system and P_i satisfies the following conditions.

$$P_i : \mathcal{X}_i \rightarrow \mathbb{R}^n \; \forall i \in I$$
$$\forall i \in I \rightarrow Sup_{x_c \in \mathcal{X}_i} |\lambda_{Max}(P_i(x_c))| < +\infty$$
$$\forall i \in I \rightarrow Sup_{x_c \in \mathcal{X}_i} |\lambda_{min}(P_i(x_c))| < +\infty \tag{3-164}$$

Possible choices of matrices $P_i(x_c)$ to guarantee the requirements on the eigenvalues are

- Continuous functions on $\mathcal{X}_i$ if $\mathcal{X}_i$ is bounded
- Constant matrices if $\mathcal{X}_i$ is unbounded

It should be mentioned that as shown in [119], the $V(x_c)$ can be discontinuous around the cell boundaries as long as the number of cells is finite. This is especially

helpful when dealing with piecewise systems. The following theorem presents the requirements for the system to be stable.

Theorem: Assume that the cardinality of the set I is finite. Let X_0 be a set of initial states, the equilibrium $x_c = 0$ of the PWA system presented in (3-162) is exponentially stable on X_0 if there exists a function $V(x_c)$ as in (3-163) which results in a negative forward difference as follows.

$$\begin{aligned}\Delta V(k+1,k) = {x_c}^T(k+1)P_i\big(x_c(k+1)\big)x_c\,(k+1)\\ - {x_c}^T(k)P_i\big(x_c(k)\big)x_c\,(k) < 0\end{aligned} \tag{3-165}$$

where i is the index for the condition $x_c(k) \in \mathcal{X}_i$.

This theorem basically means that if a lyapanov energy function can be found that is dissipative over the time horizon of the controller, then the system is exponentially stable.

Following [119] and assuming that the eigenvalues of the system are bounded for each of $P_i\big(x_c(k)\big)$ matrixes and assuming that the set I is cardinal there exist constants $\alpha, \beta > 0$ such that

$$\alpha I < P_i\big(x_c(k)\big) < \beta I\,, \forall i \in I \tag{3-166}$$

Further, there exist an arbitrarily small γ such that,

$$\begin{aligned}V\big(x_c(k+1)\big) - V\big(x_c(k)\big) \le\ -\gamma\ {x_c}^T(k)x_c(k) \le\ -\frac{\gamma}{\beta}\ {x_c}^T(k)P_i\big(x_c(k)\big)x_c(k)\\ = -\frac{\gamma}{\beta}V(x_c(k))\end{aligned} \tag{3-167}$$

Since the constant can be chosen arbitrarily small, γ can be chosen such that $0 < 1 - \frac{\gamma}{\beta} < 1$. Thus,

$$\forall k \in \mathbb{N}^+ \ \rightarrow V\left(x_c(k)\right) \leq \ \left(1 - \frac{\gamma}{\beta}\right)^k V\left(x_c(0)\right) \tag{3-168}$$

Which directly results in the following.

$$\forall k \in \mathbb{N}^+ \ \rightarrow \|x_c(k)\|^2 \leq \ \left(1 - \frac{\gamma}{\beta}\right)^k \|x_c(0)\|^2 \tag{3-169}$$

Equation (3-169) limits the norm of evolution of system trajectory based on the norm of the starting point.

The second part of our performance analysis of MPC deals with disturbance attenuation of the H_∞ platform. To begin with, the so called PWQ stability should be defined. The following class of lyapanov functions can be used to prove the stability of the continuous-time PWA systems without logic states [120].

$$\forall x_c \in \mathcal{X}_i \ \rightarrow P_i(x_c) = P_i \tag{3-170}$$

Using lyapanov functions of the class (3-170) results in the so-called Piecewise Quadratic (PWQ) stability. This result can be easily extended to systems with logic states.

Given a real number $\gamma > 0$, the exogenous signal ω is attenuated by γ if starting form a state x_0 satisfying $C(x_0) = 0$ for each integer $N \geq 0$ and for ever $\omega \in l_2([0, N], \mathbb{R}^m) - \{0\}$ it holds

$$\sum_{k=0}^{N} \|z(k)\|^2 < \gamma^2 \sum_{k=0}^{N} \|\omega(k)\|^2 \tag{3-171}$$

Following [118], some preliminary facts on the H_∞ norm of a PWA system for which the origin is PWQ stable can be established.

Lemma: Assume that the given system is PWQ stable and set $C(x_0) = 0$. Then, the H_∞ constraint is satisfied $\forall \gamma > \gamma_0$ where

$$\gamma_0 = \left(\tilde{C}^2 \bar{\gamma}^2 + \tilde{D}^2\right)^{\frac{1}{2}} \tag{3-172}$$

where,

$$\begin{gathered} \tilde{C} := \mathrm{Sup}_{i\in I}\left\|C_{c,i}\right\| \quad , \tilde{D} := \mathrm{Sup}_{i\in I}\|D_i\| \\ \gamma := \frac{\bar{L}_1 + \left(\bar{L}_1{}^2 + 4\bar{L}_2\right)^{1/2}}{2} \quad , \bar{L}_2 := \frac{L_1 \bar{P}}{\sigma} \\ L_1 := \mathrm{Sup}_{i\in I}\left\|A_{c,i}\right\|\left\|B_{c,i}\right\| \quad L_1 := \mathrm{Sup}_{i\in I}\left\|B_{c,i}\right\|^2 \quad \bar{P} := \mathrm{Sup}_{i\in I}\|P_i\| \end{gathered} \tag{3-173}$$

The proof of this lemma could be found in [118].

Lemma: Consider an initial state $x(0)$ such that $C(x(0))=0$. If there exists a function $V(x_c) = x_c{}^T P_i(x_c)\, x_c \quad \forall x_c \in \mathcal{X}_i$ satisfying the dissipative inequality (3-165), then the H_∞ performance condition (3-171) is satisfied and the PWA system is exponentially stable.

The proof of this lemma which gives a measure for performance H_∞ control of PWA systems could be found in [118].

3.5 Summary

This section discussed the problem formulation of dynamic reactive power control of the isolated power system. First, a simplified model of the system for reactive control was presented. Then, the model was linearzied in a piecewise linear form and the resulting linear model was discretized. The piecewise linear model was unified in the MLD form and the MLD model was used as a prediction model in reactive control.

4 MODEL PREDICTIVE BASED REACTIVE POWER CONTROL OF SHIPBOARD POWER SYSTEMS

4.1 Introduction

As discussed earlier, the AC/DC shipboard power system is consisted of AC generators and DC distribution zones. The DC zones add to system redundancy and reliability. The general Volt/Var control for an SPS may take a long time to converge. In order to shorten convergence time, the general voltage control problem should be divided into smaller scale sub-problems. It is commonly known that the only active power can be transmitted over DC links. Thus, the reactive power control can be decoupled into smaller scale problems by cutting the system at the DC links. Decoupling the Volt/Var control into smaller problems is beneficial since the

The high voltage AC system includes the synchronous generators, propulsion motors, and potentially high power pulsed AC loads. The high voltage AC system treats the DC zones as AC loads connected to the AC bus. The AC system also may include reactive power compensators placed close to loads at design stage. The voltage control scheme in this work, solves the voltage control problem of the AC system dynamically and sends reference voltage of generators and reactive power setpoints of compensators to these components. The optimization problem minimizes the voltage deviation of specific buses in the system, which are more vulnerable to voltage drop by setting the optimal control inputs.

The voltage control of the each DC zone is solved separately and locally in this work. Thus, each distribution zone is able to keep the voltage autonomously. The Zone is

composed of DC/DC converters, Inverters, DC and AC loads. The converters and inverters are the main components that can be used for voltage control inside the zones. Obviously, the rectifier can also be used to control the voltage level of the main DC buses of the system. The control scheme is local and the components are coordinated to keep the voltages of the buses within limits.

4.2 Implementation and Simulation Results

The sample SPS used in this paper for the case-studies is depicted in Figure 4-1. The system is composed of two synchronous generators, two zones and one propulsion motor. The objective function for the studied SPS is as follows.

$$J(\boldsymbol{x}, \boldsymbol{u}, k) = \sum_{k=0}^{N-1} \sum_{i \in \{5,6,7,8\}} \left\| V_i(k+t|t) - V_i^{Nom} \right\|_2 + \left\| \boldsymbol{W_1} \Delta \boldsymbol{u}(k) \right\|_2 \tag{4-1}$$

The control inputs to the system are reference voltages of generators (V_{ref1}, V_{ref2}) and the reactive power setpoint of the dynamic compensator (Q_c). Thus, the control input vector is as follows.

$$\boldsymbol{u}(k) = \left[V_{ref1}, V_{ref2}, Q_c \right] \tag{4-2}$$

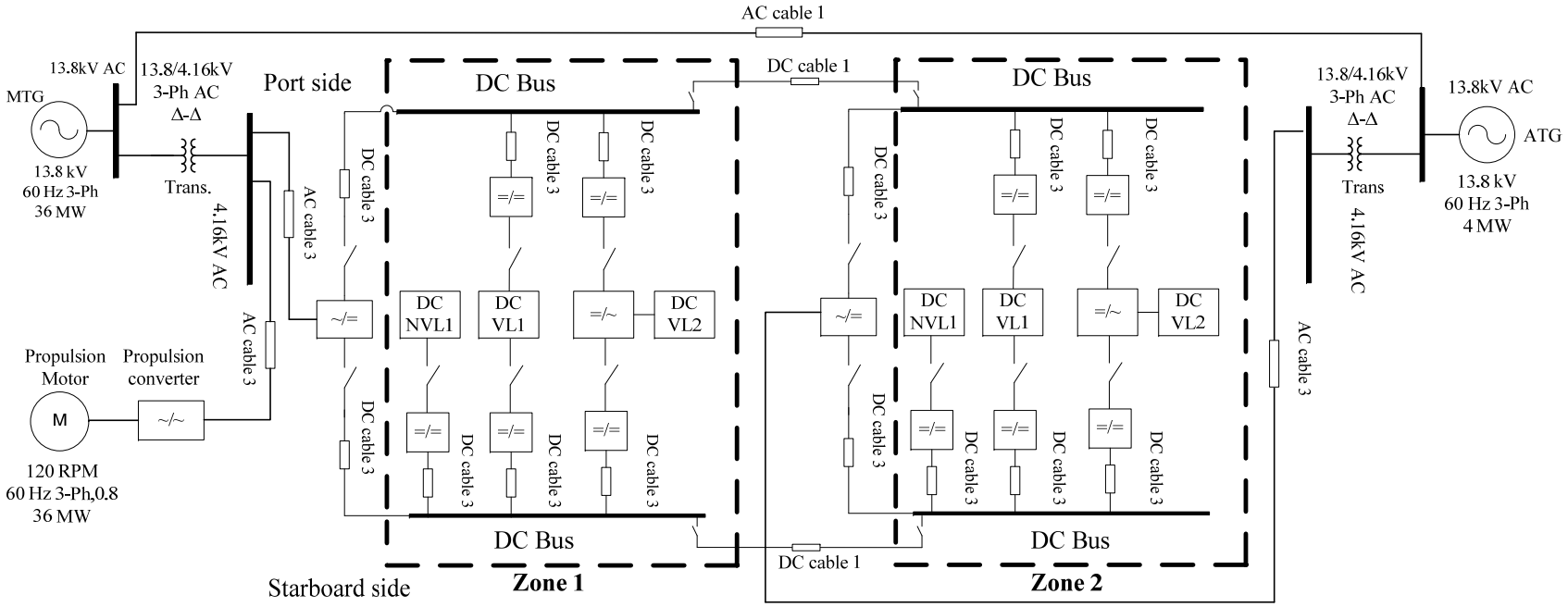

Figure 4-1 Schematic diagram of a notional all electric shipboard power system

The system has one master generator which is the main generator (MTG) and one distributed synchronous generator which is the auxiliary generator (ATG) in this case. The propulsion motor, two zones and the pulsed load are modeled as dynamic loads. Since the system had one master generator, one distributed generator, and three dynamic loads, the number of the states of the system was five.

Figure 4-2 shows the high level schematic diagram of the notional shipboard power system.

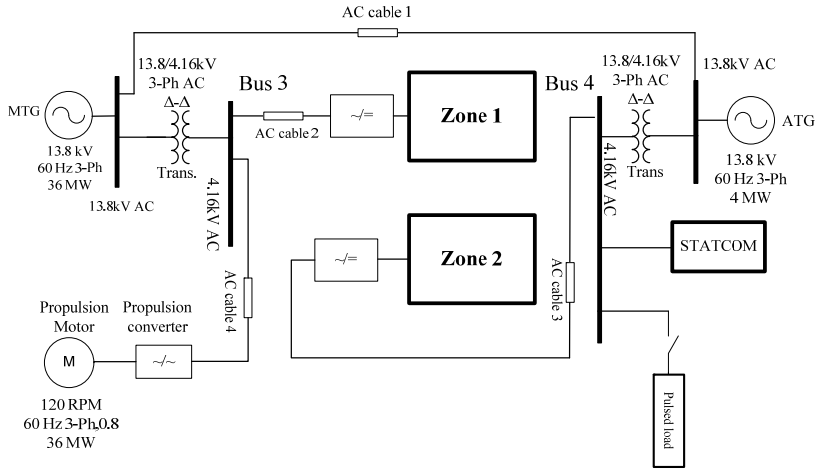

Figure 4-2 High level schematic diagram of a notional all electric shipboard power system

For the master DG, the simplified state space equations are as follows.

$$\dot{x}_1(t) = \frac{-1}{T_V}(t) + V_{ref}$$

$$V_{out}(t) = \frac{1}{T_V} x_1(t) \tag{4-3}$$

For the other DG in the system, the simplified state space equations are as follows.

$$\frac{d}{dt}\, x_2(t) = \frac{-1}{T_{Q,2}} x_2(t) + Q_{ref,2}$$

$$Q_{out,2}(t) = \frac{1}{T_{Q,2}}\, x_2(t) \tag{4-4}$$

Similarly, following (3-65) for the dynamic loads in the system, the linearized state space equations are as follows.

$$\frac{d}{dt}\, x_j = \frac{-1}{T_{q,j}} x_j + \left(D_j - \frac{C_j}{{T_{q,j}}^2} \right) V_k \,,$$

$$j = 5,6,7 \;\; , k = 4,7,8 \tag{4-5}$$

$$Q_{L,j} = Q_{L0,j} \left(\frac{1}{T_{q,j}}\, x_j + \frac{C_j}{T_{q,j}}\, V_k \right)$$

where V_k's are the voltage of the buses with the loads connected to them. Following the linearization technique discussed in [111], piecewise linear equations of the system are derived as follows.

$$\boldsymbol{x}(k+1) = \begin{cases} \boldsymbol{A_1 x}(k) + \boldsymbol{B_1 u}(k) & if\ \delta_1(k) = 1 \\ \vdots & \\ \boldsymbol{A_s x}(k) + \boldsymbol{B_s u}(k) & if\ \delta_s(k) = 1 \end{cases} \tag{4-6}$$

The bus voltages could be described in compact form as follows.

$$\boldsymbol{V} = \begin{cases} \boldsymbol{C_1 x}(k) + \boldsymbol{D_1 u}(k) & if\ \delta_1(k) = 1 \\ \vdots & \\ \boldsymbol{C_s x}(k) + \boldsymbol{D_s u}(k) & if\ \delta_s(k) = 1 \end{cases} \tag{4-7}$$

where V is the vector of the voltages that are used in the optimization formulation. Increasing the number of sets makes the prediction of voltage more accurate; however, the optimization algorithm takes more time to converge to the global minimum.

The input weight matrix is defined as $\mathbf{W}_1 = [0.1, 0.1, 0.01]$ which is designed to penalize the reactive power compensator less than the generators since providing reactive power by the reactive compensators is less costly.

The voltage, current and reactive power constraints of the SPS are given by following equations.

$$\begin{aligned} V_{b\,min} \le |V_b(k)| \le V_{b\,Max} \qquad & b = 3,4 \\ Q_{c\,min} \le Q_c(k) \le Q_{c\,Max} & \\ |I_{cl}(k)| \le I_{cl\,Max} \qquad & cl = 1, \dots, 4 \end{aligned} \tag{4-8}$$

where N_{Bus} is the number of buses, N_{Comp} is the number of compensators and N_{cl} is the number of the cables, $|V_b(k)|$ is the voltage magnitude of bus b at time k, $Q_c(k)$ reactive power setpoint of compensator c at time k and $|I_{cl}(k)|$ is the current of cable *cl* at time k.

The nonlinear SPS model with all details is implemented in SIMULINK and is considered as the actual power system. The measurements are taken from this power system and send as feedback to the model predictive controller. The MPC uses the MLD model achieved from HYSDEL compiler as the prediction model and performs the optimization over the horizon 10 seconds using the feedback of the system as the initial state. Solving the optimization problem results in the optimal control sequence, which is sent to the generators and the compensator of the SPS. The parameters of the generators are presented in Table 8.

Table 8 Generator parameters of the notional SPS

Generator Parameters			Exciter Parameters	
	MTG	ATG	MTG/ATG	
$V_{gl\text{-}l}$	13.8kV	13.8kV	*Tc*	0s
P_g	36 MW	4 MW	*Tb*	0s
p_{fg}	0.8	0.8	*Ka*	400pu
F	60 Hz	60 Hz	*Te*	0.02s
R_a	0.010Ω	0.199Ω	*Va,max*	14.5pu
X_p	0.17	0.18	*Va,min*	14.5pu (neg)
Xd	1.55	1.25	*Vr, max*	6.03pu
Xd′	0.22	0.24	*Vr,min*	5.43pu (neg)
Xd″	0.14	0.17	*kf*	0.03pu
Tdo′	8.95s	4.11s	*Tf*	1s
Tdo″	0.036s	0.023s	*Te*	0.8s
Xq	0.76	0.62	*Ke*	1pu
Xq′	N.A	N.A	*kc*	0.2pu
Xq″	0.20	0.26	*kd*	0.38pu
Tqo′	N.A	N.A	*SE(VE1)*	0.1pu
Tqo″	0.12 s	0.061s		
H	1.49s	1.06s		

The load and line parameters are summarized in Table 9 an the line lengths are presented in Table 10.

Table 9 Load and line parameters of the notional SPS

Load parameters	Value	Load parameters	Value
P_{L0-IM}	36 MW	bt	2
Q_{L0-IM}	9 MVar	T_{q-IM}	5s
P_{L0-z1} , P_{L0-z2}	4e6 MW	T_{q-z1} , T_{q-z2}	3s
Q_{L0-z1} , Q_{L0-z2}	1.8e6 MVar	$T_{q-Pulse}$	3s
bs	1		

Table 10 AC line length of the notional SPS

AC Line	Line length
Line 1	50m
Line 2	20m
Line 3	20m
Line 4	30m

Three voltage control case studies have been studied for the system.

4.2.1 Case-study 1- No Dynamic Compensator

In this case study, the SPS did not include a dynamic reactive compensator. A pulsed load was connected to bus 4 at t=2s for a duration of 2 seconds. It was assumed that the MPC knows the exact time of operation of the pulsed load. As can be seen in Figure 4-3, the MPC controller tried to compensate for the voltage drop by simultaneously boosting the excitation of the MTG and ATG generators. However, Figure 4-4 shows that the voltages of bus 3 and bus 4 dropped below the minimum acceptable level. In addition, overly boosting of the excitation of the synchronous generators resulted in a high voltage ripple on all the AC buses in the system and overcurrent of generator. This phenomenon deteriorates the electrical circuits of the generator. However, the controller could not avoid this condition since it needed to keep the system stable.

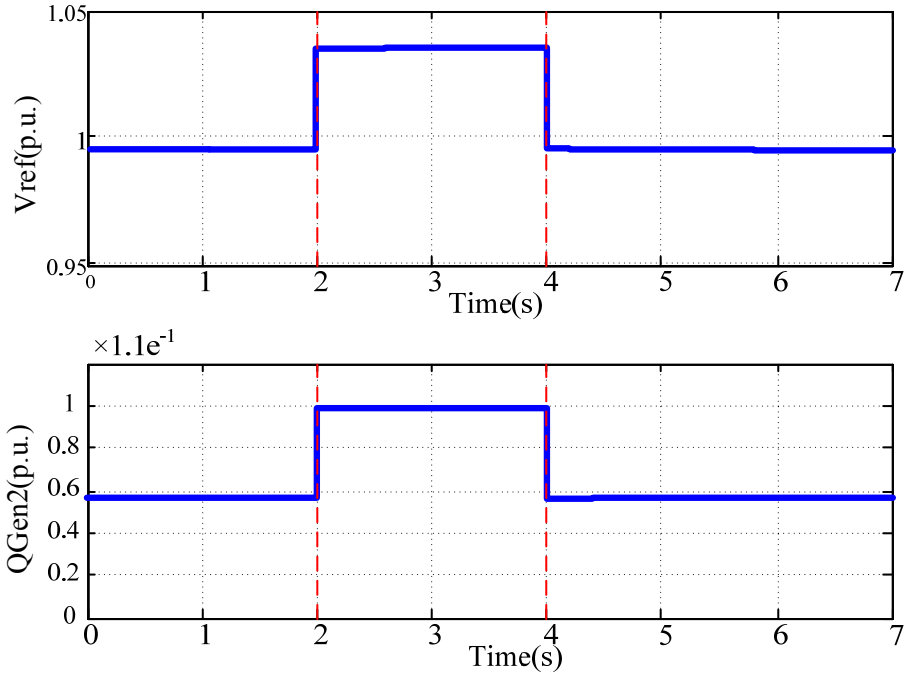

Figure 4-3 Control inputs to the SPS – Case study 1

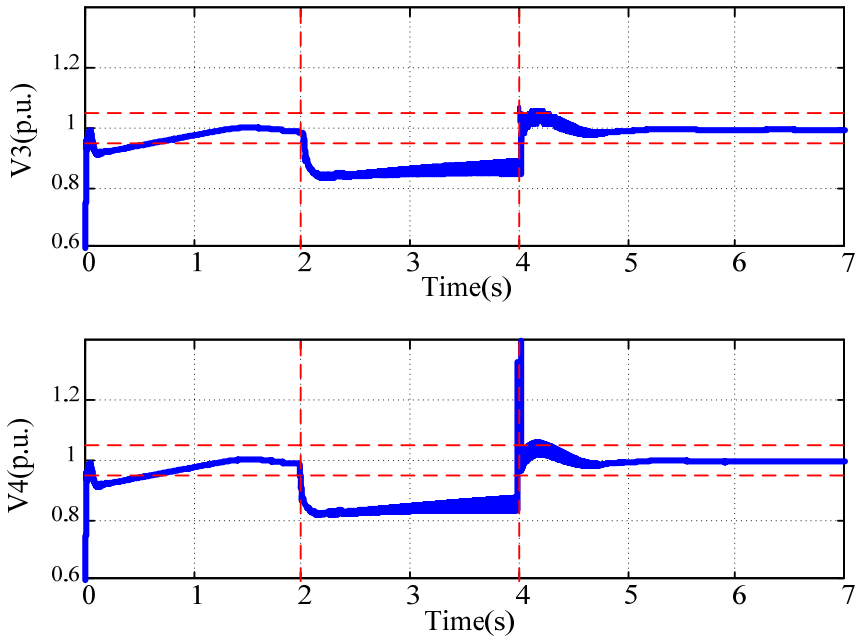

Figure 4-4 Bus voltages of the SPS – Case study 1

4.2.2 Case-study 2 – Dynamic Compensator

In this case-study, a pulsed load connected to bus gets energized at t=2s which applies a significant disturbance to the system. As can be seen in Figure 4-5, the global MPC controller tried to mitigate the effect of the disturbance on the voltages of the system by increasing the reference voltage of the master generator, increasing the reactive power setpoint of the PQ controlled generator, and increasing the reactive power setpoint of the dynamic compensator. As can be seen in Figure 4-6, SPS bus voltages stay within 5% limit and shows only small deviations. These voltage deviation satisfies the voltage requirements of section 4.6 of IEEE standard [121] for shipboard power system.

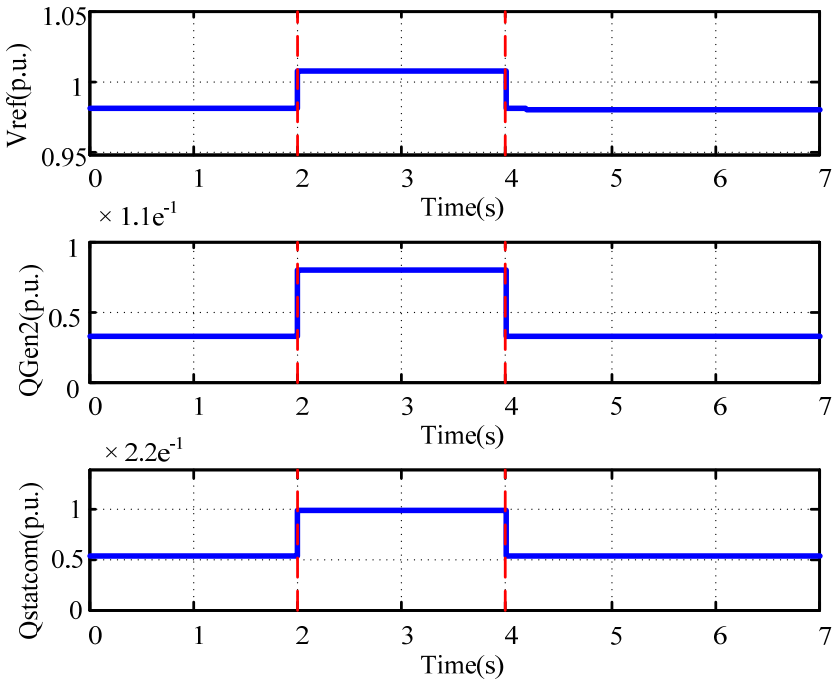

Figure 4-5 Control inputs to the SPS – Case study 2

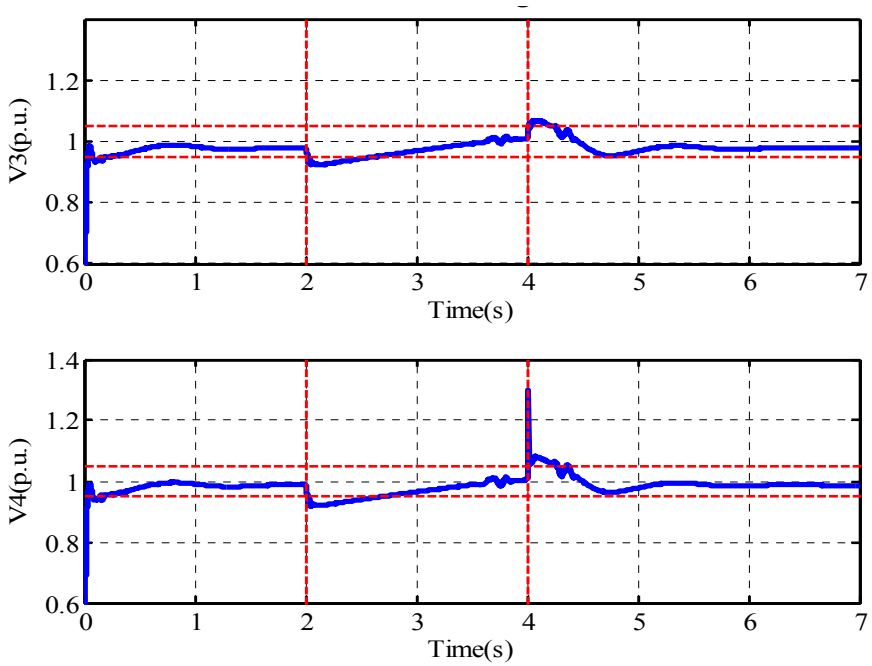

Figure 4-6 Bus voltages of the SPS – Case study 2

4.2.3 Case-study 3- Propulsion motor speed change

In this case-study, the speed of the propulsion motor changes from 2/3 of the nominal speed to the full nominal speed at t=9s. The inrush current that the induction motor is drawing from the system causes a disturbance in the system. This disturbance can be modeled as a pulse of reactive power drawn from the system, which causes voltage drop. The global MPC controller tries to mitigate the effect of the disturbance on the voltages of the system. The controller reacts to the voltage drop in 0.2 seconds. The bus voltages are depicted in Figure 4-7.

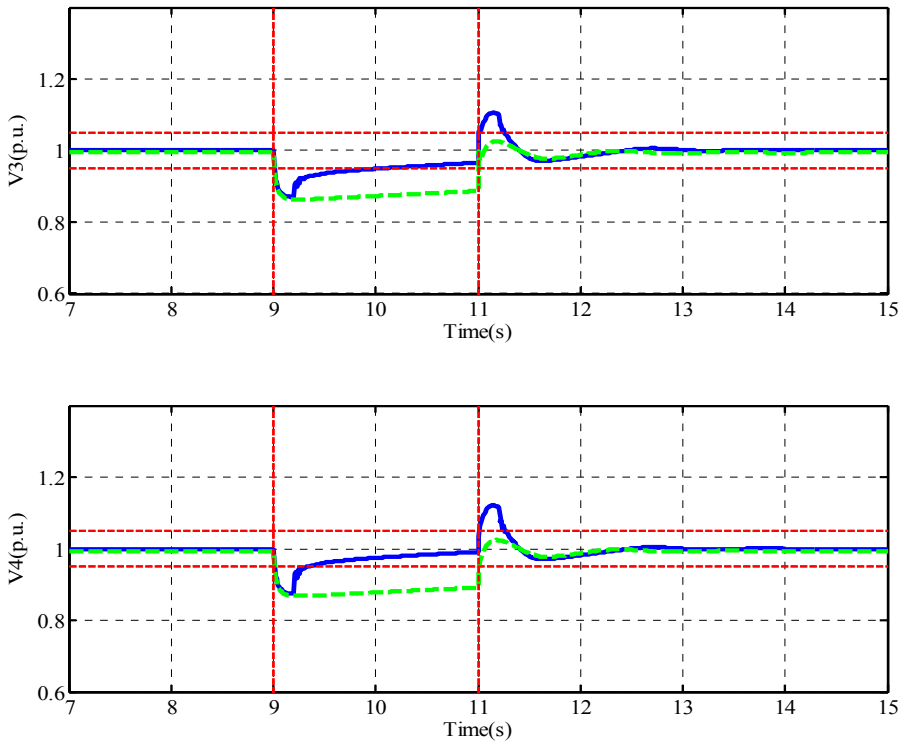

Figure 4-7 Bus voltages of the SPS – Case study 3

The control inputs generated by the MPC controller are shown in Figure 4-8. The controller increased the voltage reference of the master generator, increased the reactive power injection by the PQ generator, and increased the reactive injection by the D-STATCOM to achieve the reactive power control goals.

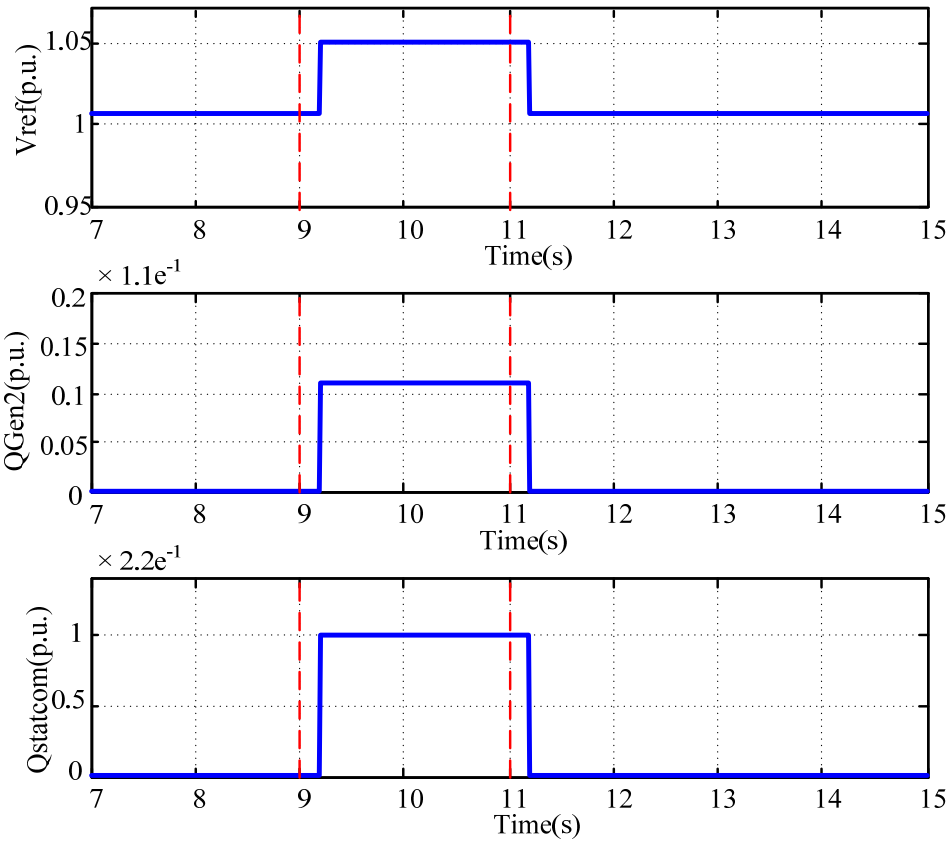

Figure 4-8 Control inputs to the SPS – Case study 3

4.3 Local Control of DC Distribution Zones

In this section, the structure of the DC distribution zone is discussed first. Then local voltage control scheme of the DC zone is discussed briefly. As mentioned before, voltage control of each DC zone is a sub-problem to the global voltage control problem and is solved locally.

The DC distribution zones are composed on DC/DC converters, Inverters, AC and DC loads. The loads can be vital and non-vital depending on the importance of their functionality. Vital loads typically have two possible paths to get energized. This

redundancy helps the system to keep the vital loads energized if one of the paths experience fault. The general structure of a DC zone is depicted in Figure 4-9. Each zone has a rectifier which supplies DC power to the zone. The rectifier, converter and the inverter are coordinated together to keep the voltage of the load at the nominal level.

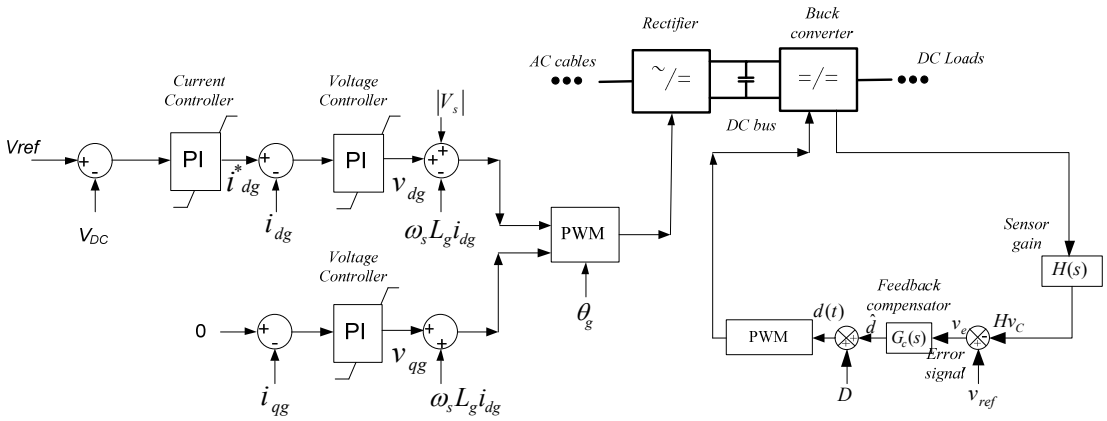

Figure 4-9 Block diagram of local controller to control the voltage of DC zones

4.4 Summary

This section discussed reactive power and voltage control of the SPS. The problem was formulated considering the dynamics of the SPS. MATLAB and CPLEX were used to implement the method. Finally, some case-studies were presented to show the effectiveness of the algorithm. Effectiveness of the methods was studied in presence of pulsed dynamic loads and changes in the propulsion of the ship.

5 MODEL PREDICTIVE BASED REACTIVE POWER CONTROL OF MICROGRIDS

5.1 Introduction

Voltage control is crucial in operation of the MicroGrid and the utility is responsible to keep the voltage at the receiving end of the distribution line within the acceptable range. The ANSI C84.1 standard specifies a guideline for the acceptable range by dividing it into emergency and normal operating ranges. The system may operate in the emergency range only for a short amount of time. Thus, the normal operating range is the focus for system operation. The ANSI C84.1 service voltage ranges are shown in Table 11.

Table 11 ANSI C84.1 voltage range for 120v [122]

	Service	
	Min	Max
Range A (Normal)	-5%	+5%
Range B (Emergency)	-8.3%	+5.8%

It should be noted that since the distribution system is usually radial, the service voltage is the main feeder voltage minus the losses on the transformers and lines in absence of DERs. Thus, the utility usually controls the service voltage by controlling the feeder voltage and sometimes by switching on load tap changers and switched capacitor banks. However, when the DERs are present in the system, the operator can also use

them to control the voltage especially when the DERs are interfaced to the system using power electronics. Further, in a system that may have to operate in islanded mode such as a MicroGrid, controlling the feeder voltage directly through the main grid is no longer possible. Thus, the DERs, reactive power compensators, and tap changers are the only voltage control inputs to the system in the islanded mode. A number of publications are available in the literature that discuss the challenges and benefits of using inverter-based DERs for voltage support [123],[124].

5.2 Photovoltaic Source

With an annual growth rate of 25-35%, photovoltaic sources are among the fastest growing energy sources over the past decade. Prior to 1999, the primary market for PV source was in off-grid applications. However, over 80% of the recent market for the PV source is for grid-connected applications where the source is connected to a strong grid or an isolated grid as a distributed generator [125]. As the use of PV sources continues to expand, research on potential benefits and risks that the PV source introduces on the stability and operation of the electricity grid grows as well.

The impact of the PV on the voltage of the grid is directly related to its penetration level. Generally, the PVs can be classified into three categories for voltage control based on their penetration level in the grid:

1) At a low PV penetration level of 5% or less, the inverters generally do not have a significant impact on the feeder's voltage regulation
2) At medium PV penetration levels which is around 10%, inverter voltage support can help reduce the size of the voltage support capacitors by nearly 40%

3) At high PV penetration levels (30% – 50%), PV inverters may be able to entirely replace voltage support capacitors

At higher penetration levels, inverter-connected PV generation takes over the place of conventional generation. In order to match the performance of the conventional generators, inverters have to be able to exchange reactive power with the grid. Certain changes in control and protection schemes may need to be performed to adapt the PV for voltage control. Inverter ratings may need to be increased to allow more significant impact on voltage control and the operation of inverters has to be coordinated to take full advantage of the available reactive power capabilities of the inverters [126]. The coordination can be performed using local methods such as the methods presented in [127],[128] or through a global optimal control scheme that sends the reactive setpoints to the inverters dynamically.

Solving the global optimization problem gives the setpoint of the reactive power Q of the units in the MicroGrid. The setpoints are used in control of the DG unit or to determine the injection by the reactive compensators. The DG units also have their own droop control which fine tunes the reactive setpoint to keep the voltage within limits. The droop control is needed for voltage stability and local reliability and to avoid voltage and reactive power oscillations. It also eliminates the effect of small errors in the setpoint [61]. The mentioned DG control structure is shown in Figure 5-1.

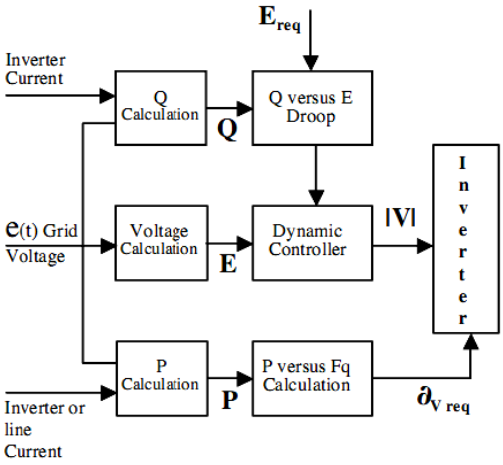

Figure 5-1 Control scheme of a DG unit [61]

Currently, standards such as IEEE 1547 and UL1741 state that the PV inverter "shall not actively regulate the voltage at the PCC." Thus, PV systems operate only provide active power to the grid in current implementations. However, this is only an agreement to make the PVs generate the maximum possible amount of active power and it is not due to the limitations of the inverters. A voltage regulation scheme that incorporates the reactive power capabilities of the PV sources would significantly increase the benefits of inverter-based DERs to the grid. Unfortunately, this interferes with most of the current anti-islanding schemes [129]. Thus, the anti-islanding schemes need to be updated as well in most cases.

With simple modifications in control scheme, most of the current inverters are capable of providing reactive power to the grid in addition to the active power but the amount is limited by the rate of the inverter and the amount of generated active power. This concept is illustrated in Figure 5-2 for a unidirectional inverter where inverter's

ratings are represented by a vector with magnitude S, the generated active power by the PV cells are denoted by *Ppv*.

The semicircle with radius *S* shows the inverter's possible operation range. Obviously, the feasible reactive range of the inverter is limited by the amount of generated active power. Reactive power limits are shown by $-Q_{limit}$ and Q_{limit} which shows that the inverter is capable of absorbing and injecting reactive power, respectively. Thus, theoretically the inverter is able to use its full rated power for reactive compensation when the generated real power is zero and cannot supply any reactive power when the full rating is used for generation of active power [126]. One method to overcome this drawback is to keep some reactive capability by over-sizing the inverter by 10-20%. The incentives for the DER operator to provide reactive power are increasing and maybe it becomes equal to the incentive of providing active power [1].

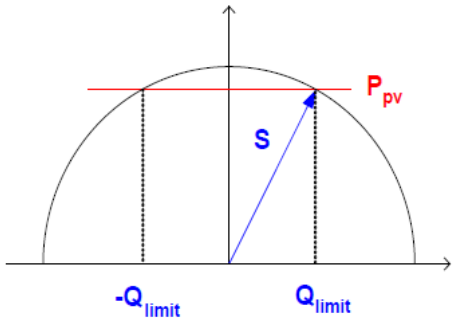

Figure 5-2 Reactive power generation limits by the PV inverter [126]

5.3 DFIG Wind Generator

DFIGs have become very common in wind power industry in the past decade. As explained before DFIGs need smaller converter than their rated power and are able to operate in variable-speed. Variable speed operation makes it possible to increase annual power production by 5% [130].

The stator of the DFIG is directly connected to the gird while the rotor is connected to the gird through a power electronics converter. The DFIG always supplies electric power to the grid from its stator and exchanges power with the grid from its rotor. The rotor power usually does not exceed 25% of the total generator power. The converter of the DFIG needs to be rated to handle rotor power and the excitation of the generator [131]. Thus, the converter rating is usually around 25% of the rated power of the generator, which results in lower component cost.

Squirrel cage induction generators were very common in wind industry two decades ago and they are still present. However, DFIGs and permanent magnet generators are taking their place due to some major advantages. These advantages include ability of DFIGs to control reactive power and voltage [132] and the potential to control active and reactive power independently through control of torque and rotor excitation current [133].

Although the grid requirements usually require the DFIGs to be reactive neutral, they can be used for reactive power control in some circumstances. The operating conditions of the DFIG can be classified into two categories based on the power grid they are connected to. These categories are as follows [134]:

- When DFIG is connected to strong power system the voltage is usually set to 1 PU. In this case, the DFIG does not exchange reactive power with the grid.
- When DFIG is connected to a weak power system, which suffers from fluctuating voltages, the DFIG can be used to produce or absorb reactive power for voltage control.

In the latter case, a PI controller can be added per customers request [135] to produce the reference signal of reactive power from the voltage error at the generator bus [136]. This type of control scheme controls reactive power locally and helps with grid voltage support. However, the results are not globally optimal due to the local nature of the control scheme.

The current grid code requires the wind farm to be reactive neutral and limits the control of reactive power absorption and generation through the wind farm to 10% of the maximum power [15]. However, it is beneficial to use reactive power capabilities of the DFIG generators for voltage compensation in weak power grid such as the MicroGrid. In MicroGrids for example, the grid side converter may be overdesigned to be able to inject or absorb 25-30% reactive power to the grid. Overdesigning the converter can be beneficial to overcome voltage fluctuations during fault condition.

Based on current grid code, the total time from the occurrence of a fault until establishment of normal voltage may not take more than 10 seconds [15]. Long voltage drops below 60-80% after a fault usually indicated that the turbine has accelerated too much that the power system cannot take it back to normal speed. The current control scheme performs a fast reduction of active power and a fast increase in reactive power to

overcome this situation. This scenario shows that overdesigning the converter can be helpful to post-fault voltage drops since more reactive power could be generated with less decrease in active power generation. Thus post-fault voltage compensation takes shorter time.

5.4 Connecting DERs to the Grid

Recent surveys show that the interconnection concerns from the electric utility point of view include reliability of the existing grid, the safety of electric power system personnel, and quality control. Thus, universal technical standards that permit standardized grid interconnection of the DERs while maintaining power system stability and worker safety is important in the MicroGrid design. The Institute of Electrical and Electronic Engineers (IEEE) presented a universal interconnection standard in winter of 1999 which is currently called IEEE P1547 standard [137]. The IEEE P1547 standard presents a uniform design standard for interconnection of DERs of 10 MVA or smaller with electric power systems. The requirements relevant to performance, operation, testing, safety, and maintenance of the interconnection are also included in the standard. Currently, the states of California, Texas, New York, and others have also set forth their own DER interconnection requirements [138].

The reactive power requirements of the MicroGrid during the islanded mode are important to consider in the design stage. DERs and compensators should be able to provide real and reactive requirements of the loads at an acceptable voltage level in the islanded mode operation of the MicroGrid. The reactive power requirements of the load during islanded mode operation and the reactive power resources should be studied in

the design stage. Particularly, reactive power resources need to be sufficient not only to provide steady-state reactive power demands, but also to provide dynamic reactive power demands, such as those related to motor starting within islanded MicroGrid. There needs to be sufficient reactive power resources available when operating induction machines or some inverter-based loads. Synchronous generators can typically provide rated power at 0.8 lagging power factor. Thus, it is important to include other sources of reactive power (e.g. capacitors) when designing the island system if the load's reactive requirements are far greater than the rating. Otherwise, the MicroGrid may not be able to provide the full-rated real power and that the generator's operation may be degraded [137].

In the local control scheme, the reactive power sharing operates under the following control method. The system reactive load level is provided to all of the generators operating on the common isolated bus. Then, each generator adjusts its own reactive power output to match the system-average reactive load. This is a closed-loop control method that is usually implemented with a proportional, integral, derivative (PID) algorithm, which results in more even control with less required readjustment to maintain satisfactory results. Unlike droop control, voltage control of the islanded system can be maintained by a control algorithm that corrects for low or high system voltage. The voltage-correction feedback is applied to all of the generators to maintain the desired system voltage.

Reactive power sharing requires that the system reactive power average be communicated to all generators. This is commonly achieved using an analog control

signal or digital control communication. In this approach, specifics of the equipment, interfaces, and available communications protocols may present challenges [106].

The protection devices placed at the interconnection of the DER to the power system measure the effective voltage and the fundamental frequency of the phase-to-phase voltages and if the measured voltage is in a range given in Table 12, the DER should stop energizing the area within the clearing time as indicated in the table. Clearing time is the maximum allowed time between the start of the abnormal condition and the DER disconnection from the system. For DERs smaller than or equal to 30 kW, the clearing time and voltage setpoint could be field adjustable or fixed. However, the voltage set points should be field adjustable for the DERs greater than 30 kW. The voltages shall be detected at either the PCC or the point of DER connection when any of the following conditions exist:

a) The aggregate capacity of DER systems connected to a single PCC is less than or equal to 30 kW,

b) The interconnection equipment is certified to pass a non-islanding test for the system to which it is to be connected,

c) The aggregate DER capacity is less than 50% of the total Local EPS minimum annual integrated electrical demand for a 15 minute time period, and export of real or reactive power by the DER to the area is not permitted [139].

It should be mentioned that the numbers mentioned in Table 12 are subject to change for isolated power systems. Isolated power systems typically have less strict requirements on voltage levels than grid connected systems [106]. The requirements for

isolated systems may vary from one system to another and are usually defined during system design.

Table 12 Requested fault clearing time for isolated power systems

Voltage range (% of base voltage[a])	Clearing time(s)
V<50	0.16
50<V<88	2.00
110<V<120	1.00
V>120	0.16

Placement of the DGs requires extensive studies on the MicroGrid. The weakest bus searching [140] is a simple method for DG placement. This method tries to maximize the loadability of a distribution system by placing a single DG at the weakest bus of the system. However, methods such as weakest bus or the largest load bus may not always lead to the best location for loss reduction and are not effective for placement of multiple DGs. Thus, an optimization problem to minimize the total cost and the active power loss should be solved in most cases. Optimal distributed generation (DG) placement [141] is usually formulated as a mixed integer nonlinear programming problem aiming at minimizing the total cost or the total active power loss. The optimal placement problem has been solved by a variety of optimization and search methods in the literature including repetitive load flow [142], the weakest bus searching [140], particle swarm intelligence [143], genetic algorithm [144], and linear programming [145].

5.5 Implementation and Simulation Results

As mentioned earlier, direct modeling of hybrid systems in MLD form is usually time consuming. In this work, HYbrid Systems DEscription Language (HYSDEL) [83] was used to derive the MLD form of the system. This program has a compiler that converts the textual description of the system to the MLD form. The MLD model of the system is then used as the prediction model in the MPC scheme. The MPT toolbox was used to solve the optimization problem. The MPT toolbox uses a branch and bound algorithm to solve the multi-parametric programming. Solving the multi-parametric problem leads to solving LP or QP problem and efficient solvers exist for these problems. CPLEX 12.2 engine was used to solve the MIQP.

5.5.1 Studies on an 11 bus MicroGrid

One MicroGrid studied in this work is depicted in Figure 5-3. The system was composed of four Distributed Generators (DGs), 11 buses, and some dynamic and static loads. The DGs were consisted of one diesel generator, 2 wind generators, and one solar generator. Two reactive power compensators were also present in the system which will be discussed more in the case-studies.

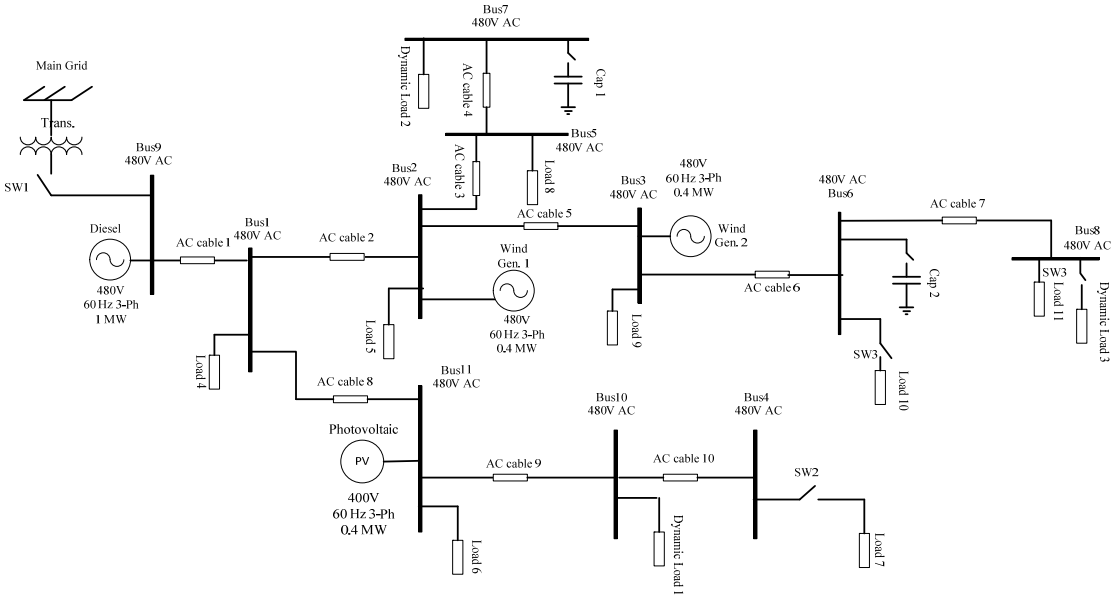

Figure 5-3 Schematic diagram of the studied MicroGrid

Parameters of the sources are presented in Table 13.

Table 13 Source parameters of the 11 bus MicroGrid

Diesel	Quantity	Wind & Solar	Quantity
$V_{gl\text{-}l}$	575V	$V_{gl\text{-}l}$ *(wind)*	575V
P_g	1MW	P_g *(wind)*	0.4 MW
p_{fg}	0.8	*Vs*	400 V
f	60 Hz	*Vr*	1975 V
R_a	0.199Ω	*F*	60 Hz
X_p	0.18	*Rs*	0.023 (p.u.)
Xd	1.25	*Ls*	0.18 (p.u.)
Xd'	0.24	*Rr*	0.016 (p.u.)
Xd''	0.17	*Lr*	0.16 (p.u.)
Tdo'	4.11s	*Lm*	2.9 (p.u.)
Tdo''	0.023s	*H*	0.685 (p.u.)
Xq	0.62	*f (wind)*	0.01 (p.u.)
Xq'	N.A	*Poles*	3
Xq''	0.26		
Tqo'	N.A	$V_{gl\text{-}l}$ *(solar)*	575V
Tqo''	0.061s	P_g *(solar)*	0.4 MW
H	1.06s	*f (solar)*	60 Hz

The objective function for reactive power control of the MicroGrid shown in Figure 5-3 was chosen as follows.

$$J(x,u,k)=\sum_{k=0}^{N-1}\left\{\begin{array}{c}\left\{\sum_{i\in\{5,6,7,8\}}\left\|V_i(k+t_0|t_0)-V_i^{Nom}\right\|_2\right\}\\ +\|\boldsymbol{W_1}\Delta\boldsymbol{v}(k)\|_2+\|\boldsymbol{W_2}\Delta\boldsymbol{\sigma}(k)\|_2\end{array}\right\} \tag{5-1}$$

Control inputs to the system were the reference voltage of synchronous diesel generator (V_{ref}), reactive power setpoints of the DGs, and the reactive power setpoint of the dynamic compensator (Q_{c1}, Q_{c2}). Thus, the control input vectors were as follows for the case where power electronics compensators were placed in the MicroGrid.

$$\boldsymbol{v}(k)=\left[V_{ref},Q_{W1},Q_{W2},Q_{PV},Q_{c1},Q_{c2}\right]^T,\quad \boldsymbol{\sigma}(k)=\ [0,0]^T \tag{5-2}$$

For the case studies where capacitor banks were placed in the system the control input vectors were as follows.

$$\boldsymbol{v}(k)=\left[V_{ref},Q_{W1},Q_{W2},Q_{PV}\right]^T,\quad \boldsymbol{\sigma}(k)=\ [Q_{c1},Q_{c2}]^T \tag{5-3}$$

Since the system had four distributed generators, and two dynamic loads, the number of the states of the system was six. For the master DG, the simplified state space equations were as follows.

$$\begin{aligned}\dot{x}_1(t)&=\frac{-1}{T_V}x_1(t)+V_{ref}(t)\\ V_1(t)&=\frac{1}{T_V}x_1(t)\end{aligned} \tag{5-4}$$

For the other DGs in the system, the simplified state space equations were as follows.

$$\frac{d}{dt}\, x_i(t) = \frac{-1}{T_{Q,i}} x_i(t) + Q_{ref,i}(t)$$
$$Q_{DG,i}(t) = \frac{1}{T_{Q,i}}\, x_i(t) \quad , \quad i = 2,3,4 \tag{5-5}$$

Similarly, following (3-65) for the dynamic loads in the system, the linearized state space equations were as follows.

$$\frac{d}{dt}\, x_j(t) = \frac{-1}{T_{q,j}} x_j(t) + \left(D_j - \frac{C_j}{{T_{q,j}}^2}\right) V_k(t)\,,$$
$$j = 5,6,7 \;, k = 4,7,8 \tag{5-6}$$
$$Q_{L,j}(t) = Q_{L0,j}\left(\frac{1}{T_{q,j}}\, x_j(t) + \frac{C_j}{T_{q,j}}\, V_k(t)\right)$$

where V_k's are the voltage of the buses with the loads connected to them. Following the linearization technique discussed in [111], piecewise linear equations of the system were derived as follows.

$$\boldsymbol{x}(k+1) = \begin{cases} \boldsymbol{A_1 x}(k) + \boldsymbol{B_1 u}(k) & if\ \delta_1(k) = 1 \\ \vdots & \\ \boldsymbol{A_s x}(k) + \boldsymbol{B_s u}(k) & if\ \delta_s(k) = 1 \end{cases} \tag{5-7}$$

The bus voltages can be described in compact form as follows.

$$\boldsymbol{V} = \begin{cases} \boldsymbol{C_1 x}(k) + \boldsymbol{D_1 u}(k) & if\ \delta_1(k) = 1 \\ \vdots & \\ \boldsymbol{C_s x}(k) + \boldsymbol{D_s u}(k) & if\ \delta_s(k) = 1 \end{cases} \tag{5-8}$$

where V is the vector of the voltages that are used in the optimization formulation. Increasing the number of sets makes the prediction of voltage more accurate; however, the optimization algorithm takes more time to converge to the global minimum.

The voltage, current and reactive power constraints of the SPS are given by following equations.

$$\begin{aligned} V_{b\,min} \le |V_b(k)| \le V_{b\,Max} \qquad & b = 3,4 \\ Q_{c\,min} \le Q_c(k) \le Q_{c\,Max} \qquad & c = 1,2 \\ |I_{cl}(k)| \le I_{cl\,Max} \qquad & cl = 1,\dots,4 \end{aligned} \tag{5-9}$$

where N_{Bus} is the number of buses, N_{Comp} is the number of compensators and N_{cl} is the number of the cables, $|V_b(k)|$ is the voltage magnitude of bus b at time k, $Q_c(k)$ reactive power setpoint of compensator c at time k and $|I_{cl}(k)|$ is the current of cable *cl* at time *k*.

A partial sample of the MLD model of the MicroGrid is presented in Table 14.

Table 14 Sample of the MLD model for the studied MicroGrid

No	Constraint type	Description
1	Eq. 7x1	x_2 == A*x_1 + B1*u_1 + B2*d_1 + B3*z_1 + B5
2	Eq. 7x1	y_1 == C*x_1 + D1*u_1 + D2*d_1 + D3*z_1 + D5
3	Ineq. 20x1	E2*d_1 + E3*z_1 <= E1*u_1 + E4*z_1 + E_5
4	Ineq. 20x1	MLD.zl < z_1 < MLD.zu
5	Ineq. 12x1	umin < u_0 < umax
6	Eq. 1x1	u_0(5) in [0 0.2 0.3]
7	Eq. 1x1	u_0(6) in [0 0.2 0.3]
8	Ineq. 12x1	xmin < x_0 < xmax
9	Ineq. 12x1	ymin < y_0 < ymax
…	…	…

The photovoltaic source was controlled using an MPPT algorithm. The controller of the wind generator was also designed to send the maximum active power to the system and the reactive power was regulated through an external PID. Details of the MPPT and local controller are beyond the scope of this dissertation.

The loads are modeled in the prediction model as dynamic loads and the MLD model of the system was derived with the approach discussed in the paper for a horizon of 12 time steps ahead and each time step is 0.2 seconds. The input weight matrix was defined as $\boldsymbol{W_1} = [0.1, 0.01, 0.01, 0.01]$, $\boldsymbol{W_2} = [15, 15]$ which was designed to penalize the reactive power compensator less than the generators since providing reactive power by the reactive compensators is less costly.

The studied MicroGrid with all details was implemented in SIMULINK and was considered as the actual power system. The measurements were taken from this power system and sent as feedback to the model predictive controller. The MPC used the MLD model achieved from HYSDEL compiler as the prediction model and performed the optimization over the horizon *N* using the feedback of the system as the initial state. Solving the optimization problem resulted in the optimal control sequence, which was sent to the sources and the compensators of the MicroGrid.

The load and line parameters of the studied MicroGrid are summarized in Table 15.

Table 15 Load and line parameters of the 11 bus MicroGrid

Symbol	Quantity	Symbol	Quantity
PL0-1	0.1 MW	*QL-4*	0.03 MVar
QL0-1	0.2 MVar	*PL-5*	0.1 p.u.
PL0-2	0.1 MW	*QL-5*	0
QL0-2	0.1 MVar	*PL-6*	0.02 p.u.
PL0-3	0.1 MW	*QL-6*	0.07 p.u.
QL0-3	0.1 MVar	*PL-7*	0.1 p.u.
bs1-3	1	*QL-7*	0
bt1-3	2	*PL-8*	0.10 MW
Tq1-3	3sec	*QL-8*	0 MVar
PL 10	0.05 MW	*PL-9*	0.2 MW
QL 10	0.2 MVar	*QL-9*	0.1 MVar
PL 11	0.2 MW	*QL 11*	0 MVar
PL-4	0.05 MW		

5.5.1.1 Case-study 1

In this case-study, loads 7,10 got connected at t=2s in the sample MicroGrid shown in Figure 5-3. These loads remained connected until *t*=3.2*s* where load 7 was disconnected but load 10 stayed connected to the system. In this case study, capacitor banks were considered as reactive power compensators and were connected to bus 6,7. In this case study, capacitor banks were considered as reactive power compensators and were connected to bus 6,7. Two capacitor banks rated 150 kVar were connected to bus 6 and two capacitor banks each rated at 100 kVar were connected to bus 7. The time horizon was selected as 12 and the step time was considered to be 0.2s. The prediction model was implemented in HYSDEL which transfers the model to MLD form. The

MLD was used as prediction model and the optimization was performed using CPLEX 12.2.

The optimization problem led to solving a Mixed Integer Quadratic Programming (MIQP) problem since norm 2 was used in the objective function. The voltages of the load buses are shown in Figure 5-4 and the control inputs are depicted in Figure 5-5. As can be seen in the figure, the dynamic reactive controller responded faster to the change in the load and results in smoother voltage profile. The active and reactive power tracking of the wind generator 1 and the PV source are depicted in Figure 5-6 and Figure 5-7 respectively.

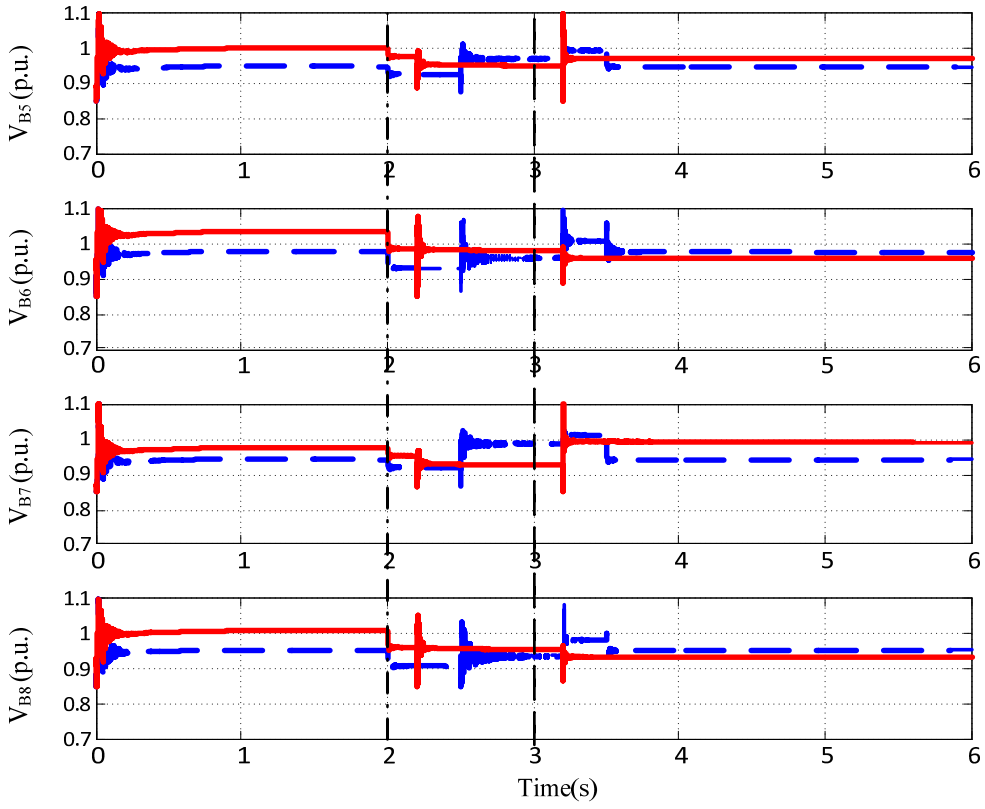

Figure 5-4 RMS voltage of bus 5,6,7,8 – MPC (solid line), Local Control (dashed line) in case study 1

As can be seen in Figure 5-5, the controller adjusted the reactive power coordination by decreasing the voltage reference of the master generator, decreasing the reactive power setpoint of wind generators and the solar generator, and adding two capacitor banks at the connection point of capacitor 2. After one the loads gets energized, the controller responds by disconnecting one capacitor at the connection point of capacitor 2 and connecting two capacitors at the connection point of capacitor 1. These changes add up to the best compensation that results in the voltages to stay within limits. Figure 5-6 and Figure 5-7 show how one wind generator and one solar generator responded to the reactive power setpoint change.

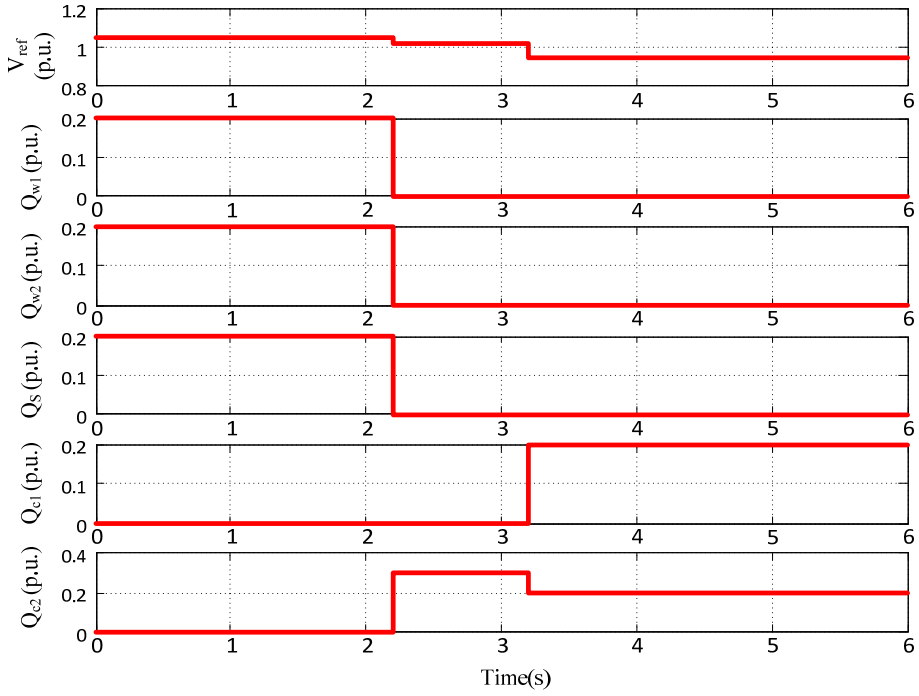

Figure 5-5 Control inputs to the MicroGrid in case study 1

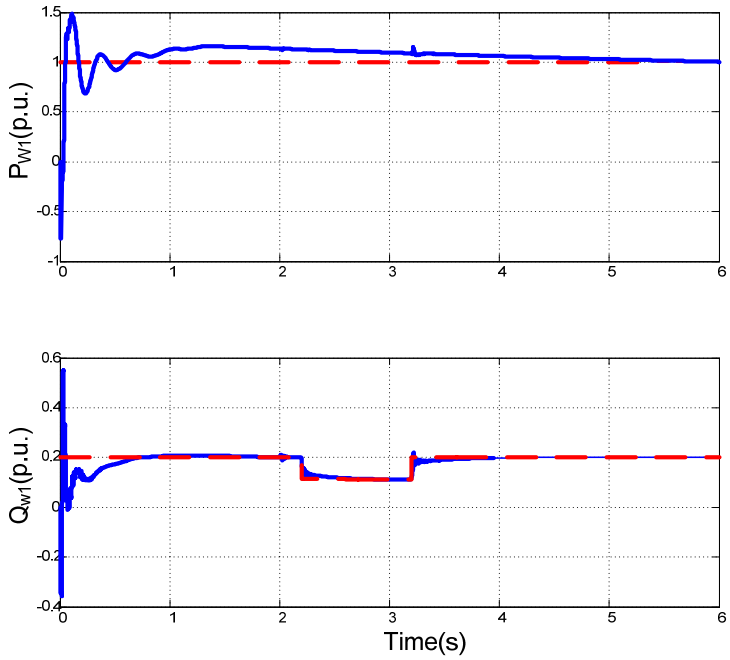

Figure 5-6 Active and reactive response of wind generator 1 for case study 1 (solid line), control inputs (dotted line)

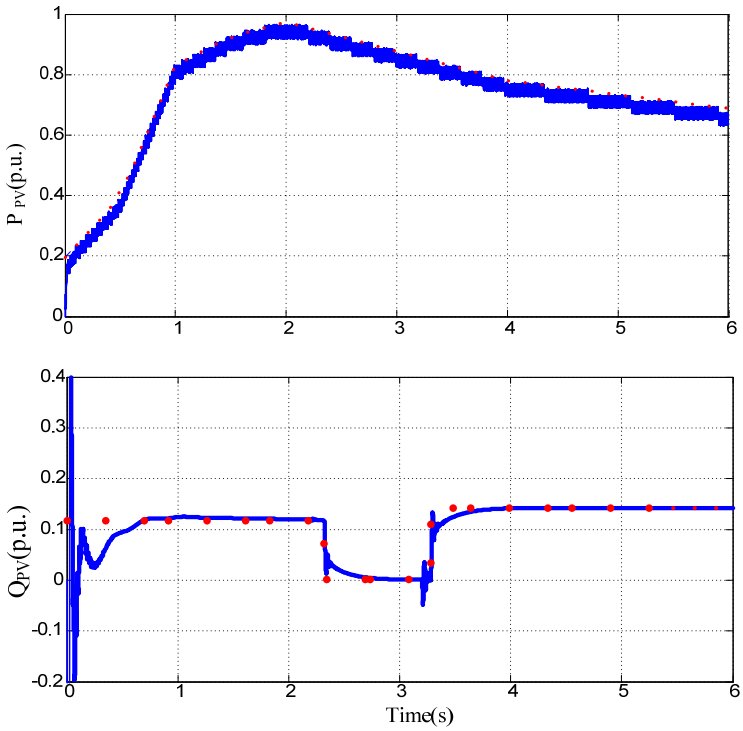

Figure 5-7 Active and reactive response of the PV source for case study 1 (solid line) – control inputs (dotted line)

5.5.1.2 Case-study 2:

In this case-study, the same load change pattern as case-study 1 occurred in the system. However, STATCOMs were used for reactive power compensation instead of capacitor banks. The problem formulation was the same as case-study 1. The voltage of the load buses are shown in Figure 5-8 and the control inputs are depicted in Figure 5-9. The results demonstrate that the dynamic reactive controller successfully kept the system close to nominal voltage; however, the local control scheme was unable to satisfy system voltage constraints in this case.

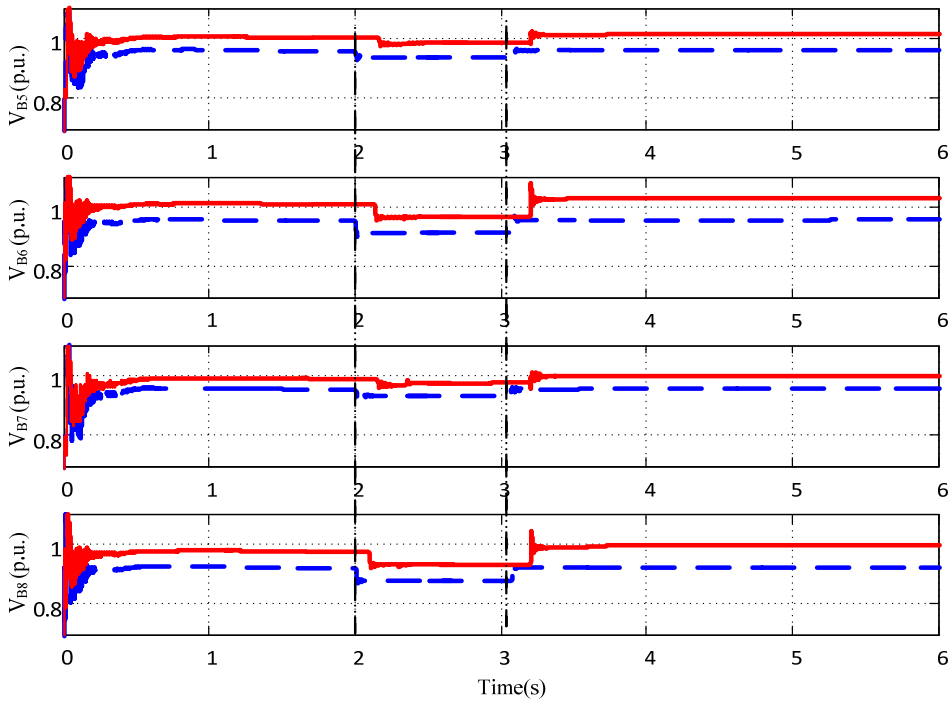

Figure 5-8 Voltage of Bus 5,6,7,8 – MPC (solid line), Local Control (dashed line) in case study 2

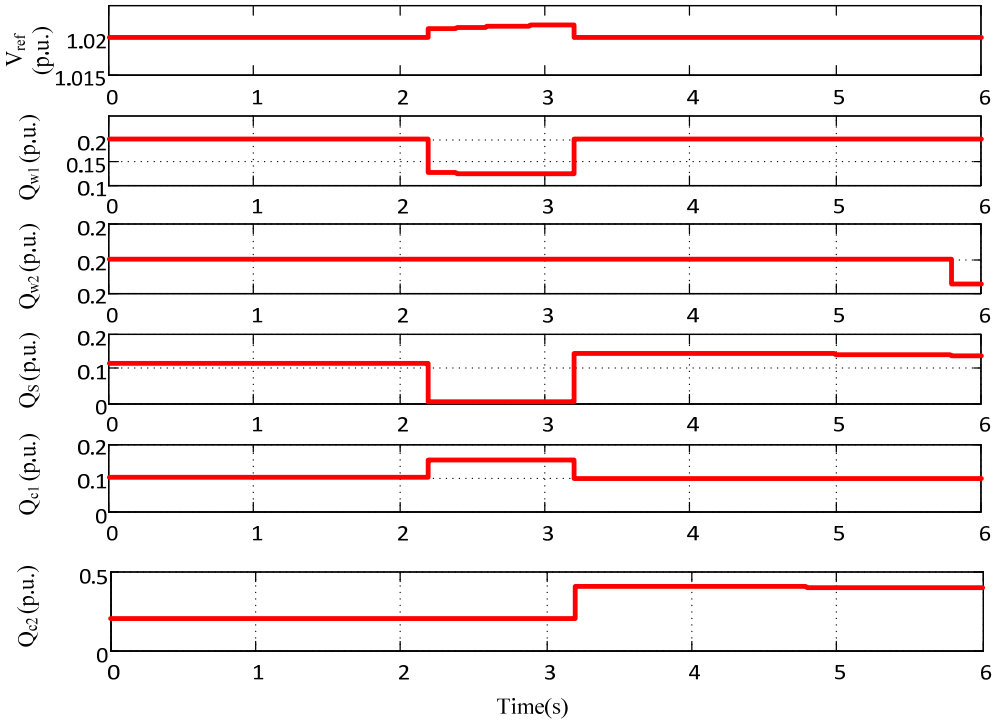

Figure 5-9 Control inputs to the MicroGrid in case study 2

Since the reactive demand decreased at t=2s, the controller had to decrease the reactive power injection to the system. As can be seen in Figure 5-9, the controller responded to the load change by decreasing the reactive injection of one wind generator, decreasing the reactive power injection of the solar generator, slightly increasing the reactive power injection of the D-STATCOM 1, and slightly increasing the reference voltage of the master generator. These changes added up to keep all the bus voltages within limits after the load change at t=2s. After one load was energized again, the controller responded by increasing the reactive injection of one wind generator, solar generator, and DSTATCOM 2. The controller also slightly decreased the voltage setpoint of the master generator, and the reactive setpoint of DSTATCOM 1. These changes added up to keeping the MicroGrid bus voltages within desired limits.

5.5.1.3 Case-study 3

As mentioned earlier renewable energy sources are intermittent and the amount of power production varies due to climate changes. The effect of changes in production of active and reactive power on the sample MicroGrid shown in Figure 5-3 is studied in this case-study.

In this case-study, capacitor banks were connected to bus 6,7 as reactive power compensator instead of D-STATCOMS. The wind generator 1 stopped the production of reactive power at t=2.2s due to changes in weather condition and then went back to normal operation at t=3.2s. Further, wind generator 2 stopped production of reactive power at t=3.2s and remained in the same condition until t=6s.

Similar to case-study 1, the optimization problem yielded to solving an MIQP problem since norm 2 was used in the objective function. The voltage of the load buses are shown in Figure 5-10 and the control inputs are depicted in Figure 5-11. The results demonstrate that the controller used alternative reactive capabilities of the system to achieve smooth voltage profile when one of the sources was unavailable.

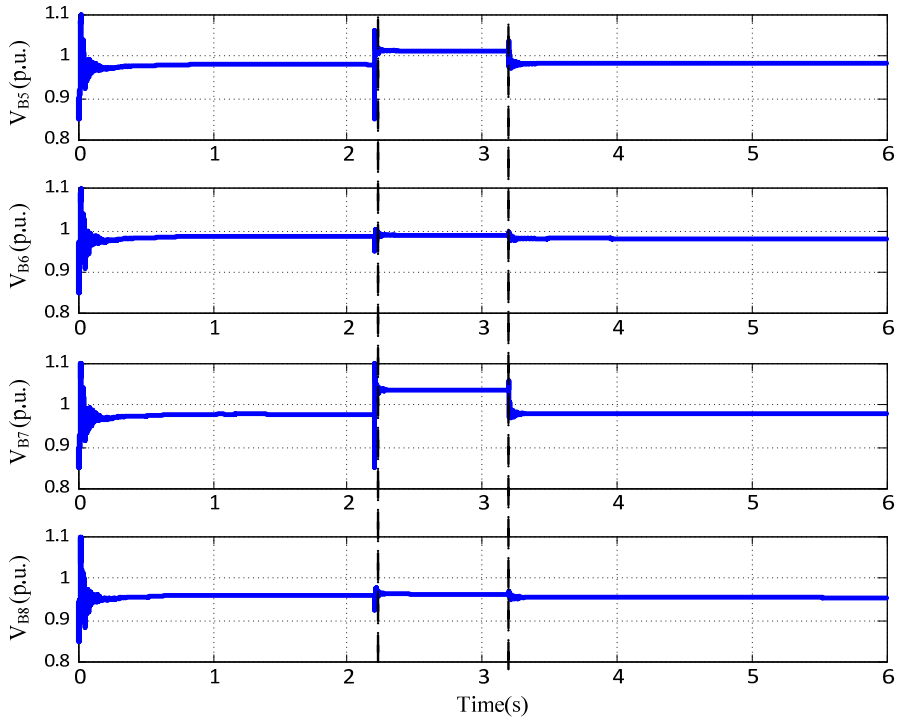

Figure 5-10 RMS voltage of Bus 5,6,7,8 in case study 3

As can be seen in Figure 5-11, wind generator 1 was not able to inject reactive power to the system from *t*=2.2*s* until *t*=3.2*s*.Therefore, the reactive power controller had to increase the reactive injection by connecting two capacitor banks at the connection point of capacitor 1. Since capacitor bank reactive injection is quantized, the controller had to decrease the reactive injection of wind generator to coordinate the reactive power to maintain the bus voltages within limits. At t=3.2s wind generator 2 lost its capability to produce reactive power. The dynamic reactive controller increased the reactive injection of solar source, wind generator 1 and disconnected the capacitor banks at connection point of capacitor 1 to compensate for the loss of reactive generation.

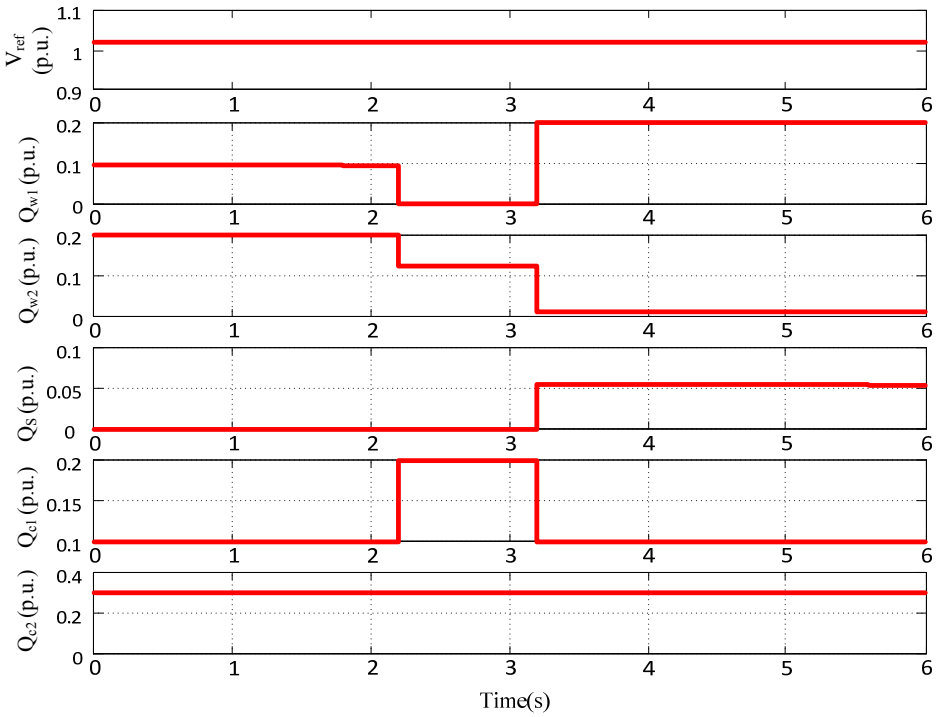

Figure 5-11 Control inputs to the MicroGrid in case study 3

5.5.1.4 Case-study 4

In this case-study, the same generation changes as case-study 3 occurred in the system. However, D-STATCOMs were used for reactive power compensation instead of capacitor banks. The problem formulation was the same as case-study 3, and the optimization problem led into solving a QP problem. The voltage of the load buses are shown in Figure 5-12 and the control inputs are depicted in Figure 5-13. Similar to case-study 3, the dynamic reactive controller used alternative reactive capabilities of the system to achieve smooth voltage profile when one reactive power source was unavailable.

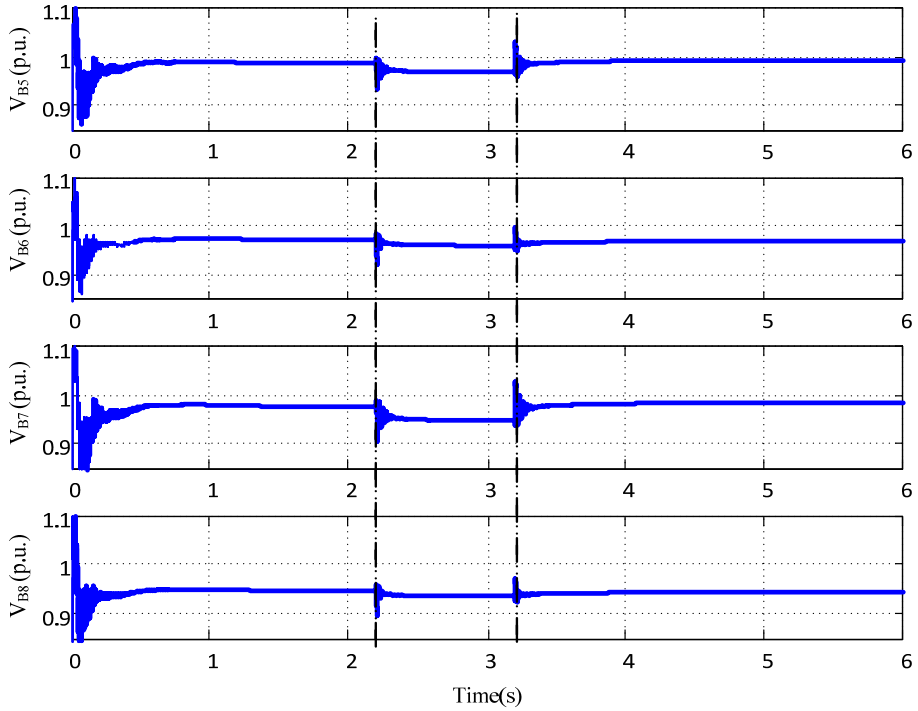

Figure 5-12 RMS voltage of Bus 5,6,7,8 in case study 4

As can be seen in Figure 5-13, wind generator 1 lost its capability to produce reactive power at t=2.2s. Therefore, the dynamic reactive controller had to increase the reactive power injection of the solar source and the voltage reference of the master generator. These changes alone would cause overvoltage in some buses in the system. Therefore, the reactive controller had to decrease the reactive injection of wind generator 2 and the D-STATCOMs. At t=3.2s, wind generator 2 lost its capability to produce reactive power. Therefore, the dynamic reactive controller increased the reactive injection of both reactive compensators as well as wind generator 1. In this case, the reactive controller had to slightly decrease the reactive injection of the solar source. As can be seen in Figure 5-12, these controller was able to maintain bus voltages within limits taking these control actions.

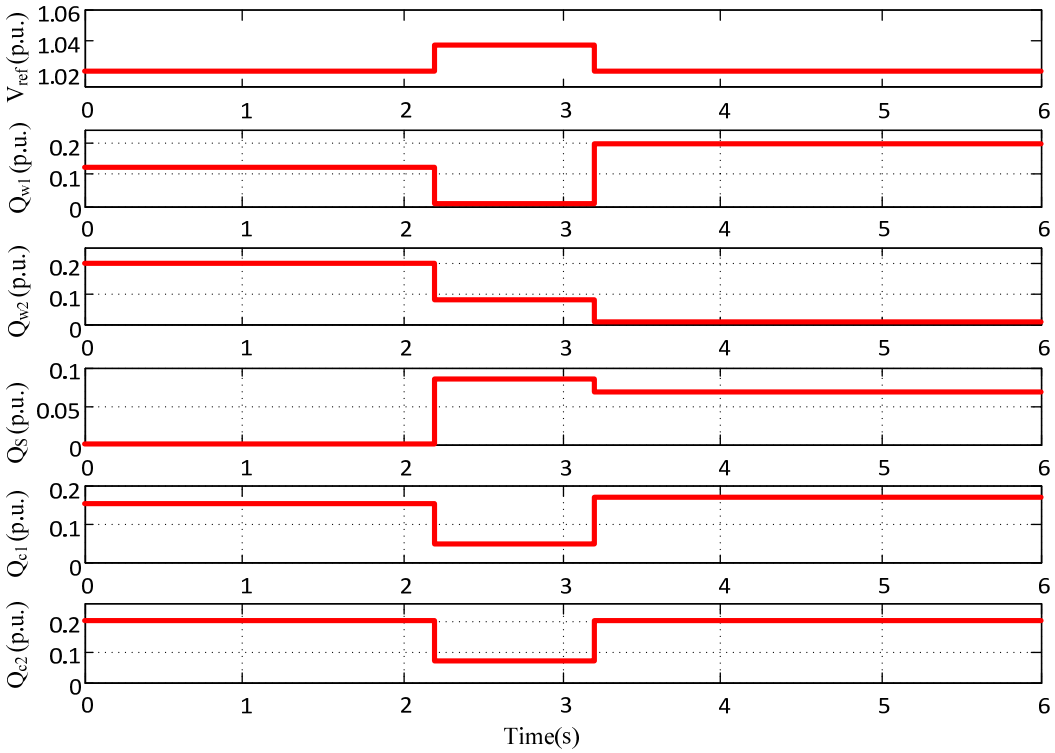

Figure 5-13 Control inputs to the MicroGrid in case study 4

5.5.2 Studies on IEEE 34 node MicroGrid

Figure 5-14 shows a MicroGrid based designed based on the IEEE34 node. The system is divided into three zones and each zone contains a DER. The system was designed such that the DERs were capable of providing active and reactive power to the loads when the MicroGrid was operating in islanded mode. Two capacitor banks were used as switched capacitor banks in the case-study which means that the general controller was capable of connecting and disconnecting them.

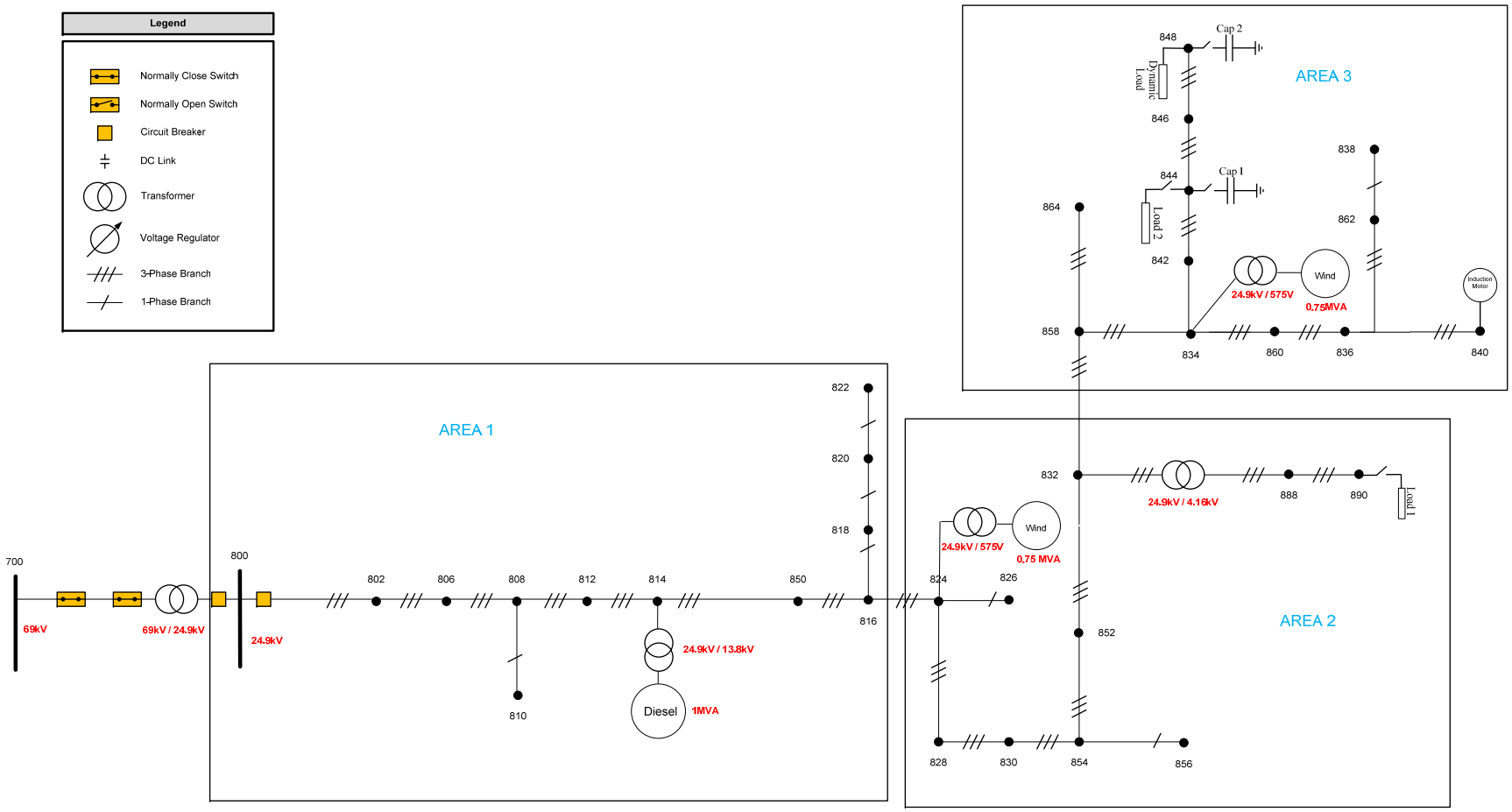

Figure 5-14 MicroGrid based on the IEEE 34 node feeder

The distributed loads of the MicroGrid are listed in Table 16. The spot loads of the MicroGrid are shown in Table 17. Source parameters of the MicroGrid shown in Figure 5-14 is are listed in Table 18.

Table 16 Distributed loads of the IEEE 34 node system

Node A	Node B	Load Model	Ph-1 kW	Ph-1 kVAr	Ph-2 kW	Ph-2 kVAr	Ph-3 kW	Ph-3 kVAr
802	806	Y-PQ	0	0	30	15	25	14
808	810	Y-I	0	0	16	8	0	0
818	820	Y-Z	34	17	0	0	0	0
820	822	Y-PQ	135	70	0	0	0	0
816	824	D-I	0	0	5	2	0	0
824	826	Y-I	0	0	40	20	0	0
824	828	Y-PQ	0	0	0	0	4	2
828	830	Y-PQ	7	3	0	0	0	0
854	856	Y-PQ	0	0	4	2	0	0
832	858	D-Z	7	3	2	1	6	3
858	864	Y-PQ	2	1	0	0	0	0
858	834	D-PQ	4	2	15	8	13	7
834	860	D-Z	16	8	20	10	110	55
860	836	D-PQ	30	15	10	6	42	22
836	840	D-I	18	9	22	11	0	0
862	838	Y-PQ	0	0	28	14	0	0
842	844	Y-PQ	9	5	0	0	0	0
844	846	Y-PQ	0	0	25	12	20	11
846	848	Y-PQ	0	0	23	11	0	0
Total			262	133	240	120	220	114

Table 17 Spot loads of the IEEE 34 node system

Node	Load	Ph-1	Ph-1	Ph-2	Ph-2	Ph-3	Ph-3
	Model	kW	kVAr	kW	kVAr	kW	kVAr
860	Y-PQ	20	16	20	16	20	16
840	Y-I	9	7	9	7	9	7
844	Y-Z	135	105	135	105	135	105
848	D-PQ	20	16	20	16	20	16
890	D-I	150	75	150	75	150	75
830	D-Z	10	5	10	5	25	10
Total		344	224	344	224	359	229

Table 18 Source parameters of the IEEE 34 node system

Diesel	Quantity	Wind	Quantity
VgI-I	13.8 kV	*VgI-I*	575V
Pg	1MW	*Pg*	0.75 MW
pfg	0.85	*Vs*	575 V
f	60 Hz	*Vr*	1975 V
Ra	0.199Ω	*F*	60 Hz
Xp	0.18	*Rs*	0.023 (p.u.)
Xd	1.305	*Ls*	0.18 (p.u.)
Xd'	0.296	*Rr*	0.016 (p.u.)
Xd''	0.252	*Lr*	0.16 (p.u.)
Tdo'	1.01s	*Lm*	2.9 (p.u.)
Tdo''	0.053s	*H*	0.685 (p.u.)
Xq	0.474	*f*	0.01 (p.u.)
Xq'	N.A	*Poles*	3
Xq''	0.243		
Tqo'	N.A		
Tqo''	0.061s	*Pg (solar)*	0.4 MW
H	1.06s	*f (solar)*	60 Hz

The result of steady state load flow of the MicroGrid when the diesel generator was off and the MicroGrid was connected to the main grid is shown in Table 19 and Table 20. The result of steady state load flow of the MicroGrid when it was operating in the islanded mode is shown in

Table 21 and

Table 22.

Table 19 Power flow of the system when connected to the grid and the Diesel generator is off – Bus voltages

	Voltage				Voltage Angle		
Bus	**A**	**B**	**C**		**A**	**B**	**C**
800	1.05	1.05	1.05		0.00	-118.97	119.96
802	1.05	1.05	1.05		-0.07	-119.04	119.89
806	1.05	1.05	1.05		-0.11	-119.08	119.85
808	1.04	1.04	1.04		-0.93	-119.88	119.01
810	1.04	1.04	1.04		-0.93	-119.88	119.01
812	1.02	1.03	1.03		-1.90	-120.84	118.02
814	1.01	1.02	1.02		-2.68	-121.62	117.21
850	1.01	1.02	1.02		-2.68	-121.62	117.21
816	1.01	1.02	1.02		-2.69	-121.63	117.20
818	1.01	1.02	1.02		-2.68	-121.63	117.20
820	1.01	1.02	1.01		-2.55	-121.63	117.07
822	1.01	1.02	1.01		-2.53	-121.63	117.05
824	1.01	1.01	1.01		-2.99	-121.92	116.95
826	1.01	1.01	1.01		-2.99	-121.92	116.95
828	1.01	1.01	1.01		-3.04	-121.97	116.90
830	0.99	0.99	0.99		-4.31	-123.24	115.72
854	0.99	0.99	0.99		-4.35	-123.28	115.69
856	0.99	0.99	0.99		-4.35	-123.28	115.69
852	0.95	0.95	0.95		-6.74	-125.67	113.48
832	0.95	0.95	0.95		-6.74	-125.67	113.48
888	1.05	1.05	1.05		-14.36	-133.23	106.13
890	0.90	0.90	0.90		-18.56	-137.42	102.08
858	0.95	0.95	0.95		-7.04	-125.97	113.20
864	0.95	0.95	0.95		-7.04	-125.97	113.20
834	0.95	0.95	0.95		-7.39	-126.33	112.87
842	0.95	0.95	0.95		-7.42	-126.35	112.85
844	0.95	0.95	0.95		-7.55	-126.48	112.73
846	0.95	0.95	0.95		-7.82	-126.74	112.47
848	0.95	0.95	0.95		-7.86	-126.78	112.43
860	0.95	0.95	0.95		-7.40	-126.33	112.87
836	0.95	0.95	0.95		-7.41	-126.34	112.87
862	0.95	0.95	0.95		-7.41	-126.34	112.87
838	0.95	0.95	0.95		-7.41	-126.34	112.87
840	0.95	0.95	0.95		-7.41	-126.34	112.87

Table 20 Power flow of the system when connected to the grid and the Diesel generator is off – Line currents

Current					
From Bus	**To Bus**		**A**	**B**	**C**
800	**802**		29.88	29.33	28.85
802	**806**		29.88	29.33	28.85
806	**808**		29.88	27.54	27.37
808	**810**		29.88	27.54	27.37
808	**812**		29.88	26.61	27.37
812	**814**		29.88	26.61	27.37
814	**850**		29.88	26.61	27.37
850	**816**		29.81	26.71	27.03
816	**818**		10.59	0.00	0.00
818	**820**		9.53	0.00	0.00
820	**822**		9.53	0.00	0.00
816	**824**		20.68	26.43	27.03
824	**826**		0.00	1.25	0.00
824	**828**		65.64	69.29	71.24
828	**830**		65.25	69.29	71.24
830	**854**		63.61	67.64	68.75
854	**856**		0.00	0.12	0.00
854	**852**		63.61	67.42	68.75
852	**832**		63.61	67.42	68.75
832	**888**		21.61	21.60	21.58
888	**890**		21.61	21.60	21.58
832	**858**		21.61	21.60	21.58
858	**864**		0.06	0.00	0.00
858	**834**		48.63	52.05	53.03
834	**842**		87.94	89.61	88.21
842	**844**		87.54	89.61	88.21
844	**846**		67.04	67.91	66.88
846	**848**		67.04	67.91	66.88
834	**860**		4.63	5.36	4.30
860	**836**		4.63	5.36	4.30
836	**862**		0.00	1.66	0.00
862	**838**		0.00	1.66	0.00
836	**840**		2.34	2.45	1.81

Table 21 Power flow of the system isolated from the grid – Bus voltages

	Voltage				Voltage angle		
Bus	**A**	**B**	**C**		**A**	**B**	**C**
800	1.05	1.05	1.06		0.00	-119.66	121.06
802	1.05	1.05	1.06		0.00	-119.66	121.06
806	1.05	1.05	1.06		0.00	-119.66	121.06
808	1.05	1.05	1.06		0.03	-119.64	121.06
810	1.05	1.05	1.06		0.03	-119.64	121.06
812	1.05	1.05	1.06		0.08	-119.61	121.06
814	1.05	1.06	1.06		0.12	-119.59	121.06
850	1.05	1.06	1.06		0.12	-119.59	121.06
816	1.05	1.06	1.06		0.10	-119.60	121.04
818	1.05	1.06	1.06		0.11	-119.60	121.04
820	1.05	1.06	1.05		0.24	-119.60	120.91
822	1.05	1.06	1.05		0.25	-119.60	120.89
824	1.05	1.05	1.05		-0.30	-120.02	120.67
826	1.05	1.05	1.05		-0.30	-120.02	120.67
828	1.04	1.05	1.05		-0.35	-120.08	120.62
830	1.02	1.02	1.02		-1.68	-121.49	119.31
854	1.02	1.02	1.02		-1.72	-121.52	119.28
856	1.02	1.02	1.02		-1.72	-121.53	119.28
852	0.98	0.98	0.98		-4.24	-124.19	116.80
832	0.98	0.98	0.98		-4.24	-124.19	116.80
888	1.07	1.07	1.08		-11.59	-131.84	109.26
890	0.93	0.93	0.93		-15.64	-136.05	105.08
858	0.98	0.98	0.98		-4.56	-124.53	116.48
864	0.98	0.98	0.98		-4.56	-124.53	116.48
834	0.97	0.97	0.98		-4.94	-124.93	116.11
842	0.97	0.97	0.98		-4.97	-124.96	116.08
844	0.97	0.97	0.98		-5.09	-125.09	115.96
846	0.97	0.97	0.97		-5.35	-125.36	115.69
848	0.97	0.97	0.97		-5.39	-125.40	115.66
860	0.97	0.97	0.98		-4.95	-124.94	116.10
836	0.97	0.97	0.98		-4.95	-124.94	116.10
862	0.97	0.97	0.98		-4.95	-124.94	116.10
838	0.97	0.97	0.98		-4.95	-124.94	116.10
840	0.97	0.97	0.98		-4.95	-124.94	116.10

Table 22 Power flow of the system isolated from the grid – Line currents

Current				
From Bus	**To Bus**		**A**	**B**	**C**
800	**802**		0.00	0.00	0.00
802	**806**		0.00	0.00	0.00
806	**808**		0.00	1.93	1.66
808	**810**		0.00	1.93	1.66
808	**812**		0.00	0.00	0.00
812	**814**		0.00	2.96	1.66
814	**850**		0.00	2.96	1.66
850	**816**		53.12	49.85	50.81
816	**818**		10.90	0.00	0.00
818	**820**		9.81	0.00	0.00
820	**822**		4.36	0.00	0.00
816	**824**		4.36	0.00	0.00
824	**826**		0.00	1.28	0.00
824	**828**		82.28	85.96	88.37
828	**830**		81.87	85.96	88.37
830	**854**		80.15	84.23	85.80
854	**856**		0.00	0.12	0.00
854	**852**		80.15	84.00	85.80
852	**832**		80.15	84.00	85.80
832	**888**		25.86	25.81	25.84
888	**890**		25.86	25.81	25.84
832	**858**		58.79	62.43	63.76
858	**864**		0.06	0.00	0.00
858	**834**		88.85	90.35	89.14
834	**842**		88.85	90.35	89.14
842	**844**		88.85	90.35	89.14
844	**846**		88.44	90.35	89.14
846	**848**		67.72	68.47	67.60
834	**860**		4.68	5.41	4.34
860	**836**		2.89	4.79	1.83
836	**862**		0.00	1.67	0.00
862	**838**		0.00	1.67	0.00
836	**840**		2.36	2.47	1.83

The objective function for reactive power control of the MicroGrid shown in Figure 5-14 was chosen as follows.

$$J(\boldsymbol{x},\boldsymbol{u},k) = \sum_{k=0}^{N-1}\sum_{i\in N_t}\Big\{\big\|{V_i}^A(k+t|t) - V_i^{Nom}\big\|_{\{1,\infty\}} + \big\|{V_i}^B(k+t|t) - V_i^{Nom}\big\|_{\{1,\infty\}} + \big\|{V_i}^C(k+t|t) - V_i^{Nom}\big\|_{\{1,\infty\}} + \|\boldsymbol{W_1}\Delta\boldsymbol{v}(k)\|_{\{1,\infty\}} + \|\boldsymbol{W_2}\Delta\boldsymbol{\sigma}(k)\|_{\{1,\infty\}}\Big\} \tag{5-10}$$

where ${V_i}^A(k+t|t)$, ${V_i}^B(k+t|t)$, ${V_i}^C(k+t|t)$ are the predicted voltage of phase A, B and C of bus *i*, respectively.

The control inputs to the system were the reference voltage of synchronous diesel generator (V_{ref}), and reactive power setpoints of the DGs and the switched capacitors (Q_{c1}, Q_{c2}). Thus, the control input vectors were defined as follows.

$$\boldsymbol{v}(k) = \left[V_{ref}, Q_{W1}, Q_{W2}\right]^T, \quad \boldsymbol{\sigma}(k) = [Q_{c1}, Q_{c2}]^T \tag{5-11}$$

Since the system had three distributed generators, and one dynamic load, the number of the states of the system was four. So the optimization problem was solved subject to the following simplified differential algebraic equations.

$$x_1(k+1) = x_1(k) + \Delta t\left(\frac{-1}{T_V}x_1(k) + v_{ref}(k)\right)$$
$$V_1(k) = \frac{1}{T_V}x_1(k) \tag{5-12}$$

$$x_i(k+1) = x_i(k) + \Delta t\left(\frac{-1}{T_{Q,i}}x_i(k) + Q_{ref,i}(k)\right)$$
$$Q_{DG,i}(k) = \frac{1}{T_{Q,i}}\, x_i(k) \quad , \quad i = 2,3 \tag{5-13}$$

$$x_4(k+1) = x_4(k) - \Delta t\left(\frac{x_4(k)}{T_q} + Q_{L0}(V^{b_s}(k) - V^{b_t}(k))\right)$$
$$Q_L(k) = \left(\frac{x_4(k)}{T_q} + Q_{L0}\left(V^{b_t}(k)\right)\right) \tag{5-14}$$

$$\boldsymbol{V_{ABC}}^{\boldsymbol{n}} = \boldsymbol{a_t}\, \boldsymbol{V_{abc}}^{\boldsymbol{m}} + \boldsymbol{b_t}\, \boldsymbol{I_{abc}}^{\boldsymbol{m}}$$
$$\boldsymbol{I_{abc}}^{\boldsymbol{n}} = \boldsymbol{c_t}\, \boldsymbol{V_{abc}}^{\boldsymbol{m}} + \boldsymbol{d_t}\, \boldsymbol{I_{abc}}^{\boldsymbol{m}} \tag{5-15}$$

$$V_{b_{min}} \le |V_b(k)| \le V_{b\,Max} \qquad b = 1, \dots, N_{Bus}$$
$$\frac{|V_m(k) - V_n(k)|}{|Z_{cl}|} = |I_{cl}(k)| \le I_{cl\,Max} \qquad cl = 1, \dots, N_{cl} \tag{5-16}$$

Following the linearization technique discussed in [111], system state space equations were derived in the piecewise linear form as follows.

$$\boldsymbol{x}(k+1) = \begin{cases} \boldsymbol{A_1 x}(k) + \boldsymbol{B_1 u}(k) & if\ \delta_1(k) = 1 \\ \vdots & \\ \boldsymbol{A_s x}(k) + \boldsymbol{B_s u}(k) & if\ \delta_s(k) = 1 \end{cases} \tag{5-17}$$

The bus voltages can be described in compact form as follows.

$$\boldsymbol{V} = \begin{cases} \boldsymbol{C_1 x}(k) + \boldsymbol{D_1 u}(k) & if\ \delta_1(k) = 1 \\ \vdots & \\ \boldsymbol{C_s x}(k) + \boldsymbol{D_s u}(k) & if\ \delta_s(k) = 1 \end{cases} \tag{5-18}$$

where V is the vector of the voltages that are used in the optimization formulation and it includes the voltage of all three buses in the system. Increasing the number of sets makes

the prediction of voltage more accurate; however, the optimization algorithm takes more time to converge to the global minimum.

5.5.2.1 Case-study 1: Load change with local control

Sharp load changes during islanded operation can cause instability and oscillatory voltage in the MicroGrid. Further, the on load tap changers are not fast enough to avoid the effect of sharp load changes efficiently.

This case-study is demonstrating the effect of sharp load change in the islanded MicroGrid with local voltage control and fixed capacitors. The exciter of the master generator usually damps the voltage oscillations in time if the relays do not operate and isolate the system any further. However, if the protection relays are triggered the system may experience a blackout. Figure 5-15 and Figure 5-16 show the voltage oscillations resulting from the load change in the system.

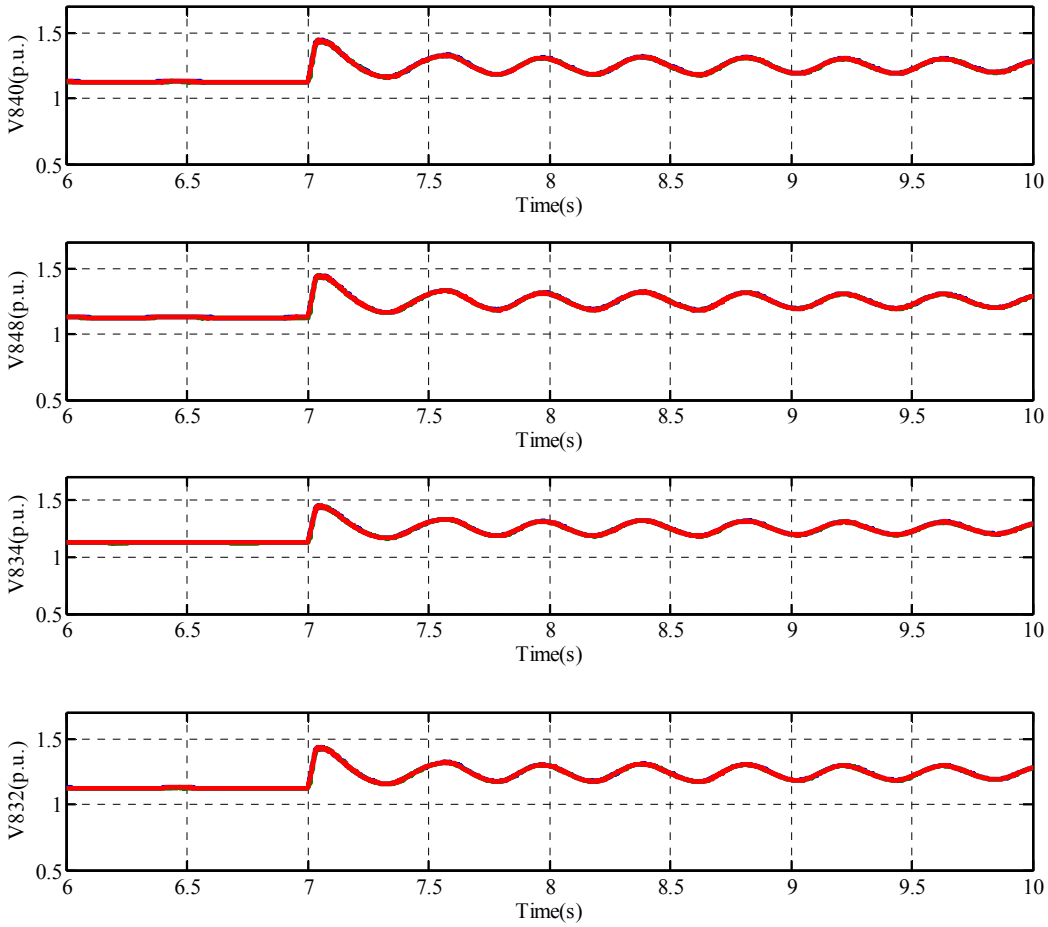

Figure 5-15 Bus voltages with fixed capacitor – case study 1

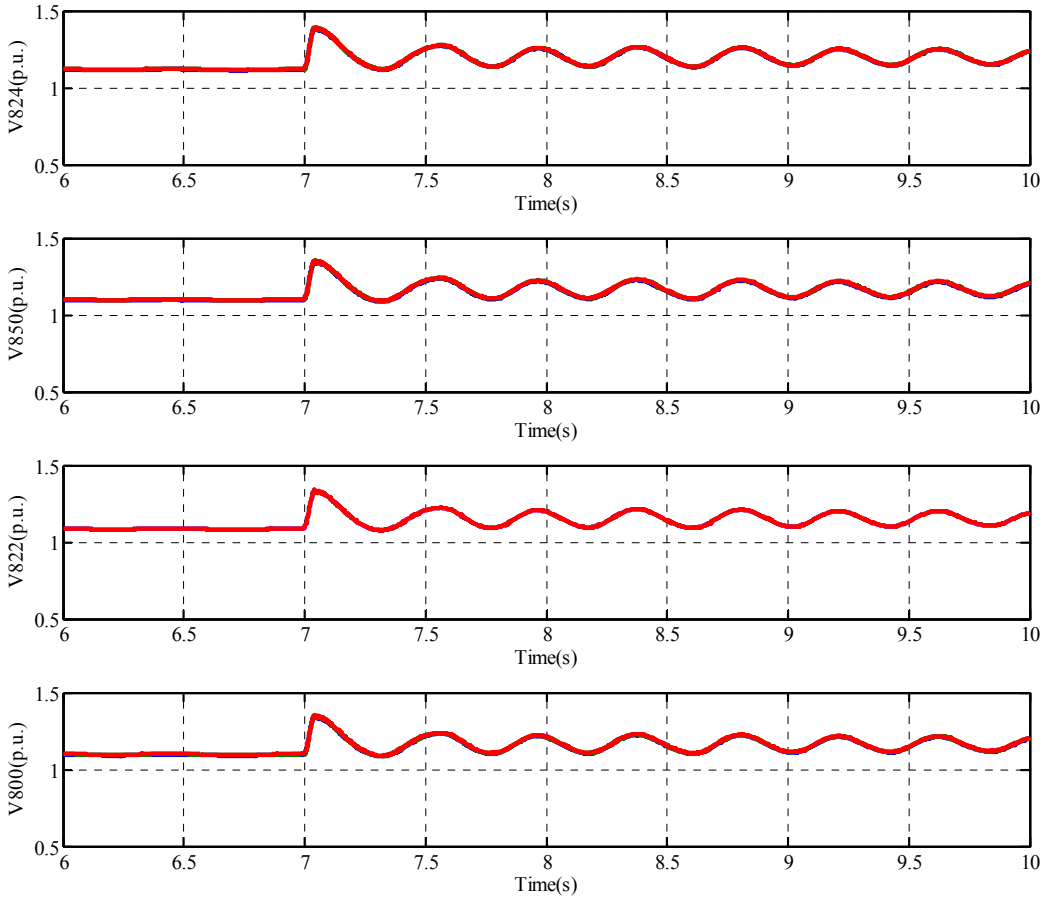

Figure 5-16 Bus voltages with fixed capacitor - case study 1

5.5.2.2 Case –study 2: Load change

MicroGrids may experience sharp load changes during their operation. As shown in case-study1, if cautions are not taken by the power management unit, the system might experience voltage oscillations. This case-study is demonstrating the performance of the MPC controller during sharp load changes in the system.

Load 2 which was connected to node 844 got disconnected from the system at t=2.5s. Further, load 1 which was connected to node 890 got disconnected at t=3.5s and

both of the loads were energized again at t=5.5s. The generalized MPC controller tried to reduce the effect of the load change in the system by sending optimal control inputs to the system. The assumption in this case-study was that the MPC controller does not have a prediction of the exact time of load change. Therefore, after the load status changed, it took 0.2 seconds for the controller to send the updated control inputs to the system. As can be seen in Figure 5-17 and Figure 5-18, the MPC controller was able to keep the voltages within the limits by adjusting the control input.

Each of loads 1 and 2 are approximately 25% of the system's total load. Given that the load change was significantly large in this case-study and the system was operating in islanded mode, the bus voltage experience a spike immediately after the voltage change. This transient behavior is acceptable with current requirements presented in IEEE Standard for isolated power systems [106]. The IEEE Std 1547.4 mentions that the under-voltage tripping time are 0.16*s* for voltage less than 50% and 2*s* for voltages less than 88%. In this case-study, the variations in the voltage beyond the 12% limit occurred for less than 0.2 seconds, which is acceptable according to IEEE 1547.4 Standard for isolated power systems and does not cause relays to trip.

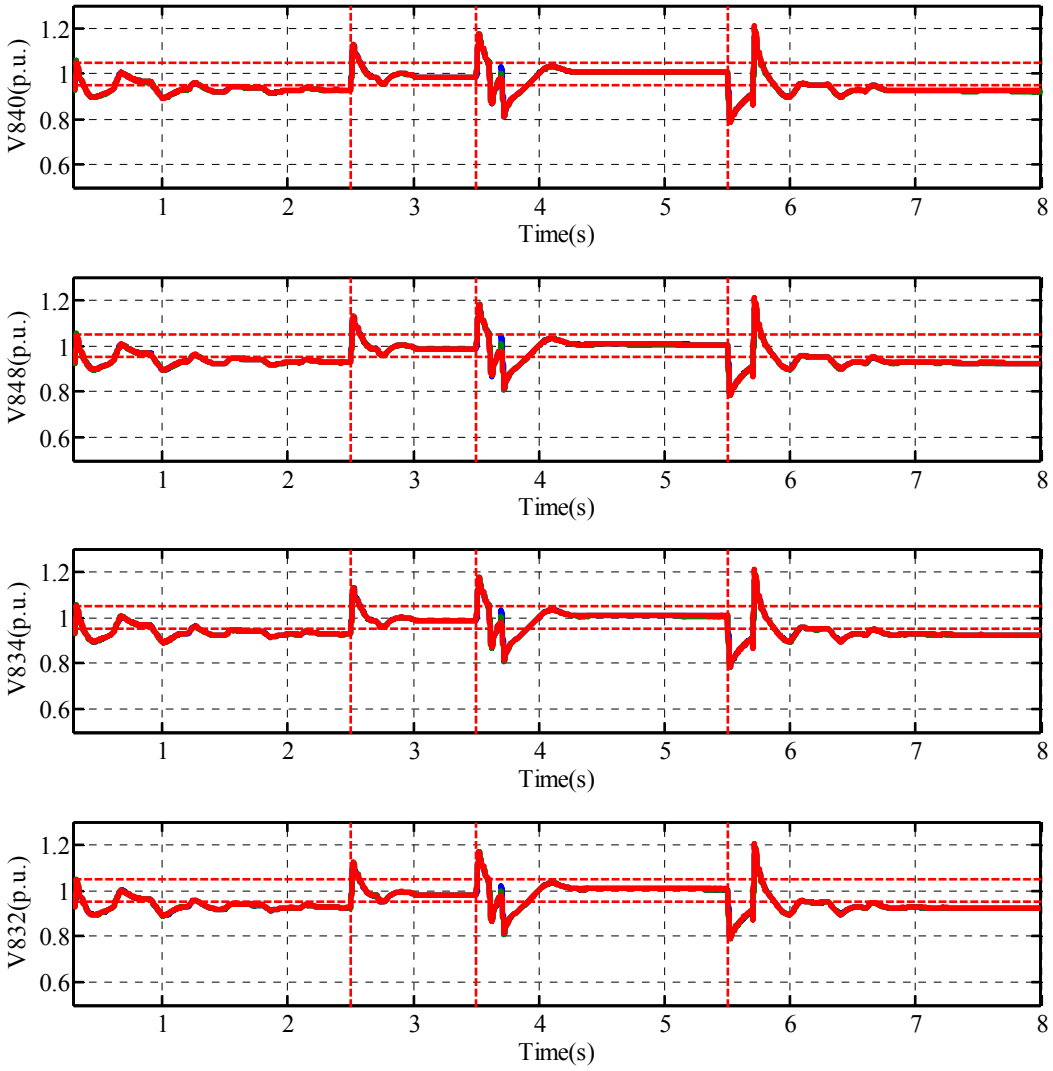

Figure 5-17 Bus voltages with MPC – case study 2

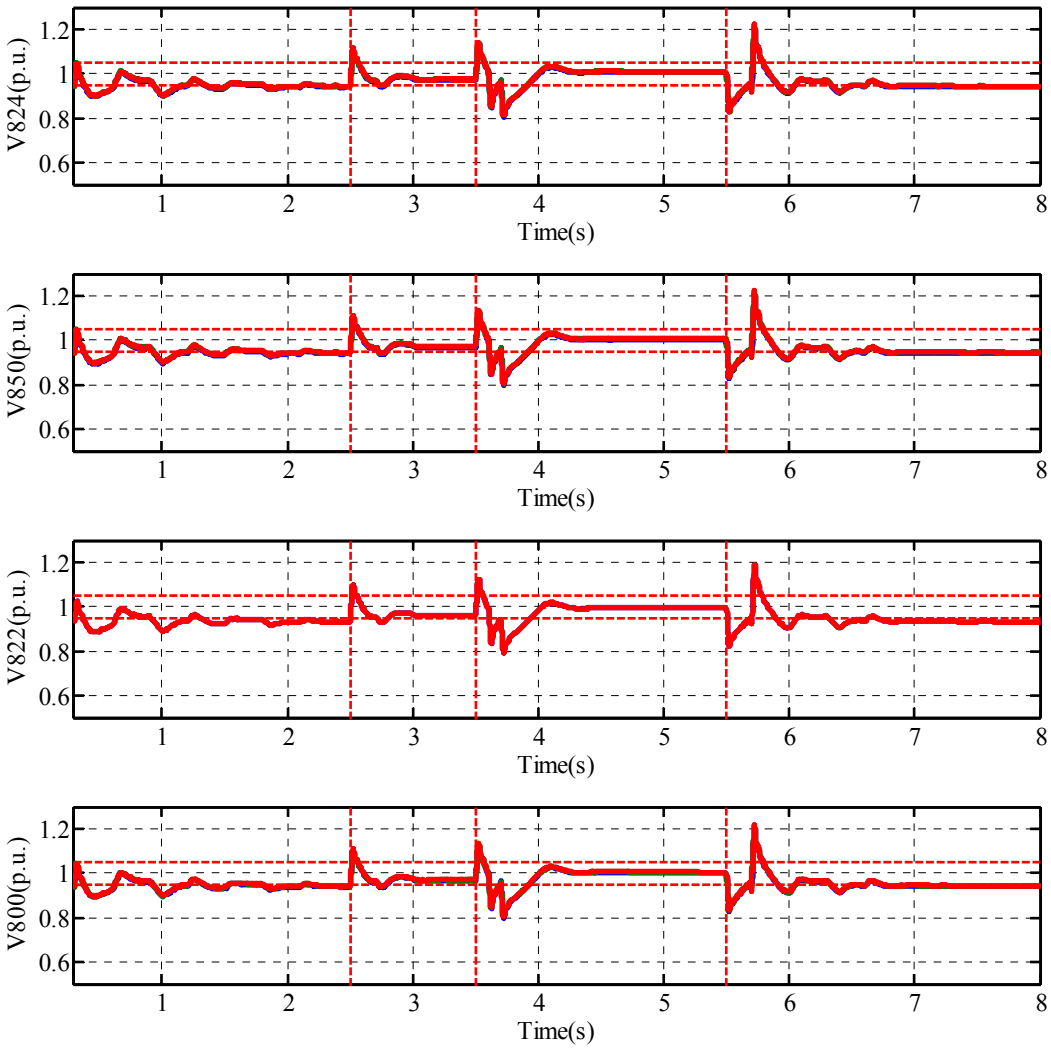

Figure 5-18 Bus voltages with MPC – case study 2

Figure 5-19 shows how the proposed dynamic reactive controller coordinated the reactive power sources in the system to achieve the optimal solution. After the first load change at t=2.5s, the controller responded by decreasing the local reactive power injection of the wind generators. After the second load change, the controller responded by disconnecting the capacitor banks from the system, increasing the reactive injection of the wind generators, and increasing the voltage reference of the master generator. It

should be noted that disconnecting the capacitor banks alone would have resulted in an overvoltage in the system. On the other hand, the controller could not keep the bus voltages within limits without turning the capacitor banks off.

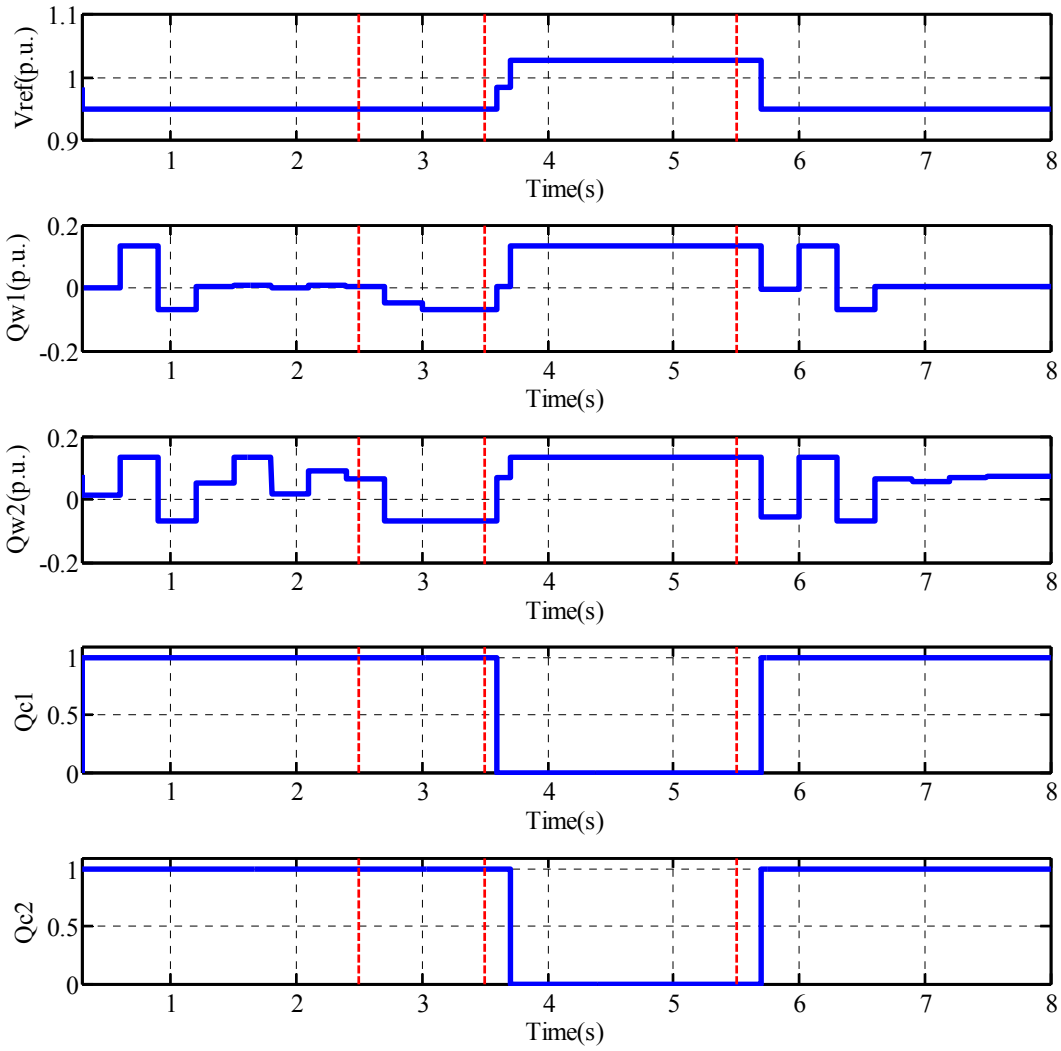

Figure 5-19 Control inputs to the MicroGrid generated by MPC – case study 2

5.5.2.3 Case –study 3: Wind change

In this case-study, the wind speed changed to 60% of rated speed from t=4s to t=15s. The variations in wind speed resulted in variation in the output power of the wind generator. Wind speed variations may affect the stability of the system as well as the voltage level of the load buses. The model predictive control had an estimate of the wind variation, which is provided by the user based on the weather forecast. This forecast does not need to be exactly accurate and the reactive controller can operate as long as it can estimate the reactive power injection capacity of the wind sources. The controller had to determine what percentage of the output power may be assigned to reactive power generation based on the total generated power of the wind generator. The reactive power generation limit of the wind generator was tighter in this case, so reactive power had to be provided by other sources of reactive power in the system.

The bus voltages of some buses in the system are shown in Figure 5-20and Figure 5-21. The system also experiences a temporary fault at t=8.5s which results in a glitch in bus voltages.

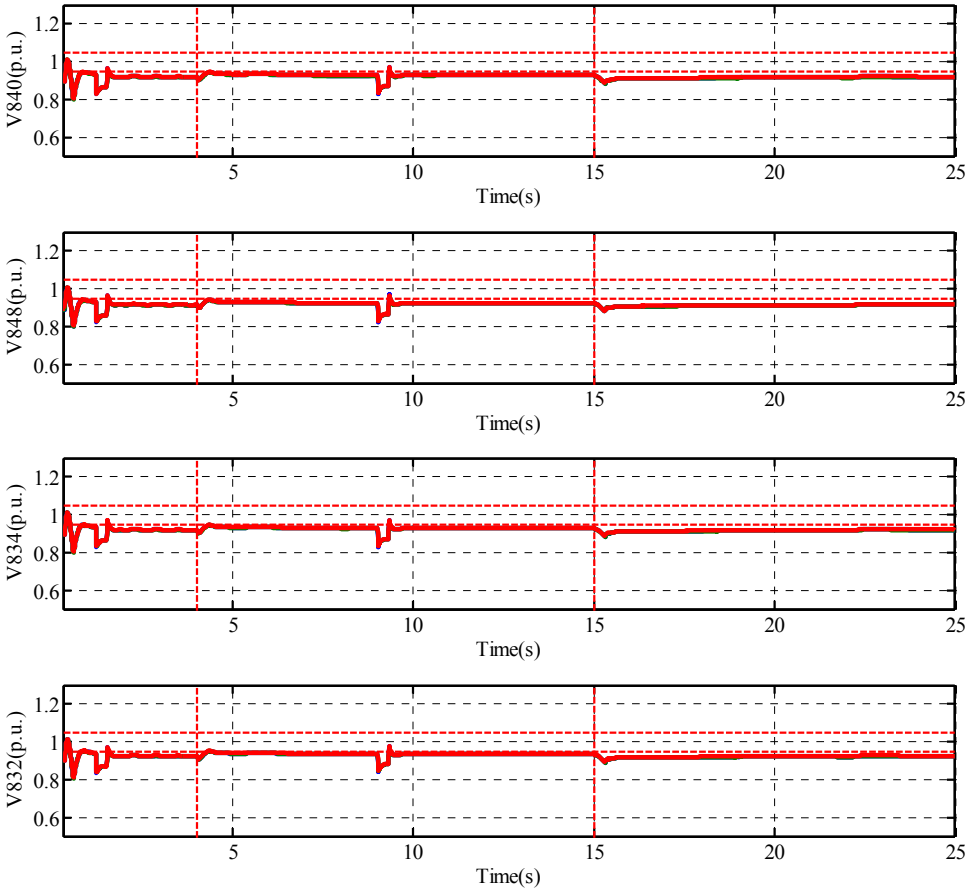

Figure 5-20 Bus voltages of MicroGrid – case study 3

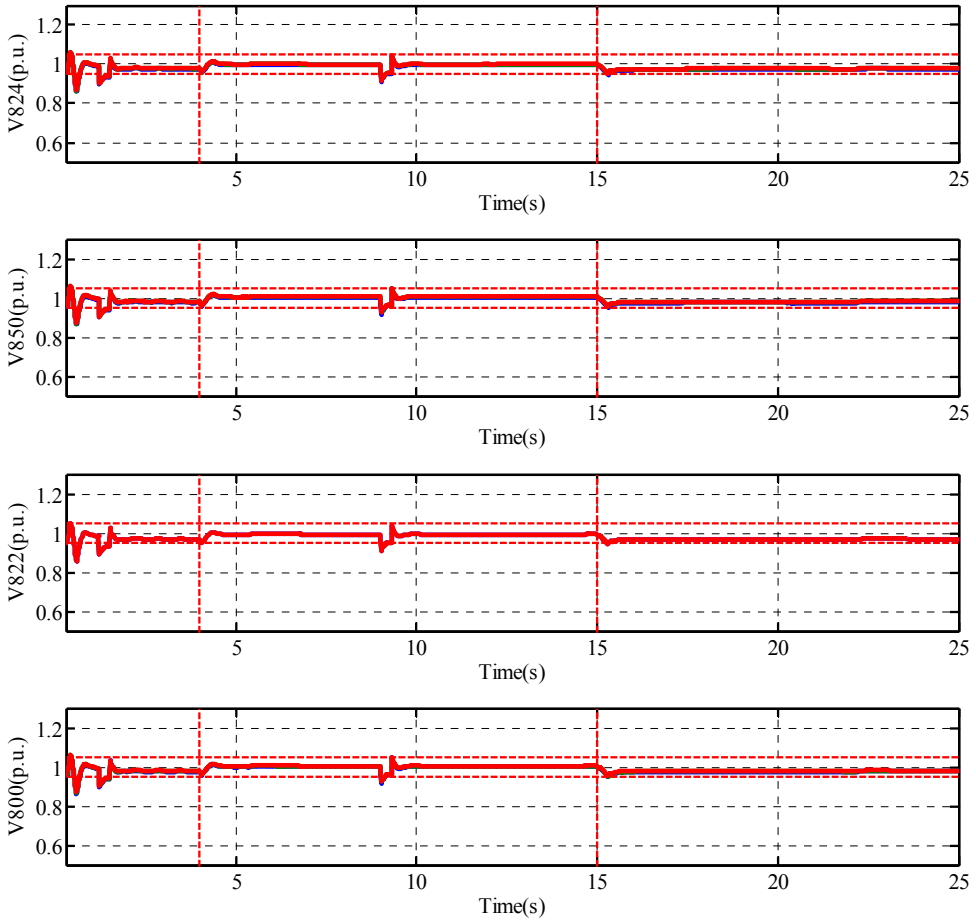

Figure 5-21 Bus voltages of the MicroGrid – case study 3

As can be seen in Figure 5-22, the reactive controller lowered the reactive power reference of the wind generators and increased the voltage setpoint of the master generator. Increasing the voltage setpoint of the master generator resulted in a bus voltage increase in all the buses of the microgrid. This is a wasteful method to keep bus voltage within limits and it puts stress on the diesel generator. However, in this case, the controller does not have access to any other local reactive injectors.

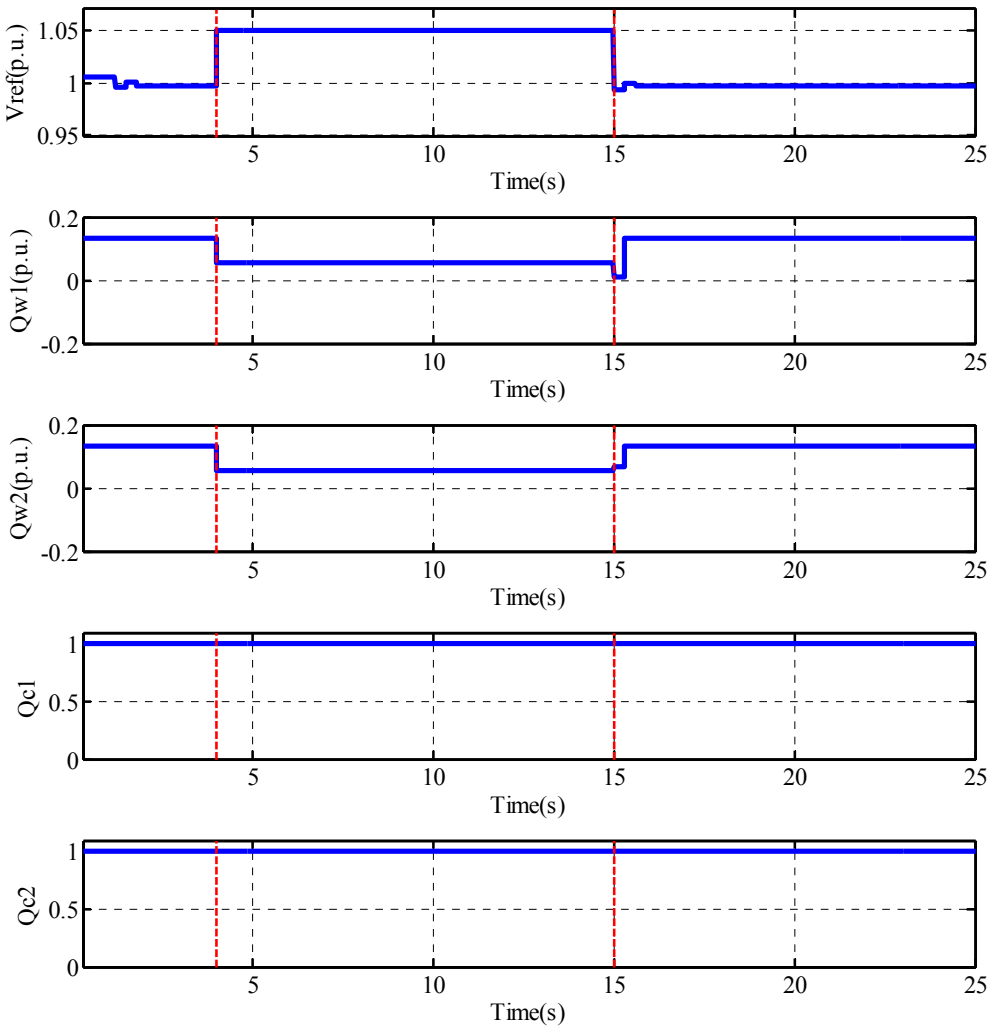

Figure 5-22 Control inputs to the MicroGrid generated by MPC – case study 3

Figure 5-23 shows the active and reactive power injection of wind generators in this case-study.

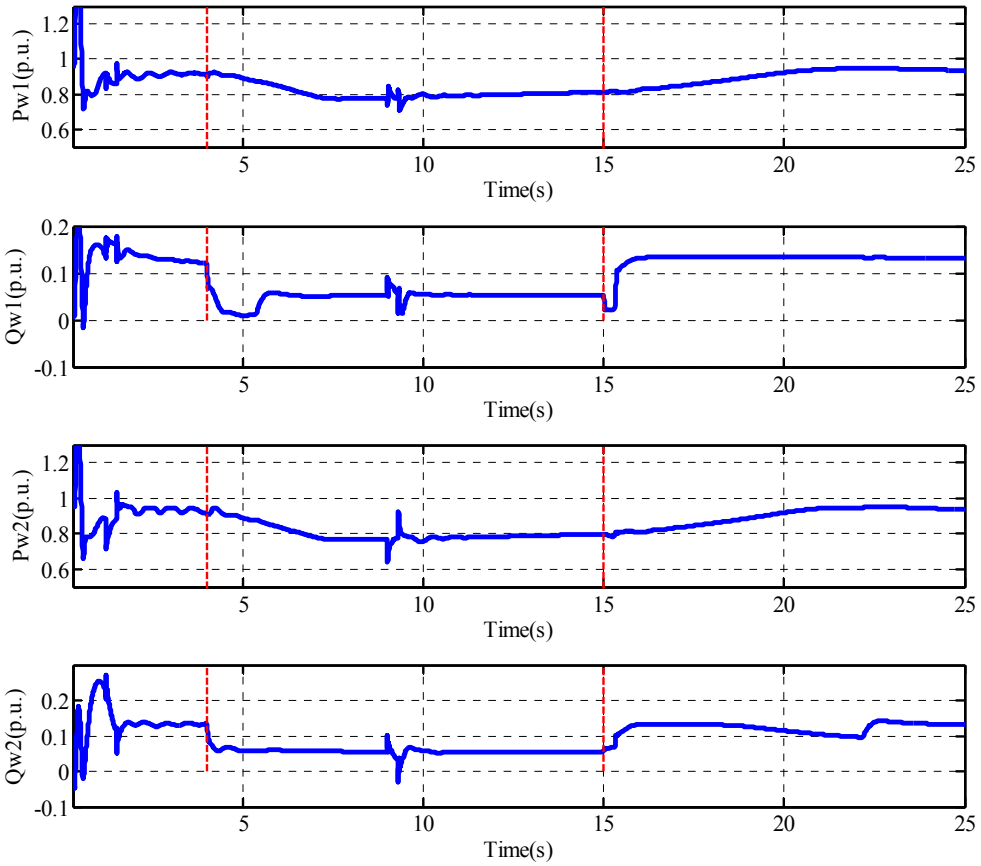

Figure 5-23 Active and reactive power generation of the wind generators – case study 3

5.5.2.4 Case-study 4: Motor starting

In this case-study, all the loads of the IEEE 34 node system were connected to the system. The induction motor connected to bus 840 started operating at t=2s and drew the starting current for about one second. The MPC controller used the available control inputs to achieve the voltage goals, but was still not capable of providing the extra voltage and reactive support to keep the bus voltage within limits during the motor

startup. This is normal in most induction motor startups in heavily loaded power systems.

Figure 5-24, Figure 5-25 shows the bus voltages dropped below the requirement during motor startup. This drop did not make the system go unstable or the relays to trip. However, this voltage drop can result in flickering lights in the distribution system.

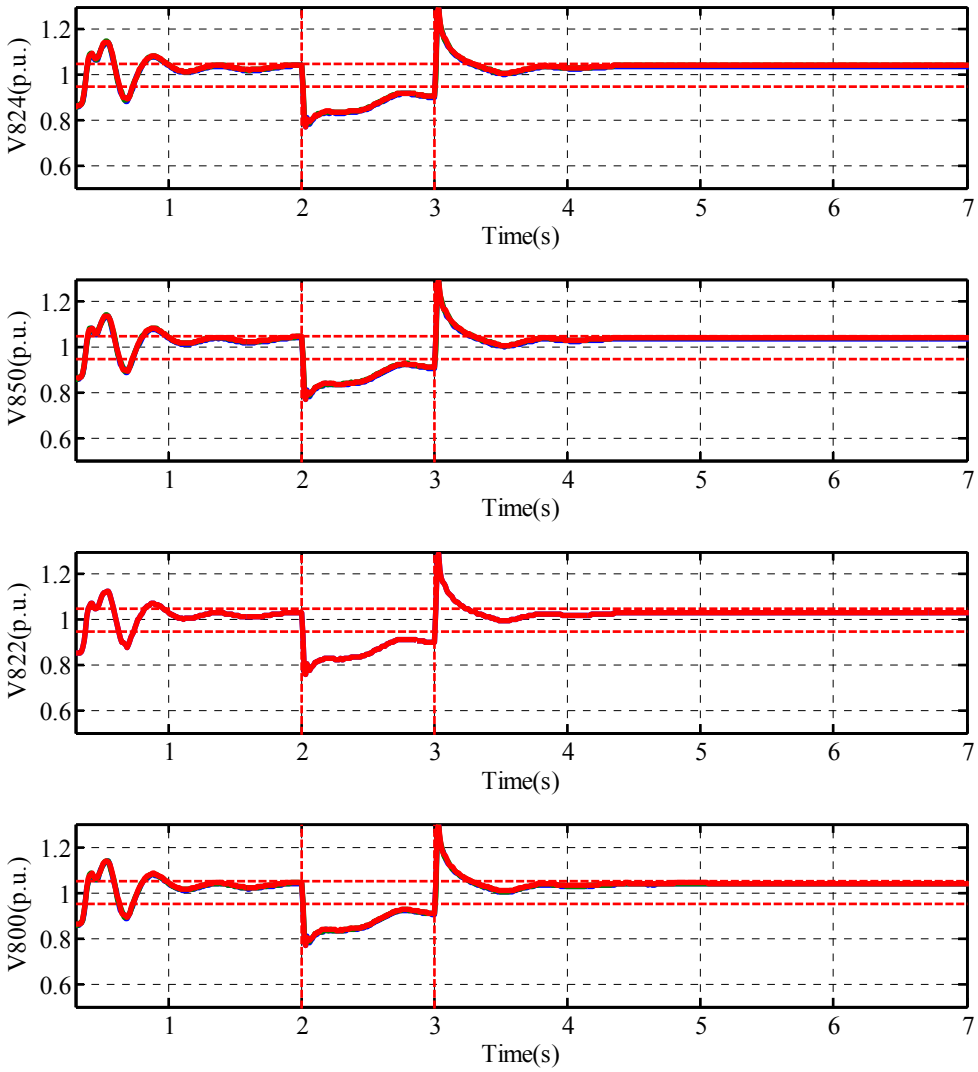

Figure 5-24 Bus voltages of MicroGrid – case study 4

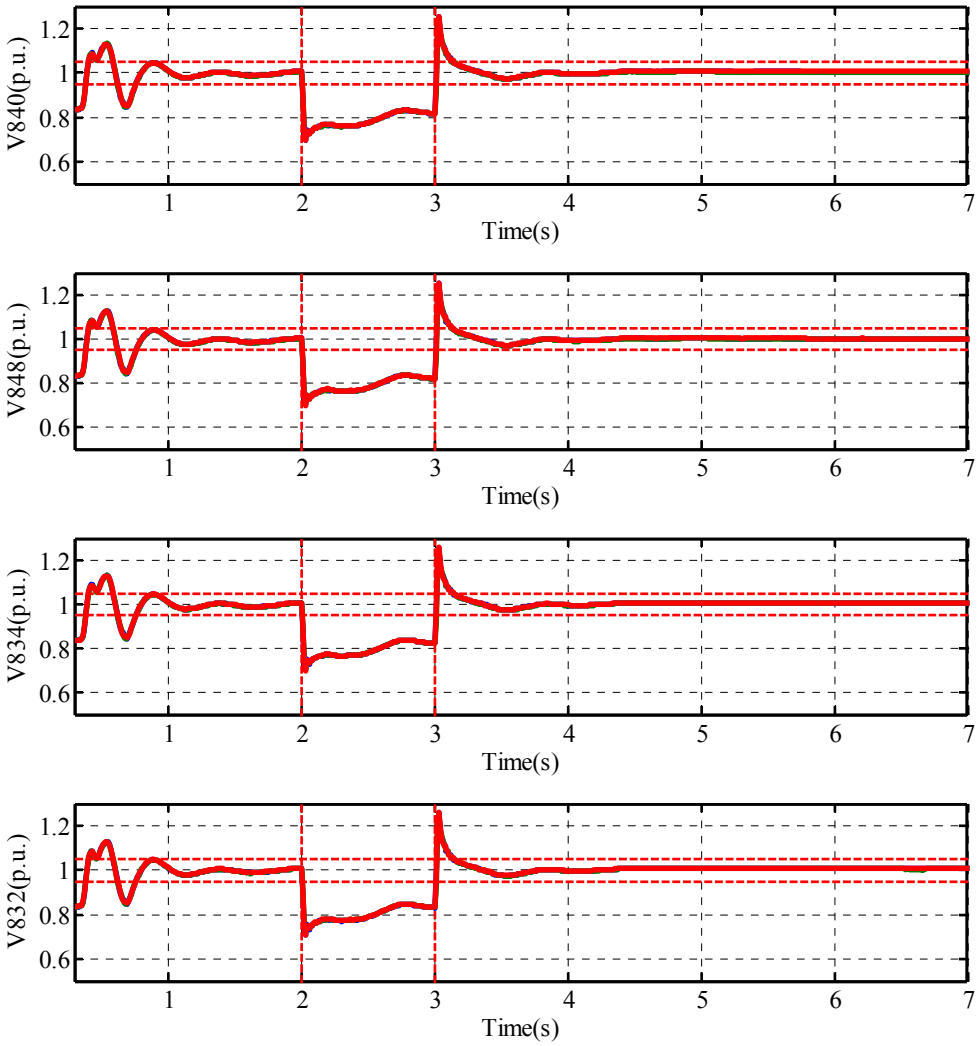

Figure 5-25 Bus voltages of MicroGrid – case study 4

As can be seen in Figure 5-26, the reactive power controller adjusted the voltage reference of the master generator to compensate for the voltage drop in the system. In this case-study, the reactive controller could not keep bus voltages within limits since

there were no additional reactive capabilities in the system to inject reactive power locally.

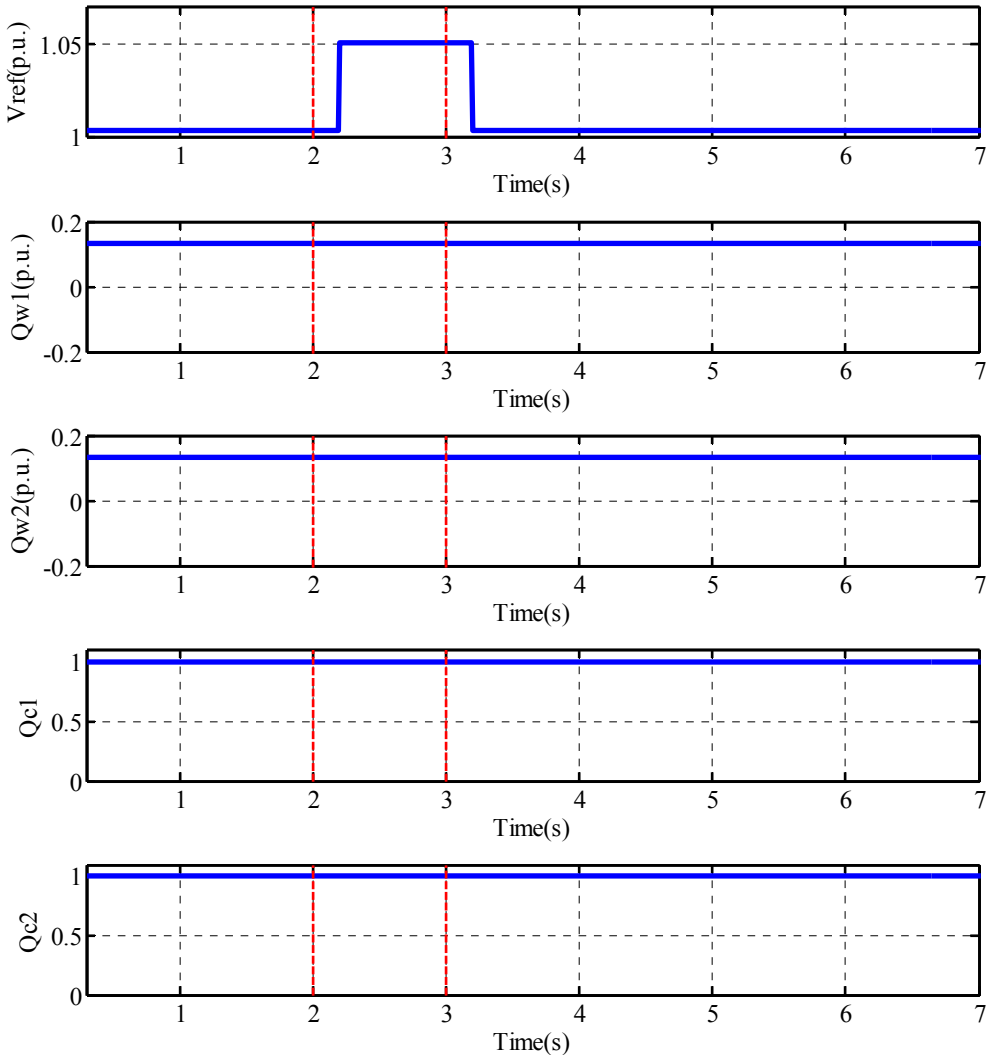

Figure 5-26 Control inputs to the MicroGrid – case study 4

5.5.2.5 Case-study 5: Induction motor starting and demand-response

In this case-study, all the loads of the IEEE 34 node system were connected to the system. The spot load connected to bus 890 was considered a non-sensitive load that had

a demand response contract with the utility. The induction motor connected to bus 840 started operating at t=2s and drew the starting current for about one second. The MPC controller used the available control inputs to achieve the voltage goals. The control signals generated by the MPC controller are depicted in Figure 5-27. As can be seen in Figure 5-28 and Figure 5-29, the MPC controller used the demand response load to reduce the reactive power consumption of the whole system, which resulted in less voltage drop in the buses comparing to case-study 4.

Compared to case-study 5, in this case the controller also disconnected the demand-response load during the startup period of the motor. The demand-response load was disconnected when Q_{DR}=1 and connected when Q_{DR}=0 Disconnecting the demand-response load resulted in a less voltage drop in the buses in the system. The voltage of some buses are depicted in Figure 5-28, Figure 5-29.

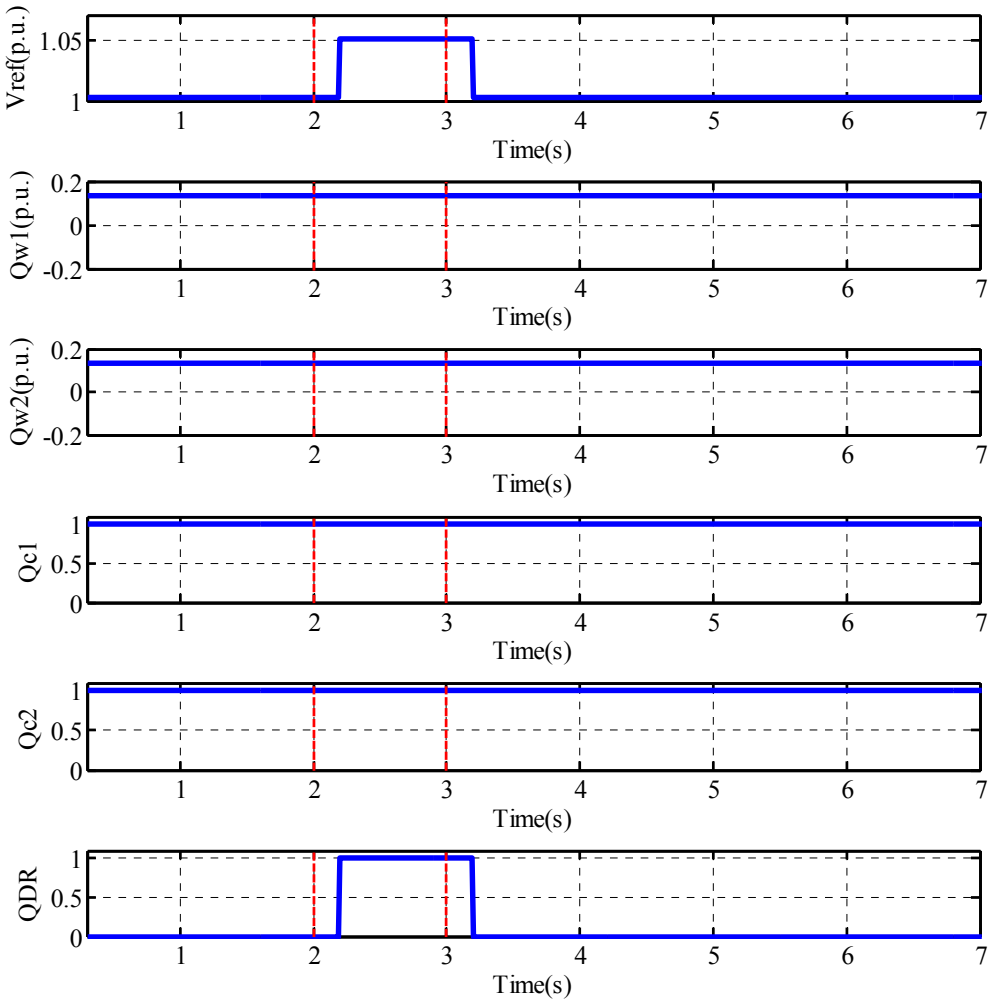

Figure 5-27 Control inputs to the MicroGrid – case study 5

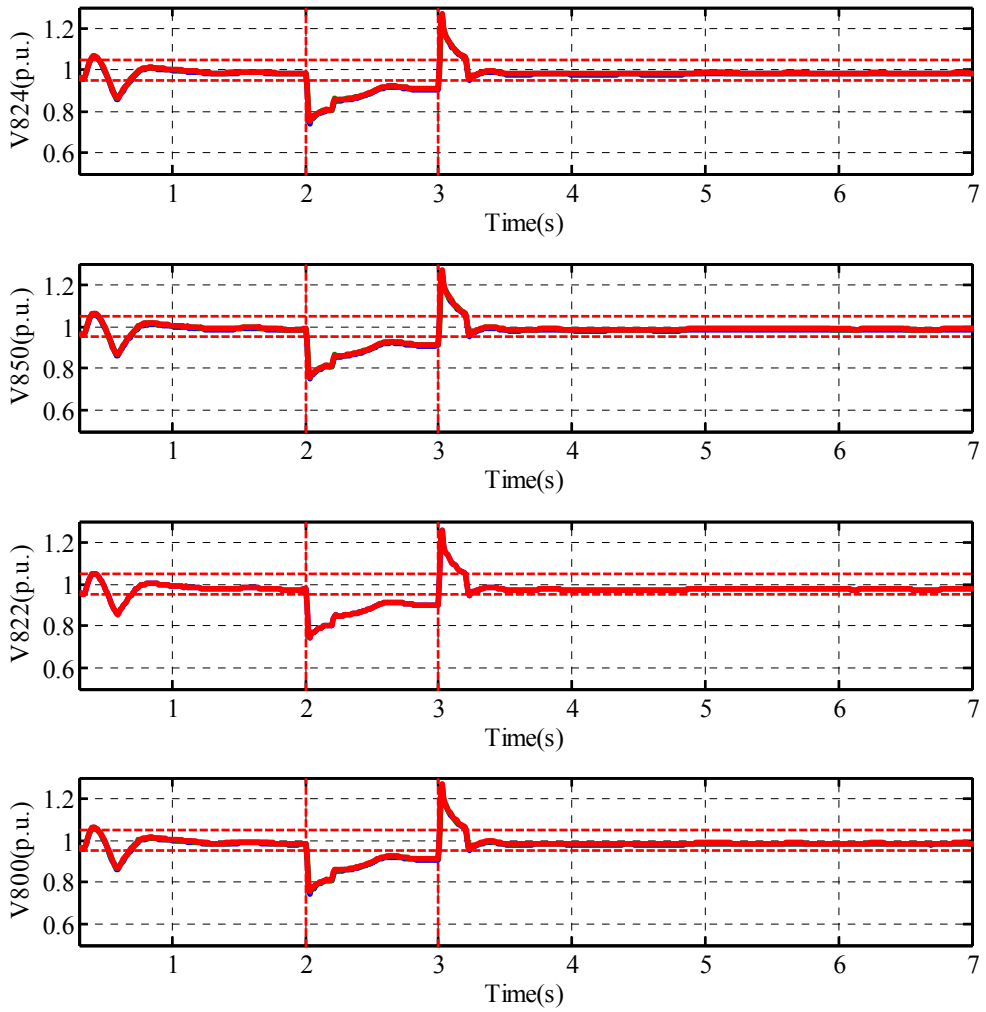

Figure 5-28 Bus voltages of MicroGrid – case study 5

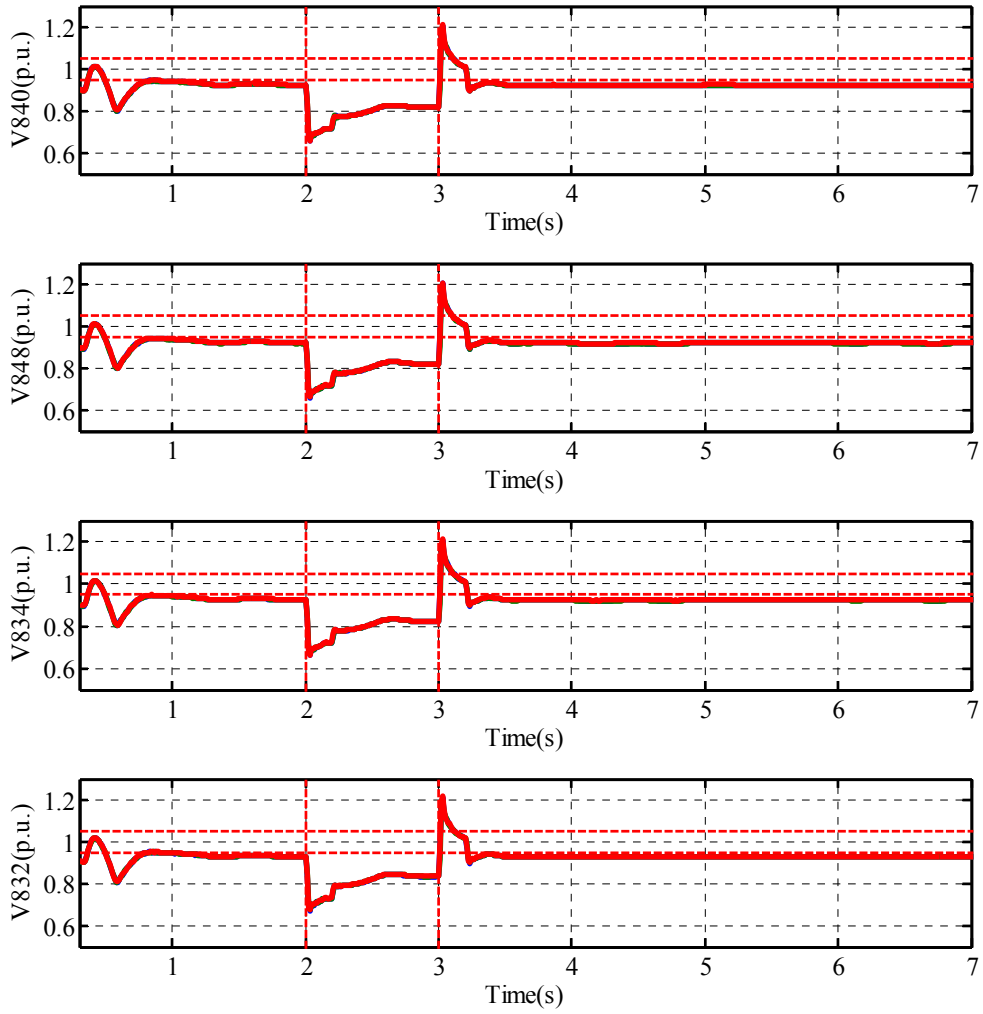

Figure 5-29 Bus voltages of MicroGrid – case study 5

5.5.2.6 Case-study 6: Motor starting with demand-response

In this case-study, the spot load at 844 was disconnected from the system all through the case-study. The induction motor connected to bus 840 started operating at t=2s and drew the starting current for about one second. A non-sensitive load with a demand-response contract with the utility was connected at bus 890. The MPC controller used the available control inputs to achieve the voltage goals. Figure 5-30and Figure 5-31 show

that compared to case-study 4 and 5, the controller was more successful in keeping the voltage close to required level during motor startup. During the transient condition, the system experienced voltage spikes and voltage drops. As mentioned earlier, the present requirements in IEEE Std 1547.4 [106] for under-voltage tripping time are 0.16 s for voltage less than 50% and 2 s for voltages less than 88%. The variations in the voltage beyond the 12% limit occurred for less than 0.2 seconds, which is acceptable according to IEEE 1547.4 Standard for isolated power systems and does not cause relays to trip. Some bus voltages remained outside the 5% limit for around one second.

As can be seen in Figure 5-32, the MPC controller increased the reference voltage of the master generator, disconnected the DR load, and connected the capacitor bank to be able to provide enough reactive power for the induction motor startup.

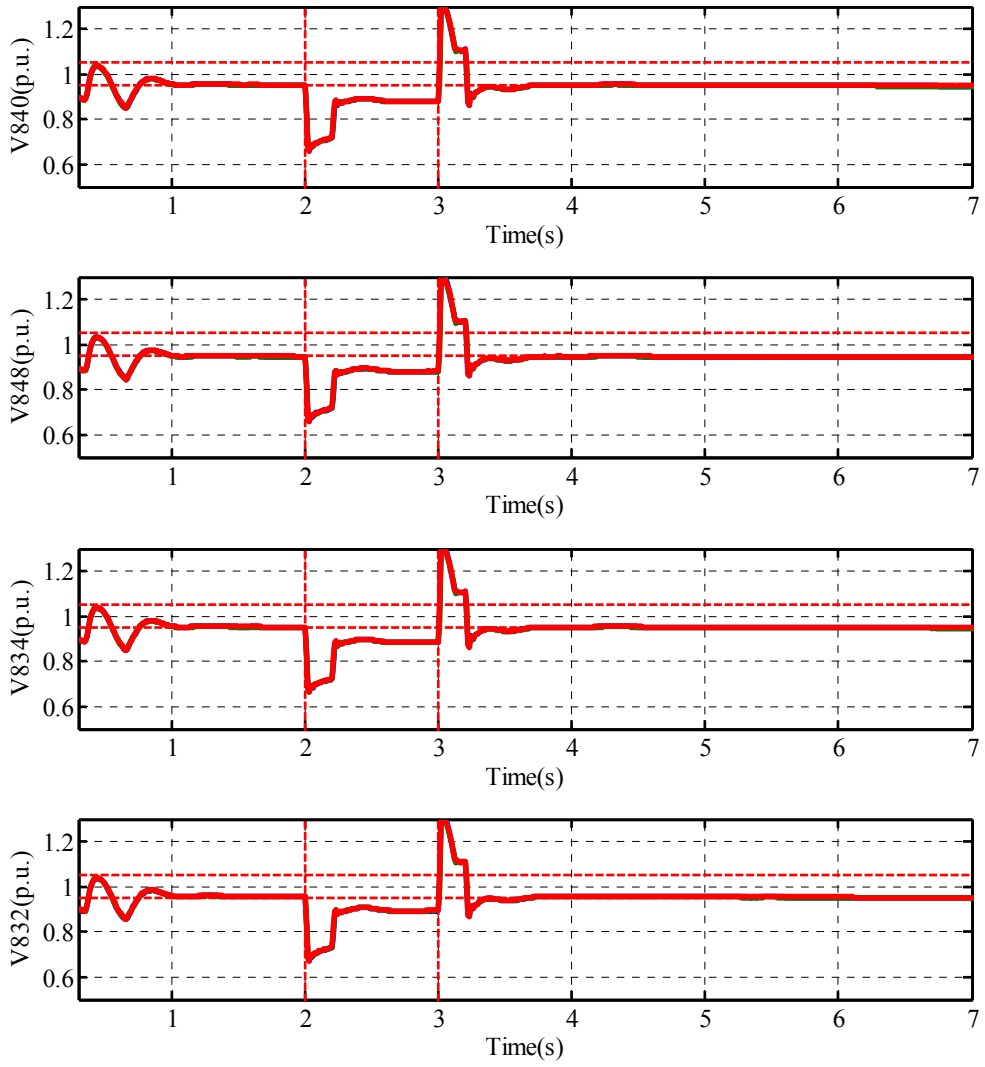

Figure 5-30 Bus voltages of MicroGrid – case study 6

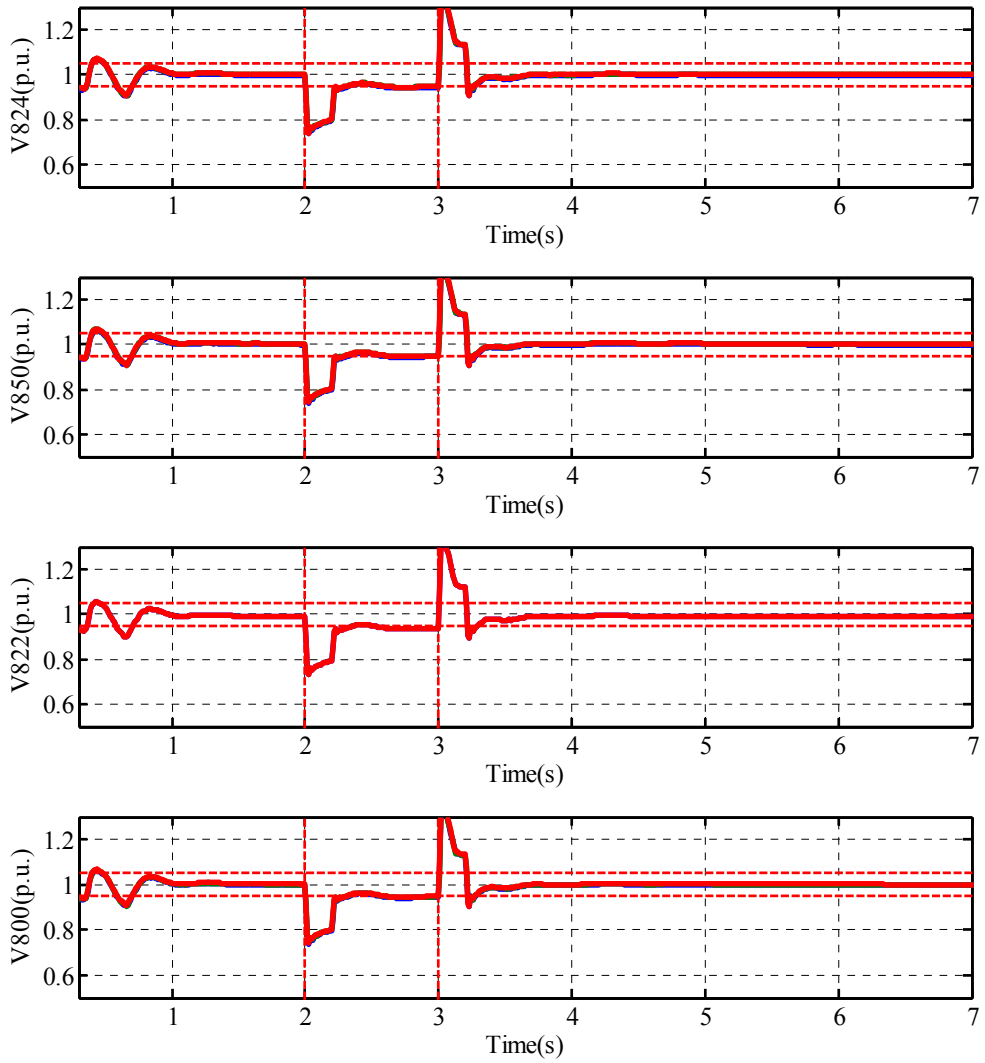

Figure 5-31 Bus voltages of MicroGrid – case study 6

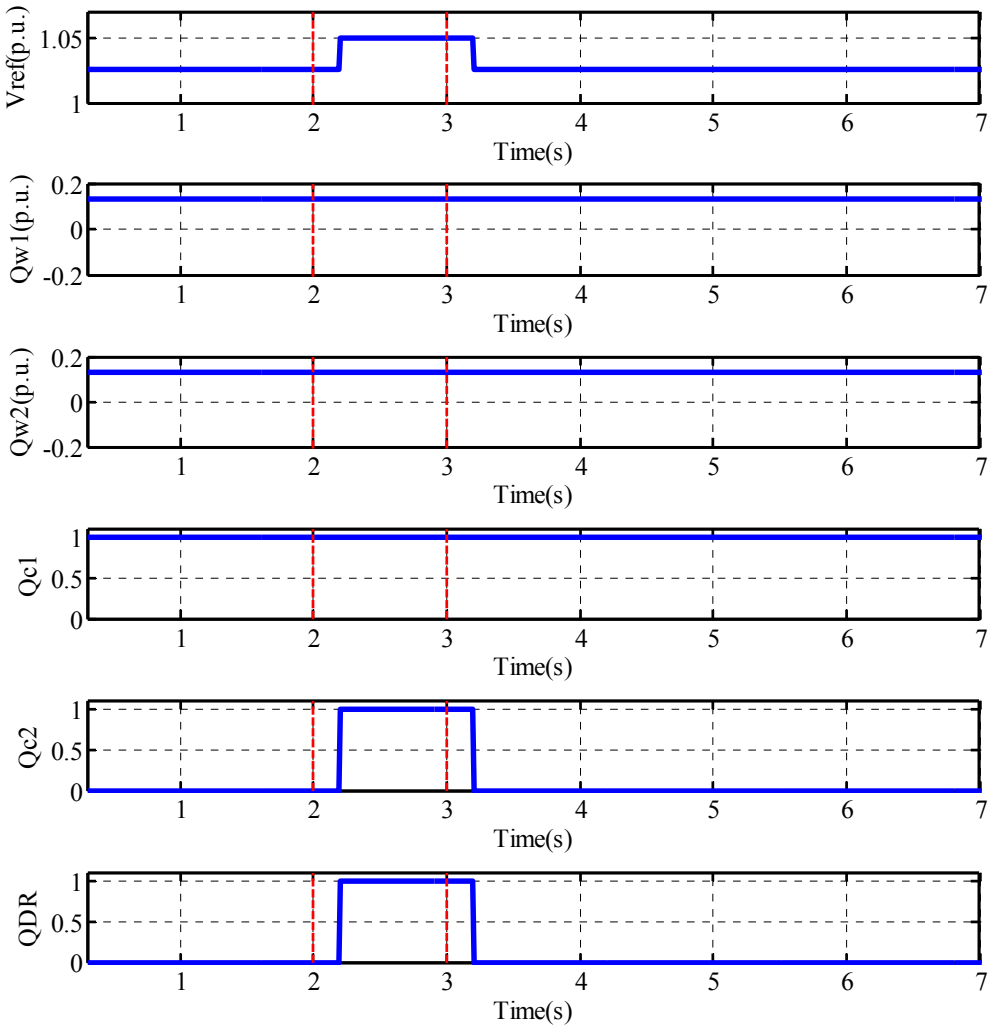

Figure 5-32 Control inputs to the MicroGrid – case study 6

5.5.2.7 Case-study 7: Induction starting with demand response and increasing reactive support

In this case-study, the spot load at 844 was disconnected from the system all through the case-study. The induction motor connected to bus 840 started operating at t=2s and

drew the starting current for about one second. A non-sensitive load with demand response contract with the utility was connected to bus 890.

In this case-study, when the demand response load was disconnected from the system, the PQ generators in the system had higher reactive power production capacity, since less active power was being consumed by the loads in the system. Thus, the MPC controller adjusted the reactive power production limit of the wind generators. Figure 5-33 shows how the reactive power controller increased the reactive power production setpoint of the wind generator to achieve the voltage requirements. Similar to the previous case-study, the reactive power controller increased the voltage reference of the master generator and disconnected the demand-response load. As can be seen in Figure 5-34 and Figure 5-35, the MPC controller was able to maintain the voltage within limits in this case with proper adjustment and demand-response load. In this case the system only experiences voltage drop and voltage spike for short periods of time. The light flickering in the distribution system is not visible in that short duration. Compared to case-study 4,5, and 6, the controller performed better in case-study since it had more flexibility in terms of control inputs to achieve the required criteria.

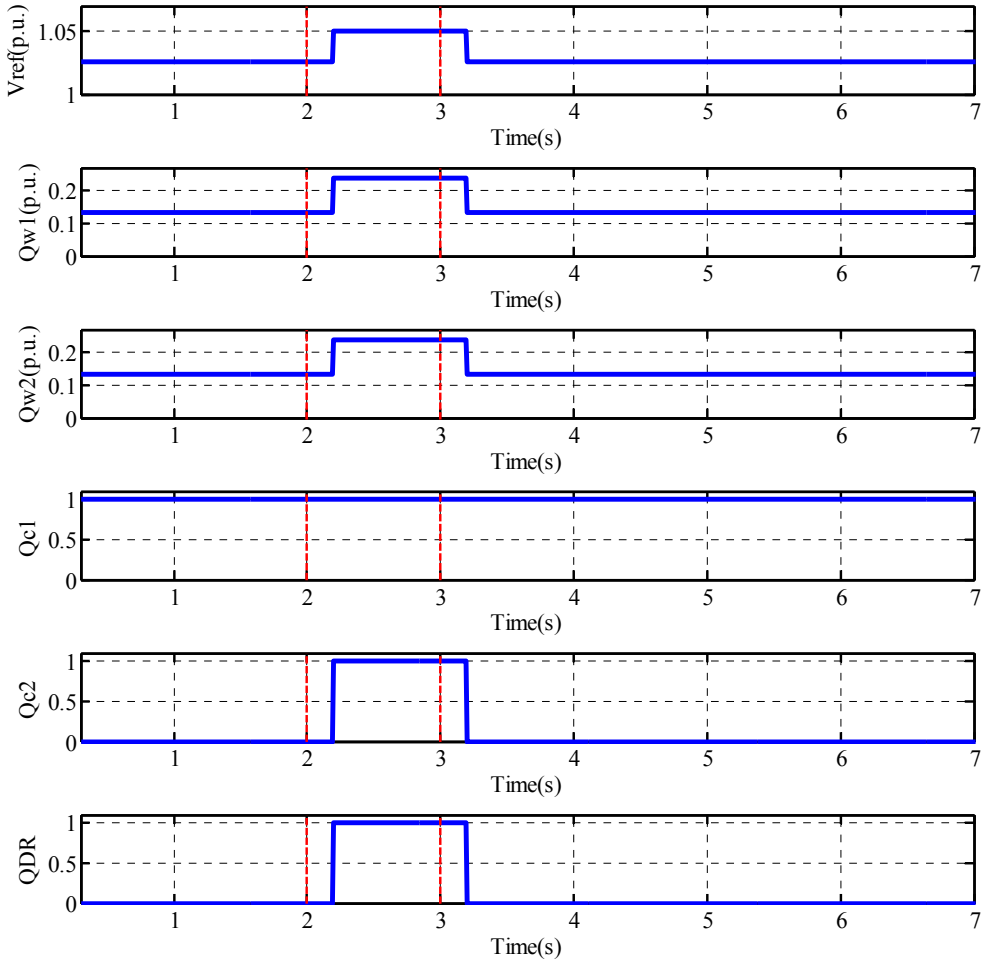

Figure 5-33 Control inputs to the MicroGrid – case study 7

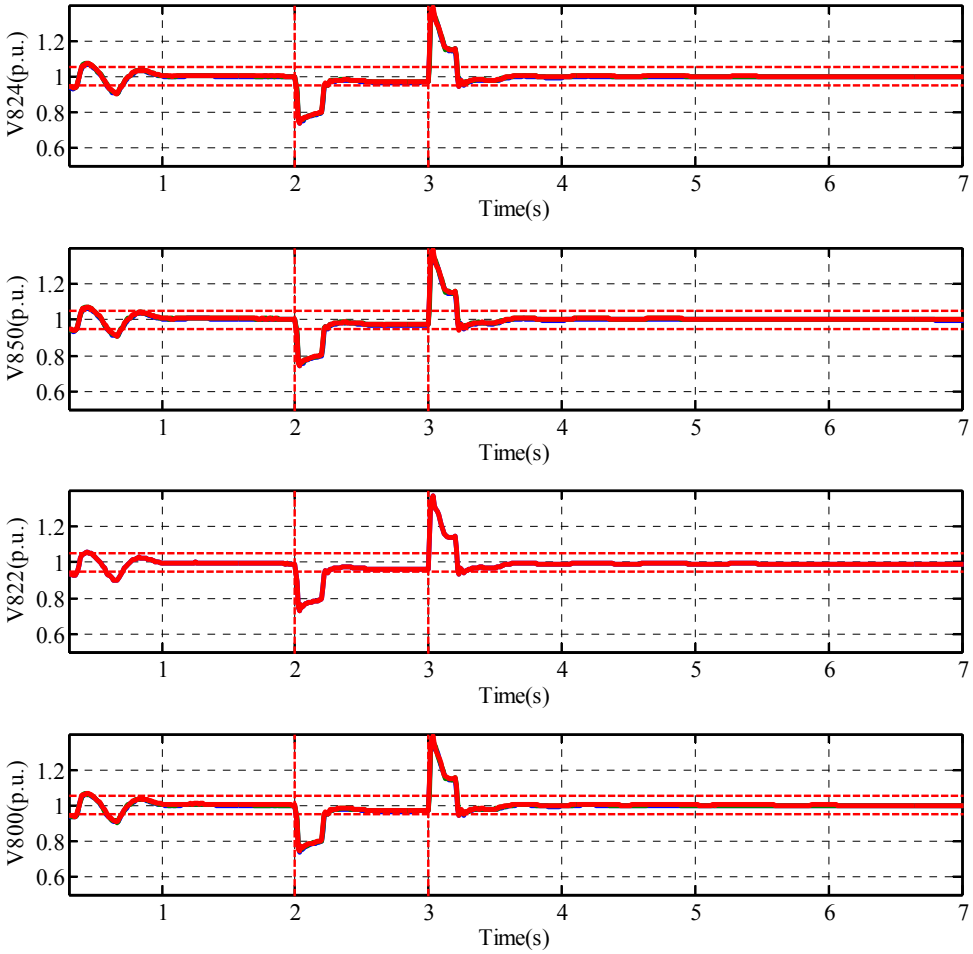

Figure 5-34 Bus voltages of MicroGrid – case study 7

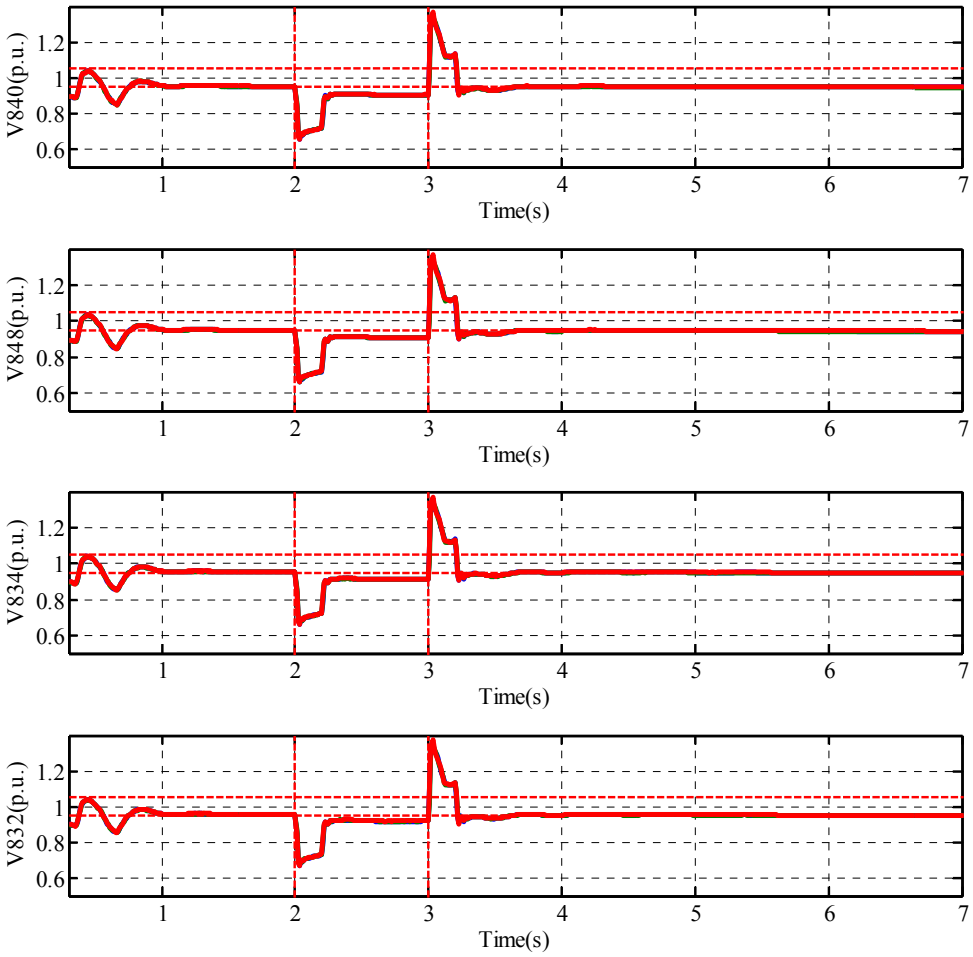

Figure 5-35 Bus voltages of MicroGrid – case study 7

5.5.2.8 Case –study 8: Load change with varying wind

This case-study is demonstrating the performance of the MPC controller during small load changes in the system. Load 2 which was connected to node 844 was reduced to half at t=2.5s. Further, load 1 which is connected to node 890 was reduced to half at t=3.5s and both of the loads got back to their nominal value at *t*=5.5*s*. In addition, the wind speed was changing moderately during this case-study. The generalized MPC controller tried to reduce the effect of the load change and wind change in the system.

The assumption in this case-study was that the MPC controller did not have a prediction of the exact time of load change. Therefore, after the load changed, it took 0.3 seconds for the controller to send the updated control inputs to the system since the step time of the control algorithm was set to 0.3s. As can be seen in Figure 5-37 and Figure 5-38, the MPC controller was able to keep the voltages within the limits by adjusting the control inputs. In this case-study, to reduce the losses in the system and to reduce the peak power, the reference voltage setpoint was chosen equal to 0.96 p.u. The wind profile in this case-study is shown in Figure 5-36.

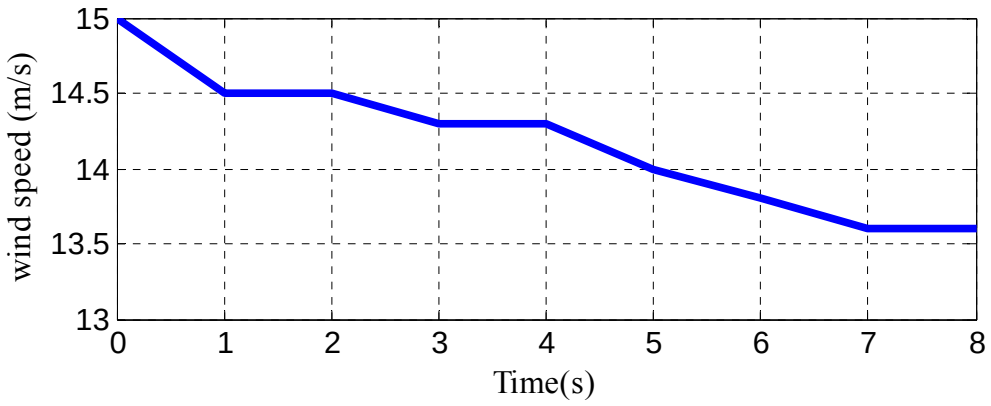

Figure 5-36 Wind profile

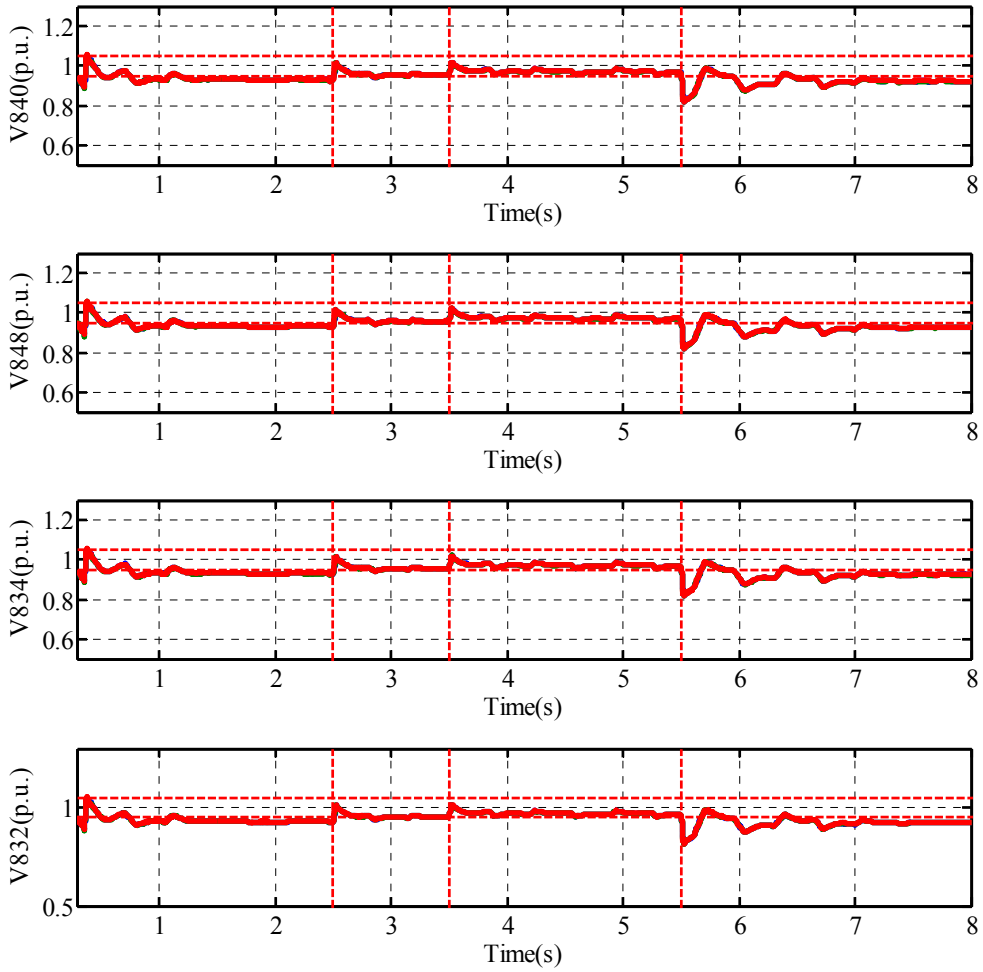

Figure 5-37 Bus voltages with MPC – case study 8

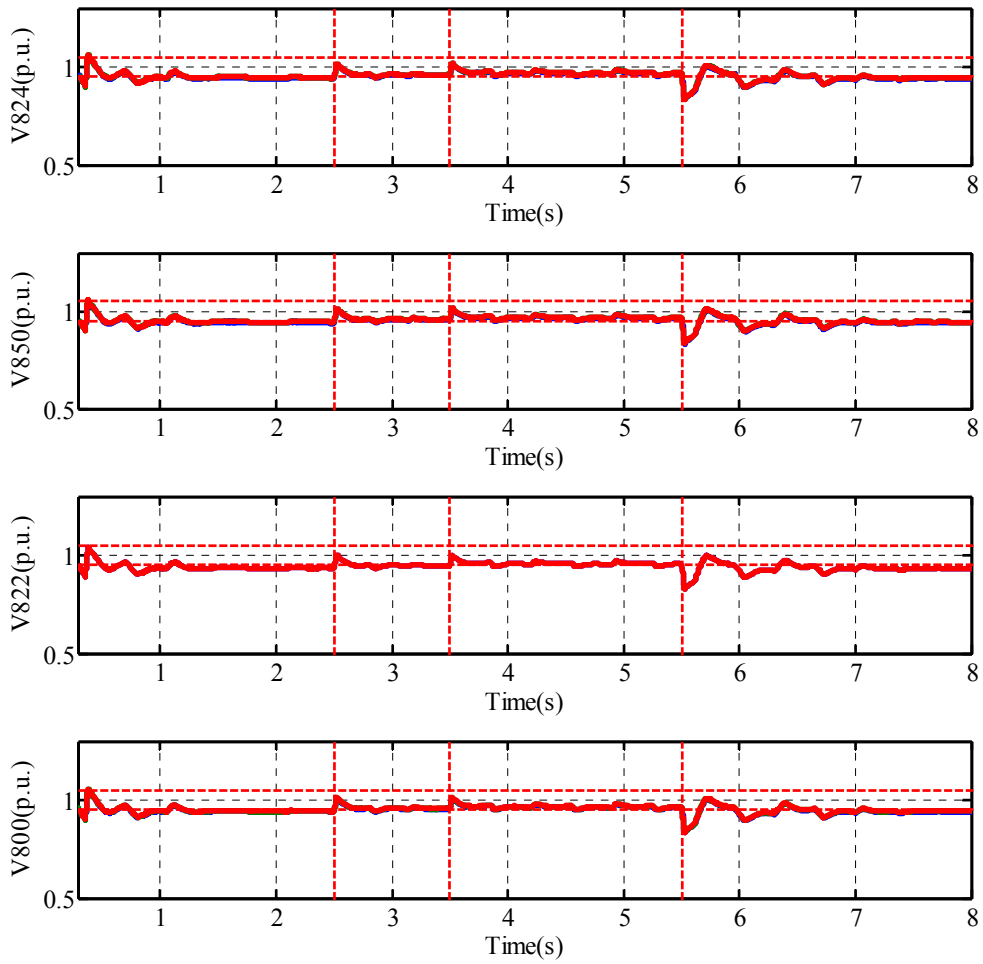

Figure 5-38 Bus voltages with MPC – case study 8

As can be seen in Figure 5-39, the controller decreased the reactive injection of the second wind generator to keep the voltage within limits after the decrease in load at t=2.5s. This decrease resulted in the voltage being maintained within the 5% limits at no extra cost to the system as can be seen in Figure 5-37 and Figure 5-38. The system's total load again decreased at t=3.5s. The controller responded to this load change by slowly decreasing the reactive injection of both wind generators 1 and 2. The system's total load increased at t=5.5s. Further, the wind speed decreased resulting in an

additional demand for reactive support. The designed controller responded by increasing the reactive injection of both wind generators. The controller also increased the voltage reference of the master generator for a short period of time. These changes in the control input resulted in the voltages of the system to stay within the 5% limits except for a very short period as can be seen in Figure 5-37 and Figure 5-38.

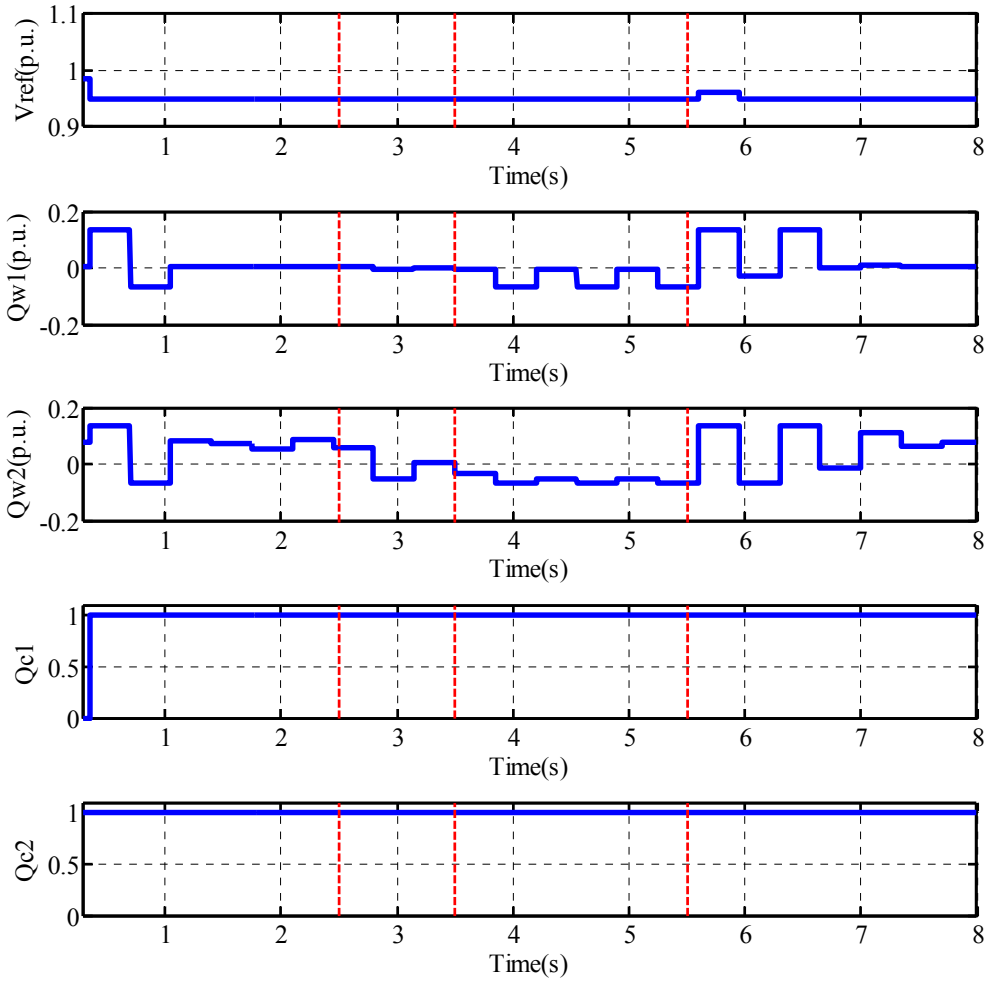

Figure 5-39 Control inputs to the MicroGrid generated by MPC – case study 8

5.5.2.9 Case –study 9: Controller failure due to capacitor bank malfunction

This case-study is demonstrating the effect of malfunction of the actuators of the components on the performance the MPC controller during sharp load changes in the system. Load 2 which was connected to node 844 got disconnected from the system at t=2.5s. Further, load 1 which was connected to node 890 got disconnected at t=3.5s and both of the loads were energized again at t=5.5s. The generalized MPC controller tried to reduce the effect of the load change in the system by sending optimal control inputs to the system. The assumption in this case-study was that the MPC controller does not have a prediction of the exact time of load change. Therefore, after the load changed, it took 0.2 seconds for the controller to send the updated control inputs to the system. After the load change at t=3.5s, the controller tried to disconnect the capacitor banks one by one to coordinate the reactive power in the system. However, the actuators of the capacitor banks malfunctioned, which resulted in the capacitor banks to remain connected to the system. As a result the MicroGrid buses experienced an overvoltage for a few seconds as can be seen in Figure 5-40 and Figure 5-41. This overvoltage can be destructive to the system and cause insulation damaging.

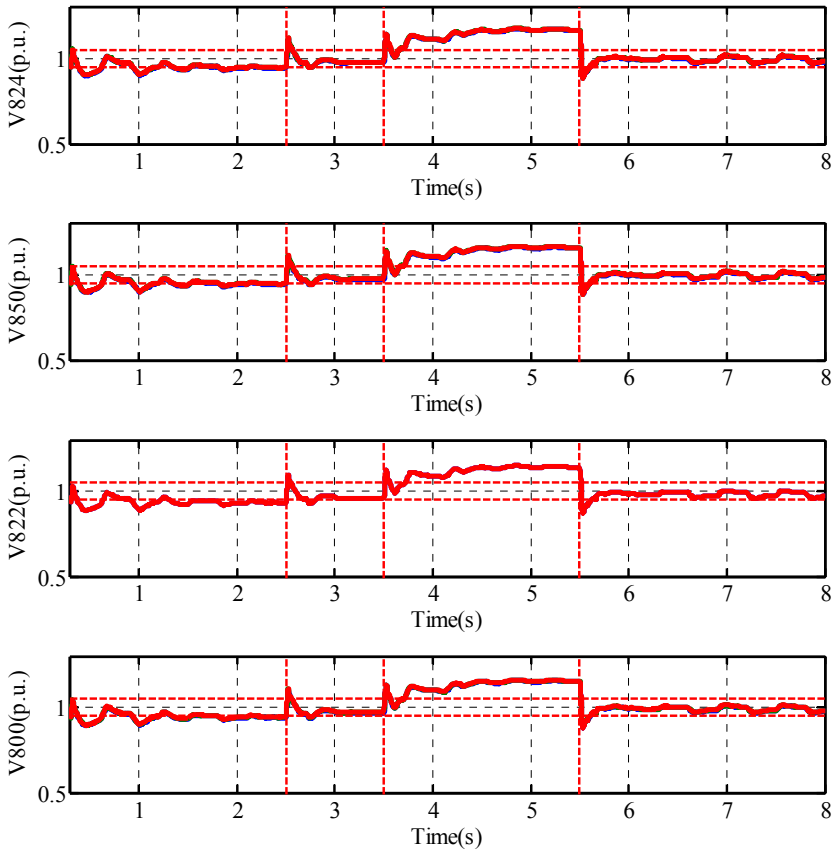

Figure 5-40 Bus voltages with MPC – case study 9

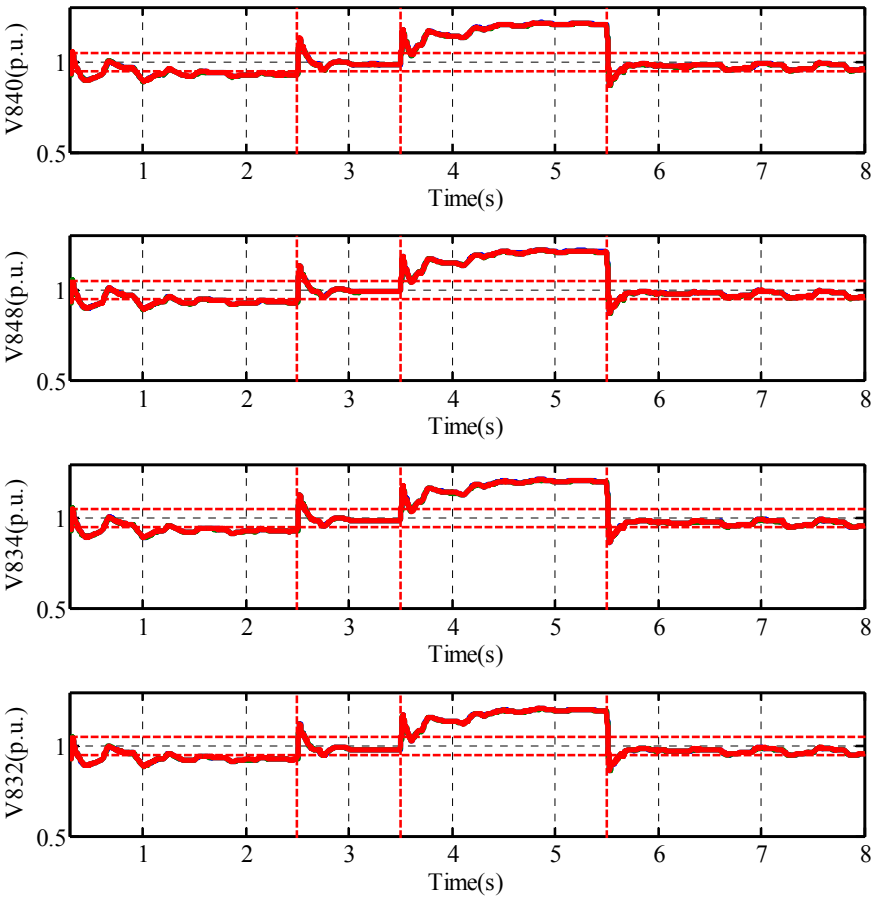

Figure 5-41 Bus voltages with MPC – case study 9

The control inputs to the system in case-study 9 are depicted in Figure 5-42.

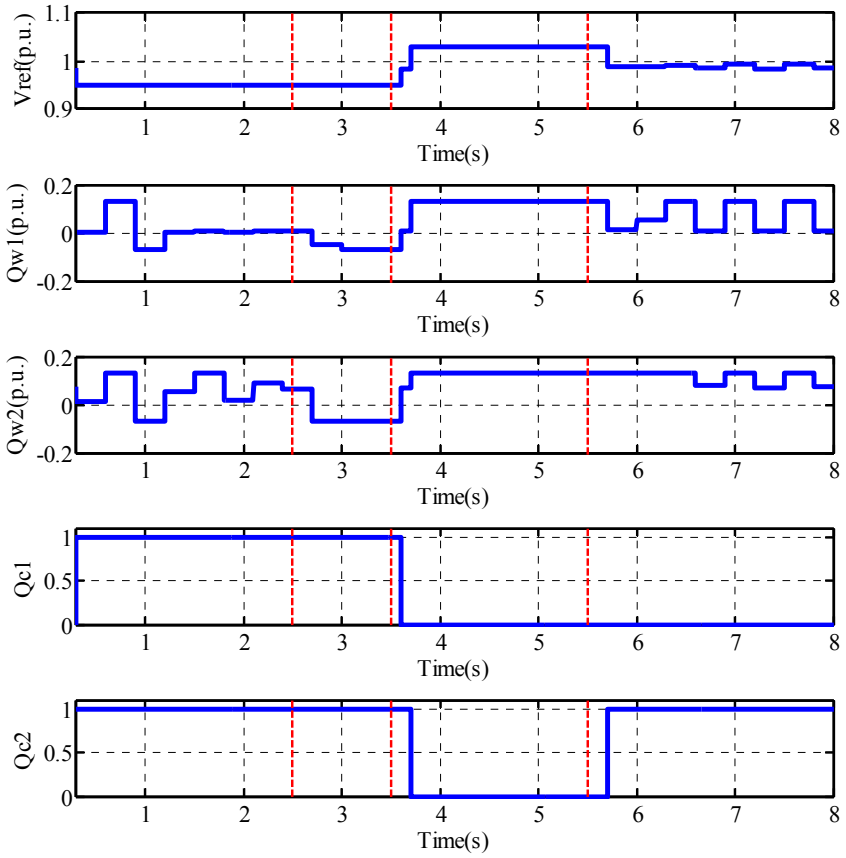

Figure 5-42 Control inputs to the MicroGrid generated by MPC – case study 9

5.5.2.10 Case –study 10: Failure due communication delay

This case-study is demonstrating the effect of communication delay on the performance the MPC controller during sharp load changes in the system. Load 2, connected to node 844, got disconnected from the system at t=2.5s. Further, load 1 connected to node 890, got disconnected at t=3.5s. Both of these loads were energized again at t=5.5s. The generalized MPC controller tried to reduce the effect of the load change in the system by sending optimal control inputs to the system. After the load change at t=3.5s, the controller tried to disconnect the capacitor banks one by one to

coordinate the reactive power in the system. However, the communication between the centralized controller and the capacitor banks experienced 1 second delay. This communication delay resulted in an overvoltage for around one second and an abnormal behavior in the system voltages as can be seen in Figure 5-43and Figure 5-44. In addition, the controller tried to connect the capacitor banks back to the system after the load change at t=5.5s. The system experienced the same communication delay for one second resulting in an undervoltage in the system buses for one second.

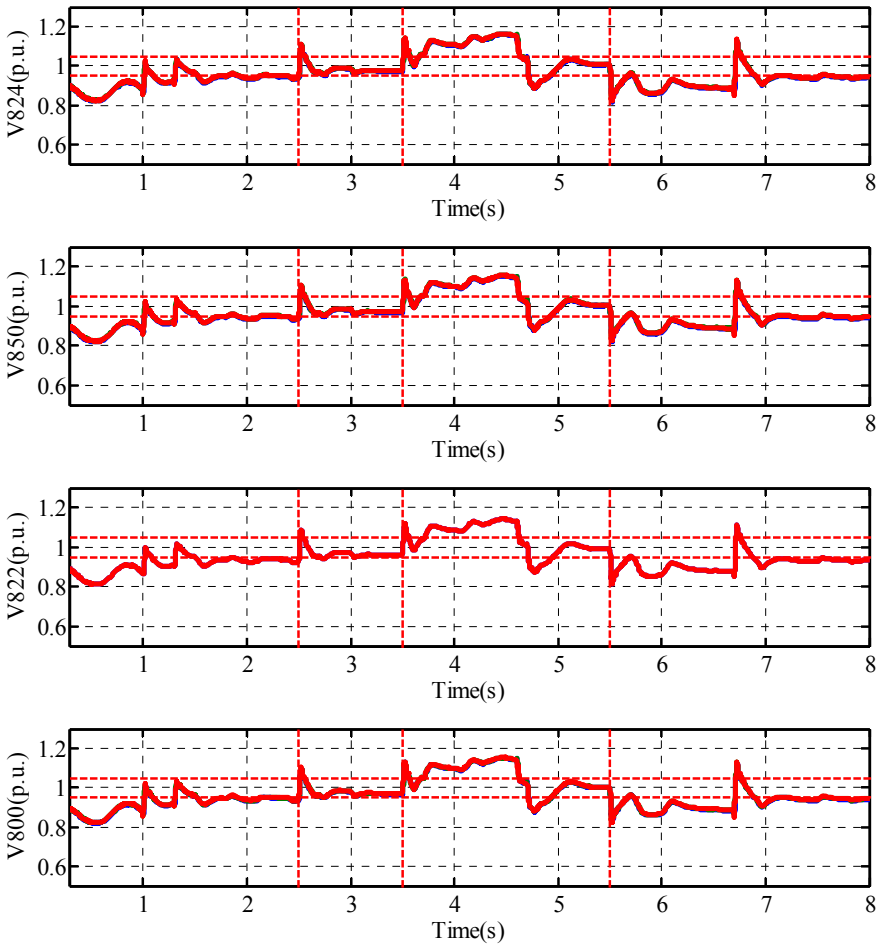

Figure 5-43 Bus voltages with MPC – case study 10

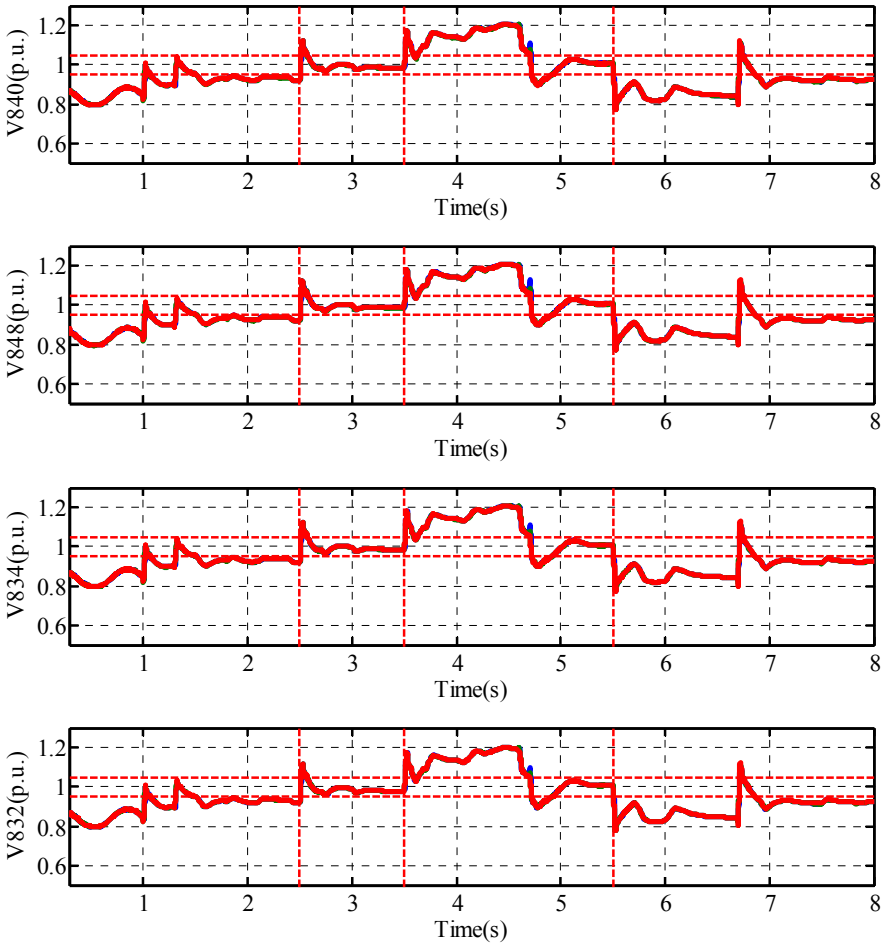

Figure 5-44 Bus voltages with MPC – case study 10

The control inputs to the system in case-study 10 are depicted in Figure 5-45.

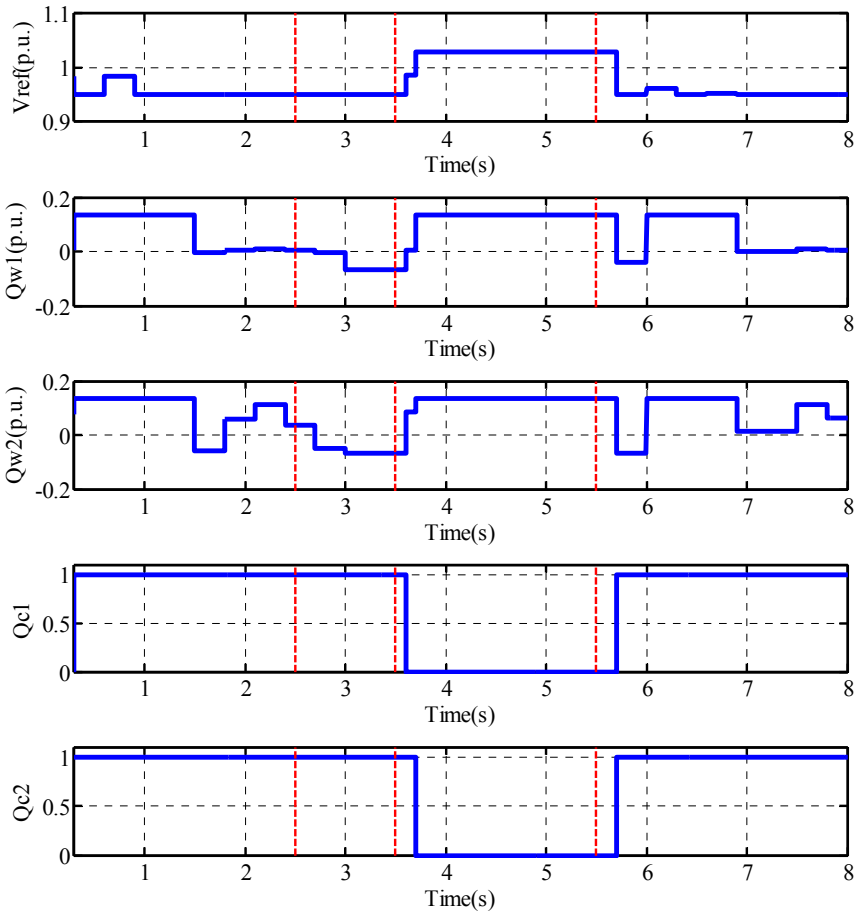

Figure 5-45 Control inputs to the MicroGrid generated by MPC – case study 10

5.6 Summary

This section discussed reactive power and voltage control of the MicroGrid. The problem was formulated considering the dynamics of the MicroGrid. MATLAB and CPLEX were used to implement the method. Finally, some case-studies were presented to show the effectiveness of the algorithm.

6 CONCLUSIONS AND FUTURE WORK

6.1 Conclusions

This dissertation presented a dynamic reactive control approach to control isolated power systems. Isolated power systems are vulnerable to changes in loads or generation and can easily get unstable. The reactive power control problem is a nonlinear problem integrating discrete inputs. This work proposed using model predictive control for reactive control of isolated systems. The system was linearized using a piecewise linear approach. Then the piecewise linear model was unified in the MLD framework. Replacing the nonlinearities by piecewise linear approximation introduces very small modeling error. The modeling error hardly manifests itself in the control experiments thus proving the usefulness of the MLD modeling approach. This dissertation showed that the bus voltages can be stabilized by an MPC controller using only nominal control moves. Tuning of the MPC controller is straightforward and systematic. The MPC controller can effectively use discrete inputs such as capacitor banks and Demand/Response loads as well as continuous inputs such as setpoint of dynamic reactive compensators and DGs to achieve smooth bus voltage profile.

The study in this dissertation concludes that if the communication and control infrastructure is available, MPC based reactive power control is viable option. MPC requires a model of the system to be able to predict the behavior of the system ahead of time; however, the model can be as simple as reactive power balance equations. The study in this dissertation used a simplified reactive power flow model in MPC and the simplified model achieved satisfactory results.

The author believes that in scope of 10-20 years, model predictive methods replace the current control scheme of power systems not only in reactive control but also in protection, and active power dispatch. The inherent robustness and reliability of MPC controllers can adequately deal with the changing structure of power systems. To achieve this goal, communication and control infrastructures of power systems need to be improved. In addition, accurate measurements of power system in certain buses should be available. With current trend in development of smart-grid and adding smart-meters to power systems, these measurements will be available to the operator in the distribution systems of the next decade.

6.2 Future Research

This dissertation only focused on dynamic reactive control of power systems. The major assumption in this dissertation was that the active power loop is already designed and works cooperatively with the reactive power control loop. Active and reactive power control loops are usually studied separately in power systems. It is interesting to design a dynamic active control loop using model predictive control and try to operate the two loops together. Further, it is interesting to try design a controller that can control active and reactive power together using one loop.

A challenge that the design in this dissertation faced was that the MPC resulted in too much control action in some cases. To the knowledge of the author, MPC usually results in more control action than other control methods. It is interesting to investigate methods to penalize control action over a long horizon of time. Penalizing the control action over a long horizon can help MPC to avoid too much control action. Another

challenge that this work experience was that from a control point of view the model complexity was unnecessarily increased when a large number of binary variables were associated with the approximations. As a result, the computation time for solving the underlying MILP or MIQP problems became relatively large. The method used in this dissertation was to limit the number of sectors in the piecewise linear system. In other words, the piecewise linear system was limited to a small number of pieces. Other methods can be further investigated to address the computation time increase. Since most current designs and testbeds of MicroGrids and shipboard power systems do not include an On-Load Tap Changer (OLTC), this dissertation did not focus on OLTCs. Adding OLTCs as a control input to the control problem can be further investigated.

It is common in industry that the utility desired to pick a sub-optimal solution to the reactive problem at the cost of not making too many changes in the system. In other words, sometimes utilities prefer to only change the status of one component and achieve a suboptimal solution. This approach slows down the aging of components in the system. This dissertation did not focus on such an approach; however, the method presented in this dissertation can be easily expanded to include such constraints.

REFERENCES

[1] J. D. Kueck, D. T. Rizy, F. Li, Y. Xu, H. Li, S. Adhikari, and P. Irminger, "Local dynamic reactive power for correction of system voltage problems," Oak Ridge National Laboratory, ORNL/TM-2008/174, 2008.

[2] E. Fuchs and M. Masoum, *Power Quality in Power Systems and Electrical Machines* Academic Press, 2008.

[3] C. J. Dafis, "An observability formulation for nonlinear power systems modeled as differential algebraic systems," Ph.D. dissertation, Dept. Elect. Eng., Drexel University, 2005.

[4] F. Katiraei and M. R. Iravani, "Power management strategies for a Microgrid with multiple distributed generation units," *IEEE Trans. Power Syst.,* vol. 21, pp. 1821-1831, Nov. 2006.

[5] K. L. Butler, N. D. R. Sarma, and V. Ragendra Prasad, "Network reconfiguration for service restoration in shipboard power distribution systems," *IEEE Trans. Power Syst.,* vol. 16, pp. 653-661, Nov. 2001.

[6] G. Gates, D. Shipp, and W. Vilcheck, "Electrical distribution system analysis for off-shore oil production facilities," in *Proc. Annual Petroleum and Chemical Industry Conf.*, 1998, pp. 129-137.

[7] F. McNamara, "Optimising unit commitment in an island power system," in *Proc. IEE Colloquium on Effective Response of a Public Electricity Network to Independent Generators*, 1993, pp. 1-7.

[8] W. Wei, W. Daifeng, A. Arapostathis, and K. Davey, "Optimal power generation scheduling of a shipboard power system," in *Proc. IEEE Elect. Ship Tech. Symp.*, 2007, pp. 519-522.

[9] S. Kulkarni and S. Santoso, "Estimating transient response of simple AC and DC shipboard power systems to pulse load operations," in *Proc. IEEE Conf. Electric Ship Technologies Symp.*, 2009, pp. 73-78.

[10] C. Yan, G. K. Venayagamoorthy, and K. Corzine, "AIS-based coordinated and adaptive control of generator excitation systems for an electric ship," *IEEE Trans. Indust. Electron.,* vol. 59, pp. 3102-3112, Aug. 2012.

[11] J. D. Kueck, R. H. Staunton, S. D. Labinov, and B. J. Kirby, "Microgrid energy management system," Oak Ridge National Laboratory, P500-03-091F, 2003.

[12] J. Stevens, "Characterization of microgrids in the United States," Sandia National Laboratories, Vienna, Virginia, 2005.

[13] D. Salomonsson, "Modeling, control and protection of low-voltage DC Microgrids," Ph.D. dissertation, Dept. Elect. Eng., KTH University, Stockholm, 2008.

[14] M. Innorta, P. Marannino, G. P. Granelli, M. Montagna, and A. Silvestri, "Security constrained dynamic dispatch of real power for thermal groups," *IEEE Trans. Power Syst.,* vol. 3, pp. 774-781, May 1988.

[15] Eltra, "Specifications for connecting wind farms to the transmission network," Eltra doc. no. 74174, 2000, available at: http://www.offshorecenter.dk/log/bibliotek/Specifications-Eltra.pdf.

[16] S. Morozumi, "Micro-grid demonstration projects in Japan," in *Proc. Power Conversion Conf.*, 2007, pp. 635-642.

[17] T. Funabashi and R. Yokoyama, "Microgrid field test experiences in Japan," in *Proc. IEEE Power Eng. Soc. General Meeting*, 2006, p. 2 pp.

[18] T. Geyer, "Low complexity model predictive control in power electronics and power systems," Ph.D. dissertation, Dept. Elect. Eng., ETH Zurich University, 2005.

[19] M. Barnes, "An evaluation of Microgrid structures and their relative merits," in *Proc. IET Power Conv.*, 2007, pp. 1-34.

[20] N. Hatziargyriou, H. Asano, R. Iravani, and C. Marnay, "Microgrids - an overview of ongoing research, development, and demonstration projects," *IEEE Power & Energy Mag.,* vol. 5, pp. 78-94, 2007.

[21] I. Roytelman, B. K. Wee, and R. L. Lugtu, "Volt/Var control algorithm for modern distribution management system," *IEEE Trans. Power Syst.,* vol. 10, pp. 1454-1460, Aug. 1995.

[22] J. Dréo, A. Pétrowski, P. Siarry, and E. Taillard, *Metaheuristics for hard optimization: Methods and case studies*, 1 ed. Berlin, Germany: Springer-Verlag, 2006.

[23] Y. C. Huang, H. T. Yang, and C. L. Huang, "Solving the capacitor placement problem in a radial distribution system using tabu search approach," *IEEE Trans. Power Syst.,* vol. 4, pp. 1868-1873, Nov. 1996.

[24] D. E. Goldberg, *Genetic Algorithms in Search, Optimization, and Machine Learning*, 1 ed. Boston, MA: Addison-Wesley Professional, 1989.

[25] Y. d. Valle, S. Mohagheghi, J. C. Hernandez-Mejia, G. K. Venayagamoorthy, and R. G. Harley, "Particle swarm optimization- basic concepts, variants and applications in power system," *IEEE Trans. Evol. Comput.,* vol. 12, pp. 171 - 195, Apr. 2008.

[26] A. G. Beccuti, T. Geyer, and M. Morari, "A hybrid system approach to power systems voltage control," in *Proc. IEEE Conf. Decision and Control*, Seville, Spain, 2005, pp. 6774-6779.

[27] M. Zima and G. Anderson, "Model predictive control employing trajectory sensitivities for power systems applications," in *Proc. IEEE Conf. on Decision and Control, and the Europ. Control Conf.*, Seville, Spain, 2005, pp. 4452-4456.

[28] B. Gong and I. A. Hiskens, "Two-stage model predictive control for voltage collapse prevention " in *Proc. North Amer. Power Symp.*, 2008, pp. 1-7.

[29] B. Gong and A. Pinheiro, "Online voltage collapse prevention through optimal load shedding and dynamic generation control," in *Proc. Power Energy Engineering Conf.*, 2010, pp. 1-6.

[30] I. A. Hiskens and M. A. Pai, "Trajectory sensitivity analysis of hybrid systems," *IEEE Trans. Circuits Systems I: Fundamental Theory Appl.,* vol. 47, pp. 204 - 220, Feb. 2000.

[31] L. Jin, R. kumar, and N. Elia, "Model predictive control-based real-time power system protection schemes," *IEEE Trans. Power Syst.,* vol. 25, pp. 988-998, May 2010.

[32] P. Kienast, "Optimal overload response in electric power systems applying model predictive control," M.S. thesis, Dept. Elect. Eng., ETH Zurich University, 2007.

[33] M. Maxwell, "The economic application of capacitors to distribution feeders," *Trans. Am. Inst. Electr. Eng. Part 3,* vol. 79, pp. 353-359, Apr. 1960.

[34] R. F. Cook, "Optimizing the application of shunt capacitors for reactive-volt-ampere control and loss reduction," *Trans. Am. Inst. Electr. Eng. Part 3,* vol. 80, pp. 430-444, Aug. 1961.

[35] R. F. Cook, "Calculating loss reduction afforded by shunt capacitor application," *IEEE Trans. Power App. Syst.,* vol. 83, pp. 1227-1230, Dec. 1964.

[36] J. V. Schmill, "Optimum size and location of shunt capacitors on distribution feeders," *IEEE Trans. Power App. Syst.,* vol. 84, pp. 825-832, Sept. 1965.

[37] N. E. Chang, "Locating shunt capacitors on primary feeder for voltage control and loss reduction," *IEEE Trans. Power App. Syst.,* vol. 88, pp. 1574-1577, Oct. 1969.

[38] M. E. Baran and F. F. Wu, "Optimal capacitor placement on radial distribution system," *IEEE Trans. Power Del.,* vol. 4, pp. 725-734, Jan. 1989.

[39] H. Durán, "Optimum number, location, and size of shunt capacitors in radial distribution feeders- a dynamic programming approach," *IEEE Trans. Power App. Syst.,* vol. 87, pp. 1769-1774, Sept. 1968.

[40] M. Ponnavaikko and K. S. P. Rao, "Optimal choice of fixed and switched shunt capacitors on radial distributors by the method of local variations," *IEEE Trans. Power App. Syst.,* vol. 102, pp. 1607-1615, June 1983.

[41] Y. Y. Hsu and H. C. Kuo, "Dispatch of capacitors on distribution system using dynamic programming," *IEE Proc. Gen., Transm. and Distrib.,* vol. 140, pp. 433-438, Nov. 1993.

[42] S. H. Lee and J. J. Grainger, "Optimum placement of fixed and switched capacitors on primary distribution feeders," *IEEE Trans. Power App. Syst.,* vol. 100, pp. 345-352, Jan. 1981.

[43] Y. Y. Hsu and C. C. Yang, "A hybrid artificial neural network dynamic programming approach for feeder capacitor scheduling," *IEEE Trans. Power Syst.,* vol. 9, pp. 1069-1075, May 1994.

[44] M. Kaplan, "Optimization of number, location, size, control type and control settings of shunt capacitors on radial distribution feeders," *IEEE Trans. Power App. Syst.,* vol. 103, pp. 2569-2663, Sept. 1984.

[45] M. M. A. Salama and A. Y. Chikhani, "A simplified network approach to the Var control problem for radial distribution systems," *IEEE Trans. Power Del.,* vol. 8, pp. 1529-1535, July 1993.

[46] M. M. A. Salama, E. A. A. Mansour, A. Y. Chikhani, and R. Hackam, "Control of reactive power in distribution system with an end-load and varying load condition," *IEEE Trans. Power App. Syst.,* vol. 104, pp. 941-947, Apr. 1985.

[47] H. D. Chiang, J. C. Wang, O. Cockings, and H. D. Shin, "Optimal capacitors placements in distribution systems- Part I: a new formulation of the overall problem," *IEEE Trans. Power Del.,* vol. 5, pp. 634-642, Apr. 1990.

[48] H. D. Chiang, J.C. Wang, O. Cockings, and H.D. Shin, "Optimal capacitor placements in distribution systems- part II: solution algorithms and numerical results," *IEEE Trans. Power Del.,* vol. 5, pp. 643-649, Apr. 1990.

[49] S. Sundhararajan and A. Pahwa, "Optimal selection of capacitors for radial distribution systems using a genetic algorithm," *IEEE Trans. Power Syst.,* vol. 9, pp. 1499-1505, Aug. 1994.

[50] H. H. Happ, "Optimal Power Dispatch," *IEEE Trans. Power App. Syst.,* vol. 93, pp. 820-830, May/June 1974.

[51] K. H. Kim and S. K. You, "Voltage profile improvement by capacitor placement and control in unbalanced distribution systems using GA," in *Proc. IEEE Power Eng. Soc. Summer Meeting*, Alberta, Canada, 1999, pp. 800-805.

[52] R. A. Gallego, A. J. Monticelli, and R. Romero, "Optimal capacitor placement in radial distribution networks," *IEEE Trans. Power Syst.,* vol. 16, pp. 630-637, Nov. 2001.

[53] G. Ramakrishna and N. D. Rao, "A fuzzy logic framework for control of switched capacitors in distribution systems," in *Proc. Canadian Conf. Elect. & Comp. Eng.*, Montreal, Canada, 1995, pp. 676-679.

[54] I. Jonasson and L. Soder, "Power quality on ships. A questionnaire evaluation concerning island power system," in *Proc. 9th Int. Conf. Harmonics and Quality of Power*, 2000, pp. 639-644.

[55] V. Arcidiacono, S. Castellan, R. Menis, and G. Sulligoi, "Integrated voltage and reactive power control for all electric ship power systems," in *Proc. Int. Sym.on Power Electronics, Elect. Drives, Autom. and Motion*, 2006, pp. 878-882.

[56] M. Steurer, M. Andrus, J. Langston, L. Qi, S. Suryanarayanan, S. Woodruff, and P. F. Ribeiro, "Investigating the impact of pulsed power charging demands on shipboard power quality," in *Proc. IEEE Elect. Ship Tech. Symp.*, 2007, pp. 315-321.

[57] S. Quaia, "All electric ship power stations: Dynamic coordination between controls and protections," in *Proc. 43rd Int. Universities Power Eng. Conf.*, 2008, pp. 1-5.

[58] V. Arcidiacono, R. Menis, and G. Sulligoi, "Improving power quality in all electric ships using a voltage and VAR integrated regulator," in *Proc. IEEE Elect. Ship Tech. Symp.*, 2007, pp. 322-327.

[59] N. D. Hatziargyriou and A. P. Sakis Meliopoulos, "Distributed energy sources: technical challenges," in *Proc. IEEE Power Eng. Soc. Winter Meeting*, 2002, pp. 1017-1022.

[60] R. J. Konopinski, P. Vijayan, and V. Ajjarapu, "Extended reactive capability of dfig wind parks for enhanced system performance," *IEEE Trans. Power Syst.,* vol. 24, pp. 1346-1355, Aug. 2009.

[61] P. Piagi and R. H. Lasseter, "Autonomous control of microgrids," in *Proc. IEEE Power Eng. Soc. Gen. Meeting*, 2006.

[62] B. H. Chowdhury, H. T. Ma, and N. Ardeshna, "The challenge of operating wind power plants within a microgrid framework," in *Proc. Power and Energy Conf.*, Illinois, 2010, pp. 93-98.

[63] H. Laaksonen, P. Saari, and R. Komulainen, "Voltage and frequency control of inverter based weak LV network microgrid," in *Proc. Int. Conf. on Future Power Syst.*, 2005.

[64] F. Katiraei, M. R. Iravani, and P. W. Lehn, "Micro-grid autonomous operation during and subsequent to islanding process," *IEEE Trans. Power Del.,* vol. 20, pp. 248-257, Jan. 2005.

[65] R. Majumder, A. Ghosh, G. Ledwich, and F. Zare, "Power management and power flow control with back-to-back converters in a utility connected microgrid," *IEEE Trans. Power Syst.,* vol. 25, pp. 821 - 834, May 2010.

[66] S. A. Al-Askari, S. J. Ranade, and J. Mitra, "Designing a sufficient reactive power supply scheme to multi islands in a microgrid," in *Proc. IEEE Power Eng. Soc. General Meeting*, 2006.

[67] A. A. Ghadimi and H. Rastegar, "Optimal control and management of distributed generation units in an islanded MicroGrid," in *Proc. IEEE Symp. Integration of Wide-Scale Renewable Resources Into the Power Delivery Syst.*, 2009, pp. 1-7.

[68] A. G. Madureira and J. A. P. Lopes, "Voltage and reactive power control in MV networks integrating microgrids," in *Proc. Int. Conf. Renewable Energy Power Quality* Seville, Spain, 2007.

[69] A. G. Madureira and J. A. Pecas Lopes, "Coordinated voltage support in distribution networks with distributed generation and microgrids," *IET Renewable Power Gen.,* vol. 3, pp. 439-454, Dec. 2009.

[70] J. R. O. Soto, C. R. R. Domellas, and D. M. Falcao, "Optimal reactive power dispatch using a hybrid formulation: genetic algorithms and interior point," in *Proc. IEEE Power Tech*, Porto, 2001.

[71] L. Min, W. Jie, Z. Jun, and G. La-Mei, "Power dispatching of distributed wind-Solar power generation hybrid system based on genetic algorithm," in *Proc. Inter. Conf. Power Electronics Systems and Applications*, 2009, pp. 1-4.

[72] B. M. Nickell. Wind Dispatchability and Storage Interconnected Grid Perspective. *[On-line] Energy Efficiency & Renewable Energy available at http://www.austinenergy.com/About%20Us/Newsroom/Reports/taskForce/tfWind Dispatchability.pdf*.

[73] D. Karlsson and D. J. Hill, "Modelling and identification of nonlinear dynamic loads in power systems," *IEEE Trans. Power Syst.,* vol. 9, pp. 157–166, Feb. 1994.

[74] R. Lasseter and M. Erickson, "Integration of battery-based energy storage element in the CERTS Microgrid," University of Wisconsin-Madison, DE-FC02-06CH11350, 2009.

[75] H. Laaksonen and K. Kauhaniemi, "Fault type and location detection in islanded microgrid with different control methods based converters," in *Proc. 19th Int. Conf. Electr. Distribution*, 2007.

[76] E. D. Sontag, "Nonlinear regulation: The piecewise linear approach," *IEEE Trans. Autom. Control,* pp. 346-358, Apr. 1981.

[77] W. P. M. H. Heemels, B. D. Schutter, and A. Bemporad, "Equivalence of hybrid dynamical models," *Automatica,* pp. 1085-1091, July 2001.

[78] A. Bemporad, "Model predictive control of hybrid systems," *1st HYCON PhD School on Hybrid Systems,* July 19-22 2005.

[79] A. Bemporad and M. Morari, "Control of systems integrating logic, dynamics, and constraints," *Automatica,* vol. 35, pp. 407-427, March 1999.

[80] A. Bemporad, "An efficient technique for translating mixed logical dynamical systems into piecewise affine systems," in *Proc. 41st IEEE Conf. Decision and Control*, Las Vegas, NV, 2002.

[81] F. Borrelli, *Constrained Optimal Control of Linear and Hybrid Systems*: Springer, 2003.

[82] G. Ferrari-Trecate, D. Mignone, and M. Morari, "Moving horizon estimation for hybrid systems," *IEEE Trans. Autom. Control,* vol. 47, pp. 1663-1676, Oct. 2002.

[83] F. D. Torrisi and A. Bemporad, "HYSDEL - A tool for generating computational hybrid models for analysis and synthesis problems," *IEEE Trans. Control Syst. Tech.,* pp. 235-249, March 2004.

[84] R. Raman and I. E. Grossmann, "Relation between MILP modeling and logical inference for chemical process synthesis," *Computers and Chemical Engineering,* vol. 15, pp. 73-84, 1991.

[85] C. A. Floudas, *Nonlinear and Mixed-Integer Optimization: Fundamentals and Applications (Topics in Chemical Engineering)*: Oxford University Press, 1995.

[86] R. Fletcher and S. Leyffer, "Numerical experience with lower bounds for MIQP branch-and-bound," *SIAM Journal on Optimization,* vol. 8, pp. 604-616, 1998.

[87] V. Dua and E. N. Pistikopoulos, "An algorithm for the solution of multiparametric mixed integer linear programming problems," *Annals of Operations-Research,* pp. 123-139, 2000.

[88] V. Dua, N. A. Bozinis, and E. N. Pistikopoulos, "A multiparametric programming approach for mixed-integer quadratic engineering problems," *Computers and Chemical Engineering,* vol. 26, pp. 715-733, May 2002.

[89] F. Borrelli, M. Baotic, A. Bemporad, and M. Morari, "Dynamic programming for constrained optimal control of discrete-time linear hybrid systems," *Automatica,* vol. 41, pp. 1709-1721, June 2005.

[90] P. Kundur, N. J. Balu, and M. G. Lauby, *Power System Stability and Control*. New York: McGraw-Hill, 1994.

[91] P. Sauer and M. A. Pai, *Power System Dynamics and Stability*: Prentice-Hall, 1998.

[92] J. G. Slootweg, "Wind power modelling and impact on power systems dynamics," Ph.D. dissertation, Dept. Elect. Eng., Delft Univ. Technol., Delft, The Netherlands, 2003.

[93] R. S. Pena, "Vector control strategies for a doubly-fed induction generator driven by a wind turbine," Ph.D. dissertation, Dept. Elect. Eng., Univ. Nottingham, Nottingham, U.K., 1996.

[94] F. Blaabjerg, Z. Chen, and S. B. Kjaer, "Power electronics as efficient interface in dispersed power generation systems," *IEEE Trans. Power Electron.,* vol. 19, pp. 1184-1194, Sept. 2004.

[95] F. Blaabjerg, F. lov, R. Teodorescu, and Z. Chen, "Power electronics in renewable energy systems," in *Proc. IEEE Power Elec. Motion Conf.*, Portoroz, Slovenia, 2006.

[96] M. G. Villalva, J. R. Gazoli, and E. R. Filho, "Comprehensive approach to modeling and simulation of photovoltaic arrays," *IEEE Trans. Power Electron.,* vol. 24, pp. 1198-1208, May 2009.

[97] C. Lin, Y. Chen, C. Chiou, C. Huang, H. Chiang, J. Wang, and L. Fekih-Ahmed, "Dynamic load models in power systems using the measurement approach," *IEEE Trans. Power Syst.,* vol. 8, pp. 309-315, Feb. 1993.

[98] Y. Liang, R. Fischl, A. DeVito, and S. C. Readinger, "Dynamic reactive load model," *IEEE Trans. Power Syst.,* vol. 13, pp. 1365-1372, Nov. 1998.

[99] I. R. Navarro, "Dynamic load models for power systems," Ph.D. dissertation, Dept. Elect. Eng., Lund University, Sweden, 2002.

[100] A. J. Wigington, "A comparison of induction motor starting methods being powered by a diesel-generator set," M.S. Thesis, Dept. Elect. Eng., University of Nebraska at Lincoln, 2010.

[101] J. Kay, R. Paes, J. Seggewiss, and R. Ellis, "Methods for the control of large medium-voltage motors: application considerations and guidelines," *IEEE Trans. Indust. Appl.,* vol. 36, pp. 1688--1696, 1999.

[102] *IEEE Recommended Practice for Industrial and Commercial Power Systems Analysis,* IEEE Standard 399-1997, Aug. 1998

[103] S. J. Chapman, *Electric Machinery Fundamentals*, 4 ed. New York: NY: McGraw-Hill, 2005.

[104] R. Natarajan, *Power System Capacitors (Power Engineering (Willis))*, 1 ed.: CRC Press, 2005.

[105] S. Khushalani, J. M. Solanki, and N. N. Schulz, "Development of three-phase unbalanced power flow using PV and PQ models for distributed generation and study of the impact of DG models," *IEEE Trans. Power Syst.,* vol. 22, pp. 1019-1025, Aug. 2007.

[106] *IEEE Guide for design, operation, and integration of distributed resource island systems with electric power Systems,* IEEE Standard 1547.4™-2011, 2011

[107] W. H. Kersting, *Distribution System Modeling and Analysis*, 2 ed.: CRC Press, 2006.

[108] Y. Zhu and K. Tomsovic, "Adaptive power flow method for distribution systems with dispersed generation," *IEEE Trans. Power Del.,* vol. 17, pp. 822 - 827, July 2002.

[109] C. S. Cheng and D. Shirmohammadi, "A three-phase power flow method for real-time distribution system analysis," *IEEE Trans. Power Syst.,* vol. 10, pp. 671-679, May 1995.

[110] M. E. Baran and E. A. Staton, "Distribution transformer models for branch current based feeder analysis," *IEEE Trans. Power Syst.,* vol. 12, pp. 698-703, May 1997.

[111] G. Ferrari-Trecate, M. Muselli, D. Liberati, and M. Morari, "A clustering technique for the identification of piecewise affine and hybrid systems," *Automatica,* vol. 39, pp. 205-217, 2003.

[112] G. Ferrari-Trecate, "Identification algorithms for hybrid systems," *1st HYCON PhD School on Hybrid Systems,* July 19-22 2005.

[113] C. E. Garcia, D. M. Prett, and M. Morari, "Model predictive control: theory and practice - a survey," *Automatica,* vol. 25, pp. 335-348, May 1989.

[114] D. Q. Mayne, "Constrained model predictive control: stability and optimality," *Automatica,* vol. 36, pp. 789-814, June 2000.

[115] J. M. Maciejowski, *Predictive Control*: Prentice Hall, 2002.

[116] S. Boyd and L. Vandenberghe, *Convex Optimization*: Cambridge University Press, 2004.

[117] D. Mignone, "Control and estimation of hybrid systems with mathematical optimization," Ph.D. dissertation, Dept. Elect. Eng., ETH Zurich University, 2002.

[118] G. F. Ferrari-Trecate, F. A. Cuzzola, and M. Morari, "Lagrange stability and performance analysis of discrete-time piecewise affine systems with logic states," *Inter. Jour. Control,* vol. 76, pp. 1585-1598, 2003.

[119] G. Ferrari-Trecate, F. A. Cuzzola, D. Mignone, and M. Morari, "Analysis of discrete-time piecewise affine and hybrid systems," *Automatica,* vol. 38, pp. 2139-2146, Dec. 2002.

[120] M. Johansson and A. Rantzer, "Computation of piecewise quadratic lyapunov functions for hybrid systems," *IEEE Trans. Autom. Control,* vol. 43, pp. 555-559, Apr. 1998.

[121] *IEEE Recommended Practice for Electrical Installations on Shipboard,* IEEE Standard 45, 2002

[122] T. Short, *Electric Power Distribution Handbook*, 1 ed.: CRC Press, 2003.

[123] J. D. Kueck, B. J. Kirby, L. M. Tolbert, and D. T. Rizy, "Voltage regulation - Tapping Distributed Energy Resources," *Public Utilities Fortnightly,* Sept. 2004.

[124] Y. Xu, D. T. Rizy, F. LI, and J. D. Kueck, "Dynamic voltage regulation using distributed energy resources," in *Proc. Inter. Conf. Electrical Distribution*, 2007.

[125] R. McMonagle, "The potential of solar PV in Ontario," The Canadian Solar Industries Association, V2.1, Jan. 30, 2006.

[126] E. Liu and J. Bebic, "Distribution systems voltage performance analysis for high-penetration photovoltaics," *Subcontract Report , NREL/SR-581-42298,* 2008.

[127] H. Yu, J. Pan, and A. Xiang, "A multi-function grid-connected PV system with reactive power compensation for the grid," *Elsevier Solar Energy Journal,* vol. 79, pp. 101-106, 2005.

[128] K. Turitsyn, P. Sulc, S. Backhaus, and M. Chertkov, "Local control of reactive power by distributed photovoltaic generators," in *Proc. IEEE Inter. Conf. Smart Grid Communications*, Gaithersburg, MD, 2010, pp. 79-84.

[129] C. Whitaker, J. Newmiller, M. Ropp, and B. Norris, "Distributed photovoltaic systems design and technology requirements," Sandia national lab, SAND2008-0946 P, 2008.

[130] "OptiSpeed, Vestas converter system, General Edition," *Item no. 947543.R0 - Class 1, Ringkobing, Denmark.*

[131] I. Cadirci and M. Ermis, "Double-output induction generator operating at subsynchronous and supersynchronous speeds: steady-state performance optimization and wind-energy recovery," *IEE Proc. B. Electric Power Appl.,* vol. 139, pp. 429-442, 1992.

[132] V. Akhmatov, "Modelling of variable-speed wind turbines with doubly-fed induction generators in short-term stability investigations," in *Proc. 3rd Int. Workshop Transmission Networks for Offshore Wind Farms*, Stockholm, Sweden, 2002, pp. 1–23.

[133] L. Zhang, C. Watthanasarn, and W. Shepher, "Application of a matrix converter for the power control of a variable-speed wind-turbine driving a doubly-fed induction generator," in *Proc. 23rd Int. Conf. Indust. Electr., Control and Instrument.*, 1997, pp. 906 - 911.

[134] V. Akhmatov, "Analysis of dynamic behaviour of electric power systems with large amount of wind power," Ph.D. dissertation, Dept. Elect. Eng., Technical University of Denmark, Lyngby, 2003.

[135] G. W. Energy, "Patented VAR Control Technology," GE Wind Energy, General Electric Company, GEA-13345 (05/02 5M), 2002.

[136] V. Akhmatov, "Variable speed wind turbines with doubly-fed induction generators Part II: power system stability," *Wind Engineering,* vol. 26, pp. 171-188, July 2002.

[137] *IEEE Standard for interconnecting distributed resources with electric power systems,* IEEE Standard 1547, 2008

[138] D. L. Hornak and N. H. Joe, "Distributed generation interconnections: protection, monitoring, and control opportunities," Basler Electric Company, available at: www.basler.com/downloads/disgen_interc2.pdf.

[139] N. R. Friedman, "Distributed energy resources interconnection systems: technology review and research needs," National Renewable Energy Laboratory, NREL/SR-560-32459, 2002.

[140] N. Mithulannthan and T.Oo, "Distributed generation placement to maximize the loadability of a distribution system," *Inter. Journal Electr. Eng. Education,* vol. 2, pp. 107–118, 2006.

[141] W. Prommee and W. Ongsakul, "Optimal multiple distributed generation placement in microgrid system by improved reinitialized social structures particle swarm optimization," *Euro. Trans. Electr. Power,* vol. 21, pp. 489–504, May 2011.

[142] P. Mahat, W. Ongsakul, and T. Kerdchuen, "Optimal placement of wind turbine DG in primary distribution system for real power loss reduction," *Environ. Sciences Division Publ.,* March 2006.

[143] W. Kuersuk and W. Ongsakul, "Optimal placement of distributed generation using particle swarm optimization," in *Proc. Australian Universities Power Eng. Conf.*, Victoria, Australia, 2006.

[144] H. Hedayati and S. Nabaviniaki, "A new method for placement of DG unit in distribution networks," in *Proc. IEEE Power Syst. Conf. and Exp.*, Atlanta, Georgia, 2006.

[145] A. Keane and M. O. Malley, "Optimal allocation of embedded generation on distribution networks," *IEEE Trans. Power Syst.,* vol. 3, pp. 1640–1646, Aug. 2005.

APPENDIX A

The NEMA Codes by letter grade are reproduced here for convenience from (NEMA, 2007) and (NEMA, 2009) in Tables 5 and 6.

Table 5: NEMA Letter Code Typical Characteristics (NEMA Standards Publication Condensed MG 1-2007)

Polyphase Characteristics	Locked Rotor Torque (Percent Rated Load Torque	Pull-Up Torque (Percent Rated Load Torque)	Breakdown Torque (Percent Rated Load Torque)	Locked Rotor Current (Percent Rated Load Current)	Slip	Typical Applications	Relative Efficiency
Design A High locked rotor torque and high locked rotor current	70-275*	65-190	175-300*	Not defined	0.5-5%	Fans, blowers, centrifugal pumps and compressors, motor-generator sets, etc., where starting torque requirements are relatively low	Medium or high
Design B Normal locked rotor torque and normal locked rotor current	70-275*	65-190	175-300*	600-700	0.5-5%	Fans, blowers, centrifugal pumps and compressors, motor-generator sets, etc., where starting torque requirements are relatively low	Medium or high
Design C High locked rotor torque and normal locked rotor current	200-285*	140-195	190-225*	600-700	1-5%	Conveyors, crushers, stirring motors, agitators, reciprocating pumps and compressors, etc., where starting under load is required	Medium
Design D High locked rotor torque and high slip	275	NA	275	600-700	5-8%	High peak loads with or without flywheels such as punch presses, shears, elevators, extractors, winches, hoists, oil-well pumping and wire-drawing motors	Low
Design N Small motor	—	NA	—	—	NA	Centrifugal loads where starting torque requirements are relatively low	Low
Design O Small motor	—	NA	—	—	NA		
Design L Medium motor	—	100%	—	—	NA	Fans, blowers, centrifugal pumps and compressors, motor-generator sets, etc., where starting torque requirements are relatively low	Medium or Low
Design M Medium motor	—	100%	—	—	NA	Fans, blowers, centrifugal pumps and compressors, motor-generator sets, etc., where starting torque requirements are relatively low	Medium or high

*Higher values are for motors having lower horsepower ratings.

Table 6: NEMA Code Letter Locked-Rotor kVA (NEMA, 2009)

NEMA Code Letter	Locked Rotor kVA per HP
A	0.0 - 3.15
B	3.15 - 3.55
C	3.55 - 4.0
D	4.0 - 4.5
E	4.5 - 5.0
F	5.0 - 5.6
G	5.6 - 6.3
H	6.3 - 7.1
J	7.1 - 8.0
K	8.0 - 9.0
L	9.0 - 10.0
M	10.0 - 11.2

APPENDIX B

IEEE 34 Node Test Feeder

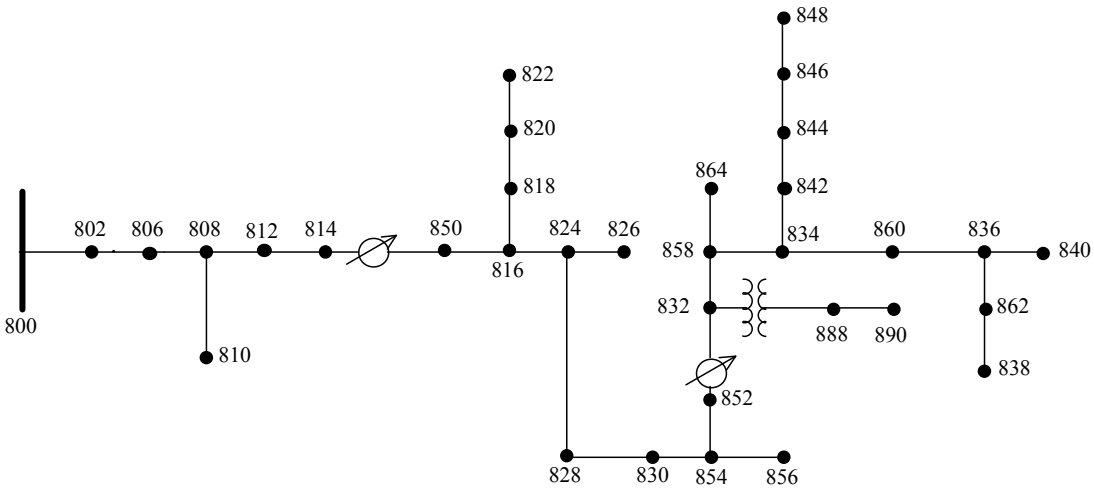

Overhead Line Configurations (Config.)

Config.	Phasing	Phase ACSR	Neutral ACSR	Spacing ID
300	B A C N	1/0	1/0	500
301	B A C N	#2 6/1	#2 6/1	500
302	A N	#4 6/1	#4 6/1	510
303	B N	#4 6/1	#4 6/1	510
304	B N	#2 6/1	#2 6/1	510

Line Segment Data

Node A	Node B	Length(ft.)	Config.
800	802	2580	300
802	806	1730	300
806	808	32230	300
808	810	5804	303
808	812	37500	300
812	814	29730	300
814	850	10	301
816	818	1710	302
816	824	10210	301
818	820	48150	302
820	822	13740	302
824	826	3030	303
824	828	840	301
828	830	20440	301
830	854	520	301
832	858	4900	301
832	888	0	XFM-1
834	860	2020	301
834	842	280	301
836	840	860	301
836	862	280	301
842	844	1350	301
844	846	3640	301
846	848	530	301
850	816	310	301
852	832	10	301
854	856	23330	303
854	852	36830	301
858	864	1620	302
858	834	5830	301
860	836	2680	301
862	838	4860	304
888	890	10560	300

Transformer Data

	kVA	kV-high	kV-low	R - %	X - %
Substation:	2500	69 - D	24.9 -Gr. W	1	8
XFM -1	500	24.9 - Gr.W	4.16 - Gr. W	1.9	4.08

Spot Loads

Node	Load Model	Ph-1 kW	Ph-1 kVAr	Ph-2 kW	Ph-2 kVAr	Ph-3 kW	Ph-4 kVAr
860	Y-PQ	20	16	20	16	20	16
840	Y-I	9	7	9	7	9	7
844	Y-Z	135	105	135	105	135	105
848	D-PQ	20	16	20	16	20	16
890	D-I	150	75	150	75	150	75
830	D-Z	10	5	10	5	25	10
Total		344	224	344	224	359	229

Distributed Loads

Node A	Node B	Load Model	Ph-1 kW	Ph-1 kVAr	Ph-2 kW	Ph-2 kVAr	Ph-3 kW	Ph-3 kVAr
802	806	Y-PQ	0	0	30	15	25	14
808	810	Y-I	0	0	16	8	0	0
818	820	Y-Z	34	17	0	0	0	0
820	822	Y-PQ	135	70	0	0	0	0
816	824	D-I	0	0	5	2	0	0
824	826	Y-I	0	0	40	20	0	0
824	828	Y-PQ	0	0	0	0	4	2
828	830	Y-PQ	7	3	0	0	0	0
854	856	Y-PQ	0	0	4	2	0	0
832	858	D-Z	7	3	2	1	6	3
858	864	Y-PQ	2	1	0	0	0	0
858	834	D-PQ	4	2	15	8	13	7
834	860	D-Z	16	8	20	10	110	55
860	836	D-PQ	30	15	10	6	42	22
836	840	D-I	18	9	22	11	0	0
862	838	Y-PQ	0	0	28	14	0	0
842	844	Y-PQ	9	5	0	0	0	0
844	846	Y-PQ	0	0	25	12	20	11
846	848	Y-PQ	0	0	23	11	0	0
Total			262	133	240	120	220	114

Shunt Capacitors

Node	Ph-A kVAr	Ph-B kVAr	Ph-C kVAr
844	100	100	100
848	150	150	150
Total	250	250	250

Regulator Data

Regulator ID:	1		
Line Segment:	814 - 850		
Location:	814		
Phases:	A - B -C		
Connection:	3-Ph,LG		
Monitoring Phase:	A-B-C		
Bandwidth:	2.0 volts		
PT Ratio:	120		
Primary CT Rating:	100		
Compensator Settings:	Ph-A	Ph-B	Ph-C
R - Setting:	2.7	2.7	2.7
X - Setting:	1.6	1.6	1.6
Volltage Level:	122	122	122

Regulator ID:	2		
Line Segment:	852 - 832		
Location:	852		
Phases:	A - B -C		
Connection:	3-Ph,LG		
Monitoring Phase:	A-B-C		
Bandwidth:	2.0 volts		
PT Ratio:	120		
Primary CT Rating:	100		
Compensator Settings:	Ph-A	Ph-B	Ph-C
R - Setting:	2.5	2.5	2.5
X - Setting:	1.5	1.5	1.5
Volltage Level:	124	124	124

IEEE 34 Node Test Feeder

Impedances

```
Configuration 300:

--------- Z & B Matrices Before Changes ---------

           Z (R +jX) in ohms per mile
 1.3368  1.3343   0.2101  0.5779   0.2130  0.5015
                  1.3238  1.3569   0.2066  0.4591
                                   1.3294  1.3471
          B in micro Siemens per mile
            5.3350   -1.5313   -0.9943
                      5.0979   -0.6212
                                4.8880
Configuration 301:

           Z (R +jX) in ohms per mile
 1.9300  1.4115   0.2327  0.6442   0.2359  0.5691
                  1.9157  1.4281   0.2288  0.5238
                                   1.9219  1.4209
          B in micro Siemens per mile
            5.1207   -1.4364   -0.9402
                      4.9055   -0.5951
                                4.7154

Configuration 302:

           Z (R +jX) in ohms per mile
 2.7995  1.4855   0.0000  0.0000   0.0000  0.0000
                  0.0000  0.0000   0.0000  0.0000
                                   0.0000  0.0000
          B in micro Siemens per mile
            4.2251    0.0000    0.0000
                      0.0000    0.0000
                                0.0000

Configuration 303:

           Z (R +jX) in ohms per mile
 0.0000  0.0000   0.0000  0.0000   0.0000  0.0000
                  2.7995  1.4855   0.0000  0.0000
                                   0.0000  0.0000
          B in micro Siemens per mile
            0.0000    0.0000    0.0000
                      4.2251    0.0000
                                0.0000

Configuration 304:

           Z (R +jX) in ohms per mile
0.0000  0.0000   0.0000  0.0000   0.0000  0.0000
                 1.9217  1.4212   0.0000  0.0000
                                  0.0000  0.0000
         B in micro Siemens per mile
           0.0000    0.0000    0.0000
                     4.3637    0.0000
                               0.0000
```

Power Flow Results

```
-  R A D I A L   F L O W   S U M M A R Y  - DATE:  6-24-2004 AT 16:34:11 HOURS ---
SUBSTATION:  IEEE 34;   FEEDER:  IEEE 34
--------------------------------------------------------------------------------
SYSTEM        PHASE             PHASE             PHASE             TOTAL
INPUT -------(A)-------|-------(B)-------|-------(C)-------|------------------
kW   :       759.136   |       666.663   |       617.072   |      2042.872
kVAr :       171.727   |        90.137   |        28.394   |       290.258
kVA  :       778.318   |       672.729   |       617.725   |      2063.389
PF   :        .9754    |        .9910    |        .9989    |        .9901

LOAD  --(A-N)----(A-B)-|--(B-N)----(B-C)-|--(C-N)----(C-A)-|---WYE-----DELTA--
kW   :   359.9    246.4|   339.3    243.3|   221.8    359.0|   921.0    848.8
 TOT :       606.322   |       582.662   |       580.840   |      1769.824
                       |                 |                 |
kVAr :   230.9    128.7|   216.9    128.7|   161.8    184.6|   609.6    441.9
 TOT :       359.531   |       345.609   |       346.407   |      1051.547
                       |                 |                 |
kVA  :   427.6    278.0|   402.7    275.3|   274.6    403.7|  1104.5    957.0
 TOT :       704.903   |       677.452   |       676.293   |      2058.647
                       |                 |                 |
PF   :   .8417    .8864|   .8425    .8840|   .8078    .8894|   .8339    .8870
 TOT :        .8601    |        .8601    |        .8589    |        .8597

LOSSES ------(A)-------|-------(B)-------|-------(C)-------|------------------
kW   :       114.836   |        80.389   |        77.824   |       273.049
kVAr :        14.200   |        10.989   |         9.810   |        34.999
kVA  :       115.711   |        81.137   |        78.440   |       275.283

CAPAC --(A-N)----(A-B)-|--(B-N)----(B-C)-|--(C-N)----(C-A)-|---WYE-----DELTA--
R-kVA:   250.0       .0|   250.0       .0|   250.0       .0|   750.0       .0
 TOT :       250.000   |       250.000   |       250.000   |       750.000
                       |                 |                 |
A-kVA:   265.7       .0|   264.8       .0|   265.9       .0|   796.3       .0
 TOT :       265.658   |       264.760   |       265.869   |       796.287
```

--- **V O L T A G E P R O F I L E** ---- DATE: 6-24-2004 AT 16:34:18 HOURS ----
SUBSTATION: IEEE 34; FEEDER: IEEE 34

NODE	MAG	ANGLE	MAG	ANGLE	MAG	ANGLE	mi.to SR
	A-N		B-N		C-N		
800	1.0500 at	.00	1.0500 at	-120.00	1.0500 at	120.00	.000
802	1.0475 at	-.05	1.0484 at	-120.07	1.0484 at	119.95	.489
806	1.0457 at	-.08	1.0474 at	-120.11	1.0474 at	119.92	.816
808	1.0136 at	-.75	1.0296 at	-120.95	1.0289 at	119.30	6.920
810			1.0294 at	-120.95			8.020
812	.9763 at	-1.57	1.0100 at	-121.92	1.0069 at	118.59	14.023
814	.9467 at	-2.26	.9945 at	-122.70	.9893 at	118.01	19.653
RG10	1.0177 at	-2.26	1.0255 at	-122.70	1.0203 at	118.01	19.654
850	1.0176 at	-2.26	1.0255 at	-122.70	1.0203 at	118.01	19.655
816	1.0172 at	-2.26	1.0253 at	-122.71	1.0200 at	118.01	19.714
818	1.0163 at	-2.27					20.038
820	.9926 at	-2.32					29.157
822	.9895 at	-2.33					31.760
824	1.0082 at	-2.37	1.0158 at	-122.94	1.0116 at	117.76	21.648
826			1.0156 at	-122.94			22.222
828	1.0074 at	-2.38	1.0151 at	-122.95	1.0109 at	117.75	21.807
830	.9894 at	-2.63	.9982 at	-123.39	.9938 at	117.25	25.678
854	.9890 at	-2.64	.9978 at	-123.40	.9934 at	117.24	25.777
852	.9581 at	-3.11	.9680 at	-124.18	.9637 at	116.33	32.752
RG11	1.0359 at	-3.11	1.0345 at	-124.18	1.0360 at	116.33	32.752
832	1.0359 at	-3.11	1.0345 at	-124.18	1.0360 at	116.33	32.754
858	1.0336 at	-3.17	1.0322 at	-124.28	1.0338 at	116.22	33.682
834	1.0309 at	-3.24	1.0295 at	-124.39	1.0313 at	116.09	34.786
842	1.0309 at	-3.25	1.0294 at	-124.39	1.0313 at	116.09	34.839
844	1.0307 at	-3.27	1.0291 at	-124.42	1.0311 at	116.06	35.095
846	1.0309 at	-3.32	1.0291 at	-124.46	1.0313 at	116.01	35.784
848	1.0310 at	-3.32	1.0291 at	-124.47	1.0314 at	116.00	35.885
860	1.0305 at	-3.24	1.0291 at	-124.39	1.0310 at	116.09	35.169
836	1.0303 at	-3.23	1.0287 at	-124.39	1.0308 at	116.09	35.677
840	1.0303 at	-3.23	1.0287 at	-124.39	1.0308 at	116.09	35.839
862	1.0303 at	-3.23	1.0287 at	-124.39	1.0308 at	116.09	35.730
838			1.0285 at	-124.39			36.650
864	1.0336 at	-3.17					33.989
XF10	.9997 at	-4.63	.9983 at	-125.73	1.0000 at	114.82	32.754
888	.9996 at	-4.64	.9983 at	-125.73	1.0000 at	114.82	32.754
890	.9167 at	-5.19	.9235 at	-126.78	.9177 at	113.98	34.754
856			.9977 at	-123.41			30.195

---------- **VOLTAGE REGULATOR DATA** ---- DATE: 6-24-2004 AT 16:34:22 HOURS --
SUBSTATION: IEEE 34; FEEDER: IEEE 34

[NODE]	[VREG]	[SEG]	[NODE]	MODEL	OPT	BNDW
814	RG10	850	850	Phase A & B & C, Wye	RX	2.00

PHASE	LDCTR	VOLT HOLD	R-VOLT	X-VOLT	PT RATIO	CT RATE	TAP
1		122.000	2.700	1.600	120.00	100.00	12
2		122.000	2.700	1.600	120.00	100.00	5
3		122.000	2.700	1.600	120.00	100.00	5

[NODE]	[VREG]	[SEG]	[NODE]	MODEL	OPT	BNDW
852	RG11	832	832	Phase A & B & C, Wye	RX	2.00

PHASE	LDCTR	VOLT HOLD	R-VOLT	X-VOLT	PT RATIO	CT RATE	TAP
1		124.000	2.500	1.500	120.00	100.00	13
2		124.000	2.500	1.500	120.00	100.00	11
3		124.000	2.500	1.500	120.00	100.00	12

```
- R A D I A L  P O W E R  F L O W  ---  DATE:  6-24-2004 AT 16:34:32 HOURS ---
SUBSTATION:  IEEE 34;   FEEDER:  IEEE 34
--------------------------------------------------------------------------------
   NODE      VALUE         PHASE A         PHASE B         PHASE C     UNT O/L<
                           (LINE A)        (LINE B)        (LINE C)        60.%
--------------------*--------A-------*-------B-------*-------C-------*--------
NODE: 800       VOLTS:   1.050     .00   1.050 -120.00   1.050  120.00 MAG/ANG
kVll  24.900           NO LOAD OR CAPACITOR REPRESENTED AT SOURCE NODE

TO NODE 802   .......:   51.56  -12.74   44.57 -127.70   40.92  117.37 AMP/DG
<802   > LOSS=  3.472:    (  1.637)       (   .978)       (   .858)    kW
--------------------*--------A-------*-------B-------*-------C-------*--------
NODE: 802       VOLTS:   1.047    -.05   1.048 -120.07   1.048  119.95 MAG/ANG
                  -LD:     .00     .00     .00     .00     .00     .00 kW/kVR
kVll  24.900      CAP:             .00             .00             .00 kVR

FROM NODE 800   .....:   51.58  -12.80   44.57 -127.76   40.93  117.31 AMP/DG
<802   > LOSS=  3.472:    (  1.637)       (   .978)       (   .858)    kW
TO NODE 806   .......:   51.58  -12.80   44.57 -127.76   40.93  117.31 AMP/DG
<806   > LOSS=  2.272:    (  1.102)       (   .618)       (   .552)    kW
--------------------*--------A-------*-------B-------*-------C-------*--------
NODE: 806       VOLTS:   1.046    -.08   1.047 -120.11   1.047  119.92 MAG/ANG
                  -LD:     .00     .00     .00     .00     .00     .00 kW/kVR
kVll  24.900      CAP:             .00             .00             .00 kVR

FROM NODE 802   .....:   51.59  -12.83   42.47 -126.83   39.24  118.52 AMP/DG
<806   > LOSS=  2.272:    (  1.102)       (   .618)       (   .552)    kW
TO NODE 808   .......:   51.59  -12.83   42.47 -126.83   39.24  118.52 AMP/DG
<808   > LOSS= 41.339:    ( 20.677)       ( 10.780)       (  9.882)    kW
--------------------*--------A-------*-------B-------*-------C-------*--------
NODE: 808       VOLTS:   1.014    -.75   1.030 -120.95   1.029  119.30 MAG/ANG
                  -LD:     .00     .00     .00     .00     .00     .00 kW/kVR
kVll  24.900      CAP:             .00             .00             .00 kVR

FROM NODE 806   .....:   51.76  -13.47   42.46 -127.59   39.28  117.76 AMP/DG
<808   > LOSS= 41.339:    ( 20.677)       ( 10.780)       (  9.882)    kW
TO NODE 810   .......:                    1.22 -144.62                 AMP/DG
<810   > LOSS=   .002:                    (   .002)                    kW
TO NODE 812   .......:   51.76  -13.47   41.30 -127.10   39.28  117.76 AMP/DG
<812   > LOSS= 47.531:    ( 24.126)       ( 11.644)       ( 11.761)    kW
--------------------*--------A-------*-------B-------*-------C-------*--------
NODE: 810       VOLTS:                   1.029 -120.95                 MAG/ANG
                  -LD:                     .00     .00                 kW/kVR
kVll  24.900      CAP:                             .00                 kVR

FROM NODE 808   .....:                     .00     .00                 AMP/DG
<810   > LOSS=   .002:                    (   .002)                    kW
```

```
- R A D I A L  P O W E R  F L O W  ---  DATE:  6-24-2004 AT 16:34:32 HOURS ---
SUBSTATION:  IEEE 34;   FEEDER:  IEEE 34
--------------------------------------------------------------------------------
   NODE      VALUE         PHASE A         PHASE B         PHASE C     UNT O/L<
                           (LINE A)        (LINE B)        (LINE C)        60.%
--------------------*--------A-------*-------B-------*-------C-------*--------
NODE: 812       VOLTS:    .976   -1.57   1.010 -121.92   1.007  118.59 MAG/ANG
                  -LD:     .00     .00     .00     .00     .00     .00 kW/kVR
kVll  24.900      CAP:              .00             .00             .00 kVR

FROM NODE 808   .....:   51.95  -14.18   41.29 -127.99   39.33  116.90 AMP/DG
<812   > LOSS= 47.531:    ( 24.126)       ( 11.644)       ( 11.761)    kW
TO NODE 814   .......:   51.95  -14.18   41.29 -127.99   39.33  116.90 AMP/DG
<814   > LOSS= 37.790:    ( 19.245)       (  9.140)       (  9.404)    kW
--------------------*--------A-------*-------B-------*-------C-------*--------
NODE: 814       VOLTS:    .947   -2.26    .994 -122.70    .989  118.01 MAG/ANG
                  -LD:     .00     .00     .00     .00     .00     .00 kW/kVR
kVll  24.900      CAP:              .00             .00             .00 kVR

FROM NODE 812   .....:   52.10  -14.73   41.29 -128.69   39.37  116.23 AMP/DG
<814   > LOSS= 37.790:    ( 19.245)       (  9.140)       (  9.404)    kW
TO NODE RG10  .<VRG>.:   52.10  -14.73   41.29 -128.69   39.37  116.23 AMP/DG
<RG10  > LOSS=   .000:    (   .000)       (   .000)       (   .000)    kW
--------------------*--------A-------*-------B-------*-------C-------*--------
NODE: RG10      VOLTS:   1.018   -2.26   1.026 -122.70   1.020  118.01 MAG/ANG
                  -LD:     .00     .00     .00     .00     .00     .00 kW/kVR
kVll  24.900      CAP:              .00             .00             .00 kVR

FROM NODE 814   <VRG>:   48.47  -14.73   40.04 -128.69   38.17  116.23 AMP/DG
<RG10  > LOSS=   .000:    (   .000)       (   .000)       (   .000)    kW
TO NODE 850   .......:   48.47  -14.73   40.04 -128.69   38.17  116.23 AMP/DG
<850   > LOSS=   .017:    (   .008)       (   .005)       (   .005)    kW
--------------------*--------A-------*-------B-------*-------C-------*--------
NODE: 850       VOLTS:   1.018   -2.26   1.026 -122.70   1.020  118.01 MAG/ANG
                  -LD:     .00     .00     .00     .00     .00     .00 kW/kVR
kVll  24.900      CAP:              .00             .00             .00 kVR

FROM NODE RG10  .....:   48.47  -14.73   40.04 -128.69   38.17  116.23 AMP/DG
<850   > LOSS=   .017:    (   .008)       (   .005)       (   .005)    kW
TO NODE 816   .......:   48.47  -14.73   40.04 -128.69   38.17  116.23 AMP/DG
<816   > LOSS=   .538:    (   .254)       (   .145)       (   .139)    kW
--------------------*--------A-------*-------B-------*-------C-------*--------
NODE: 816       VOLTS:   1.017   -2.26   1.025 -122.71   1.020  118.01 MAG/ANG
                  -LD:     .00     .00     .00     .00     .00     .00 kW/kVR
kVll  24.900      CAP:              .00             .00             .00 kVR

FROM NODE 850   .....:   48.47  -14.74   40.04 -128.70   38.17  116.23 AMP/DG
<816   > LOSS=   .538:    (   .254)       (   .145)       (   .139)    kW
TO NODE 818   .......:   13.02  -26.69                                  AMP/DG
<818   > LOSS=   .154:    (   .154)                                     kW
TO NODE 824   .......:   35.83  -10.42   40.04 -128.70   38.17  116.23 AMP/DG
<824   > LOSS= 14.181:    (  4.312)       (  5.444)       (  4.425)    kW
```

```
- R A D I A L  P O W E R  F L O W  ---  DATE:  6-24-2004 AT 16:34:32 HOURS ---
SUBSTATION:  IEEE 34;   FEEDER:  IEEE 34
--------------------------------------------------------------------------------
   NODE      VALUE         PHASE A         PHASE B         PHASE C     UNT O/L<
                           (LINE A)        (LINE B)        (LINE C)        60.%
--------------------*--------A-------*-------B-------*-------C-------*--------
NODE: 818       VOLTS:   1.016   -2.27                                 MAG/ANG
                  -LD:     .00     .00                                 kW/kVR
kVll  24.900      CAP:              .00                                 kVR

FROM NODE 816   .....:   13.03  -26.77                                 AMP/DG
<818   > LOSS=   .154:    (   .154)                                    kW
TO NODE 820   .......:   13.03  -26.77                                 AMP/DG
<820   > LOSS=  3.614:    (  3.614)                                    kW
--------------------*--------A-------*-------B-------*-------C-------*--------
NODE: 820       VOLTS:    .993   -2.32                                 MAG/ANG
                  -LD:     .00     .00                                 kW/kVR
kVll  24.900      CAP:              .00                                 kVR

FROM NODE 818   .....:   10.62  -28.98                                 AMP/DG
<820   > LOSS=  3.614:    (  3.614)                                    kW
TO NODE 822   .......:   10.62  -28.98                                 AMP/DG
<822   > LOSS=   .413:    (   .413)                                    kW
--------------------*--------A-------*-------B-------*-------C-------*--------
NODE: 822       VOLTS:    .990   -2.33                                 MAG/ANG
                  -LD:     .00     .00                                 kW/kVR
kVll  24.900      CAP:              .00                                 kVR

FROM NODE 820   .....:     .00     .00                                 AMP/DG
<822   > LOSS=   .413:    (   .413)                                    kW
--------------------*--------A-------*-------B-------*-------C-------*--------
NODE: 824       VOLTS:   1.008   -2.37   1.016 -122.94   1.012  117.76 MAG/ANG
                  -LD:     .00     .00     .00     .00     .00     .00 kW/kVR
kVll  24.900      CAP:              .00             .00             .00 kVR

FROM NODE 816   .....:   35.87  -10.70   39.82 -129.02   38.05  116.25 AMP/DG
<824   > LOSS= 14.181:    (  4.312)       (  5.444)       (  4.425)    kW
TO NODE 826   .......:                    3.10 -148.92                 AMP/DG
<826   > LOSS=   .008:                    (   .008)                    kW
TO NODE 828   .......:   35.87  -10.70   36.93 -127.39   38.05  116.25 AMP/DG
<828   > LOSS=  1.108:    (   .361)       (   .393)       (   .354)    kW
--------------------*--------A-------*-------B-------*-------C-------*--------
NODE: 826       VOLTS:                   1.016 -122.94                 MAG/ANG
                  -LD:                     .00     .00                 kW/kVR
kVll  24.900      CAP:                             .00                 kVR

FROM NODE 824   .....:                     .00     .00                 AMP/DG
<826   > LOSS=   .008:                    (   .008)                    kW
```

```
- R A D I A L   P O W E R   F L O W  ---  DATE:  6-24-2004 AT 16:34:32 HOURS ---
SUBSTATION:  IEEE 34;   FEEDER:  IEEE 34
--------------------------------------------------------------------------------
   NODE      VALUE         PHASE A         PHASE B         PHASE C     UNT O/L<
                           (LINE A)        (LINE B)        (LINE C)        60.%
--------------------*--------A-------*-------B-------*-------C-------*--------
NODE: 828       VOLTS:   1.007   -2.38   1.015 -122.95   1.011  117.75 MAG/ANG
                  -LD:     .00     .00     .00     .00     .00     .00 kW/kVR
kVll  24.900      CAP:             .00             .00             .00 kVR

FROM NODE 824   .....:   35.87  -10.72   36.93 -127.41   37.77  116.42 AMP/DG
<828   > LOSS=  1.108:    (   .361)       (   .393)       (   .354)    kW
TO NODE 830   .......:   35.87  -10.72   36.93 -127.41   37.77  116.42 AMP/DG
<830   > LOSS= 26.587:    (  8.443)       (  9.214)       (  8.930)    kW
--------------------*--------A-------*-------B-------*-------C-------*--------
NODE: 830       VOLTS:    .989   -2.63    .998 -123.39    .994  117.25 MAG/ANG
                 D-LD:    9.95    4.98    9.86    4.93   24.55    9.82 kW/kVR
kVll  24.900    Y CAP:             .00             .00             .00 kVR

FROM NODE 828   .....:   35.43  -11.06   36.91 -127.92   37.79  115.96 AMP/DG
<830   > LOSS= 26.587:    (  8.443)       (  9.214)       (  8.930)    kW
TO NODE 854   .......:   34.22   -9.97   36.19 -127.47   36.49  116.26 AMP/DG
<854   > LOSS=   .635:    (   .197)       (   .227)       (   .211)    kW
--------------------*--------A-------*-------B-------*-------C-------*--------
NODE: 854       VOLTS:    .989   -2.64    .998 -123.40    .993  117.24 MAG/ANG
                  -LD:     .00     .00     .00     .00     .00     .00 kW/kVR
kVll  24.900      CAP:             .00             .00             .00 kVR

FROM NODE 830   .....:   34.23   -9.99   36.19 -127.48   36.49  116.25 AMP/DG
<854   > LOSS=   .635:    (   .197)       (   .227)       (   .211)    kW
TO NODE 852   .......:   34.23   -9.99   35.93 -127.72   36.49  116.25 AMP/DG
<852   > LOSS= 44.798:    ( 13.996)       ( 15.778)       ( 15.023)    kW
TO NODE 856   .......:                     .31  -98.70                 AMP/DG
<856   > LOSS=   .001:                    (   .001)                    kW
--------------------*--------A-------*-------B-------*-------C-------*--------
NODE: 852       VOLTS:    .958   -3.11    .968 -124.18    .964  116.33 MAG/ANG
                  -LD:     .00     .00     .00     .00     .00     .00 kW/kVR
kVll  24.900      CAP:             .00             .00             .00 kVR

FROM NODE 854   .....:   34.35  -11.00   35.90 -128.66   36.52  115.41 AMP/DG
<852   > LOSS= 44.798:    ( 13.996)       ( 15.778)       ( 15.023)    kW
TO NODE RG11  .<VRG>.:   34.35  -11.00   35.90 -128.66   36.52  115.41 AMP/DG
<RG11  > LOSS=   .000:    (   .000)       (   .000)       (   .000)    kW
--------------------*--------A-------*-------B-------*-------C-------*--------
NODE: RG11      VOLTS:   1.036   -3.11   1.035 -124.18   1.036  116.33 MAG/ANG
                  -LD:     .00     .00     .00     .00     .00     .00 kW/kVR
kVll  24.900      CAP:             .00             .00             .00 kVR

FROM NODE 852   <VRG>:   31.77  -11.00   33.59 -128.66   33.98  115.41 AMP/DG
<RG11  > LOSS=   .000:    (   .000)       (   .000)       (   .000)    kW
TO NODE 832   .......:   31.77  -11.00   33.59 -128.66   33.98  115.41 AMP/DG
<832   > LOSS=   .011:    (   .003)       (   .004)       (   .004)    kW
```

- **R A D I A L P O W E R F L O W** --- DATE: 6-24-2004 AT 16:34:32 HOURS ---
SUBSTATION: IEEE 34;   FEEDER: IEEE 34

NODE	VALUE	PHASE A (LINE A)		PHASE B (LINE B)		PHASE C (LINE C)		UNT	O/L< 60.%
NODE: 832	VOLTS:	1.036	-3.11	1.035	-124.18	1.036	116.33	MAG/ANG	
	-LD:	.00	.00	.00	.00	.00	.00	kW/kVR	
kVll 24.900	CAP:		.00		.00		.00	kVR	
FROM NODE RG11	:	31.77	-11.00	33.59	-128.66	33.98	115.41	AMP/DG	
<832 > LOSS= .011	:	(.003)		(.004)		(.004)		kW	
TO NODE 858	:	21.31	.47	23.40	-116.89	24.34	128.36	AMP/DG	
<858 > LOSS= 2.467	:	(.643)		(.997)		(.827)		kW	
TO NODE XF10	:	11.68	-32.29	11.70	-152.73	11.61	87.39	AMP/DG	<
<XF10 > LOSS= 9.625	:	(3.196)		(3.241)		(3.187)		kW	
NODE: 858	VOLTS:	1.034	-3.17	1.032	-124.28	1.034	116.22	MAG/ANG	
	-LD:	.00	.00	.00	.00	.00	.00	kW/kVR	
kVll 24.900	CAP:		.00		.00		.00	kVR	
FROM NODE 832	:	20.86	.86	23.13	-116.39	24.02	128.48	AMP/DG	
<858 > LOSS= 2.467	:	(.643)		(.997)		(.827)		kW	
TO NODE 834	:	20.73	1.01	23.13	-116.39	24.02	128.48	AMP/DG	
<834 > LOSS= 2.798	:	(.717)		(1.145)		(.936)		kW	
TO NODE 864	:	.14	-22.82					AMP/DG	
<864 > LOSS= .000	:	(.000)						kW	
NODE: 834	VOLTS:	1.031	-3.24	1.029	-124.39	1.031	116.09	MAG/ANG	
	-LD:	.00	.00	.00	.00	.00	.00	kW/kVR	
kVll 24.900	CAP:		.00		.00		.00	kVR	
FROM NODE 858	:	20.29	2.18	22.37	-116.07	23.23	130.06	AMP/DG	
<834 > LOSS= 2.798	:	(.717)		(1.145)		(.936)		kW	
TO NODE 842	:	14.75	34.68	16.30	-95.63	15.12	151.05	AMP/DG	
<842 > LOSS= .064	:	(.015)		(.032)		(.017)		kW	
TO NODE 860	:	11.16	-43.05	9.09	-154.82	10.60	99.34	AMP/DG	
<860 > LOSS= .141	:	(.021)		(.104)		(.017)		kW	
NODE: 842	VOLTS:	1.031	-3.25	1.029	-124.39	1.031	116.09	MAG/ANG	
	-LD:	.00	.00	.00	.00	.00	.00	kW/kVR	
kVll 24.900	CAP:		.00		.00		.00	kVR	
FROM NODE 834	:	14.74	34.67	16.30	-95.64	15.12	151.03	AMP/DG	
<842 > LOSS= .064	:	(.015)		(.032)		(.017)		kW	
TO NODE 844	:	14.74	34.67	16.30	-95.64	15.12	151.03	AMP/DG	
<844 > LOSS= .306	:	(.068)		(.156)		(.083)		kW	

```
- R A D I A L  P O W E R  F L O W  ---  DATE:  6-24-2004 AT 16:34:32 HOURS ---
SUBSTATION:  IEEE 34;   FEEDER:  IEEE 34
--------------------------------------------------------------------------------
   NODE      VALUE         PHASE A         PHASE B         PHASE C     UNT O/L<
                           (LINE A)        (LINE B)        (LINE C)        60.%
--------------------*--------A-------*-------B-------*-------C-------*--------
NODE: 844       VOLTS:   1.031   -3.27   1.029 -124.42   1.031  116.06 MAG/ANG
                 Y-LD:  143.41  111.54  142.97  111.20  143.51  111.62 kW/kVR
kVll  24.900    Y CAP:          106.23          105.90          106.31 kVR

FROM NODE 842   .....:   14.47   37.12   16.29  -95.71   15.11  150.97 AMP/DG
<844   > LOSS=   .306:    (   .068)       (   .156)       (   .083)    kW
TO NODE 846   .......:    9.83   78.88    9.40  -63.87    9.40 -170.67 AMP/DG
<846   > LOSS=   .323:    (   .043)       (   .212)       (   .068)    kW
--------------------*--------A-------*-------B-------*-------C-------*--------
NODE: 846       VOLTS:   1.031   -3.32   1.029 -124.46   1.031  116.01 MAG/ANG
                  -LD:     .00     .00     .00     .00     .00     .00 kW/kVR
kVll  24.900      CAP:             .00             .00             .00 kVR

FROM NODE 844   .....:    9.76   78.80    9.40  -52.54    9.78 -161.93 AMP/DG
<846   > LOSS=   .323:    (   .043)       (   .212)       (   .068)    kW
TO NODE 848   .......:    9.76   78.80    9.40  -52.54    9.78 -161.93 AMP/DG
<848   > LOSS=   .048:    (   .007)       (   .031)       (   .010)    kW
--------------------*--------A-------*-------B-------*-------C-------*--------
NODE: 848       VOLTS:   1.031   -3.32   1.029 -124.47   1.031  116.00 MAG/ANG
                 D-LD:   20.00   16.00   20.00   16.00   20.00   16.00 kW/kVR
kVll  24.900    Y CAP:          159.43          158.86          159.56 kVR

FROM NODE 846   .....:    9.76   78.79    9.77  -42.47    9.78 -161.94 AMP/DG
<848   > LOSS=   .048:    (   .007)       (   .031)       (   .010)    kW
--------------------*--------A-------*-------B-------*-------C-------*--------
NODE: 860       VOLTS:   1.030   -3.24   1.029 -124.39   1.031  116.09 MAG/ANG
                 Y-LD:   20.00   16.00   20.00   16.00   20.00   16.00 kW/kVR
kVll  24.900    Y CAP:             .00             .00             .00 kVR

FROM NODE 834   .....:    5.87  -33.62    7.68 -156.52    5.29   86.10 AMP/DG
<860   > LOSS=   .141:    (   .021)       (   .104)       (   .017)    kW
TO NODE 836   .......:    4.16  -30.19    5.96 -154.63    3.60   90.25 AMP/DG
<836   > LOSS=   .039:    (  -.035)       (   .103)       (  -.028)    kW
--------------------*--------A-------*-------B-------*-------C-------*--------
NODE: 836       VOLTS:   1.030   -3.23   1.029 -124.39   1.031  116.09 MAG/ANG
                  -LD:     .00     .00     .00     .00     .00     .00 kW/kVR
kVll  24.900      CAP:             .00             .00             .00 kVR

FROM NODE 860   .....:    1.49  -19.83    4.42 -150.74    1.74   68.08 AMP/DG
<836   > LOSS=   .039:    (  -.035)       (   .103)       (  -.028)    kW
TO NODE 840   .......:    1.50  -20.01    2.33 -151.97    1.75   68.00 AMP/DG
<840   > LOSS=   .002:    (  -.014)       (   .026)       (  -.010)    kW
TO NODE 862   .......:     .00     .00    2.09 -149.38     .00     .00 AMP/DG
<862   > LOSS=   .000:    (  -.005)       (   .009)       (  -.004)    kW
```

```
- R A D I A L  P O W E R  F L O W  ---  DATE:  6-24-2004 AT 16:34:32 HOURS ---
SUBSTATION:  IEEE 34;   FEEDER:  IEEE 34
--------------------------------------------------------------------------------
   NODE      VALUE         PHASE A         PHASE B         PHASE C     UNT O/L<
                           (LINE A)        (LINE B)        (LINE C)        60.%
--------------------*--------A-------*-------B-------*-------C-------*--------
NODE: 840       VOLTS:   1.030   -3.23   1.029 -124.39   1.031  116.09 MAG/ANG
                 Y-LD:    9.27    7.21    9.26    7.20    9.28    7.22 kW/kVR
kVll  24.900    Y CAP:             .00             .00             .00 kVR

FROM NODE 836   .....:     .79  -41.11     .79 -162.26     .79   78.21 AMP/DG
<840   > LOSS=   .002:    (  -.014)       (   .026)       (  -.010)    kW
--------------------*--------A-------*-------B-------*-------C-------*--------
NODE: 862       VOLTS:   1.030   -3.23   1.029 -124.39   1.031  116.09 MAG/ANG
                  -LD:     .00     .00     .00     .00     .00     .00 kW/kVR
kVll  24.900      CAP:             .00             .00             .00 kVR

FROM NODE 836   .....:     .00     .00    2.09 -149.50     .00     .00 AMP/DG
<862   > LOSS=   .000:    (  -.005)       (   .009)       (  -.004)    kW
TO NODE 838   .......:                    2.09 -149.50                 AMP/DG
<838   > LOSS=   .004:                    (   .004)                    kW
--------------------*--------A-------*-------B-------*-------C-------*--------
NODE: 838       VOLTS:                   1.029 -124.39                 MAG/ANG
                  -LD:                     .00     .00                 kW/kVR
kVll  24.900      CAP:                             .00                 kVR

FROM NODE 862   .....:                     .00     .00                 AMP/DG
<838   > LOSS=   .004:                    (   .004)                    kW
--------------------*--------A-------*-------B-------*-------C-------*--------
NODE: 864       VOLTS:   1.034   -3.17                                 MAG/ANG
                  -LD:     .00     .00                                 kW/kVR
kVll  24.900      CAP:             .00                                 kVR

FROM NODE 858   .....:     .00     .00                                 AMP/DG
<864   > LOSS=   .000:    (   .000)                                    kW
--------------------*--------A-------*-------B-------*-------C-------*--------
NODE: XF10      VOLTS:   1.000   -4.63    .998 -125.73   1.000  114.82 MAG/ANG
                  -LD:     .00     .00     .00     .00     .00     .00 kW/kVR
kVll   4.160      CAP:             .00             .00             .00 kVR

FROM NODE 832   .....:   69.90  -32.29   70.04 -152.73   69.50   87.39 AMP/DG <
<XF10  > LOSS=  9.625:    (  3.196)       (  3.241)       (  3.187)    kW
TO NODE 888   .......:   69.90  -32.29   70.04 -152.73   69.50   87.39 AMP/DG
<888   > LOSS=   .000:    (   .000)       (   .000)       (   .000)    kW
--------------------*--------A-------*-------B-------*-------C-------*--------
NODE: 888       VOLTS:   1.000   -4.64    .998 -125.73   1.000  114.82 MAG/ANG
                  -LD:     .00     .00     .00     .00     .00     .00 kW/kVR
kVll   4.160      CAP:             .00             .00             .00 kVR

FROM NODE XF10  .....:   69.90  -32.29   70.04 -152.73   69.50   87.39 AMP/DG
<888   > LOSS=   .000:    (   .000)       (   .000)       (   .000)    kW
TO NODE 890   .......:   69.90  -32.29   70.04 -152.73   69.50   87.39 AMP/DG
<890   > LOSS= 32.760:    ( 11.638)       (  9.950)       ( 11.173)    kW
```

```
- R A D I A L  P O W E R  F L O W  ---  DATE:  6-24-2004 AT 16:34:32 HOURS ---
SUBSTATION:  IEEE 34;   FEEDER:  IEEE 34
--------------------------------------------------------------------------------
   NODE      VALUE         PHASE A         PHASE B         PHASE C     UNT O/L<
                           (LINE A)        (LINE B)        (LINE C)        60.%
--------------------*--------A-------*-------B-------*-------C-------*--------
NODE: 890       VOLTS:    .917   -5.19    .924 -126.78    .918  113.98 MAG/ANG
                 D-LD:  139.11   69.55  137.56   68.78  137.01   68.50 kW/kVR
kVll   4.160    Y CAP:             .00             .00             .00 kVR

FROM NODE 888   .....:   69.91  -32.31   70.05 -152.75   69.51   87.37 AMP/DG
<890   > LOSS= 32.760:    ( 11.638)       (  9.950)       ( 11.173)    kW
--------------------*--------A-------*-------B-------*-------C-------*--------
NODE: 856       VOLTS:                    .998 -123.41                  MAG/ANG
                  -LD:                     .00     .00                  kW/kVR
kVll  24.900      CAP:                             .00                  kVR

FROM NODE 854   .....:                     .00     .00                  AMP/DG
<856   > LOSS=   .001:                   (   .001)                      kW
```